UC Riverside

UC Riverside Electronic Theses and Dissertations

Title

Effects of Thirdhand Smoke, Nicotine and Electronic Cigarette Aerosol on Cellular Oxidative Stress and Organelle Dynamics in In Vitro and In Vivo Models

Permalink

https://escholarship.org/uc/item/9xh557qd

Author

Pozuelos, Giovanna Lissette

Publication Date

2022

Copyright Information

This work is made available under the terms of a Creative Commons Attribution License, availalbe at https://creativecommons.org/licenses/by/4.0/

Peer reviewed|Thesis/dissertation

eScholarship.org Powered by the California Digital Library
University of California

UNIVERSITY OF CALIFORNIA
RIVERSIDE

Effects of Thirdhand Smoke, Nicotine and Electronic Cigarette Aerosol on Cellular Oxidative Stress and Organelle Dynamics in *In Vitro* and *In Vivo* Models

A Dissertation submitted in partial satisfaction
of the requirements for the degree of

Doctor of Philosophy

in

Cell, Molecular, and Developmental Biology

by

Giovanna Lissette Pozuelos

March 2022

Dissertation Committee:
Dr. Prue Talbot, Chairperson
Dr. Thomas Girke
Dr. Yinsheng Wang

Copyright by
Giovanna Lissette Pozuelos
2022

The Dissertation of Giovanna Lissette Pozuelos is approved:

Committee Chairperson

University of California, Riverside

ABSTRACT OF THE DISSERTATION

Effects of Nicotine, Thirdhand Smoke, and Electronic Cigarette Aerosol on Cellular Oxidative Stress and Organelle Dynamics in *In Vitro* and *In Vivo* Models

by

Giovanna Lissette Pozuelos

Doctor of Philosophy, Graduate Program in Cell, Molecular, and Developmental Biology
University of California, Riverside, March 2022
Dr. Prue Talbot, Chairperson

Human exposure to contaminated thirdhand smoke (THS) environments and electronic cigarette (EC) e-liquid is a major concern due to the prevalence of tobacco product usage. The purpose of this dissertation was to assess the molecular effects of nicotine, THS, and ECs using *in vitro* and *in vivo* models. First, we proposed a simple and rapid method to assess THS contamination and showed that extraction of THS is dependent on fabric type, heat, chemicals, time, and humidity. These factors need to be taken into consideration when implementing remediation methods. Dermal exposure to environmental THS and EC contamination was studied using 3D EpiDerm^{TM} tissue and cultured keratinocytes. Nicotine concentrations found in THS contaminated environments and e-liquids were sufficient to alter the proteomic profile of EpiDerm^{TM} tissue.

Nicotine altered proteins involved in promoting an anti-inflammatory response, oxidative phosphorylation, and an anti-apoptotic response. Mitochondrial fragmentation and peroxisome dysfunction were also observed in keratinocytes upon nicotine exposure. Next, we analyzed the transcriptomic alterations in the nasal epithelium of non-smokers exposed to THS. Changes in the transcriptome of non-smokers acutely exposed to THS identified upregulation of pathways associated with the respiratory electron transport chain, DNA repair, and oxidative stress. These results are in agreement with those reported previously using in vitro models. Transcriptomic analysis of the nasal epithelium of former smokers who switched to ECs showed enrichment in genes associated with increased immune response, keratinization, and NADPH oxidase and a decrease in ciliogenesis. Switching to ECs may result in continual airway epithelial damage due to inflammation and oxidative stress, which can lead to diseases. In conclusion, this dissertation provides data that will be useful in developing remediation policies for THS contaminated environments. We further showed that: (1) dermal exposure to nicotine caused an anti-inflammatory response, which may lead to skin infections and impaired wound healing, (2) acute inhalation of THS caused cell stress that led to the activation of survival pathways, and (3) EC usage may impair the recovery of airway epithelium in former tobacco cigarette smokers by promoting oxidative stress and inflammatory response.

Dedication

This dissertation is dedicated to my wonderful parents, Maria and Ovidio Pozuelos.

Table of Contents

Chapter 1: Introduction ……1-44

References.....45-62

Chapter 2: Adhesion and Removal of Thirdhand Smoke from Indoor Fabrics: A Method for Rapid Assessment and Identification of Chemical Repositories

Abstract.....65-65

Introduction.....66-69

Materials and Methods.....70-74

Results.....75-83

Discussion.....84-90

References.....91-95

Chapter 3: Nicotine Affects Multiple Biological Processes in EpiDerm organotypic Tissues and Keratinocyte Monolayers

Abstract.....97-98

Introduction.....99-101

Materials and Methods.....102-107

Results.....108-124

Discussion.....125-131

References.....132-139

Chapter 4: Acute Exposure to Thirdhand Smoke Leads to Rapid Changes in the Human Nasal Epithelial Transcriptome

Abstract.....141-142

Introduction.....143-145

Materials and Methods.....146-150

Results..... 151-157

Discussion.....158-162

References.....163-167

Chapter 5: Transcriptomic evidence that switching from tobacco to electronic cigarettes does not reverse damage to the respiratory epithelium

Abstract.....169-170

Introduction.....171-173

Materials and Methods.....174-177

Results.....178-193

Discussion..... 194-200

References.....201-208

Chapter 6: Conclusion……...209-211

Appendix A: Supplemental Information for Chapter 2…….212-216

Appendix B: Supplemental Information for Chapter 3...……..217

Appendix C: Supplemental Information for Chapter 4 ……218-240

Appendix D: Supplemental Information for Chapter 5 ……240-304

Chapter 1: Introduction

Tobacco Smoke: A Public Health Hazard

Cigarette smoking is the leading cause of preventable death affecting both smokers and non-smokers (Walser *et al.,* 2008; Surgeon General 2014**)**. Though smoking has declined considerably since 1965, smoking prevalence has not decreased in recent years and smoking related mortality is expected to remain high in future decades (Surgeon General, 2014). Worldwide the number of smokers has increased to 1.1 billion adults due to population growth (WHO 2019), making it imperative to continue studying the health effects of cigarette smoke as an environmental toxicant that can affect both smokers and those passively exposed.

In the United States, 480,000 adults die each year from tobacco-related diseases and secondhand smoke exposure, while millions live and suffer with smoking related diseases (Surgeon General, 2014). Smoking causes various adverse health effects, such as respiratory diseases, cardiovascular diseases, and cancer (Surgeon General, 2014). Chronic obstructive pulmonary disease (COPD), which is a group of respiratory related problems such as emphysema and chronic bronchitis, is among the most common conditions attributed to smoking (Wheaton *et al*., 2019; Barnes *et al.,* 2003). The total smoking-attributable COPD prevalence is estimated to be between 20.4 - 21.6 million persons (Surgeon General, 2014). COPD affects both smokers and individuals exposed to secondhand smoke (Wheaton *et al*., 2019). Smoking is also the

leading cause of lung cancer (Surgeon General, 2014). Between 70% to 90% of all lung cancer deaths are attributed to smoking (Walser *et al.,* 2008). Smoking can also cause cancer in many other organs such as bladder, cervix, stomach, and pancreas (Fig 1) (CDC). It can also promote cancer relapse in previous cancer survivors. Smoking during pregnancy can cause complications for the fetus, which can lead to stillbirth and developmental defects, such as orofacial clefts (Surgeon General, 2014). Pregnant women also experience a high frequency of ectopic pregnancies if they are smokers. Other conditions attributed to smoking include increased risk of cataracts, type 2 diabetes, inflammation, as well as a decrease in immune function (Fig. 1) (Surgeon General, 2014). Overall, smoking can affect the homeostasis of every organ and negatively affect a person's overall health.

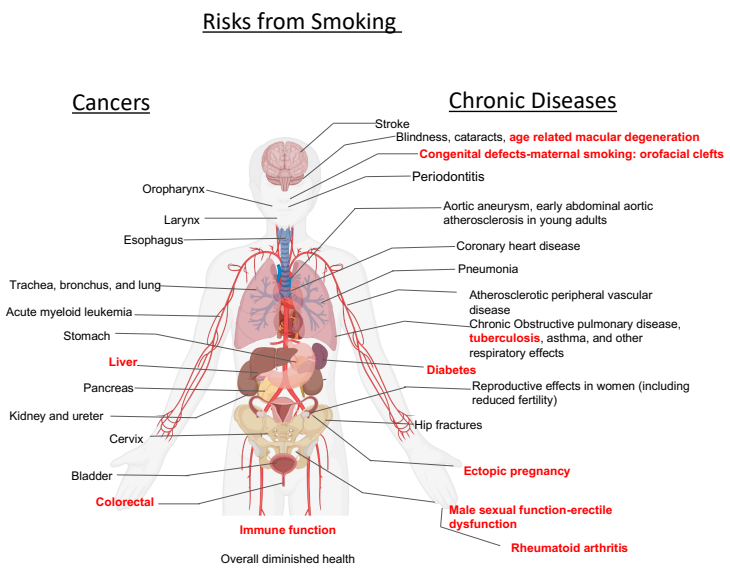

Figure 1. Chronic Diseases and Cancers Associated with Cigarette Smoking. Smoking can affect every organ of the body and overall diminishes human health.

Components of Cigarettes

Cigarette smoke contains more than 7,000 chemicals, including 69 carcinogens (Surgeon General, 2010). The delivery of these chemicals can be manipulated by altering the cigarette components, such as the type of tobacco leaf, the tobacco curing process, or the cigarette filters (Surgeon General, 2010). To further understand the health effects of tobacco smoke, it is important to characterize the components that make the cigarette and how these chemicals contribute to the toxicity of cigarette smoke.

Tobacco Composition in Cigarettes

Many types of tobacco are produced around the world, and each can vary in cultivation, harvesting conditions, and curing (leaf drying). Tobacco leaves vary in size, color, and the size of their veins, which contribute to their taste and aroma. Cigarettes are composed of blends of various tobacco types (Geiss *et al.,* 2007). The three main ways of curing tobacco are a flue, air, and sun curing.

In the United States, tobacco blends in cigarettes are mainly composed of flue-cured Virginia /Bright tobacco, Burley tobacco and Oriental tobacco (Hoffmann *et al.,* 1997; Thielen *et al.,* 2008; Hoffmann *et al.,* 1997; IARC,2004). Flue-curing Virginia tobacco, produced in the US, consists of using heated air to dry leaves over a period of 6-7 days to speed the curing process (Zou *et al.,* 2017). Flue-curing tobacco rapidly destroys chlorophyll, giving leaves a yellow appearance. During this procedure, many biological processes occur such as conversion of starch into sugar, enzymatic oxidation of amino acids, and

carbohydrate degradation, which increase the aroma and decrease the bitter taste (Geiss *et al.,* 2007; Banozic *et al,.* 2020). Flue-cured tobacco is also characterized by low nitrogen, high sugar content, acidic pH, a light aroma, and medium nicotine content (Stratton *et al.,* 2001). Burley tobacco is produced in the US and undergoes air-curing, which maintains a constant temperature (70 – 90^{o} F) and does not speed the curing process (Stratton *et al.,* 2001; Geneva: WHO, 2017). Burley tobacco leaves have a very low sugar content, produce alkaline smoke, and have a fuller aroma and a high nicotine content (Stratton *et al.,* 2001). Oriental tobacco leaves are sun-cured and a Mediterranean climate is required to cultivate this product, which originates mainly from Turkey, Greece, Yugoslavia, Bulgaria, and Russia. These sun-cured tobacco leaves have a mild aromatic smoke with low nicotine content (Stratton *et al.,* 2001; Hoffmann *et al.,* 1997). Tobacco in cigarettes is a blend of the different types mentioned above. Tobacco blends are created to achieve a specific taste, burning characteristic, and a desired nicotine concentration

In addition to tobacco leaves, cigarettes also contain reconstituted tobacco, which is composed of stems, leaves, and tobacco scrap made into a tobacco “paper”. Tobacco paper is added to the cigarette blend for economic reasons (Stratton *et al.,* 2001).

Cigarette Additives

Hundreds of additives can be introduced into cigarettes during manufacturing, and some of these can have toxic properties (Geiss *et al.,* 2007;

Stratton *et al.*, 2001). Over 599 additives have been used by cigarette manufacturers in the US. The additive list includes chemicals such as sugars, humectants, and aromatic substances. Other additives include natural extracts and essential oils, such as anise, cassia, chocolate, cinnamon, and vanilla which are categorized as safe for ingestion (Surgeon General, 2010).

After curing, additives are introduced into the tobacco blend. Each additive serves a purpose. Sugars are used to manipulate the pH of the smoke by neutralizing the alkalinity of the nitrogenous compounds (Geiss *et al.,* 2007). Ammonia is also added during the manufacturing process to influence the pH of the smoke (Stratton *et al.,* 2001; Hoffmann *et al.,* 1997). pH plays an important role in the concentration of free nicotine in tobacco smoke (Stratton *et al.,* 2001). At a high pH, the concentration of free nicotine increases in the smoke. Free nicotine has a more profound effect on the sensory nerves in the mouth and throat, which contributes to the strength of the cigarette. Free nicotine can be more readily absorbed across mucous membranes and rapidly absorbed in the lungs at higher pHs. (Stratton *et al.,*2001). Most cigarettes use glycerol as a humectant, which upon heating can lead to the formation of acrolein, a cytotoxic agent (Hoffmann *et al.,* 1997). Other additives such as cocoa are used to add flavor and aroma (Geiss *et al.,* 2007). Menthol and other sweeteners are added to improve taste and facilitate inhalation of smoke (Geiss *et al.,* 2007).

Non-tobacco Cigarette Components

The non-tobacco cigarette components include paper, filters, tipping paper and wrapping paper (Fig 2). Tobacco blend is wrapped in cigarette paper, which can be composed of cellulose, calcium carbonate, monopotassium phosphate, potassium citrate, sodium citrate and cellulose pulp from textile fibers (Geiss *et al.* 2007, Stratton *et al.* 2001). The porosity of the wrapping paper can determine how the tobacco burns *(Geiss et al. 2007)*. Pores allow for increased ventilation, which reduces the yield of CO and tar, volatile nitrosamines, tobacco specific nitrosamines (TSNAs), and benzo[a]pyrene (BaP) through dilution (Stratton *et al.,* 2001). In the United States cigarette filters are composed of cellulose acetate (Goel *at al.,* 2018; Ogundare *et al.,* 2017). Filters can trap nicotine and tar, as well as provide ventilation when smoking (Geiss *et al*., 2007). Filters are wrapped in tipping paper, which serves to connect the filter to the rest of the cigarette. The tipping paper secures the filter to the tobacco rod and contains holes that control the amount of air going through the filter. The air that passes through the tipping paper dilutes the smoke and lowers nicotine, tar, and carbon monoxide (Geiss et al., 2007).

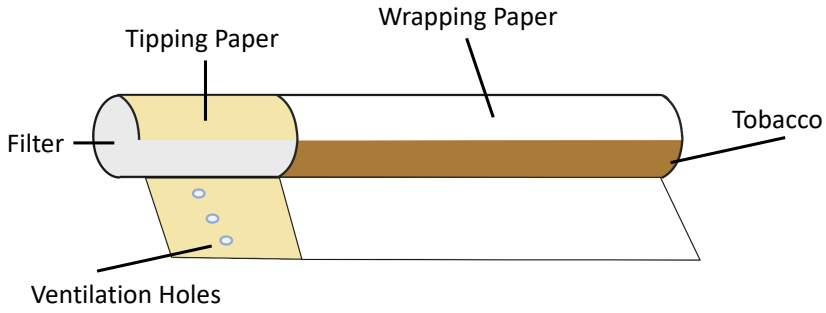

Fig 2. Schematic illustration of a tobacco cigarette. Image depicts the tobacco and non-tobacco components.

Mainstream Smoke Chemical Components

Nicotine

Nicotine is the major tobacco component responsible for addiction (Surgeon General, 2010) Tobacco leaves contain many alkaloids, and nicotine is the most abundant one. Nicotine content in a cigarette varies based on the blend that is used, as discussed above (Surgeon General, 2010). Nicotine concentration in cigarettes can range from 6 to 18 milligrams per gram (mg/g). Nicotine absorption in the body is highly dependent on pH. At a basic pH, nicotine is in a unionized state, which makes it easier for it to pass through lipoprotein membranes (Stratton *et al.,* 2001). Nicotine can be more readily absorbed into the lungs due to the large surface area of the alveoli and small airways. Nicotine

cannot be easily absorbed in the stomach due to the stomach's acidity (Stratton *et al.,* 2001).

Nicotine can rapidly transfer into the blood vessels and circulate from the lung to the brain. In the brain, nicotine binds to nicotinic acetylcholine receptors, which are ion channels. The binding of nicotine to the receptors allows the entry of sodium or calcium into the cell (Dajas-Bailador *et al.,* 2004). Stimulation of the nicotinic acetylcholine receptors causes release of neurotransmitters, such as dopamine, into the brain (Dajas-Bailador *et al.,* 2004, Wonnacott S. *et al.,* 1997). Dopamine produces a pleasurable experience that plays a critical role in addiction as a self-induced reward (Nestler *et al.,* 2005). With increased use of nicotine, some nicotinic acetylcholine receptors become desensitized *(Wang et al. 2005*. Then, in response to desensitization, there is an increase of acetylcholine receptors (Govind *et al.,* 2009, Benowitz *et al.,* 2010).

Tobacco alkaloids

The alkaloids in tobacco include anatabine, anabasine, nicotine, nicotine N-oxide, myosmine, B-nicotyrine, cotinine, and 2,3 bipyridyl. The concentration of anatabine, anabasine and nornicotine is approximately 5% of the nicotine concentration (Surgeon General, 2010; Jacob *et al.,* 1999). Minor tobacco alkaloids are pharmacologically active in humans. Anabasine and nornicotine had effects on smooth muscle fibers, blood pressure, and enzyme inhibition (General Surgeon, 2010).

Nitrate

Nitrate content is high in air-cured tobacco compared to sun-cured or flue cure tobaccos. (Stratton *et. al.,* 2001). Nitrate content can influence the carcinogenic potential of the smoke; higher nitrate concentrations inhibit the synthesis of BaP, a carcinogen. However, the higher the nitrate concentration the higher the levels of TSNAs, also known carcinogens (Stratton *et al.,* 2001).

N-Nitrosamines

N-Nitrosamines are chemical compounds containing a nitroso group attached to an amine nitrogen (General Surgeon, 2010). Tobacco smoke contains volatile nitrosamines (N-nitrosodimethylamine, N-nitrosoethylmethylamine, N-nitrosodiethylamine, N-nitro-sopyrrolidine, and N-nitrosomorpholine) and non- volatile nitrosamines (4-(N-nitroso-N-methyl- amino) butyric acid, N-nitrosopipecolic acid, N-nitroso- sarcosine, 3-(N-nitroso-N-methylamino) propionic acid, N-nitrosoproline, and N-nitrosodiethanolamine) (General Surgeon 2010). Non-volatiles also include tobacco-specific nitrosamines (TSNAs) (N'-nitrosonornicotine (NNN), 4-(methylnitrosamino)- 1-(3-pyridyl)-1-butanone (NNK), N'-nitrosoanatabine (NATB), and N'-nitrosoanabasine (NAB)), which are carcinogenic compounds that form from nicotine and other tobacco alkaloids (Schick *et al.,* 2007, General Surgeon, 2010). These compounds are found in mainstream and secondhand smoke (Schick *et al.,* 2007). Cigarette smokers are exposed to higher levels of TSNAs than any other nitrosamines (General Surgeon, 2010). Nicotine and nornicotine can react with

sodium nitrate to from NNN and NNK. TSNAs are not in freshly cut tobacco, but form during curing and storage (General Surgeon, 2010). Flue curing tobacco alters TSNAs (Morin *et al.,* 2004). Direct fire curing causes nitrogen oxides to react with tobacco alkaloids to form TSNAs (Fisher *et al.,* 1990; General Surgeon 2010; Nestor *et al.* 2003; Roton *et al.,* 2005). TSNA content can be influenced by many factors including the quantity of stems used in the tobacco mixture, the use of nitrogen fertilizer in growing the tobacco, storage times, and storage temperatures (Chamberlain *et al.*, 1986; Andersen *et al.*, 1982; General Surgeon 2010). The type of tobacco used can also influence the amount of TSNAs. Oriental tobaccos, for example, have the lowest nitrates and TSNAs (General surgeon 2010). Burley tobacco has the highest concentration in TSNAs (Fischer *et al.,* 1989). Blended tobacco has more TSNAs than bright tobacco (Fischer *et al.,* 1990; General surgeon, 2010). Since growing, curing, and blend of tobacco affects nitrosamine levels in tobacco, controlling manufacturing methods can lead to less TSNAs (General Surgeon, 2010).

Polycyclic Aromatic Hydrocarbons

There are about 539 polycyclic aromatic hydrocarbons **(**PAHs) in tobacco smoke (Rodgmen *et al.*, 2006*,* General Surgeon 2010*).* The U.S. Environment Protection Agency (EPA) has identified 16 priority environment PAHs on the basis of evidence that they cause cancer. These PAHs include acenaphthylene, acenaphthene, anthracene, benz[a] anthracene, benzo[a]pyrene (B[a]P), benzo[b]fluoranthene (B[b]F), benzo[k]fluoranthene (B[k]F), benzo[g,h,i]

perylene, chrysene, dibenz[a,h]anthracene, fluoranthene, fluorene, indeno[1,2,3-cd]pyrene, naphthalene, phenanthrene, and pyrene (USAEPA 1980, 1986) . The composition of PAHs differs in mainstream and sidestream smoke (Grimmer *et al*., 1987; General Surgeon 2010). Differences in tobacco used and nitrate content can affect the levels of PAHs.

Volatile compounds

There are 400 to 500 volatile gases in cigarette smoke (Hoffmann and Hoffmann 1997). These include oxides of nitrogen, carbon, and sulfur containing compounds (General Surgeon, 2010). CO and CO2 are generated by the combustion of tobacco and are the most abundant volatile gases in mainstream cigarette smoke (General Surgeon, 2010). Smoke also contains volatile organic compounds (VOCs), such as benzene, toluene, xylenes, ethylbenzene, and styrene, that form from the incomplete combustion of tobacco (Fowles *et al.,* 2003; General Surgeon, 2010; Pazo *et al.,* 2016). The level of volatile chemicals determines the toxicity of the tobacco smoke.

Heavy Metals

Metals and metalloids are also part of tobacco smoke. Total concentrations of metals range from 0.15 to 0.58 mg/cigarette (Cantrell,1990). These metals can be deposited on tobacco leaves from the air, fungicides, and pesticides containing toxic metals. (Frank *et al.,* 1977, General Surgeon 2010). Some metals in tobacco, such as lead and cadmium, are absorbed from the soil (Schwartz and Hecking,1991, Bache *at al.,* 1985, General Surgeon 2010). Lead

in cigarette smoke ranges from 18-83 ng/cigarette. Cigarettes also contain cobalt, arsenic, chromium, antimony, thallium, and mercury. Variations of metal content in cigarettes depends on the growing conditions of the tobacco and the cigarette manufacturing process (General Surgeon, 2010).

Aromatic and Heterocyclic Amines

Aromatic amines and heterocyclic amines are found in mainstream smoke. Some of the common amines found in tobacco smoke include aniline, 2-aminonaphthalene, 2-toluidine, and 4-aminobiphenyl. The source of nitrogen can influence the levels of aromatic amines in tobacco smoke. Cigarettes composed of dark tobacco have higher levels of aromatic amines than cigarettes composed of light tobacco (Luceri *et al.,* 1993). Bright tobacco, which has a low level of nitrogen, has a lower concentration of aromatic amines than blended tobacco (Stabbert *et al.,* 2003).

Heterocyclic amines (HCAs) are found in tobacco smoke (Manabe and Wada, 1990). Examples of HCAs in tobacco smoke include 2-amino- 9H-pyrido[2,3-b]indole; 2-amino-3-methyl-9H-pyrido[2, 3-b]indole; 3-amino-1,4-dimethyl-5H-pyrido[4,3-b]indole (Trp-P-1); 3-amino-1-methyl-5H-pyrido[4,3-b]indole (Trp- P-2); 2-amino-3-methylimidazo[4,5-f]quinoline; 2-amino- 6-methyldipyrido[1,2-a:3',2'-d]imidazole (Glu-P-1); 2-aminodipyrido[1,2-a:3',2'-d]imidazole; and 2-amino- 1-methyl-6-phenylimidazo[4,5-b]pyridine (PhIP) (Kataoka et al. 1998). The concentrations of HCAs in smoke are 0.3 to 260 .0 ng/cigarette (Hoffmann *et al.,* 2001).

Pesticides

Tobacco is contaminated with pesticides (Geiss *et al*., 2007). Since tobacco plants are sensitive to a variety of insects, they require up to 16 applications in a 3-month period (Geiss *et al.,* 2007). These chemicals are absorbed by the plant and their residues remain in the final cigarette product (Geiss *et al.,* 2007).

Health Effects of Mainstream Health

There are many health effects associated with cigarette use, as mentioned above (Figure 1). Respiratory illness (e. g. COPD and emphysema) and cancer are among the most adverse health effects caused by smoking. Other common diseases related to cigarette smoke include cardiovascular diseases.

Tobacco smoke related cancers include lung, bladder, oral, and esophageal cancer. Up to 90% of all respiratory cancers have been attributed to active smoking (Saha *et la.,* 2017). Notably inactivation of tumor suppressor genes, such as P53 and an increase of pro-oncogenes such as KRAS play a critical role in cancer formation (Saha *et la.,* 2017; Husgafvel-Pursiainen *et al.,*1996; Weston *et al.,*1999). Polymorphism of genes related to tumor suppression, oncogenes, and modulating DNA adducts play a role in the susceptibility of a cigarette smoker to the development of cancer (Saha *et la*., 2017; Weston *et al.,* 1999; Soni *et al.,* 1998; Hung *et al.,* 1997).

Chronic respiratory diseases related to cigarette smoking include COPD, chronic bronchitis, and pulmonary emphysema (Saha *et la*., 2017). Smokers are prone to upper respiratory infections due to a dysfunctional immune response,

impaired mucociliary clearance and persistent oxidative stress in the airways (Feldman *et al.,* 2013). Cigarette smoking induces an inflammatory response; it increases the release of cytokines leading to chronic recruitment of neutrophils to the airways (Feldman *et al.,* 2013; Elisia *et al.,* 2020). Though macrophages and neutrophils are recruited to the airways, cigarette smoke decreases the phagocytic activity of alveolar macrophages which impairs the clearance of dead cells. In turn, this exacerbates the inflammatory response, increases activation of neutrophils and NETosis (Feldman *et al.,* 2013). Chronic inflammation accompanied by impaired macrophage phagocytosis and mucociliary clearance causes tissue damage in the airways. These physiological abnormalities lead to the development of respiratory diseases and contribute to the onset of disease exacerbations (Feldman *et al.,* 2013).

Cigarette smoking causes an array of cardiovascular diseases including atherosclerosis (Saha *et la.,* 2017). The progression of atherosclerosis is due to damaged endothelial and smooth muscle cells. Smoking derived aromatic compounds decrease synthesis of nitric oxide, which is necessary for endothelium-dependent vascular relaxation (Powell *et al.,* 1998). Damage to the endothelium surface increases expression of leucocyte adhesion molecules that allow the recruitment of macrophages. Aggregated macrophages further release cytokines and growth factors, which recruit smooth muscle cells and lead to the development of arterial plaques (Powell *et al.,* 1998). Damaged Endothelium

damaged by cigarette smoke eventually leads to coronary artery disease (CAD) and other cardiovascular diseases (Saha *et al.,* 2007).

Secondhand smoke.

Secondhand smoke is a combination of sidestream smoke emitted from the burning cigarette and mainstream smoke exhaled by smokers. Secondhand smoke is composed of the chemicals in mainstream smoke and the additional compounds generated from the smoldering cigarette (Surgeon General, 2010; Guerin *et al.,* 1987). The chemicals generated during puffing are different than those generated from the smoldering cigarette (Guerin *et al.,* 1987). One main difference between puffing and smoldering is temperature. When puffing a cigarette, the temperature can reach 900^{o}C, while the temperature of a smoldering cigarette reaches 400^{o}C (Guerin *et al.,* 1987). Additionally, sidestream smoke emitted from the smoldering cigarette contains much higher levels of aromatic amines than mainstream smoke (Luceri *et al*., 1993). Ammonia levels are significantly higher in sidestream smoke (Adams *et al*., 1987, Surgeon General, 2010). Semi-volatile compounds in sidestream smoke include phenol, cresol, xylenols, guaiacol, formic acid, and acetic acid (Sakuma *et al.,* 1983, Surgeon General, 2010). VOCs emitted during the burning of cigarettes, such as isoprene, pyrrole and styrene, can react with environmental ozone and produce secondary volatile aldehydes (e.g., formaldehyde, acetaldehyde and benzaldehyde) (Matt *et al.,* 2011). Metals emitted from a burning cigarette can be volatilized into the gas phase due to the high combustion temperature, yet as the

secondhand smoke rises, these metals condense becoming nanoparticles that can be inhaled (Baker,1981; Chang *et al*., 2003; Surgeon general, 2010).

Secondhand smoke (SHS) health effects

The health effects of secondhand smoke exposure are similar to those induced by mainstream smoke but include diseases that affect children. Adults exposed to secondhand smoke have a higher mortality rate, from vascular disease and chronic obstructive pulmonary disease, than non-smokers (Diver *et al*., 2018). Like mainstream smoke, SHS can cause heart attacks by altering the lining of blood vessels and activating platelets (Barnoya *et al.,* 2005; Burghuber *et al.,*1986). A 30-minute exposure to secondhand smoke increases the levels of dysfunctional endothelial progenitor cells in non-smokers, which can lead to impaired vascular repair (Heiss *et al.,* 2008). People with pre-existing health conditions should take special precautions to avoid brief passive exposures (Kim *et al.,* 2008). Non-smokers exposed to secondhand smoke also have 20-30% higher chance of developing lung cancer than those who are not exposed (Asomaning *et al.,* 2008). Each year more than 7,300 non-smoker die of lung cancer due to SHS in the United States alone (CDC). SHS can lead to sudden infant death syndrome (Elliot *et al.,* 2003). Children of smokers, develop respiratory infections, such bronchitis and pneumonia, more often than children of non-smokers (Blizzard *et al.,* 2003). Animal studies showed maternal exposure to cigarette smoke led to smaller respiratory airways in offspring (Elliot *et al.,* 2001). Prenatally exposed infants have reduced respiratory rates (Maritz *et al.,*

2011). SHS can also exacerbate asthma attacks in non-smokers (Gopal *et al.,* 2016).

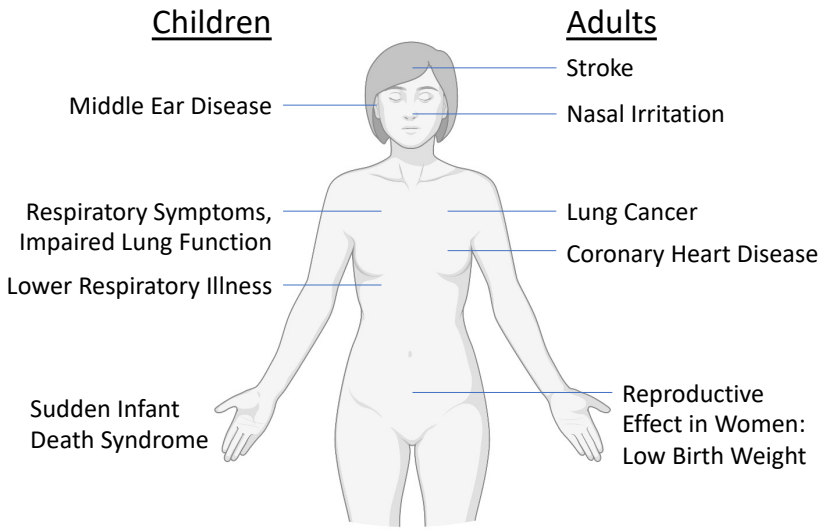

Fig 3. Secondhand Smoke Health Effects. Diseases in children and adults associated with secondhand smoke exposure.

Thirdhand smoke (THS)

Thirdhand smoke (THS) is the mixture of tobacco smoke residue derived from the burning cigarette and the smoker's exhale that settles on indoor surfaces (Matt *et al*., 2011a; Matt *et al.,* 2011b). These chemicals can remain, react, be re-emitted or resuspended months or years after smoking has ceased (Jacob *et al*., 2017; Bahl *et al.*, 2014). THS is a complex mixture of aged volatile and semi-volatile organic chemicals, PAHs, metals, TSNAs and secondary compounds generated through reactions with atmospheric pollutants, such as ozone and nitrous acid (HONO) (Destaillats *et al.,* 2006). Unlike secondhand smoke exposure, which only occurs through inhalation, THS exposure includes not only inhalation, but also ingestion and dermal absorption (Ferrante *et al*., 2013; Northrup *et al*., 2016; Becquemin *et al*., 2010). Due to the accumulation and persistence of THS in air, dust and on surfaces, non-smokers can be exposed unknowingly even when smoking has ceased (Matt *et la.,* 2008; Jacob *et al.,* 2017). Toddlers and children are particularly vulnerable to THS exposure due to their low body mass and their frequent crawling and mouthing of contaminated items. Children also have a higher respiratory rate relative to their body weight, which can exacerbate their THS exposure (Jung *et al.,* 2012).

THS Chemical Components

Nicotine and TSNAs

Nicotine, a major component of THS, can react with indoor pollutants, such as HONO, and lead to the formation of more dangerous carcinogenic

compounds, such as TSNAS (Jacob *et al.,* 2017; Schick *et al.,* 2007, Sleiman et al. 2010b). The reaction of nicotine and HONO leads to formation of three TSNAs: 1-(N-methyl-N-nitrosamino)-1-(3-pyridinyl)- 4-butanal (NNA), 4-(methylnitrosamino)- 1-(3-pyridinyl)-1-butanone (NNK), and N-nitrosonornicotine (NNN) (Sleiman et al. 2010b). NNA is not present in freshly emitted tobacco smoke but was the predominant TSNA in THS (Matt *et al.,* 2011a). NNK concentration can increase 50% to 200% every hour during the first 6 hours after smoking has stopped (Schick *et al.,* 2007). Nicotine also reacts with ozone and yields secondary oxidation products, such as cotinine, myosmine, nicotyrine, N-methyl formamide, formaldehyde, which can be reemitted into the gas phase (Destaillats *et al.,* 2006).

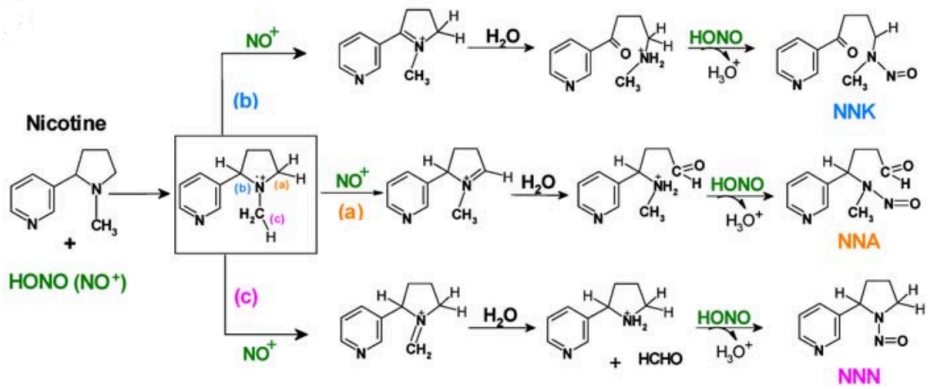

Figure 3. Formation of TSNAs. Mechanism proposed for the formation of TSNAs from nicotine. (Sleiman et al. 2010b)

Volatile Organic Compounds

More than 50 volatile organic compounds (VOCs), which include amines, aromatic hydrocarbon, furans, carbonyls and nitriles, were identified in the air after six cigarettes were smoked in a ventilated 18 m3 chamber (Sleiman *et al*. 2014). Some of these VOC's were rarely reported in SHS (e.g., acrolein, alkanes, acrylonitrile methacrolein, methyl vinyl ketone, 2-methyl furan, 1,3-pentadiene, 1-butene, propanenitrile, chloromethane, and dichloromethane) (Sleiman *et al*., 2014). The same study found that all volatile and semi-volatile amines, except for 3-ethenylpyridine, were removed from air, indicating a rapid sorption of these chemicals onto indoor surfaces (Sleiman *et al*., 2014). Other VOCs such as acetonitrile, butane and isoprene increased after 2h, which could be the result of resuspension of previously settled smoke (Sleiman *et al*., 2014). During the 18h period after smoking, carbonyls and nitriles were the most abundantly detected VOC's. Acrolein and acrylonitrile concentrations exceed the levels considered harmful by the state of California after the 18h period (Sleiman *et al*., 2014).

Measurements of VOCs in a smoker's home 8 hours after smoking had ceased detected 29 VOCs, but only 11 compounds were predominately in indoor environments (Sleiman *et al*., 2014). Since acetonitrile and 2-methyl furan were the most abundant, these could be used as THS tracers. Though isoprene is also found in ambient air, it was detected at a higher concentration in a smoker's home compared to the outdoor environment. Isoprene can also be postulated as

a THS tracer (Sleiman *et al*., 2014). Acrolein concentration in a smoker's home was 3 times higher than in outdoor environments (Sleiman *et al.,* 2014).

Polycyclic aromatic hydrocarbons

THS also contains polycyclic aromatic hydrocarbons (PAHs), semi volatile human carcinogens. PAHs has been detected in dust collected from smoker's homes and their concentrations linearly correlated with nicotine concentrations (Matt *et al.,* 2011; Hoh *et al*., 2012).

THS Accumulation in Indoor Environments

Smoker's Homes

Sampling of dust deposited on household surfaces of smokers' homes showed elevated levels of nicotine, 3-ethenylpyridine (3-EP) and ultrafine tobacco particles (Matt *et al.* 2017; Matt *et al.,* 2014; Jacob *et al.,* 2013 Whitehead *et al.,* 2009; Kim *et al.,* 2008; Singer *et al.*, 2004). Nicotine has a strong sorption tendency and can accumulate in indoor dust and on surfaces, such as tables, doors, walls, carpets, and fabrics. Concentrations of nicotine detected on smokers' household surfaces ranged from 126-16 µg/m2, and dust nicotine accumulation collected from vacuum cleaners ranged from 172-0.0046 µg/g (Table 1) (Matt *et al.,* 2017; Matt *et al.,* 2014 Jacob *et al.,* 2013; Whitehead *et al.,* 2009; Kim *et al.,* 2008). Nicotine concentrations can vary depending on the number of cigarettes smoked in each household, sample collection protocols, and the frequency in which the household living areas are cleaned. In public places where smoking is permitted, such as casinos, the amount of nicotine on

surfaces was as high as 8,520 µg/m2 and dust nicotine was 203 µg/g (Table 1) (Matt *et al*., 2018). PAHs were also found on household surfaces. PAHs in a smoker's home ranged from 74.8 - 68,900 ng/m2 of dust, compared to a non-smoker's home in which concentrations ranged from 47.8 - 18,700 ng/m2 (Hoh *et al.*, 2012; Matt *et al.*, 2011). TSNAs and minor tobacco alkaloid traces have also been detected in dust from smoker's homes (Table 2) (Whitehead *et al.,* 2015).

Table 1. Nicotine Concentrations in Casinos and Homes

Study	Surface	Surface Nicotine	Dust Nicotine
Matt *et al*. 2018	Casino	33 - 8520 $\mu g/m^2$	121 - 203 µg/g
Matt *et al.* 2017	Household (living room and bedroom)	16.2 - 59.0 $\mu g/m^2$	
Matt *et al.* 2004	Household (living room)	32.09 - 126.71 $\mu g/m^2$	
Jacob *et al.* 2013	Household		22.4-174 µg/g
Whitehead *et al.* 2009	Household (living room)		35 - 96 µg/g
Kim *et al.* 2008	Household (children's bedroom)		0.0046-3 µg/g

Table 2. TSNA and minor tobacco alkaloid concentrations in household dust*

TSNAs	**Median concentrations (ng/g)**
NNN	1.6
NNK	3.7
NNA	0.46
NAB	<.15
NAT	<4.2
Minor tobacco alkaloids	
Cotinine	430
Myosmine	440
N-formylnornicotine	480
Nicotelline	8
2,3'-Bipyridine	74

Homes of Previous Smokers

Nicotine can linger in previous smokers' homes exposing non-smokers (Matt *et al.,* 2011b). THS pollutants persist in houses previously owned by smokers even after 2 months of vacancy (Matt *et al*., 2011b). Traces of nicotine ranged from 3.1 - 28.6 μg/m^2 in homes previously owned by smokers. (Matt *et al*., 2011b). In comparison, surface nicotine in non-smoker home ranged from 0.4 to 3.7 μg/m^2 (Matt *et al*., 2011b).

Homes with Smoking Bans

Nicotine has been detected in homes with indoor smoking bans (Matt *et al.,* 2004). Nicotine concentrations found in households with strict indoor smoking bans ranged from 3.41 - 38.99 μg/m^2 (Matt *et al.,* 2004). Infants whose mothers strictly smoked outdoors to protect their children from exposure had higher levels of cotinine (1.52-3.78 ng/mL), a nicotine metabolite, in their urine compared to infants of non-smoking parents (0.20 -0.46 ng/mL) (Matt *et al.,* 2004). THS particulates in the skin and clothing of smokers can transfer to toddlers by mere contact with a smoker (Matt *et al.*, 2011a).

Cars Previously Owned by Smokers

Nicotine accumulates in cars previously owned by smokers (Matt *et al.* 2008). Dust nicotine levels in smokers' cars (19.51 μg/g) was significantly higher than non-smokers' cars (3.37 μg/g). Though some smokers implemented a car smoking ban, high levels of nicotine in dust were detected (11.61 μg/g). Cars

previously own by smokers can expose new owners to nicotine and other THS pollutants (Matt *et al.,* 2008).

Fabrics Retain THS

Common household fabrics exposed to THS retained nicotine, tobacco alkaloids, and TSNAs 19 months after the last cigarette was smoked (Bahl *et al*., 2014). High concentration of ammonia and 2-furaldehyde were found in cotton and linen fabrics exposed to THS (Ueta *et al.,* 2010). Nicotine and NNK were still detected in wool curtain extracts 50 days after being exposed to approximately 11,000 cigarettes (Whitlatch *et al*., 2018). Nicotine recovery from wool curtain was 60% of total input (Whitlatch *et al*., 2018). The concentration of NNK recovered was higher than the amount that entered the exposure chamber (Whitlatch *et al*., 2018). Though, fabrics were exposed to approximate 12 mg of NNK and a total 20 mg of NNK was recovered, a 170% recovery increased (Whitlatch *et al*. 2018). Increased recovery suggests NNK formation during the 50 days of smoke aging (Whitlatch *et al*., 2018).

Hospital Settings

Traces of THS were found in neonatal ICUs. Dust samples from the infants' incubators (0.3 0.2 μg/m^2) and hospital furniture had traces of nicotine (0.3-34.2 μg/m^2) (Northrup *et al.*, 2016). Infant's urine contained detectable levels of cotinine (0.17 -5.01 ng/mL), cotinine's major metabolites, trans-30 -hydroxycotinine (0.46 -31.58 ng/mL), and NNAL (0.47 -12.38 pg/mL). Since

hospitals have strict no smoking policies, contaminants were most likely introduced by visitors with THS contaminated clothing (Northrup et al. 2016).

Public Places

Contaminated public environments are a source of THS exposure to non-smokers. Concentrations of cotinine in the urine directly correlated with the frequency with which non-smokers used public transportation, internet cafes, and/or bars (Moon *et al.,* 2019). Sheu *et al.,* 2020 showed THS contaminants, equivalent to secondhand smoke derived from 1-10 cigarettes, were transported into a smoke-free movie theater by moviegoers' clothing (Sheu *et al.,* 2020). The widespread distribution of THS to indoor environments, such as movie theaters, hospitals, and hotels, makes non-smokers susceptible to THS exposure.

In-vitro THS studies

Genotoxicity of THS

THS chemicals have the potential to cause genotoxic effects and alter molecular processes in various cultured cells lines. *In vitro* animal and human cell lines have allowed researchers to examine the effects of THS on multiple cellular mechanisms (Bahl *et al.,* 2016; Hang *et al.* 2013).

Reports have shown that THS induces DNA damage. DNA damage was observed in a human liver cancer cell line (HepG2) exposed both acutely and chronically to THS extracts Hang *et al.* 2013. Acute exposure consisted of extracts derived from chromatography after a 20-minute exposure to cigarette smoke (Hang *et al.* 2013). Chronic exposure consisted of samples exposed for

258 hrs. to cigarette smoke over 196 days (Hang *et al.* 2013). The chromatography paper remained in the smoking chamber for 17 hrs. after smoking ceased (Hang *et al.* 2013). HepG2 treated with acute THS extracts showed an increase in DNA strand breaks compared to controls using the comet assay (Hang *et al.* 2013). Cells chronically exposed to THS showed significantly higher DNA damage compared to acutely exposure cells, most likely due to the higher concentration of THS toxicants (Hang *et al.* 2013). DNA damage from THS exposure was also observed in mouse neural stem cells (mNSC) and adult human dermal fibroblasts (hDFs) (Bahl et al. 2016). THS extracts generated from a car seat cover and carpet exposed to 20 cigarettes/day for 30 days were used to treat mNSC and hDFs (Bahl et al. 2016). Exposures to 30% and 100% of THS extract induced DNA breaks in both mNSC and hDFs using the comment assay (Bahl *et al.,* 2016).

DNA damage caused by THS could be attributed to oxidative stress. DNA base damage caused by chronic THS exposure was analyzed in two genes, hypoxanthine phosphoribosyltransferase (HPRT) and DNA polymerase beta (POLB), of THS treated human lung epithelial cells (BEAS-2B) (Hang *et al.* 2013). Using LA-QPCR, cellular DNA was treated with formamidopyrimidine DNA glycosylases (Fpg) and endonuclease VIII (Nei) to excise oxidized DNA bases. The presence of oxidized DNA bases generated single stranded DNA and prevented PCR amplification of long regions. A decrease in PCR product signifies higher amounts of oxidative damage (Hang *et al.* 2013). THS exposed

BEAS-2B cells showed a decrease in PCR production as compared to controls reflecting higher oxidative DNA damage (Hang *et al.,* 2013).

THS exposure in lung cells caused activation of DNA repair mechanisms and impaired transcription (Sarker *et al.,* 2020). THS exposure produced an increase in DNA synthesis in BEAS-2B which was attributed to the activation of the nucleotide exciton repair pathway (Sarker *et al.,* 2020). Additionally, genes involved in the DNA repair machinery, such as Rad3-related (ATR) kinase, were also activated upon THS treatment (Sarker *et al.,* 2020). Following THS treatment, both BEAS-2B cells and hPFs showed an increase in RPA 32 phosphorylation, which occurs in response to DNA replication stress and DNA damage. Increased DNA double stranded breaks were also observed in treated BEAS-2B cells. Further analysis showed THS exposure reduced ongoing RNA synthesis and caused accumulation of the elongating form of RNA Pol II in BEAS-2B, suggesting an increase in transcription blocking lesions most likely caused by bulky DNA damage (Sarker *et al.,* 2020). THS increased phosphorylation of Breast Cancer gene 1 (BRCA1), a human tumor suppressor gene, in treated BEAS-2B cells (Sarker *et al.,* 2020). Phosphorylation of BRCA1 occurs in response to DNA damage and plays a role in maintaining genomic integrity, including damage-induced cell cycle checkpoint activation and double stranded repair Sarker *et al.* 2020, Chen *et al.,* 2018).

THS inhibits cell proliferation

THS affects cell proliferation in various cells. In a study by Sarker et al. 2020, BEAS-2B cells exposed to 5% THS extract showed decreased cell proliferation. BEAS-2B cells were treated with THS extracts from exposed terry cloth to examine the impact on cell cycle progression using fluorescence-activated cell sorting (FACS). BEAS-2B cells exposed to 2.5% THS extract for 24 hrs showed a decline in G1-phase (from 60% to 47%) and an increase in S-phase cells (17% to 31%), suggesting exposed cells were not exiting the S phase (Sarker *et al.,* 2020). Impaired S-phase progression most likely leads to impaired cellular proliferation (Sarker *et al.,* 2020). Similarly, mNSC, showed decreased cell proliferation when exposed to 100% THS extract from a car seat cover and carpet. Acrolein has also been identified as a THS volatile chemical that inhibits cell proliferation (Bahl *et al.,* 2016b).

Cell toxicity

mNSC undergo morphological changes when exposed to THS for 24 hrs. mNSC exhibit blebbing, fragmentation, cytoskeletal disruption and vacuolization when treated with THS aqueous extract (Bahl *et al.,* 2016).

Oxidative stress

THS can cause stressed induced mitochondrial-hyperfusion (SIMH) in addition to increases in mitochondrial membrane potential (MMP), ATP, and reactive oxygen species (ROS) (Bahl *et al.,* 2016). SIMH is characterized by a morphological change from punctate to tubular. Mitochondria are dynamic

organelles that undergo fusion and fission for growth and to maintain proper cellular function (Collins *et al.,* 2012). Undergoing fusion allows mitochondria to exchange molecules including mitochondrial DNA, as a survival mechanism in response to pollutants (Chen *et al.,* 2010). A precise balance between these two events is essential to maintain quality control of healthy mitochondria under stress conditions (Otera *et al*., 2013; Youle *et al.,* 2012). Mitochondria are involved in a variety of biological process such as redox signaling, ATP production, apoptosis, and cell cycle regulation (Otera *et al*., 2013). mNSC undergo SIMH after being exposed for 24 hours to 100% THS extract (Bahl *et al.,* 2016). THS exposed cells also showed an increased MMP at both 24 hrs. and 15 days after exposures to 10% and 30% THS extracts. After 30 days of exposure, MMP decreased indicating THS can compromise MMP after a long exposure (Bahl *et al.,* 2016). ROS and ATP increased in cells exposed for 24 hours to 30% and 100% THS extracts (Bahl *et al.,* 2016).

Metabolomics changes

THS exposed male germ cell lines exhibit up regulation of glutathione metabolism, nucleic acid metabolism, and ammonia metabolism (Xu *et al.,* 2015). Two male germ cell lines, spermatogonia (GC-2) and Sertoli-derived cells (TM-4), were exposed to THS extract derived from chromatography paper exposed to cigarette smoke for 24 hrs. Metabolomics analysis of GC-2 THS treated cells showed an increase in glutathione (GSH) and glycine, while glutamate decreased (Xu *et al.,* 2015). Results suggest that THS caused an increase in biogenesis of

GSH, derived from the reaction of γ-glutamylcysteine and glycine. Glutathione is an important antioxidant used for the mitigation of ROS in the cell (Xu *et al.,* 2015). Though there was an increase in glutathione, there was no detectable increase in cellular ROS (Xu *et al.,* 2015), possibly because upregulation of glutathione was sufficient to inhibit an increase of ROS (Xu *et al.,* 2015). A decrease in glutamate also suggested THS inhibits catabolism glutathione (Xu *et al.,* 2015). Metabolic changes in Sertoli-derived cells (TM-4) exposed to THS included a dysregulation in multiple nucleic acid metabolites and an increase in metabolites involving ammonia metabolism (Xu *et al.,* 2015).

In Vivo THS Studies

Lung effect

THS can cause lung damage in mice exposed to fabrics containing THS residues. Mice exposed for 6 months to fabrics impregnated with THS residue developed disrupted alveoli walls in the alveolar sacs (Martins-Green *et al.,* 2014). THS exposed mice developed thickening of the respiratory alveoli walls, had elevated levels of collagen and higher number of microphages in lung tissue (Martins-Green *et al.,* 2014). Lungs showed an increase of pro-inflammatory cytokines IP10, KC, MCP1, MCSF, MIG, MIP1b, MIP2, Eotaxin, LIX, VEGF and downregulation of anti-inflammatory cytokines (IL1a, IL9, IL10) (Martins-Green *et al*., 2014). Inhalation of THS particles cause a pro-inflammatory response in lung tissue.

Skin effect

THS caused wound healing impairments in exposed mice (Martins-green *et al.,* 2014). THS exposed mice showed an upregulation of keratin genes that lead to keratinization of the epithelium and wound susceptibility to reopening (Martins-green *et al.,* 2014). Genes involved in an inflammatory response and associated with wound healing were also down regulated. Fibrillar collagen, essential for proper healing, was decreased by THS exposure (Martins-Green *et al.,* 2014; Brauer *et al.,* 2019).

Behavioral

THS exposed mice were hyperactive (Martins-Green *et al.* 2014). Mice anxiety was measured in the standard “Elevated plus” T-maze anxiety test. Anxiety is measured by the amount of time the mouse spends in the enclosed arms section of the maze. Increased time in the enclosed arms versus the open arms represents anxious behavior. THS exposed mice had significantly higher frequency of entries into open arms, suggesting hyperactivity (Martins-Green *et al*., 2014). Behavior was also tested using an open field test where walking and stationary behavior was assessed as well as rearing behavior. THS exposed mice spent a longer time walking and rearing than controls *(*Martins-Green *et al., 2014)*. Exposed mice were constantly mobile compared to controls, which were more stationary. THS mice covered longer distances at a faster pace (Martins-Green *et al.,* 2014). THS mice were more hyperactive than controls, suggesting THS contributes to this behavioral response.

Hormonal Alteration

Hormonal release was stimulated by THS exposure in mice. Mice exposed for 2 months had elevated levels of adrenocorticotropic hormone (ACTH) (Adhami *et al.* 2017). Pituitary gland release of ACTH was stimulated by pro-opiomelanocortin (POMC) hormone (Adhami *et al.,* 2017). ACTH is known to stimulate the secretion of stress related hormones, cortisol, and epinephrine serum. Epinephrine levels were increased after 2 months of exposure, while cortisol levels were elevated after 4 months of exposure (Adhami *et al.,* 2017). At 6 months of exposure, mice increased secretion of corticotropin-releasing hormone (CRH) in serum, a hypothalamus secreted hormone, which also stimulates ACTH production (Adhami *et al.,* 2017).

Oxidative Stress

THS exposure also causes an oxidative stress response in various organs. H2O2 accumulation was detected in skeletal muscle cells of THS exposed mice, while activity of antioxidant enzymes, catalase, and glutathione peroxidase (GPx) was decreased (Adhami *et al., 2016)*. Superoxide dismutase (SOD) activity, which is important for the breakdown of H2O2 and O2, was elevated in treated mice (Adhami *et al.,* 2016). Livers of exposed mice also showed higher levels of H_2O_2, but no increase in catalase or GPX activity to properly process H_2O_2 (Flores *et al.,* 2016). In the liver, activity of catalase and GPX decreased after 4-6 months of THS exposure and activity in the brain decreased after 6 months of exposure (Adhami *et al*., 2017). ATP and lactate production increased in the liver of exposed mice.

An increase of lactate is indicative of a switch to glycolysis as an alternative pathway energy production and ROS in the liver (Adhami *et al*., 2017).

Genotoxicity in animal models

It is widely known that cigarette smoking induces genotoxicity, which plays a role in carcinogenesis in both tobacco smokers and secondhand smokers. Cancer has not been associated with THS exposure, but THS chemicals are known to be genotoxic. *In vivo* studies using animal models have provided evidence that indeed THS can cause genotoxicity. Mice developed DNA adducts and DNA damage after 6 months of being exposed to THS containing fabrics (Adhami *et al.,* 2017; Adhami *et al.,* 2016). THS can also lead to lipid peroxidation and protein nitrosylation (Adhami *et al.,* 2016).

Liver Damage

Mice exposed to THS exhibit lipid accumulation in the liver (Martins-green *et al.* 2014, Flores *et al.* 2017). THS exposed mice showed increased low-density lipoprotein (LDL bad cholesterol) and decreased high density lipoprotein (HDL, good cholesterol) in the liver (Martins-green *et al*., 2014). THS inhibited the Sirt1/AMPK/SBREP1c signaling pathways in the livers of exposed mice. SIRT1 and AMPK prevent abnormal lipid metabolism by inhibiting SBREP1c, a lipogenesis enzyme in the liver (Flores *et al.,* 2016). THS exposed mice also had low levels of SIRT3 and decreased activity of isocitrate dehydrogenase 2 (IDH2). SIRT 3 is involved in fatty acid metabolism and activates IDH2 (Flores *et al.,* 2017). IDH2 activity prevents nonalcoholic fatty liver disease. Over expression of IDH2

reduces mRNA genes that are associated with lipogenesis (Gong *et al*. 2019). Low levels of apolipoprotein B, which is involved in lipid transport out of the liver, were detected in THS-exposed mice (Flores *et al.,* 2017. Abnormal lipid transport can lead to hepatic steatosis (Flores *et al.,* 2017). These molecular changes lead to lipid elevation, which can cause non-alcoholic fatty liver disease (NAFLD) and lead to fibrosis, cirrhosis, and cancer in non-smoker individuals (Martins-Green *et al,.*2014; Flores *et al.,* 2017).

Diabetes

In vivo, THS contributes to the development of diabetes. Mice exposed for 6 months to fabrics impregnated with THS residue become hyperglycemic and hyperinsulinemic suggesting THS can cause insulin resistance (Adhami *et al.,* 2017). These mice had pre-diabetic fasting glucose levels and were unable to efficiency bring down glucose with insulin (Adhami *et al.,* 2017). THS exposed mice had decreased levels of insulin receptors, P13K and AKT which are important in insulin signaling and glucose uptake (Adhami *et al*. 2016). Levels of biomarkers related to endoplasmic reticulum stress, pPERK and BiP, were elevated in the pancreas of THS exposed mice (Adhami *et al.,* 2016). When mice were treated with antioxidants N-acetyl cysteine and alpha-tocopherol, molecular damage and insulin resistant significantly reversed. These results suggest that exposed mice developed insulin resistance as a consequence of cellular oxidative stress caused by THS (Adhami *et al.,* 2016)

Hematopoiesis Alterations

Mice exposed to THS had hematopoiesis alterations. THS can affect platelet biology by enhancing platelet secretion and aggregation, increasing the risk of thrombosis (Karim *et al.,* 2015). In mice exposed to THS, platelets exhibited enhanced glycoprotein IIb-IIIa activation. A tail bleeding assay to assess hemostasis, showed that THS exposed mice had a shorter bleeding time compared to controls (Karim *et al.,* 2015). Using FeCl3-induced carotid artery injury in an *In vivo* thrombosis model showed that occlusion of the vessel was significantly quicker (2.5 minutes) in THS exposed mice than in controls (28 minutes) (Karim *et al.,* 2015).

Mice exposed for two months to THS exposed fabric had significantly higher serum levels of proinflammatory cytokines IL-1α, IL-6, GM-CSF, and TNF-α than control mice (Adhami *et al.,* 2017). Exposed mice also had increased levels of anti-inflammatory cytokines IL-4 and IL-10 (Adhami *et al.,* 2017).

THS exposed neonatal and adult mice showed changes in hematopoiesis (Hang *et al.,* 2017). Neonatal mice exposed to THS contaminated cotton fabrics in their cages from birth to 3 weeks after birth had significantly lower body weights compared to controls. After no further exposure, these mice were able to regain enough weight to catch up to controls at 5 weeks. On the contrary, exposed adult mice did not show a difference in body weight (Hang *et al.,* 2017). Neonatal exposed mice had altered hematopoiesis and cellular components (Hang *et al.,* 2017). At 17 weeks neonatal exposed mice had decreased numbers of

eosinophils, whereas adult exposed mice had an increase of eosinophils. Both neonatal and adult mice had an increased number of B cells and myeloid cells and a decrease in platelet count (Hang *et al.,* 2017). These results suggest that different exposure times yield different alterations in hematopoiesis (Hang *et al.,* 2017).

Metabolomics Dysregulation in Liver

Metabolomics in the liver were affected in mice exposed to THS (Torres *et al*., 2021). Liver biopsies from mice exposed to THS were analyzed using a multiplatform untargeted metabolomics approach (Torres *et al*., 2021). Eighty-eight metabolites were altered by THS exposure. In aqueous extracts of liver, 49 metabolites were altered by THS exposure which included an increase in serotonin, NAD, amp, and glutathione (Torres *et al*., 2021). In lipidic extracts, 39 metabolites were altered by THS exposure, which included 21 different triglycerides and other lipids. In agreement with previous studies, there was a higher lipid accumulation as well as an increase of larger lipid droplets in THS-exposed mice. Notably serotonin, which is involved in liver disease, was upregulated in THS exposed mouse livers (Torres *et al*., 2021). High concentrations of lipids suggested possible fatty liver disease (Torres *et al*., 2021). Antioxidant treated mice had a decrease in total lipid concentration in the liver, as previously shown in Flores et al. 2016. Antioxidant treatment did not revert all metabolites to normal levels. Pathway enrichment analysis of in THS exposed mice included purine, glutathione, D-glutamine and D-glutamate, and oxidative

phosphorylation pathways, which agree with previous studies showing THS causes oxidative stress (Torres *et al*., 2021).

Electronic cigarettes

Electronic cigarettes (ECs) are non-combustive devices designed to aerosolize liquids containing nicotine, solvents, and flavor chemicals (Trtchounian *et al*., 2010, Hajek *et al*.,. 2014 Caponnetto *et al*., 2012,). Initially, they were introduced as both smoking cessation devices and a safer alternative than cigarette smoke (Alexander *et al*., 2015). During the past 10-12 years, ECs have become increasingly popular with high school students and young adults (Cao *et al*., 2020; Caponnetto *et al*., 2012, Hajek *et al*., 2014).

Since their introduction in 2006, at least four generations of ECs have been marketed (Williams *et al*., 2019). Components of ECs include a battery, heating coil, wick, cartridge, atomizer, and mouth piece (Caponnetto *et al*., 2012, Williams *et al*., 2013, Cao et al. 2020). Upon heating, e-liquid is aerosolized and inhaled by the user (Caponnetto *et al*., 2012, Cao *et al*., 2020). EC devices have evolved into a wide selection of devices with different heating capabilities and refillable liquid chambers (Williams *et al*., 2019). Consumers can introduce unique e-liquid chemical combinations and alter temperatures to as high as 350oC (Kosmider *et al*., 2014). Fourth generation products, including JUUL and Puff, are currently very popular with young adults (Zaleski *et al*., 2018).

Electronic cigarette chemicals

E-liquids (refill fluids or liquids included with purchased ECs) may contain nicotine, flavorings, additives, propylene glycol, and glycerol (Hajek *et al*., 2014, Omaiye *et al*., 2021, Omaiye *et al*., 2019). Nicotine in EC liquids is usually derived from tobacco plants, but synthetic nicotine has recently been introduced into some products, such as Puff, to circumvent FDA regulation (the FDA is authorized to regulate tobacco products; producers of some ECs have argued that synthetic nicotine is not from tobacco, hence their products are not subject to FDA regulation). Nicotine derived from tobacco plants is purified and distilled, but it contains impurities, such as nicotine-related alkaloids and tobacco-specific nitrosamines (TSNAs). Nicotine concentrations in ECs are highly variable and range from 0 to 60.2 mg/mL (Omaiye *et al*., 2019). Flavorings added to e-liquids are considered safe for ingestion, but their safety as inhaled substances have generally not been studied (Cao *et al.,* 2020). More than 20,000 flavor chemicals are available to EC manufactures in the Netherlands (Havermans *et al.,* 2019, Zhu *et al.* 2014). Flavorings include menthol, tobacco-menthol blends, and other flavor categories such as fruit, dessert/candy, alcohol/drink, snacks and meals flavorings (Zhu *et al.,* 2014; Hua *et al.* 2019; Ester *et al.* 2019). EC fluids can also include diacetyl, which can cause bronchiolitis obliterans, a serious often fatal lung disorder that is not reversible (Egilman *et al*., 2012). Other additives include powder cocaine, ecstasy, hallucinogens, heroin, and methamphetamines (Cao *et al*., 2020).

Propylene glycol and glycerin are solvents in e-liquids that upon aerosolization can be pulmonary irritants (Lechasseur *et al*., 2020). These solvents are considered safe for dermal contact and ingestion, but their inhalation toxicity is not well understood (Cao *et al*., 2020). E-liquids and EC aerosols have a higher number and concentration of detectable metals than unused e-liquids. These metals are derived from atomizer components, such as the filament, thick wire, brass claps, solder joints, and sheath (Williams *et al*., 2017 Williams *et al*., 2013, Hajek *et al*., 2014). Metals reported in EC fluids and aerosols include aluminum, chromium, iron, lead, manganese, nickel, and tin (Cao *et al*., 2020). Some of the metals in EC aerosols are known to produce adverse health effects including cancer (e.g., nickel); however, EC use has not yet been directly linked to cancer.

Carcinogenic chemicals are also present in e-fluids/aerosols, probably as contaminants introduced with the major ingredients, or as reaction products formed during heating. These include formaldehyde, acetaldehyde, acrolein and pulegone. (Cao *et al*., 2020). Several margin of error (MOE) risk assessment studies have shown that pulegone is present in JUUL products in high enough concentration to be likely to produce cancer with prolonged use (Omaiye *et al*., 2019: Jabba *et al*., 2020).

Electronic cigarette health effects

In vitro, human embryonic stem cells and neural stem cells (NSCs) were highly sensitive to some EC refill fluids (Bahl *et al.,* 2012; Behar *et al.,* 2014). EC

aerosol induces mitochondrial hyperfusion accompanied with increased membrane potential, ATP, and ROS in exposed NSCs (Zahedi *et al*., 2019). EC aerosols also induced inflammatory responses in human airway epithelial cells and double stranded DNA breaks in normal human epithelial cell lines (Lerner *et al.,* 2015; Yu *et al*., 2016). Menthol, a component often used in EC liquid, induced oxidative stress and increase inflammatory cytokines (IL8) in 3D EpiAirway tissue following air liquid interphase exposure of menthol. (Nair *et al*., 2021)

In vivo animal models exposed to EC have developed damage lung tissues, dysregulated innate immunity, and impaired anti-microbial defenses (Sussan *et al*., 2015; Chun *et al*., 2017; Lerner *et al*., 2015, Schweitzer *et al*., 2015). Multiple studies have shown mice exposed to EC aerosol exhibited increased inflammatory response (Lerner *et al.* 2015; Sussan *et al*., 2015; Garcia-Arcos *et al*., 2015; Hwang *et al.* 2016, Lim *et al*., 2014). Rats exposed to EC aerosol through nose inhalation had an increase in recruitment of inflammatory cells, neutrophil and alveolar macrophages, in the lung (Werley *et al*., 2016). Chronic inflammation caused by EC can lead to tissue damage and exacerbate pulmonary diseases, such as asthma (Lim *et al*., 2014). An asthmatic airway inflammation mouse model exposed to intratracheal e-liquid showed exacerbated airway inflammation Lim et al 2014. ECs increased recruitment of eosinophils in the lungs and production of cytokines (IL 4, IL 5, IL 13) (Lim *et al*., 2014). Oxidative stress has been associated with EC exposure (Lim *et al*., 2014, Lerner *et al*., 2015). An acute inhalation murine model, demonstrated the effects of EC smoke exposure on lungs, heart, and

bladder (Lee *et al*., 2008). Mice exposed to ECs containing nicotine and VG show significant development of lung adenocarcinoma and bladder urothelial hyperplasia (Cao *et al*., 2020)

Due to relatively recent introduction of ECs, little is known about their long-term health effects. Case reports have documented adverse health conditions attributed to EC usage that included neurological, respiratory, and gastrointestinal diseases (Hua *et al.,* 2019; 2020, Hua and Talbot 2016). In a human clinical trial, acute vaping of ECs with and without nicotine, increased levels of club cell protein-16 (CC16), which is a marker for acute lung injury, were detected in urine (Chaumont *et al.,* 2019). Self-reported diagnosis analysis associated inhalation of EC aerosols to exacerbated chronic obstructive pulmonary diseases (COPD) in EC users (Bircan *et al.,* 2021). Non-smokers acutely exposed to ECs showed an increase of serum inflammatory markers, C-reactive protein (CRP), soluble intercellular adhesion molecule (sICAM), and ROS (Chatterjee *et al*., 2019). Chemical elements (e.g., Al, Cu, Mg, Zn, Pb, Cr, Mn, Ni etc.) present in EC fluids and aerosols may pose health risks in humans (Williams *et al*., 2013). Increased zinc correlated with increased ROS in EC user (Sakamaki-Ching *et al*. 2020.) In addition, infodemiological approaches have found numerous website posts by EC users on adverse health effects, including headache, coughing, malaise, asthma, dehydration, and pharyngitis. (Hua *et al.,* 2020).

Perhaps most serious, in 2019, a surge of lung injuries associated with EC usage were reported across the USA. The condition was termed e-cigarette or

vaping use-associated lung injury or EVALI. As of February 2021, 2,807 cases required hospitalization and more than 68 deaths were associated to EVALI (https://www.cdc.gov/tobacco/basic_information/e-cigarettes/severe-lung-disease.html#latest-inffebormation). In 2020, the COVID pandemic took precedence, and EVALI cases were not accurately tracked. EVALI is characterized by hypoxemia, tachycardia, and tachypnea. Individuals with EVALI had an elevated inflammatory response, which included increased inflammatory cytokines, and showed dramatic lung damage (Belok et al., 2020, Temas et al. 2020). EVALI has been attributed to vitamin E acetate (Cao *et al.,* 2020), which is used to dilute cannabis products making them vapable (Matsumoto *et al*., 2020). The pulmonary tissue is not able to metabolize vitamin E acetate, and in turn vitamin E acetate may cause disruption of lipid bilayers causing respiratory stress (Lee *et al.,* 2020). Since e-liquids vary widely, it is possible multiple chemicals can contribute to EVALI development. Chronic inflammatory response from ECs may result in lung tissue damage and could cause some cases of EVALI (Temas *et al.,* 2021).

The Purpose of this dissertation

The purpose of this is dissertation was to assess the health effects associated with THS, nicotine, and EC exposure. Specifically, the following were done: (1) a novel method was developed and used to qualify the accumulation of THS in contaminated fabrics, and this provided further insight into the release of THS chemicals from contaminated environments. (2) Nicotine concentrations

corresponding to those found in THS and EC contaminated environments were used to assess nicotine's effects during dermal exposure. (3) Human *in vivo* studies were undertaken to characterize the transcriptomic profile of the nasal airway epithelium following THS and EC aerosol exposure.

References

1. Adams, J.D., O'Mara-Adams, J., Hoffmann, D. *1987.*Toxic and carcinogenic agents in undiluted mainstream smoke and sidestream smoke of different types of cigarettes. *Carcinogenesis.*8(5):729–31.

2. Adhami, N., Starck, S. R., Flores, C., Martins-Green, M. 2016A. Health Threat to Bystanders Living in the Homes of Smokers: How Smoke Toxins Deposited on Surfaces Can Cause Insulin Resistance. *PLoS ONE* .11(3): e0149510. doi:10.1371/journal.pone.0149510

3. Adhami, N., Chen, Y., Martins-Green, M. 2017. Biomarkers of disease can be detected in mice as early as 4 weeks after initiation of exposure to thirdhand smoke levels equivalent to those found in homes of smokers. *Clinical Science*. 131 2409–2426 DOI: 10.1042/CS20171053.

4. Andersen, R.A., Kasperbauer, M.J., Burton, H.R., Hamilton, J.L., Yoder, E.E. 1982.Changes in chemical composition of homogenized leaf-cured and air cured Burley tobacco stored in controlled environments. *Journal of Agricultural and Food Chemistry* .30(4):663–8

5. Asomaning, K., Miller, D. P., Liu, G., Wain, J. C., Lynch, T. J., Su, L., & Christiani, D. C. 2008. Second hand smoke, age of exposure and lung cancer risk. *Lung cancer. 61*(1), 13–20. https://doi.org/10.1016/j.lungcan.2007.11.013

6. Bahl, V., Jacob III, P., Havel, C., Schick, S.F., Talbot, P. 2014. Thirdhand cigarette smoke: Factors affecting exposure and remediation. *PLoS ONE*. 9(10): e108258. doi:10.1371/journal.pone.0108258

7. Bahl, V., Shim, H.J., Payton, J. III, Dias, K., Schick, S.F., Talbot, P. 2016a. Thirdhand smoke: Chemical dynamics, cytotoxicity, and genotoxicity in outdoor and indoor environments. *Toxicology in Vitro*.32: 220–231

8. Bahl, V., Weng, N.J.H., Schick, S.F., Sleiman, M., Whitehead, J., Ibarra, A., Talbot, P. 2016b. Cytotoxicity of thirdhand smoke and identification of acrolein as a volatile thirdhand smoke chemical that inhibits cell proliferation. *Toxicological Sciences*.150(1): 234–246.

9. Baker, R.R. 1981. Product formation mechanisms inside a burn- ing cigarette. *Progress in Energy and Combustion Science.*7(2):135–53.

10. Barnes, P.J., Shapiro, S.D., Pauwels, R.A. 2003. Chronic obstructive pulmonary disease: molecular and cellular mechanisms. *Eur Respir J*. 22(4):672-88. doi: 10.1183/09031936.03.00040703. PMID: 14582923.

11. Becquemin, M. H., Bertholon, J. F., Bentayeb, M., Attoui, M., Ledur, D., Roy, F., Dautzenberg, B. 2010. Third-hand smoking: indoor measurements of concentration and sizes of cigarette

12. Behar, R.Z., Davis, B., Wang, Y., Bahl, V., Lin, S., Talbot, P. 2014, Identification of toxicants in cinnamon-flavored electronic cigarette refill fluids. *Toxicology in Vitro*. 198-208, 28: 2, https://doi.org/10.1016/j.tiv.2013.10.006.

13. Belok, S.H., Parikh, R., Bernardo, J., & Kathuria, H. 2020. E-cigarette, or vaping, product use-associated lung injury: a review. *Pneumonia (Nathan Qld.)*, *12*, 12. https://doi.org/10.1186/s41479-020-00075-2

14. Blizzard, L., Ponsonby, A. L., Dwyer, T., Venn, A., & Cochrane, J. A. 2003. Parental smoking and infant respiratory infection: how important is not smoking in the same room with the baby?. *American journal of public health*, *93*(3), 482–488. https://doi.org/10.2105/ajph.93.3.482

15. Banozic, M., Jokic, S., Ackar, D., Blazic, M., Subaric, D. 2020. Carbohydrates-Key Players in Tobacco Aroma formation and quality determination. *Molecules*. 25:1734

16. Barnoya, J., Glantz, S. 2005.Cardiovascular effects of second- hand smoke: nearly as large as smoking. *Circulation.*111(20):2684–98.

17. Beauman, E., Cowling, P., Leister, D.L. & Roope, R.H. 1996.*Reconstituted Tobacco Material and Method for its Production* (Patent No. 5584306 dated 17 December 1996), United States Patent Office.

18. Benowits, N.L. 2010. Nicotine Addiction N Engl J Med.; 362(24): 2295–2303. doi:10.1056/NEJMra0809890.

19. Bache, C.A., Lisk, D.J., Doss, G.J., Hoffmann, D., Adams, J.D. 1985. Cadmium and nickel in mainstream particulates of ciga- rettes containing tobacco grown on a low-cadmium soil-sludge mixture. *Journal of Toxicology and Environmental Health,* 16(3–4):547–52.

20. Brauer, E., Lippens, E., Klein, O., Nebrich, G., Schreivogel, S., Korus, G., Duda, G.N., Petersen, A. 2019. Collagen Fibrils Mechanically Contribute to Tissue Contraction in an In Vitro Wound Healing Scenario. *Adv Sci (Weinh*). 6(9):1801780. doi: 10.1002/advs.201801780.

21. Burghuber, O.C., Punzengruber, C., Sinzinger, H., Haber, P., Silberbauer, K. 1986. Platelet sensitivity to prostacyclin in smokers and non-smokers. *Chest.* 90(1):34–8.

22. California Environmental Protection Agency. Health effects of exposure to environmental tobacco smoke: the report of the California Environmental Protection Agency. Smoking and tobacco control monograph number 10. Bethesda: US Department of Health and Human Services, National Institutes of Health, National Cancer Institute; 1999 August. CEPA, 1999

23. Cantrell, D. Various aspects of menthol product devel- opment, March 1990; Bates No. 584100123; <http:// tobaccodocuments.org/ product_design/967595.html>

24. Cao, D.J., Aldy, K., Hsu, S., McGetrick, M., Verbeck, G., De Silva, I., Feng, S.Y. 2020. Review of Health Consequences of Electronic Cigarettes and the Outbreak of Electronic Cigarette, or Vaping, Product Use-Associated Lung Injury. *J Med Toxicol*. 16(3):295-310. doi: 10.1007/s13181-020-00772-w.

25. Caponnetto, P., Campagna, D., Papale, G., Russo, C., Polosa, R. 2012.The emerging phenomenon of electronic cigarettes*. Expert Rev Respir M*ed. (1):63-74. doi: 10.1586/ers.11.92.

26. Chatterjee, S., Tao, J.Q., Johncola, A., Guo, W., Caporale, A., Langham, M.C., Wehrli, F.W. 2019. Acute exposure to e-cigarettes causes inflammation and pulmonary endothelial oxidative stress in nonsmoking, healthy young subjects. *Am J Physiol Lung Cell Mol Physiol.* 2019. 317(2):L155-L166. doi: 10.1152/ajplung.00110.2019.

27. Chang MJ, Naworal JD, Walker K, Connell CT.2003. Investiga- tions on the direct introduction of cigarette smoke for trace elements analysis by inductively coupled plasma mass spectrometry. *Spectrochimica Acta Part B.Atomic Spectroscopy.*58(11):1979–96.

28. Crotty Alexander, L., Vyas, A., Schraufnagel, D., & Malhotra, A. 2015. Electronic cigarettes: the new face of nicotine delivery and addiction. *Journal Of Thoracic Disease*. 7(8), E248-E251. doi:10.3978/j.issn.2072-1439.2015.07.37

29. Centers of Disease Control and Prevention Health Effects of Cigarette Smoking https://www.cdc.gov/tobacco/data_statistics/fact_sheets/health_effects/effects_cig_smoking/index.htm Accessed December 2019

30. Centers for Disease Control and Prevention (US); National Center for Chronic Disease Prevention and Health Promotion (US); Office on Smoking and Health (US). Atlanta (GA): Centers for Disease Control and Prevention (US); 2010.

31. Chamberlain, W. J.; Severson, R. F.; Stephenson, M. G. 1984.Levels of N-nitrosonornicotine in tobaccos grown under varying agronomic conditions. *Tob. Sci*. 28, 156-158.

32. Cheng, C-Y., Huang, S-S., Yang, C-M., Tang, K-T., Yao, D-J. 2016. Detection of third-hand smoke on clothing fibers with a surface acoustic wave gas sensor. *BIOMICROFLUIDICS.* 10, 011907

33. Chun, L.F., Moazed, F., Calfee, C.S., Matthay, M.A., Gotts, J.E. 2017. Pulmonary toxicity of e-cigarettes. *Am J Physiol Lung Cell Mol Physiol*. 313(2):L193-L206. doi: 10.1152/ajplung.00071.2017.

34. Collins, Y., Chouchani E.T., James A.M., Menger K.E., Cochemé, H.M., Murphy MP.2012. Mitochondrial redox signaling at a glance. *J Cell Sci.*125(Pt 4):801-6. doi: 10.1242/jcs.098475.

35. Dajas-Bailador, F, Wonnacott, S. 2004. Nicotinic acetylcholine receptors and the regulation of neuronal signaling. *Trends Pharmacol Sci.* 25:317–24.

36. Destaillats, H., Singer, B.C., Lee, S.K., Gundel, L.A. 2006.Effect of ozone on nicotine desorption from model surfaces: evidence for heterogeneous

chemistry. *Environ Sci Technol.* 2006 Mar 15;40(6):1799-805. doi: 10.1021/es050914r. PMID: 16570600.

37. Diver, W.R., Jacobs, E.J., Gapstur, S.M. 2018. Secondhand Smoke Exposure in Childhood and Adulthood in Relation to Adult Mortality Among Never Smokers. *Am J Prev Med*. 55(3):345-352. doi: 10.1016/j.amepre.2018.05.005. PMID: 30122215.

38. Elliot, J.G., Carroll, N.G., James, A.L., Robinson, P.J. 2003.Airway alveolar attachment points and exposure to cigarette smoke in utero. *Am J Respir Crit Care Med.* 167(1):45-9. doi: 10.1164/rccm.2110005. PMID: 12502475.

39. Elisia, I., Lam, V., Cho, B. *et al.* 2020. The effect of smoking on chronic inflammation, immune function and blood cell composition. *Sci Rep* **10,** 19480. https://doi.org/10.1038/s41598-020-76556-7

40. Egilman, D. S. & Schilling, J. H. 2012.Bronchiolitis obliterans and consumer exposure to butter-flavored microwave popcorn: a case series. *Int. J. Occup. Environ. Health* **18**, 29–4

41. Fischer, S., Spiegelhalder, B., Eisenbarth, J., Preussmann, R., 1990. Investigations on the origin of tobacco-specific nitrosamines in mainstream smoke of cigarettes. *Carcinogenesis.* 11, 723–730.

42. Fischer S, Spiegelhalder B, Preussmann R. Influence of smoking parameters on the delivery of tobacco- specific nitrosamines in cigarette smoke—a contribu- tion to relative risk evaluation. *Carcinogenesis* 1989a; 10(6):1059–66.

43. Ferrante G, Simoni M, Cibella F, Ferrara F, Liotta G, Malizia V, Corsello G, Viegi G, La Grutta S. Third-hand smoke exposure and health hazards in children. Monaldi Arch Chest Dis. 2013 Mar;79(1):38-43. doi: 10.4081/monaldi.2013.108. PMID: 23741945.

44. Fowles J, Dybing E. 2003. Application of toxicological risk assessment principles to the chemical constituents of cigarette smoke. *Tobacco Control.*12(4):424–30.

45. Flores, C., Adhami, N., Martins-Green, M. 2017. The role fatty acid metabolism and apolipoproteins in mice. J Clin Toxicol. 7: 359. doi:10.4172/2161-0495.1000359

46. Flores, C., Adhami, N., Martins-Green, M. 2016. THS toxins induce hepatic steatosis by altering oxidative stress and SIRT1 levels. J Clin Toxicol. 6;5: 1000318 doi:10.4172/2161-0495.1000318

47. Feldman C, Anderson R. Cigarette smoking and mechanisms of susceptibility to infections of the respiratory tract and other organ systems. J Infect. 2013 Sep;67(3):169-84. doi: 10.1016/j.jinf.2013.05.004. Epub 2013 May 21. PMID: 23707875.

48. Frank, R., Braun, H.E., Holdrinet, M., Stonefield KI, Elliot JM, Zilkey B, Vickery L, Chang HH. Metal contents and insecticide residues in tobacco soils and cured tobacco leaves collected in southern Ontario. *Tobacco Science* 1977;21:74–80.

49. Garcia-Arcos I., Geraghty, P., Baumlin, N., Campos, M., Dabo, A.J., Jundi, B., Cummins, N., Eden, E., Grosche, A., Salathe, M., Foronjy, R. 2016. Chronic electronic cigarette exposure in mice induces features of COPD in a nicotine-dependent manner. *Thorax*. 71(12):1119-1129. doi: 10.1136/thoraxjnl-2015-208039.

50. Geiss, O., Kotzias, D. 2007. Tobacco, Cigarettes and Cigarette Smoke: An Overview. European Commission.

51. Gopal, S. H., Mukherjee, S., & Das, S. K. 2016. Direct and Second Hand Cigarette Smoke Exposure and Development of Childhood Asthma. *Journal of environment and health sciences*, *2*(6), Direct and Second Hand Cigarette Smoke Exposure and Development of Childhood Asthma. https://doi.org/10.15436/2378-6841.16.1122

52. Goel, R., Bitzer, Z.T., Reilly, S.M., Bhangu, G., Trushin, N., Elias, R.J., Foulds, J., Muscat, J., Richie Jr, J.P. 2018. Effect of Charcoal in Cigarette Filters on Free Radicals in Mainstream Smoke. *Chem. Res.* Toxicol. 2018, 31, 745−751DOI: 10.1021/acs.chemrestox.8b00092

53. Govind, A.P., Vezina, P., Green, W.N. 2009. Nicotine-induced upregulation of nicotinic receptors: underlying mechanisms and relevance to nicotine addiction. Biochem Pharmacol. 78:756–65. [PubMed: 19540212]

54. Grimmer G, Naujack K-W, Dettbarn G. Gas chromato- graphic determination of polycyclic aromatic hydrocar- bons, aza-arenes, aromatic

amines in the particle and vapor phase of mainstream and sidestream smoke of cigarettes. *Toxicology Letters* 1987;35(1):117–24.

55. Guerin MR, Higgins CE, Jenkins RA. Measuring environmental emissions from tobacco combustion: side- stream cigarette smoke literature review. *Atmospheric Environment* 1987;21(2):291–7.

56. Hajek, P., Etter J.F., Benowitz, N., Eissenberg, T., McRobbie, H. 2014. Electronic cigarettes: review of use, content, safety, effects on smokers and potential for harm and benefit. *Addiction*. 109(11):1801-1810. doi:10.1111/add.12659

57. Hang, B., Snijders, A.M., Huang, Y., Schick, S.F., Wang, P., Xia, Y., Havel, C., Jacob III, P., Benowitz, H., Destaillats, H., Gundel, L.A., Mao, J.H. 2016 Early exposure to thirdhand cigarette smoke affects body mass and development of immunity in mice. Scientific Reports . 7:41915: DOI: 10.1038/srep41915

58. Hang, B., Sarker, A.H., Havel, C., Saha, S., Hazra, T.K., Schick, S., Jacob III, P., Rehan, V.K., Channa, A., Sharan D., Sleiman, M., Destaillats, H., Gundel, L.A. 2013. Thirdhand smoke causes DNA damage in human cells. 28 (4): 381–391.

59. Havermans, A., Krüsemann, E.J.Z., Pennings, J., de Graaf, K., Boesveldt, S., Talhout, R., 2019. Nearly 20 000 e-liquids and 250 unique flavour descriptions: an overview of the Dutch market based on information from manufacturers. *Tob Control*. doi:10.1136/tobaccocontrol-2019- 055303

60. Hoffmann, D., Djordjevic, M.V., Hoffmann I. 1997. The Changing Cigarette. Preventive Medicine. 26: 427-434.

61. Hoffmann D, Hoffmann I. The changing cigarette, 1950– 1995. *Journal of Toxicology and Environmental Health* 1997;50(4):307–64.

62. Hoffmann D, Hoffmann I, El-Bayoumy K. The less harmful cigarette: a controversial issue. A tribute to Ernst L. Wynder. *Chemical Research in Toxicology* 2001;14(7):767-90.

63. Hein HO, Suadicani P, Skov P, Gyntelberg F. 1991. Indoor dust exposure: an unnoticed aspect of involuntary smoking. Archives of Environmental Health 46(2): 98- 101.

64. Heiss C, Amabile N, Lee AC, Real WM, Schick SF, Lao D, Wong ML, Jahn S, Angeli FS, Minasi P, Springer ML, Hammond SK, Glantz SA, Grossman W, Balmes JR, Yeghiazarians Y. 2008.Brief secondhand smoke exposure depresses endothelial progenitor cells activity and endothelial function: sustained vascular injury and blunted nitric oxide production. J Am Coll Cardiol.6;51(18):1760-71. doi: 10.1016/j.jacc.2008.01.040.

65. Hoh E, Hunt RN, Quintana PJ, Zakarian JM, Chatfield DA, Wittry BC, Rodriguez E, Matt GE. Environmental tobacco smoke as a source of polycyclic aromatic hydrocarbons in settled household dust. Environ Sci Technol. 2012 Apr 3;46(7):4174-83. doi: 10.1021/es300267g. Epub 2012 Mar 19. PMID: 22397504.

66. Hua, M., Omaiye, E.E., Luo, W. *et al.* 2019.Identification of Cytotoxic Flavor Chemicals in Top-Selling Electronic Cigarette Refill Fluids. *Sci Rep*. **9,** 2782. https://doi.org/10.1038/s41598-019-38978-w

67. Hua, M., Sadah, S., Hristidis, V., & Talbot, P. 2020. Health Effects Associated With Electronic Cigarette Use: Automated Mining of Online Forums. *Journal of medical Internet research*, *22*(1), e15684. https://doi.org/10.2196/15684

68. Hua, M., Talbot, P. 2016.Potential health effects of electronic cigarettes: A systematic review of case reports*. Prev Med Rep*. 4:169-78. doi: 10.1016/j.pmedr.2016.06.002.

69. Husgafvel-Pursiainen K, Kannio A. Cigarette smoking and p53 mutations in lung cancer and bladder can- cer. *Environmental Health Perspectives* 1996;104 (Suppl 3):553–6.

70. IARC Working Group on the Evaluation of Carcinogenic Risks to Humans. Tobacco Smoke and Involuntary Smoking. Lyon (FR): International Agency for Research on Cancer; 2004. (IARC Monographs on the Evaluation of Carcinogenic Risks to Humans, No. 83.) Available from: https://www.ncbi.nlm.nih.gov/books/NBK316407/

71. Jabba, S.V., and Jordt, S.E. 2020. Turbocharged Juul device challenges European tobacco regulators. *Eur Respir J.* 13;56(2):2002430. doi: 10.1183/13993003.02430-2020.

72. Jacob, P., Benowitz, N.L., Destaillats, H., Gundel, L., Hang, B., Martins-Green, M., Matt, G.E., Quintana, P.J.E., Samet, J.M., Schick, S.F., Talbot, P., Aquilina, N.J., Hovell, M.F., Mao, J.H., Whitehead, T.P., 2017. Thirdhand

smoke: new evidence, challenges, and future directions. Chem. Res. Toxicol. 30 (1), 270–294. https://doi.org/10.1021/ acs.chemrestox.6b00343.

73. J.C. Leffingwell Leffingwell and Associates Canton, Georgia, USATobacco: Production, Chemistry, And Technology, D. Layten Davis and Mark T. Nielson, Eds., Blackwell Science (Pub.), 1999 Basic Chemical Constituents of Tobacco Leaf and Differences among Tobacco Types.

74. Jung, J.W., Ju, Y.S. and Kang, H.R., 2012. Association between parental smoking behavior and children's respiratory morbidity: 5-year study in an urban city of South Korea. *Pediatric pulmonology*, *47*(4), pp.338-345.

75. Karim, Z.A., Alshbool, F.Z., Vemana, H.P., Adhami, N., Dhall, S., Espinosa, E.V.P., Martins-Green, M., Khasawneh, F.T. 2015. Third Hand Smoke: Impact on Hemostasis and Thrombogenesis. Journal of Cardiovascular Pharmacology Publish Ahead of Print. DOI: 10.1097/FJC.0000000000000260

76. Kataoka H, Kijima K, Maruo G. Determination of muta genic heterocyclic amines in combustion smoke sam ples. *Bulletin of Environmental Contamination and Toxicology* 1998;60(1):60–7.

77. Kim S, Aung T, Berkeley E, Diette GB, Breysse PN. Measurement of nicotine in household dust. Environ Res. 2008 Nov;108(3):289-93. doi: 10.1016/j.envres.2008.07.004. Epub 2008 Aug 27. PMID: 18755452.

78. Kosmider, L., Sobczak, A., Fik, M., Knysak, J., Zaciera, M., Kurek, J., & Goniewicz, M. L. 2014. Carbonyl compounds in electronic cigarette vapors: effects of nicotine solvent and battery output voltage. *Nicotine & tobacco researc : official journal of the Society for Research on Nicotine and Tobacco*, *16*(10), 1319–1326. https://doi.org/10.1093/ntr/ntu078

79. Lee, H. W., Park, S. H., Weng, M. W., Wang, H. T., Huang,W. C., Lepor, H., et al. 2018. E-cigarette smoke damages DNA and reduces repair activity in mouse lung, heart, and bladder as well as in human lung and bladder cells. *Proceedings of the National Academy of Sciences*, *115*(7), E1560-E1569.

80. Lerner, C.A., Sundar, I.K., Yao, H., Gerloff, J., Ossip, D.J., McIntosh, S., Robinson, R., Rahman, I. 2015. Vapors produced by electronic cigarettes

and e-juices with flavorings induce toxicity, oxidative stress, and inflammatory response in lung epithelial cells and in mouse lung. PLoS One. 6;10(2):e0116732. doi: 10.1371/journal.pone.0116732.

81. Li, Y., Shi, H., Yang, H., Zhou, J., Want, J., Bai, R., Xu, D. 2017. Difference between burley tobacco and flue-cured tobacco in nitrate accumulation and chemical regulation of nitrate and TSNA contents. *Journal of Chemistry*. doi.org/10.1155/2017/4357456

82. Luceri F, Pieraccini G, Moneti G, Dolara P. Primary aro- matic amines from side-stream cigarette smoke are common contaminants of indoor air. *Toxicology and Industrial Health* 1993;9(3):405–13.

83. Matsumoto, S., Fang, X., Traber, M.G., Jones, K.D., Langelier, C., Hayakawa Serpa, P., Calfee, C.S., Matthay , M.A., Gotts, J.E. 2020. Dose-Dependent Pulmonary Toxicity of Aerosolized Vitamin E Acetate. *Am J Respir Cell Mol Biol*.63(6):748-757. doi: 10.1165/rcmb.2020-0209OC.

84. Morin, A., Porter, A., Ratavicius, A. Joly, J. 2004. Evolution of Tobacco-Specific Nitrosamines and Microbial Populations During Flue-Curing of Tobacco Under Direct and Indirect Heating. Beiträge zur Tabakforschung International. DOI: 10.2478/cttr-2013-0770

85. Marom-Haham, L., Shulman, A. 2016. Cigarette smoking and hormones. Curr Opin Obstet Gynecol 2016, 28:230-235.DOI:10.1097/GCO.0000000000000283

86. Maritz, G. S., & Harding, R. 2011. Life-long programming implications of exposure to tobacco smoking and nicotine before and soon after birth: evidence for altered lung development. *International journal of environmental research and public health*, *8*(3), 875–898. https://doi.org/10.3390/ijerph8030875

87. Manabe S, Wada O. Carcinogenic tryptophan pyrolysis products in cigarette smoke condensate and cigarette smoke-polluted indoor air. *Environmental Pollution* 1990;64(2):121–32.

88. Matt, G.E., Quintana, P.J.E., Destaillats, H., Gundel, L.A., Sleiman, M., Singer, B.C., Jacob, P., Benowitz, N., Winickoff, J.P., Rehan, V., Talbot, P., Schick, S., Samet, J., Wang, Y., Hang, B., Martins-Green, M., Pankow, J.F., Hovell, M.F., 2011. Thirdhand tobacco smoke: emerging evidence and arguments for a multidisciplinary research agenda. Environ. Health Perspect. 119 (9), 1218–1226. https://doi.org/10.1289/ehp. 1103500.

89. Matt GE, Quintana PJ, Hovell MF, Bernert JT, Song S, Novianti N, et al. 2004. Households contaminated by envi- ronmental tobacco smoke: sources of infant exposures. Tob Control 13:29–37.

90. Matt GE, Quintana PJ, Hovell MF, Chatfield D, Ma DS, Romero R, et al. 2008a. Residual tobacco smoke pollution in used cars for sale: air, dust, and surfaces. Nicotine Tob Res 10(9):1467–1475.

91. Matt GE, Quintana PJE, Zakarian JM, Fortmann AL, Chatfield DA, Hoh E, et al. 2011. When smokers move out and nonsmokers move in: residential thirdhand smoke pollution and exposure. Tob Control 20:e1; doi:10.1136/ tc.2010.037382 [Online 30 October 2010].

92. Matt, G.E., Romero, R., Ma, DS., Quintana PJ, Hovell MF, Donohue M, et al. 2008b. Tobacco use and asking prices of used cars: prevalence, costs, and new opportunities for changing smoking behavior. Tob Induc Dis 4:2; doi:10.1186/1617-9625-4-2 [Online 31 July 2008].

93. Martins-Green M, Adhami N, Frankos M, Valdez M, Goodwin B. , Lyubovitsky, J., , Dhall, S., Garcia, M., Egiebor, I., Martinez, B., [1], Green, H. W., Havel, C., Yu, L., Liles, S., Matt, G., Destaillats, H·, Sleiman, M., Gundel, L. A., Benowitz, N., Jacob III P.,, Hovell, M., Winickoff , J.P., Curras-Collazo[1] M.(2014) Cigarette Smoke Toxins Deposited on Surfaces: Implications for Human Health. PLoS ONE 9(1): e86391. doi:10.1371/journal.pone.0086391

94. Moon, S.Y., Kim, T.W., Kim, Y-J., Kim, Y., Kim, S.Y., Kang, D. 2019. Public facility utility and third-hand smoking exposure without first and second-hand smoking according to urinary cotinine level. Int. J. Environ. Res. Public Health 16;855 doi:10.3390/ijerph16050855

95. Nestor, T.B., Gentry, J.S., Riddick, M.G., Conner, B.T., Peele, D.M., Edwards, M.E., 2003. Role of oxides of nitrogen in tobacco-specific nitrosamine formation in flue-cured tobacco. Beiträge Tabakforsch./ Contrib. Tob. Res. 20, 467.

96. Nair, V., Tran, M., Behar, R.Z., Zhai, S., Cui, X., Phandthong, R., Wang, Y., Pan, S., Luo, W., Pankow, J.F., Volz, D.C., Talbot, P. 2020. Menthol in electronic cigarettes: A contributor to respiratory disease?. *Toxicol Appl Pharmacol*. 15;407:115238. doi: 10.1016/j.taap.2020.115238.

97. Nestler EJ. Is there a common molecular pathway for addiction? Nat Neurosci 2005;8:1445–9. [PubMed: 16251986]

98. Northrup, T. F., Jacob, P., 3rd, Benowitz, N. L., Hoh, E., Quintana, P. J., Hovell, M. F., Matt, G. E., & Stotts, A. L. 2016. Thirdhand Smoke: State of the Science and a Call for Policy Expansion. *Public health reports (Washington, D.C. : 1974)*, *131*(2), 233–238. https://doi.org/10.1177/003335491613100206

99. Omaiye, E.E., Luo, W., McWhirter, K.J., et al. 2021. Flavour chemicals, synthetic coolants and pulegone in popular mint-flavoured and menthol-flavoured e-cigarettes. *Tobacco Control*. doi: 10.1136/tobaccocontrol-2021-056582

100. Omaiye, E.E., McWhirter, K.J., Luo, W. *et al.* 2019.High concentrations of flavor chemicals are present in electronic cigarette refill fluids. *Sci Rep*.**9,** 2468. https://doi.org/10.1038/s41598-019-39550-2

101. Omaiye, E.E., Luo, W., McWhirter, K.J., et al. 2021. Flavour chemicals, synthetic coolants and pulegone in popular mint-flavoured and menthol-flavoured e-cigarettes. *Tobacco Control*. doi: 10.1136/tobaccocontrol-2021-056582

102. Omaiye, E. E., Luo, W., McWhirter, K.J., James F. Pankow, and Prue Talbot. 2020. Electronic Cigarette Refill Fluids Sold Worldwide: Flavor Chemical Composition, Toxicity, and Hazard Analysis. *Chemical Research in Toxicology.* 33(12):2972-2987 DOI: 10.1021/acs.chemrestox.0c00266

103. Ogundare, S.A., Moodley, V., Van Zyl, W.E. 2017. Nanocyrstalline cellulose isolated from discarded cigarette filters. *Carbohydrate Polymers*. 175: 273–281 doi.org/10.1016/j.carbpol.2017.08.008

104. Outbreak of Lung Injury Associated with the Use of E-Cigarette, or Vaping, Products https://www.cdc.gov/tobacco/basic_information/e-cigarettes/severe-lung-disease.html#latest-inffebormation

105. Otera, H., Ishihara, N., Mihara, K. 2013 New insights into the function and regulation of mitochondrial fission. Biochimica et Biophysica Acta 1833. 1256–1268. doi.org/10.1016/j.bbamcr.2013.02.002

106. Pazo, D.Y., Moliere, F., Sampson, M.M., Reese, C.M., Agnew-Heard, K.A., Walters, M.J., Holman, M.R., Blount, B.C., Watson, C.H., Chamber,s D.M. 2016 Mainstream Smoke Levels of Volatile Organic Compounds in 50 U.S. Domestic Cigarette Brands Smoked With the ISO and Canadian Intense Protocols. Nicotine Tob Res. 2016 Sep;18(9):1886-94. doi: 10.1093/ntr/ntw118.

107. Pitsavos, C., Panagiotakos, D. B., Chrysohoou, C., Skoumas, J., Tzioumis, K., Stefanadis, C., et al. 2002) Association between exposure to environmental tobacco smoke and the development of acute coronary syndromes: The CARDIO2000 case- control study. Tobacco Control, 11(3), 220−225.

108. Powell, J.T. 1 Vascular damage from smoking: disease mechanisms at the arterial wall. Vasc Med. 1998;3(1):21-8. doi: 10.1177/1358836X9800300105. PMID: 9666528.

109. Roberts, J.W., Wallace, L.A., Camann, D.E., Dickey, P., Gilbert, S.G., Lewis, R.G., et al. 2009. Monitoring and reducing exposure of infants to pollutants in house dust. Rev Environ Contam Toxicol 201:1–39.

110. Rodgman, A, Perfetti TA. *The Chemical Components of Tobacco and Tobacco Smoke.* Boca Raton (FL): CRC Press, Taylor & Francis Group, 2009.

111. Sakuma, H, Kusana M, Munakata S, Ohsumi T, Sugawara S. The distribution of cigarette smoke components between mainstream and sidestream smoke. I: acidic components. *Beiträge zur Tabakforschung International* 1983;12(2):63–71

112. Sakamaki- Ching S, Williams M, Hua M, et al. 2020. Correlation between biomarkers of exposure, effect and potential harm in the urine of electronic cigarette users.*BMJ Open Respiratory7:e000452. doi: 10.1136/bmjresp-2019-000452*

113. Sarker, A.H., Trego, K.S., Zhang, W., Jacob III, P., Snijders, A.M., Mao, J.H., Schick, S.F., Cooper, P.K., Hang, B. 2020. Thirdhand smoke exposure causes replication stress and impaired transcription in human lung cells. Environ Mol Mutagen. 1–12. DOI: 10.1002/em.22372

114. Saha, S. P., Bhalla, D. K., Whayne, T. F., Jr, & Gairola, C. 2007. Cigarette smoke and adverse health effects: An overview of research trends and future needs. *The International journal of angiology: official publication of the International College of Angiology, Inc.16*(3), 77–83. https://doi.org/10.1055/s-0031-1278254

115. Schwartz, R.S., Hecking, L.T. 1991. Determination of geographic origin of agricultural products by multivariate analysis of trace element composition. *Journal of Analytical Atomic Spectrometry.*6(8):637–42.

116. Schick, S. F., and Glantz, S. 2007.Concentrations of the carcinogen 4-(methylnitrosamino)-1-(3-pyridyl)-1-butanone in side- stream cigarette smoke increase after release into indoor air: results from unpublished tobacco industry research. Cancer Epidemiol., Biomarkers Prev. 16, 1547−53.

117. Schweitzer, K.S., Chenm, S.X., Law, S., Van Demark, M., Poirier, C., Justice, M.J., Hubbard, W.C., Kim, E.S., Lai, X., Wang, M., Kranz, W.D., Carroll, C.J., Ray, B.D., Bittman, R., Goodpaster, J., Petrache, I. 2015. Endothelial disruptive proinflammatory effects of nicotine and e-cigarette vapor exposures. *Am J Physiol Lung Cell Mol Physiol*.;309(2):L175-87. doi: 10.1152/ajplung.00411.2014.

118. Singer, B.C., Revzan, K. L., Hotchi, T., Hodgson, A.T., Brown, N.J. 2004. Sorption of organic gases in a furnished room. Atmospheric Environment.38(16):2483-2494. https://doi.org/10.1016/j.atmosenv.2004.02.003.

119. Sheu, R., Stonner, C., Ditto, J.C., Klupfel, T., Williams, J., Gentner, D.R. 2020. Human transport of thirdhand tobacco smoke: A prominent source of hazardous air pollutants into indoor nonsmoking environments. Sci Adv. 6 (10): eaay4109. DOI: 10.1126/sciadv.aay4109

120. Sleiman, M., Logue, J. M., Luo, W., Pankow, J. F., Gundel, L. A., and Destaillats, H. (2014) Inhalable constituents of thirdhand tobacco smoke: chemical characterization and health impact considerations. Environ. Sci. Technol. 48, 13093−101.

121. Sturm, J. J., Yeatts, K., & Loomis, D. (2004). Effects of tobacco smoke exposure on asthma prevalence and medical care use in North Carolina middle school children. American Journal of Public Health, 94(2), 308−313.

122. Stabbert R, Schäfer K-H, Biefel C, Rustemeier K. Analysis of aromatic amines in cigarette smoke. *Rapid Commu- nications in Mass Spectrometry* 2003a;17(18):2125–32

123. Stratton, K, Shetty, P, Wallace, R, et al. 2001. editors Institute of Medicine (US) Committee to Assess the Science Base for Tobacco Harm Reduction. Clearing the Smoke: Assessing the Science Base for Tobacco Harm Reduction. Washington (DC): National Academies Press (US);. https://www.ncbi.nlm.nih.gov/books/NBK222363/

124. Sussan, T.E., Gajghate, S., Thimmulappa, R.K., Ma, J., Kim, J.H., Sudini, K., Consolini, N., Cormier, S.A., Lomnicki, S., Hasan, F., Pekosz, A., Biswal, S. 2015. Exposure to electronic cigarettes impairs pulmonary anti-bacterial and anti-viral defenses in a mouse model. *PLoS One*. 10(2):e0116861. doi: 10.1371/journal.pone.0116861.

125. Temas, D., & Meyer, A. 2020. E-Cigarette- and Vaping-Related Lung Injury (EVALI) at a Regional Hospital System in South Carolina. *Case reports in pulmonology*. 5370606. https://doi.org/10.1155/2020/5370606

126. Thielen, A., Klus, H., Muller, L. 2008. Tobacco smoke: unravelling a controversial subject. *Experimental and Toxicologic Pathology*. 60 :141–156

127. Torres, S., Samino, S., Rafols, P., Martins-Green, M., Correig, X. 2020. Unravelling the metabolic alterations of liver damage induce by thirdhand smoke. Environment International. 146:106242. doi.org/10.1016/j.envint.2020.106242

128. Tobacco and its environmental impact: an overview. Geneva: World Health Organization; 2017. Licence: CC BY-NC-SA 3.0 IGO. Retrieved November 23, 2019.

129. Trtchourian and Talbot. 2010 Electronic nicotine delivery systems: is there a need for regulation? *Tobacco Control.* 20: 47e52. doi:10.1136/tc.2010.037259

130. U.S. Department of Health and Human Services. *The Health Consequences of Smoking: 50 Years of Progress. A Report of the Surgeon General*. Atlanta, GA: U.S. Department of Health and Human Services, Centers for Disease Control and Prevention, National Center for Chronic Disease Prevention and Health Promotion, Office on Smoking and Health, 2014.

131. Ueta, I., Saito, Y., Teraoka, K., Miura, T., Jinno, K., 2010. Determination of volatile organic compounds for a systematic evaluation of third-hand smoking. *Anal Sci*. 26(5):569-74. doi: 10.2116/analsci.26.569.

132. Walser, T., Cui, X., Yanagawa, J., Lee, J. M., Heinrich, E., Lee, G., Sharma, S., & Dubinett, S. M. (2008). Smoking and lung cancer: the role of inflammation. *Proceedings of the American Thoracic Society*. *5*(8), 811–815. https://doi.org/10.1513/pats.200809-100TH

133. Wang H, Sun X. Desensitized nicotinic receptors in brain. Brain Res Brain Res Rev 2005;48:420– 37. [PubMed: 15914250]

134. Werley, M. S., Kirkpatrick, D. J., Oldham, M. J., Jerome, A. M., Langston, T. B., Lilly, P. D., Smith, D. C., & Mckinney, W. J., Jr .2016. Toxicological assessment of a prototype e-cigarette device and three flavor formulations: a 90-day inhalation study in rats. *Inhalation toxicology*, *28*(1), 22–38.https://doi.org/10.3109/08958378.2015.1130758

135. Weston A, Perrin LS, Forrester K, Hoover RN, Trump BF, Harris CC, Caporaso NE. Allelic frequency of a p53 polymorphism in human lung cancer. Cancer Epidemiology, Biomarkers & Prevention 1992;1(6):481–3.

136. Williams, M.; Talbot, P. 2019. Design Features in Multiple Generations of Electronic Cigarette Atomizers. *Int. J. Environ. Res. Public Health*.*16*, 2904. https://doi.org/10.3390/ijerph16162904

137. Williams, M., Villarreal, A., Bozhilov, K., Lin, S., Talbot, P. 2013. Metal and silicate particles including nanoparticles are present in electronic cigarette cartomizer fluid and aerosol. *PLoS One*. 8(3):e57987. doi: 10.1371/journal.pone.0057987.

138. Whitehead, T.P., Metayer, C., Ward, M.H., Nishioka, M.G., Gunier, R., Colt, J.S., Reynolds, P., Steve Selvin, Patricia Buffler, Stephen M. Rappaport. 2009. Is House-Dust Nicotine a Good Surrogate for Household Smoking? *American Journal of Epidemiology* .169(9):1113–1123, https://doi.org/10.1093/aje/kwp021

139. Whitehead, T.P, Havel, C., Metayer, C., Benowitz , N.L., Jacob, P. 2015. 3rd. Tobacco alkaloids and tobacco-specific nitrosamines in dust from homes of smokeless tobacco users, active smokers, and nontobacco users. *Chem Res Toxicol*. 28(5):1007-14. doi:10.1021/acs.chemrestox.5b00040.

140. Whitlatch, A., Schick, S. 2019. Thirdhand Smoke at Philip Morris. Nicotine Tob Res.21;12:1680-1688. doi: 10.1093/ntr/nty153. PMID: 30053240.

141. Wheaton, A.G., Lui, Y., Croft, J.B., VanFrank, B., Croxton, T.L., Punturieri, A., Postow, L., Greenlund, K.J. 2019. Chronic obstructive pulmonary disease and smoking status: United States 2017. Morbidity and Mortality Weekly Report: 68:534-538

142. WHO Report on the Global Tobacco Epidemic, 2019. Geneva: World Health Organization; 2019. Licence: CC BY-NC-SA 3.0 IGO. https://www.who.int/tobacco/global_report/en/

143. Wonnacott S. 1997. Presynaptic nicotinic ACh receptors. Trends Neurosci. 20:92–8. [PubMed: 9023878]

144. Youle, R.J., Van der Bliek, A.M. 2012. Mitochondrial fission, fusion and stress. Science. 337:1062 DOI: 10.1126/science.1219855

145. Yu, V., Rahimy, M., Korrapati, A., Xuan, Y., Zou, A. E., Krishnan, A. R., Tsui, T., Aguilera, J. A., Advani, S., Crotty Alexander, L. E., Brumund, K. T., Wang-Rodriguez, J., & Ongkeko, W. M. 2016. Electronic cigarettes induce DNA strand breaks and cell death independently of nicotine in cell lines. *Oral oncology*, *52*, 58–65. https://doi.org/10.1016/j.oraloncology.2015.10.018

146. Zahedi, A., Phandthong, R., Chaili, A., Leung, S., Omaiye, E., Talbot, P. 2019. Mitochondrial Stress Response in Neural Stem Cells Exposed to Electronic Cigarettes, *iScience*.16,250-269, https://doi.org/10.1016/j.isci.2019.05.034.

147. Zaleski O E-Cigarette Maker Juul Labs Is Raising $1.2 Billion Bloomberg. https:// www.bloomberg.com/news/articles/2018-06-29/e-cigarette-maker-juul-labs-is-raising-1-2-billion. Published June 29, 2018. Accessed September 9, 2018

148. Zhu S, Sun JY, Bonnevie E*, et al.* 2014*.* Four hundred and sixty brands of e-cigarettes and counting: implications for product regulation. *Tobacco Control* 2014;23:iii3-iii9.

149. Zou, C., Hu, X., Huang, W., Zhao, G., Yang, Jin, Y., Gu, H., Yan, F., Li, Y., Wu, Q., Xiong, K. 2017. Different yellowing degrees and the industrial utilization of flue-cured tobacco leaves. Sci. Agric. 76:1;1-9

Chapter 2

Adhesion and Removal of Thirdhand Smoke from Indoor Fabrics: A Method for Rapid Assessment and Identification of Chemical Repositories

Pozuelos, G.L.; Jacob, P., III; Schick, S.F.; Omaiye, E.E.; Talbot, P. Adhesion and Removal of Thirdhand Smoke from Indoor Fabrics: A Method for Rapid Assessment and Identification of Chemical Repositories. *Int. J. Environ. Res. Public Health* **2021**, *18*, 3592. https://doi.org/10.3390/ijerph18073592

Abstract

Thirdhand smoke (THS) is an environmental contaminant that may cause adverse health effects in smokers and non-smokers. Currently, time-consuming analytical methods are necessary to assess chemicals in THS repositories, like upholstered furniture and clothing. Our goal was to develop a rapid accessible method that can be used to measure THS contamination in common household fabrics and to evaluate remediation. Cotton, terry cloth, polyester, and wool were exposed to THS for various times in a controlled laboratory environment and then extracted in various media at room temperature or 600C to develop an autofluorescent method to quantify THS. Concentrations of nicotine and related alkaloids in the extracts were determined using liquid chromatography-tandem mass spectrometry (LC-MS/MS) and high-performance liquid chromatography (HPLC). The autofluorescence of extracts was proportional to the time and amount of THS exposure received by cotton and terry cloth. Extracts of polyester and wool did not show autofluorescence unless heat was applied during extraction. Nicotine, nicotine alkaloids, and TSNA concentrations were higher in THS extracts from cotton and terry cloth than extracts of polyester and wool carpet, in agreement with the autofluorescence data. For fabrics spiked with 10 mg of nicotine, extraction efficiency was much higher from terry cloth (7 mg) than polyester (0.11 mg). In high relative humidity, nicotine recovery from both cotton and polyester was 80% (~8 mg). Our results provide a simple, rapid method to assess THS contaminants in household fabrics and further show that THS

extraction is influence by fabric type, heat, and humidity. Thus, remediation of THS environments may need to vary depending on the fabric reservoirs being treated. Understanding the dynamics of THS in fabrics can help set up appropriate remediation policies to protect humans from exposure.

Introduction

Thirdhand smoke (THS) is an environmental pollutant that can be absorbed through dermal contact, inhalation, or ingestion by both smokers and non-smokers. THS is comprised of secondhand smoke from the burning end of a cigarette plus exhaled mainstream smoke that settles on indoor surfaces where the residue can remain, react, be re-emitted, or be resuspended for months or years after smoking has ceased. (Matt *et al*., 2011a; Jacob *et al*., 2017). THS is a mixture of hazardous volatile and semi-volatile organic chemicals, polycyclic aromatic hydrocarbons, metals, and secondary compounds generated through reactions with atmospheric pollutants (e.g., ozone and nitrous acid) (Sleiman *et al/,* 2010a). Nicotine, a major component of THS, can react with ambient concentrations of oxidants like nitrous acid or ozone to form carcinogenic tobacco-specific nitrosamines (TSNAs), such as 4-(methylnitrosamino)-1-(3-pyridinyl)-1-butanone (NNK), and N-nitrosonornicotine (NNN) (Sleiman *et al*., 2010a; Sleiman *et al.*, 2010b; Jacob *et al.,* 2017; Schick *et al.* 2007). Concentrations of TSNAs can increase as THS ages, increasing the toxicity of THS overtime (Schick *et al.,* 2007; Bahl *et al.,* 2014).

THS causes genotoxic damage and a stress-induced cellular defense response in cultured cells (Hang *et al.,* 2013; Bahl *et al.,* 2016b). Alterations in DNA occurred in cells from mice and humans during both short and long-term exposure to THS (Hang *et al.,* 2013). Mouse neural stem cells undergo morphological changes such as blebbing, fragmentation, cytoskeletal disruption,

and vacuolization when treated with aqueous THS extracts (Bahl *et al.*, 2016c). THS also caused stressed-induced mitochondrial-hyperfusion (SIMH) and increases in mitochondrial membrane potential, ATP levels, and reactive oxygen species (ROS) (Bahl *et al.,* 2016a). In a metabolomics study, male germ cells exposed to THS down-regulated molecular pathways involved in nucleic acid and ammonia metabolism and up-regulated glutathione metabolism (Xu *et al.*, 2015). Three-week old mice exposed to THS fabric for 6 months showed an increase of inflammatory cytokines in lung tissue and impaired wound healing (Martins-Green *et al*., 2014). Mice also became insulin resistance as a result of oxidative stress (Adhami *et al.*, 2016). Oxidative stress in skeletal muscle cells and accumulation of H2O2 accompanied with low catalase activity were also found in exposed mice (Adhami *et al.*, 2016). Hang *et al.* 2017 showed that THS exposed neonatal and adult mice had changes in hematopoiesis.

Unlike secondhand smoke exposure, which occurs mainly through inhalation, human exposure to THS can also include ingestion and absorption through the skin (Ferrante *et al*., 2013; Northrup *et al*., 2016). Children and toddlers are particularly vulnerable to THS due to their low body mass and frequent contact with indoor surfaces during crawling and mouthing. A toddler mouthing a small piece of fabric exposed to THS can be exposed to 2.2 µg of nitrosamines/day, a concentration approximately 16-fold greater than the inhalation exposure of an adult passive smoker (0.14 µg/day) (Balh *et al.*, 2014*).* In addition, young children have a high respiratory rate relative to their body

weight, which increases the amount of THS they can inhale when compared to adults *(Jung et al., 2012)*. Recently, we showed that acute inhalation of THS alters the nasal epithelium transcriptome of non-smoking women in a manner consistent with stress induced mitochondrial hyperfusion (SIMH), demonstrating that even short exposure to THS produces adverse effects in humans (Pozuelos *et al.*, 2019).

THS toxicants are found in both smoking and non-smoking environments (Matt *et al*., 2011b; Matt *et al.*, 2008). Infants whose mother smoked outdoors to protect their children from exposure still had much higher levels of cotinine, a nicotine metabolite, in their urine than infants of non-smoking parents (Matt *et al.*, 2004). Detectable concentrations of THS were found on incubators and cribs from neonatal intensive care units (ICU) in hospitals. ICU infants showed detectable levels of cotinine and NNAL, a metabolite of NNK (Northrup *et al*., 2016). THS can be absorbed in the clothes of smokers and non-smokers who are exposed to SHS (Matt *et al.*, 2011b). Sheu *et al.* 2020 showed that THS contaminants can be transported into a smoking-free movie theater by moviegoers clothing equal to secondhand smoke generated from 1-10 cigarettes. The widespread distribution of THS in indoor environments, such as movie theaters, hospitals, and hotels, makes non-smokers susceptible to THS exposure.

The widespread distribution of THS and its potential toxicity demonstrate a need to (1) develop rapid, accessible methods to quantify THS so that it can be

compared across laboratories and field sites, (2) measure THS retention in indoor fabric reservoirs, and (3) determine how to best remediate indoor environments, especially when there is a need to protect non-smokers and vulnerable populations. One goal of this paper is to introduce a rapid method based on autofluorescence of chemicals in smoke that permits cross comparisons of THS from different samples and environments. Additional goals were to compare the release of THS and its chemicals from various household fabric repositories and determine the factors that affect extraction of THS and remediation of indoor environments. We tested the sorption and desorption of THS chemicals using household fabrics that are not frequently washed and would therefore likely be long-term repositories of THS. These included upholstery cotton, terry cloth, upholstery polyester, and wool carpet that were exposed to THS in a controlled laboratory environment for 1, 6, 12 or 18 months.

Materials and Methods

Exposure of household fabrics to THS

Cotton, terry cloth, polyester, polyester/linen, wool carpet, and polyester carpet were purchased in Riverside, California and sent to Dr. Suzaynn Schick at the University of California, San Francisco where they were exposed to THS as previously described (Schick *et al.,* 2014) Briefly, Marlboro Red cigarettes (Philip Morris Co. Richmond, VA) were smoked using an automatic smoking machine (Model TE- 10z smoking machine, Teague Enterprises, Woodland, California, USA). The smoke was diluted with conditioned and filtered air and passed through a 6-m3 stainless steel smoke aging chamber where the fabrics were hung (Schick *et al.,* 2012). Airflow through the chamber was measured using an air velocity transmitter (model 641-b Dwyer Instruments, Michigan City IN). Particle concentration was measured using a laser photometer (Dusttrak II, model 8530, TSI Inc., Shoreview MI) located in the ducting immediately before the aging chamber.

Pieces (11” x 8”) of cotton, terry cloth, polyester, and wool carpet were exposed to different concentrations of particulate material derived from smoke for 1, 6, 12 or 18 months. Prior to exposure, fabrics were washed three times in a domestic washing machine using an unscented, enzyme-free laundry detergent (Country Save, Arlington, WA) in hot water with two rinses/cycle after each wash. After a fourth and final wash with no detergent, fabrics were line-dried. After exposure, fabrics were stored in tightly-sealed Mylar bags at -20 °C and shipped to UCR on dry ice. Once received, they were stored at -80°C until used.

Preparation of THS aqueous extracts for fluorescent intensity and LC-MS/MS analysis

Aqueous extractions of THS and unexposed control fabric (stored in a smoke-free laboratory) were prepared in serum-free keratinocyte medium (GIBCO 17005-042) supplemented with keratinocyte supplements (Gibco 37000-015), PBS (-), or dimethyl sulfoxide (DMSO). THS exposed and unexposed fabrics were soaked at a ratio 0.1 g of fabric/mL of cell medium, PBS (-), or DMSO on a rotating shaker for 1 hr at room temperature. For heated extractions, 15 mL conical tubes containing fabric and 3 mL of buffer were placed on a heating block for 1 hr at 60oC. Extract was recovered from fabric using a 30 mL Luer Henke Syringe (Henke Sass Wolf, Germany), and sterilized by passing through a 0.22 μM filter (Pall Corporation, Port Washington, NY). The extract was aliquoted and stored at -80 °C for further use.

Fluorescence Intensity

Samples (200 μL) of extracts of cotton, terry cloth, polyester and wool carpet extract in DMSO, PBS and cell medium were added to a 96 well plate. Fluorescence intensity was measured at excitation/emissions of 360/460, 485/528, 540/ 590 using a Bio-Tek Synergy HTX, multi-mode microplate reader. Control extracts of cloth samples without THS exposure were measured in triplicate.

LC–MS/MS analysis of nicotine, tobacco alkaloids, and TSA's

Quantification of nicotine, other tobacco alkaloids (cotinine, myosmine, n-formylnornicotine, nicotelline, bipyridine) and TSNAs in PBS was done at the University of California, by liquid chromatography coupled with tandem mass spectrometry (LC–MS/MS) as previously described (Whitehead *et la.* 2015). The limits of quantitation for each of the chemicals analyzed are as follows: nicotine: 1.02 ng/ml; myosmine: 0.305 ng/ml; 2,39- bipyridine: 0.914 ng/ml; cotinine: 0.914 ng/ml; N-formylnornicotine: 0.305 ng/ml; nicotelline: 0.030 ng/ml; NNN: 0.030 ng/ml; NNK; 0.0130 ng/ml; NNA 0.010 ng/ml.

Exposure to Pure Nicotine.

Samples of cotton, terry cloth, and polyester were exposed to pure nicotine to test factors affecting autofluorescence. Fabrics were exposed at room temperature to 10 mg of nicotine (Sigma, St. Louis, MO) in 50 µL droplets of purified water (10mg/50µL) for 24 hrs at room temperature. During the 24 hrs incubation, an additional piece of cotton fabric was placed underneath each treated fabric to test for fabric permeability. The cotton fabric served as a reservoir for residual nicotine that soaked through the exposed fabrics. A set of fabrics were also treated for a short incubation period of 3 hrs at room temperature. In addition, a separate 24 hrs exposure experiment was performed in a tightly sealed vial to minimize air drying and increase humidity.

Preparation of aqueous extracts from nicotine treated fabrics for HPLC analysis

After exposure, fabrics were cut and soaked in 3 mL of HPLC unbuffered mobile phase (UBMP) made of 76.9% water, 23% acetonitrile, and 0.1% triethylamine. Extraction efficiency was determined by soaking the same fabric in buffer three consecutive times for a duration of 3 minutes each in 15 mL conical tubes. For heated extractions, 15 mL conical tubes containing fabric and 3 mL unbuffered mobile phase were placed on a heating block for 1 hr at 60oC. After incubation, extracts were sterilized with a 0.22 µM filter (Pall Corporation, Port Washington, NY).

HPLC Analysis of Nicotine

The high-performance liquid chromatography (HPLC) method for quantifying nicotine in fabric was adopted from the calibration protocol described previously (Davis *et al.*, 2015). The accuracy and precision of the calibration curve were validated by injecting three samples of nicotine, 333 µg/ml, 500 µg/ml, and 637 µg/ml, and determining the percent error at each concentration. For each concentration, the error was < 1% (0.681% for 333 µg/ml, 0.319% for 500 µg/ml and 0.654% for 637 µg/ml). Periodic validation of the calibration curve was performed to ensure there were no changes or drift.

Nicotine concentrations in fabric extract were analyzed using a Hewlett Packard Series 1100 HPLC with adjustments to a method previously described (Davis *et al.*, 2015). Since the extraction was performed in the unbuffered mobile

phase, no further dilution was required. 100 % extracts of the exposed fabric were used for the analysis. Care was taken to accurately aspirate the solution so as not to introduce air bubbles. The injection volume for all samples was 5 µl. The limit of quantification for nicotine was 10 µg/ml, with a limit of detection of 50 ng/ml. Each sample was injected and analyzed three times. The values reported are the means and standard deviations of three independent experiments.

Results

THS fabric exposure

Cotton, terry cloth, polyester, and wool carpet were exposed for 1, 6, 12, and 18 months to 696, 1569, 1795 and 3617 mg of total particulate material, respectively (Fig.1 A; Table 1). THS accumulation can be visualized in terry cloth, which gradually turned brown with increased exposure (Fig. 1 B).

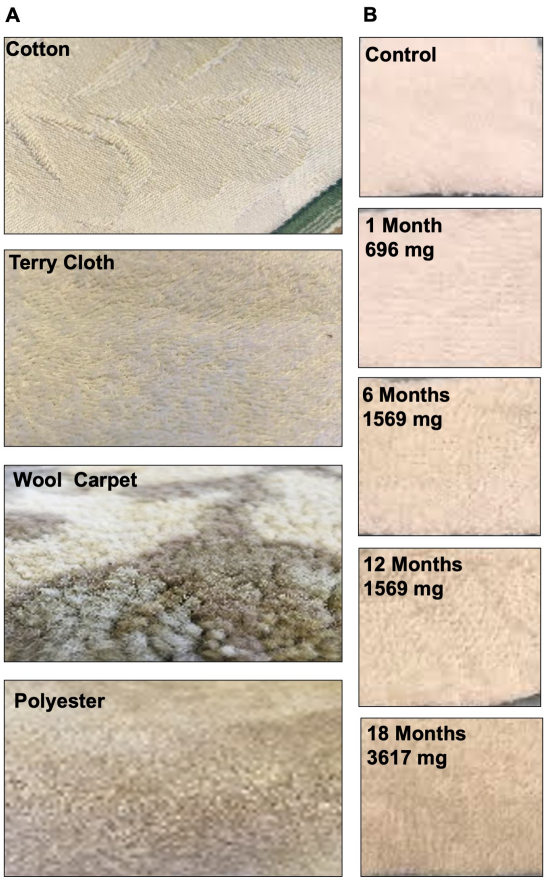

Figure 1. **Common house fabric exposed to THS**. (A) Cotton, terry cloth, wool carpet and polyester were exposed to THS. (B) Terry cloth exposed to different concentrations (mg) of particular material from cigarette smoke at 1, 6, 12 and 18 months.

Table 1. Fabric THS Exposure

Months of THS exposure	1	6	12	18
Total mg of particulate material exposed at each time interval	696	873	226	1833
Total mg of particulate material accumulated over time	696	1569	1795	3917

Autofluorescence of THS extracts is directly related to the length of exposure.

We measured autofluorescence of THS extracts as a quick and efficient method to evaluate THS accumulation in exposed fabrics using various extraction media (Fig. 2 A-D). While extracts from control fabrics had low levels of autofluorescence, extracts from THS exposed cotton showed progressively more fluorescence with longer exposures in all extraction media (Fig. 2 A). Terry cloth produced similar results when extracted in PBS or culture medium; however, DMSO extracts from all groups contained highly autofluorescent material (Fig. 2 B). THS extracts from polyester and wool carpet showed little fluorescence above the control, and fluorescence did not increase with longer THS exposures (Fig. 2 C-D). Regression analysis showed a significant correlation between length of exposure and autofluorescence for extracts of cotton fabric in each medium and for terry cloth in PBS and cell culture medium, but not in DMSO

(Fig.2). Autofluorescence also proved to be an excellent method to test extraction efficiency (Fig.3 A). Using this method, we showed that most (74-89%) THS residue is extracted from terry cloth in the first of three extractions in PBS (Fig. 3 A).

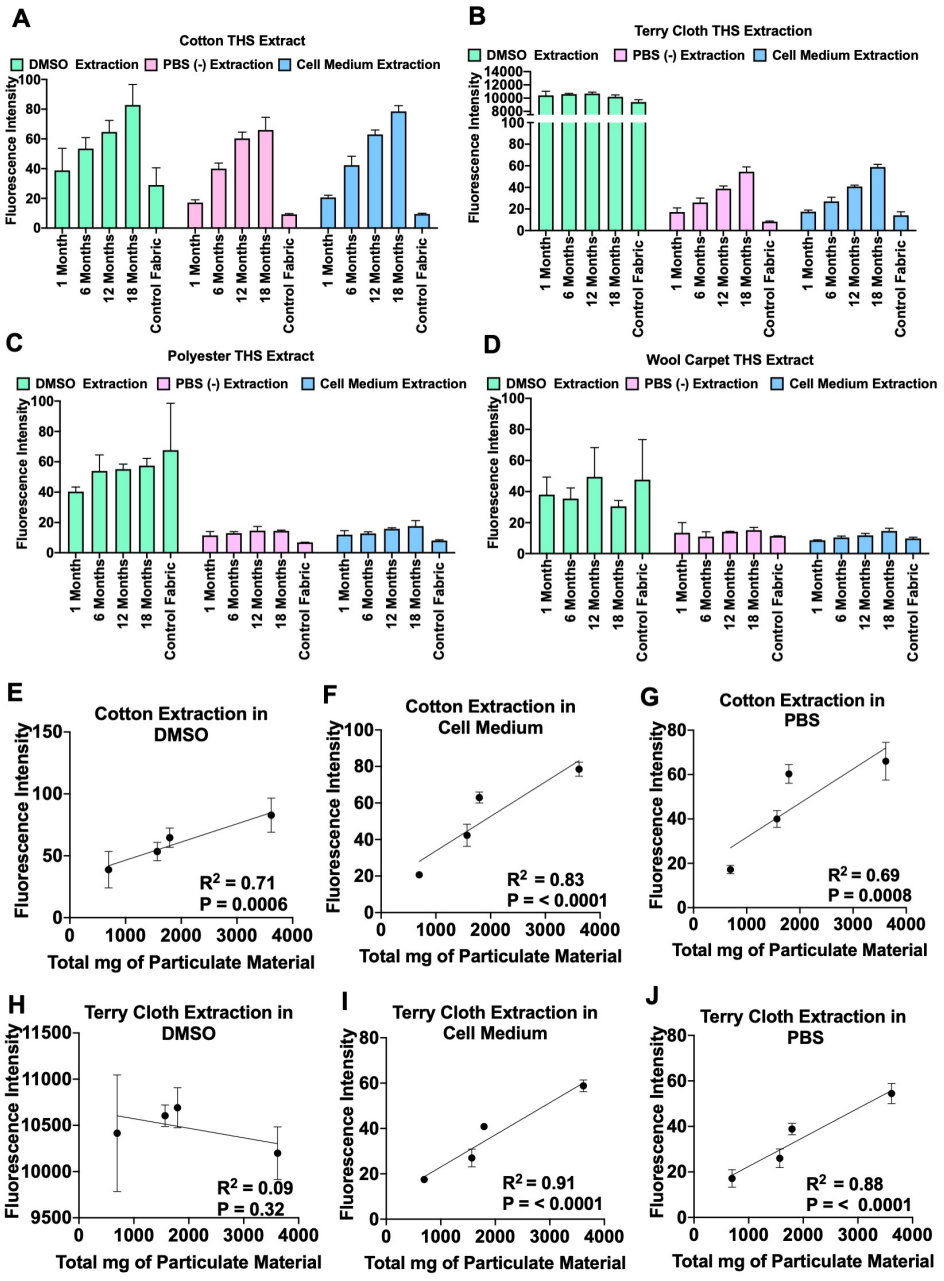

Figure 2. THS extracts from fabrics were autofluorescent. (A-D) Excitation wavelength 360/40 with emission at 460/40 detected THS residue in fabrics extracted in DMSO, PBS and cell medium. (E-J) Fluorescent intensity was proportional to the amount of THS exposure received by the fabrics extracted in PBS and cell medium but not extracts in DMSO.

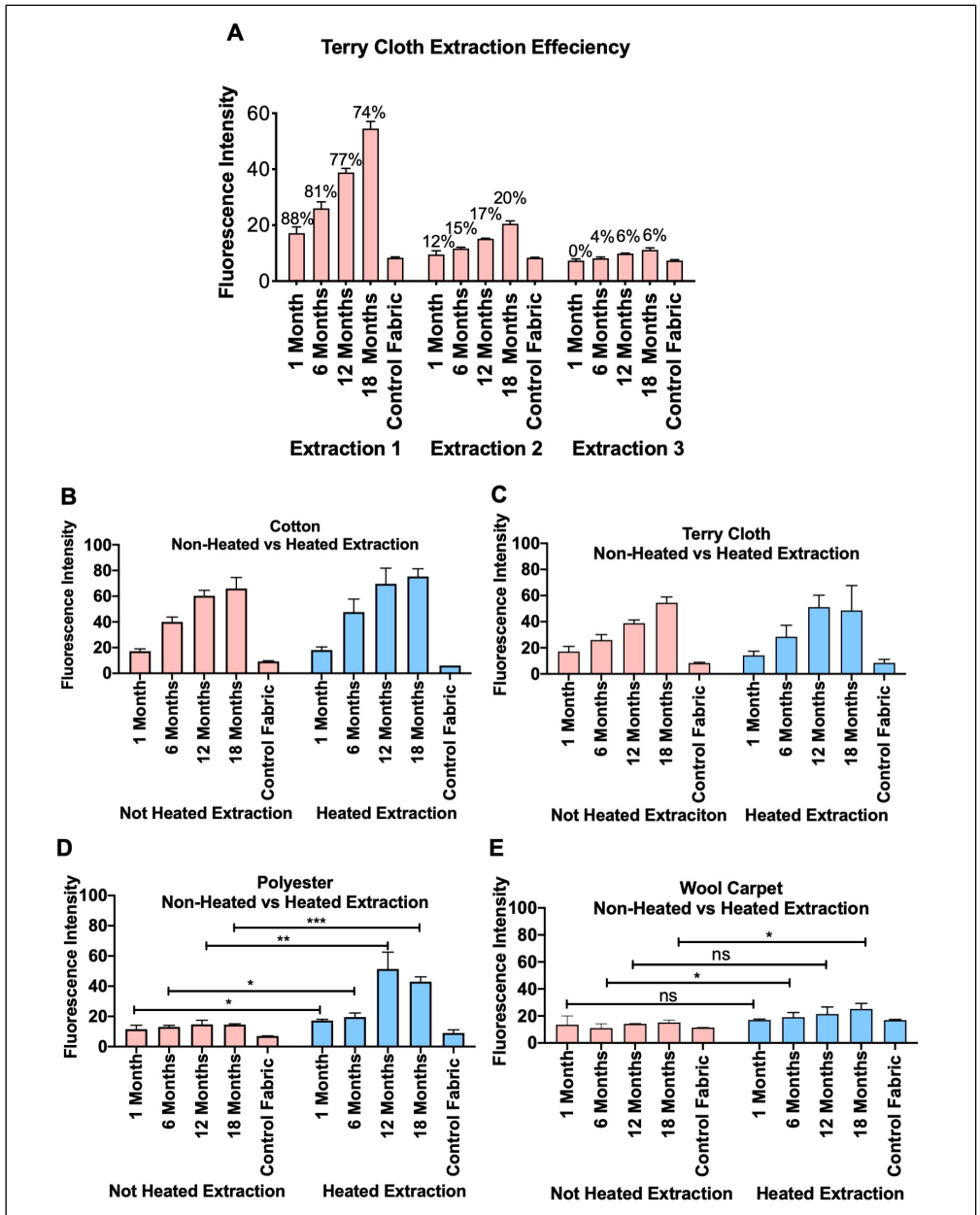

Figure 3. Effect of multiple extractions and heating on extraction efficiency. (A) Most residue was removed in the first of three extractions. (B-E) Extraction was improved in some fabrics by heating for 1 hr at 60°C.

Heating increased the release of THS from polyester and wool carpet

To facilitate the release of THS from polyester and wool carpet, fabrics in PBS were heated to 60o C for 1 hour. Extracts were analyzed using autofluorescence. Heating did not alter the fluorescent intensity between heated and non-heated extracts for both cotton and terry cloth. In contrast, heating facilitated the release of THS from polyester and wool carpet (**Fig. 3 B-E**). THS release from polyester was significantly higher in extracts at all time points, while for wool carpet it was only significantly higher for the 6 and 18-month fabric extracts (**Fig. 3 D-E**).

Analysis of chemicals released into PBS from THS exposed fabrics

Concentrations of nicotine, tobacco alkaloids and TSNAs were higher in extracts from cotton and terry cloth than those from polyester and wool carpet (**Fig. 4**). Unlike our autofluorescence analysis, nicotine concentrations did not show a progressive increase with exposure for any of the fabrics (**Fig. 4 A**). However, concentrations of cotinine, n-formylnornicotine, bipyridine, and NNK did increase progressively with longer exposures for both terry cloth and cotton, but not for polyester or wool carpet (**Fig. 4**). Wool carpet THS extracts from 6, 12, and 18-month fabrics had higher concentrations of myosmine, nicotelline, NNA, and NNN than the 1-month extracts, although the relationships were not always linear (**Fig. 4)**.

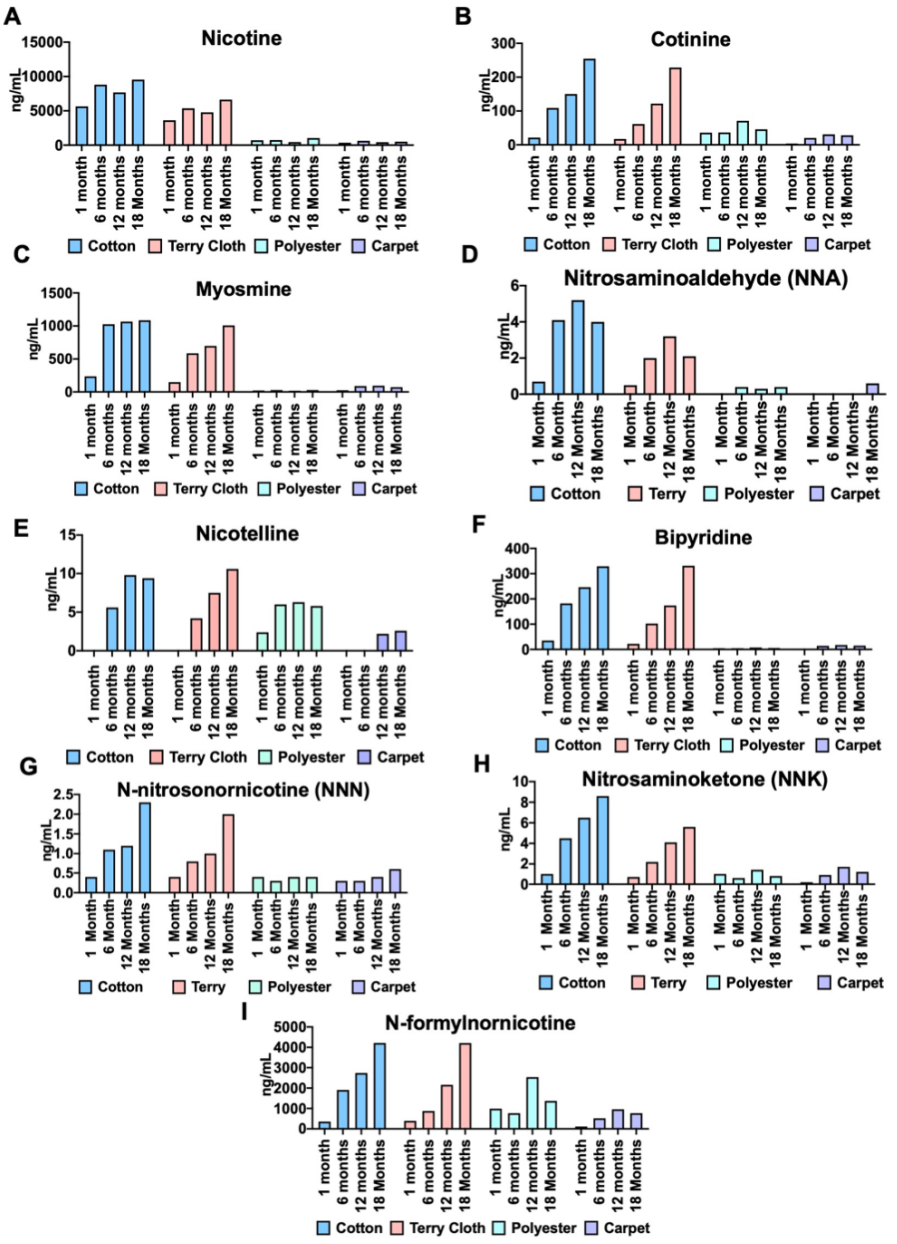

Figure 4. Concentrations of various chemicals in THS extracts of cotton, terry cloth, polyester and wool carpet. (A- I) Nicotine, nicotine alkaloids, and TSNA concentrations were higher in THS extracts from cotton and terry cloth compared to polyester and wool carpet.

Factors affecting the efficiency of nicotine extraction from fabrics

We treated terry cloth and polyester fabric with 10 mg of pure nicotine for 24 hrs before extracting the nicotine in HPLC unbuffered mobile phase. Similar to our THS exposed fabrics, higher concentrations of nicotine were recovered from cotton (5 mg) and terrycloth (7 mg) than from polyester (0.11 mg) (**Fig. 5A**). Most nicotine was recovered in the first extraction, while very little nicotine was recovered in any of the polyester extractions of polyester (**Fig. 5 B-C)**.

Loss of nicotine to the surface below the test fabric was investigated by placing a second piece of cotton fabric beneath the test fabric and measuring nicotine in it. Extracts from the cotton fabric beneath the test fabric had low nicotine concentrations (~0.2 mg total of nicotine), showing that minimal amounts of nicotine leaked through the test fabric (**Fig. 5D**). Nicotine recovery did not differ in heated and not-heated cotton and polyester extracts (**Fig. 5E**). To test the effect of incubation time on nicotine recovery, we tested a 3 hour nicotine exposure. In this assay, nicotine droplets soaked into the fabric, but the fabric did not fully dry out prior to extraction. 80% of the nicotine was successfully recovered from both cotton and polyester when the incubation was only 3 hours indicating that the time on fabrics and dryness of the fabrics influences extractability of nicotine (**Fig. 5F**). In a third experiment, droplets containing nicotine were added to fabrics which were maintained in a humid environment for 24 hours before extraction. An average of 8 mg of nicotine were recovered from both the cotton and polyester that were

incubated in high humidity (**Fig.5F**), indicating that extraction efficiency of nicotine is also dependent on ambient humidity.

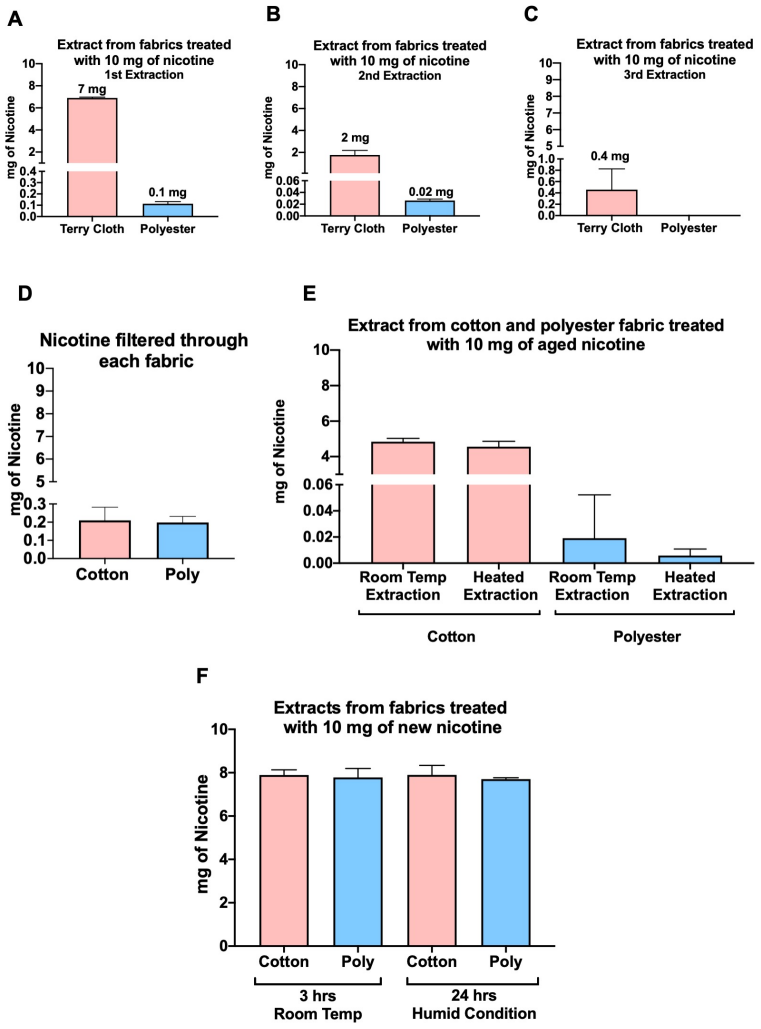

Figure 5. Nicotine extraction was more efficient from polyester when fabrics were exposed in humid conditions. 10 mg of nicotine were placed on cotton or polyester, and 24 hours later nicotine was extracted in water. (A-C) Most nicotine (7 of 10 mg) was recovered in the first extract of terry cloth, while only 0.11 mg were recovered from polyester. (D) Nicotine did not filter through either of the fabrics. (E) Heating did not improve the release of nicotine from cotton or polyester. (F) About 80% of the nicotine was recovered from both cotton and polyester when exposure was done for 3 hours at room temp or for 24 hours in humid conditions.

Discussion

Proper assessment and remediation of THS is necessary to reduce exposure for people who can't move out of THS-contaminated housing. Here we describe a rapid autofluorescence method that can be used to evaluate changes in the THS content of common household fabric. We have taken advantage of the autofluorescence associated with tobacco tar and total particulate matter (Paszkiewicz *et al*., 2008; Pauly *et al.,* 1995) to develop a rapid assay for quantitatively evaluating THS contamination. Many research facilities have fluorescent spectrometers and the sample processing, instrument reading and data analysis time is far shorter than for assays that quantify specific chemicals. We demonstrated an increase in autofluorescence intensity with increased accumulation of THS in fabrics (Fig 2). A linear relationship was observed between the length of time that cotton and terry cloth were exposed to THS and fluorescent intensity in culture medium and PBS extracts. However, extraction of terry cloth with DMSO produced non-linear results, perhaps because DMSO removed chemical surface treatments, such as fire retardant, that interfered with THS evaluation. It is also possible that the loose weave of the terry cloth tended to dissociate more readily in DMSO than the upholstery cotton. In PBS extracts, results were reproducible, with little variation between extractions of the same fabric, as shown by the small standard deviations (Fig 3A). This assay proved to be a quick, reproducible, and inexpensive method to evaluate THS chemicals in aqueous extracts and a valuable tool to compare or normalize THS extracts

between different experiments, batches, or labs. Being able to rapidly compare THS levels in different fabrics or in different labs is currently a hurdle, which may be overcome by taking advantage of this autofluorescence assay.

Autofluorescence was also used to gain insight into THS absorption to and desorption from cotton, terry cloth, polyester, and wool carpet. Most THS residue was removed from terry cloth after one extraction (Fig 3). Only cotton and terry cloth extracts had a progressive increase in fluorescent intensity with increased length of exposure; however, a significant increase in THS recovery from polyester and wool was obtained by heating during extraction. Previous studies have concluded that polyester fabric does not absorb THS (Petrick *et al.,* 2010; Noble *et al.,* 2000; Cheng *et al*., 2016; Saini *et al.*, 2016). However, these studies tested THS extraction using aqueous media without heat or by analyzing off-gas chemicals from smoked exposed fabrics (Saini *et al.*, 2016; Petrick *et al.*, 2010; Chien *et al.,* 2011). Without heat, aqueous extraction and chemical off-gassing might not give complete information on polyester absorption/desorption dynamics. Other studies have shown that polyester fibers gain less weight than cotton when exposed to smoke for 15 minutes (Noble *et al.,* 2000, Cheng *et al.*, 2016), which is consistent with our data showing that even after heated extractions, cotton extracts had higher levels of fluorescence than polyester (Fig 3).

Our chemical analysis of THS extracts showed that absorption and desorption are chemical and fabric dependent. In agreement with our fluorescent

analysis and prior study on THS (Bahl *et al.*, 2014), cotton and terry cloth released higher concentrations of nicotine than polyester and wool carpet. However, nicotine did not increase linearly over time. The lower-than-expected concentrations of these chemicals in the 18-month samples may be due to several factors. First, nicotine can react with atmospheric pollutants, such as ozone and nitrous acid (Destaillats *et al.*, 2006; Sleiman *et al*., 2010b), which would lower its concentration in the fabric. Secondly, nicotine can desorb from cotton, as shown by off gassing analysis (Destaillats *et al.*, 2006). Even though some THS nicotine is likely desorbed and may be chemically converted during aging, microgram concentrations were retained over 18 months. Similar retention of nicotine has been reported in field sites where nicotine was found in smoker's homes that had been vacant for over 2 months (Matt *et al.*, 2011b).

Like nicotine, myosmine and nicotelline did not increase linearly in cotton extracts but did in terry cloth, suggesting that desorption/conversion of chemicals is fabric dependent. Characteristics of the cotton and terry cloth fabric, such as stain release and anti-wrinkle treatments, may have contributed to the lack of linear accumulation of myosmine and nicotelline (Fig. 4). These characteristics affect in the off-gassing of volatile organic chemicals in fabrics exposed for 15 minutes to cigarette smoke (Chien *et al.*, 2011).

Unlike most chemicals, nicotelline and n-formylnornicotine were extracted from polyester in concentrations similar to those seen in cotton and terry cloth. For nicotelline, polyester was the only fabric extract with detectable

concentrations in the 1-month sample. These findings show that: (1) some THS alkaloids, such as nicotine and myosmine, turn over during aging of THS either by desorption or chemical conversion, (2) the turnover of myosmine varied with the type of fabric (cotton vs terry cloth) and (3) some chemicals are readily released from polyester but not from other fabrics (e.g., nicotelline and N-formyl-nornicotine).

The nitrosamines, NNN and NNK, but not NNA, showed linear accumulation over 18 months. While NNN and NNK can remain stable overtime, up to 50% of NNA can be lost within the first 2 hours after smoking (Sleiman *et al.,* 2010b). Our fabrics were exposed for months allowing off-gassing or chemical reactions of NNA from THS over time. For polyester and carpet, there was little accumulation over time in the extracts, perhaps because TSNAs cannot be extracted from these fabrics or because they are desorbed more readily (Fig. 4 G-I). This analysis suggests THS chemicals can be absorbed and desorbed at different rates and fabrics play a crucial role in how THS can is desorbed.

Our data show that THS can accumulate in household fabrics over time and support the idea that remediation of the affected surfaces is important to prevent adverse health effects. The Margin of Exposure (MOE) can be used to predict the possibility of cancer developing with prolonged exposure of a toddler to NNK. When a chemical has a MOE < 10,000, the risk of developing cancer increases (Barlow *et al.,* 2006; Cunningham *et al.,* 2011). Based on 1 hour of mouthing 5 grams of cotton fabric exposed to approximately 362 cigarettes for 18

months, a toddler weighting 2.3 kg could be exposed to 0.00016mg/kg body weight/day of NNK. Using the BMLD (benchmark dose lower limit) of 0.0052 mg/kg day for NNK (Naufal *et al*., 2009), MOE can be calculated as MOE = BMDL / Estimated Exposure Dose (EFSA, 2006). The MOE for a toddler exposed to 0.00016mg/kg body weight/day of NNK is 32. This value, which is well below the threshold of 10,000, indicates that chronic exposure to 0.00016 mg of NNA/kg body weight/day carries with it a risk of developing cancer in the future.

Our data also underrepresent a real environmental THS exposure. The average smoker consumes 14 cigarettes a day (CDC,2018). or 7560 cigarettes in 18-months versus the ~ 362 cigarettes used in our 18-month exposed fabrics. In 0.1g of cotton fabric exposed for 18 months, we recovered 8 ng of NNK. If the same fabric is exposed to 7,560 cigarettes, THS could accumulate ~160 ng of NNK/ 0.1g of fabric. Accumulation of THS can occur over many years, which would further increase these numbers. TSNA levels found in dust collected in smokers' houses have exceeded the lifetime cancer risk recommended by the WHO (Ramirez *et al.,* 2014). Our data support the idea that protect non-smokers from TSNAs and other toxicants, remediation methods need to be implemented that are tailored to each fabric.

To further understand differences in the binding affinity of chemicals to cotton, terry cloth and polyester, all fabrics were exposed to known amounts of nicotine (10 mg/mL) prior to extraction. Nicotine recovery from polyester after a

24 h room temperature incubation was minimal compared to cotton and terry cloth (Fig 5 A-B). Although nicotine was completely absorbed by polyester, aqueous extraction did not efficiently remove it. When polyester was treated with nicotine in a container with high humidity for 24 hrs, 89% of nicotine was recovered (Fig. 5 F). Equivalent nicotine concentrations were also recovered from cotton and polyester after treating fabrics with nicotine for 3 hrs (Fig.5 F). Clearly, nicotine was absorbed by polyester, but once the fabric was well dried, nicotine became tightly bound and extraction was difficult. This phenomenon could also be true for other THS chemicals, which can be absorbed by polyester but under dry conditions, they bind tightly and cannot be easily desorbed. THS may be more extractable from nonpolar fabrics like polyester in geographic regions with high humidity, such as Florida.

Conclusion

We demonstrate that: (1) autofluorescence is an inexpensive, one-step method to quantify THS, and (2) absorption and desorption of THS chemicals depends on the chemical of interest, the fabric that it has sorbed to, the temperature of extraction, the time on the fabric, and the ambient humidity during sorption. THS absorption to fabrics increased with increasing exposure. THS and its associated chemicals were readily extracted from cotton and terry cloth into aqueous media. For polyester, extraction of most chemicals was not efficient unless fabrics were heated or maintained in a humid environment. In contrast with other chemicals, nicotelline was recovered in aqueous extracts of polyester using standard

extraction protocols. Our simple, rapid autofluorescence method can be used to compare and normalize THS concentrations in different batches, laboratories, and field sites. In experimental work and remediation, the extraction of THS chemicals is dependent on the chemicals per se, fabric type, heat, and humidity. Understanding the dynamics of THS in fabrics can help set up appropriate remediation policies to protect humans from exposure.

References

1. Adhami, N., Starck, S.R., Flores, C., Martins Green, M. 2016. A health threat to bystanders living in the homes of smokers: How smoke toxins deposited on surfaces can cause insulin resistance. PLoS ONE. 11(3):e0149510.

2. Bahl, V., Jacob III, P., Havel, C., Schick, S.F., Talbot, P. 2014. Thirdhand cigarette smoke: Factors affecting exposure and remediation. PLoS ONE. 9(10):e108258.

3. Bahl, V., Johnson, K., Phandthong, R., Zahedi, A., Schick, S.F., Talbot, P. 2016a. Thirdhand cigarette smoke causes stress-induced mitochondrial hyperfusion and alters the transcriptional profile of stem cells. *Toxicological Sciences*.153(1):55–69.

4. Bahl, V., Shim, H.J., Jacob III, P., Dias, K., Schick, S.F., Talbot, P. 2016b. Thirdhand smoke: Chemical dynamics, cytotoxicity, and genotoxicity in outdoor and indoor environments. *Toxicology in Vitro*. 32:220–231.

5. Bahl, V., Weng, N.J.H., Schick, S.F., Sleiman, M., Whitehead, J., Ibarra, A., Talbot, P. 2016c. Cytotoxicity of thirdhand smoke and identification of acrolein as a volatile thirdhand smoke chemical that inhibits cell proliferation. *Toxicological Sciences*.150(1):234–246.

6. Barlow, S., Renwick, A.G., Kleiner, J., Bridges, J.W., Busk, L., Dybing, E., Edler, L., Eisenbrand, G., Fink-Gremmels, J., Knaap, A., Kroes, R., Liem, D., Müller, D.J., Page, S., Rolland, V., Schlatter, J., Tritscher, A., Tueting, W., Würtzen, G. 2006. Risk assessment of substances that are both genotoxic and carcinogenic report of an International Conference organized by EFSA and WHO with support of ILSI Europe. *Food and Chemical Toxicology*. 44(10):1636-50.

7. CDC (Centers for Disease Control and Prevention)**.** 2018**.** Smoking is down, but almost 38 million American adults still smoke**.** https://www.cdc.gov/media/releases/2018/p0118-smoking-rates-declining.html. Available: Accessed 30 November 2020.

8. Cheng, C-Y., Huan S-S., Yan C-M., Tang, K-T., Yao, D-J. 2016. Detection of third-hand smoke on clothing fibers with a surface acoustic wave gas sensor. *Biomicrofluidics*.10: 011907-1. doi: 10.1063/1.4939941

9. Chien, Y.C., Chang, C.P., Liu, Z.Z. 2011. Volatile organics off-gassed among tobacco-exposed clothing fabrics. *Journal of Hazardous Material.*193:139-148.

10. Cunningham, F.H., Fiebelkorn, S., Johnson, M., Meredith, C. 2011. A novel application of the Margin of Exposure approach: Segregation of tobacco smoke toxicants. *Food and Chemical Toxicology*. 49:2921–2933.

11. Davis, B., Dang, M., Kim, J., Talbot P. 2015. Nicotine Concentrations in Electronic Cigarette Refill and Do-It-Yourself Fluids. *Nicotine & Tobacco Research*.17(2):134-141 doi:10.1093/ntr/ntu080

12. Destaillats, H., Singer, B.C., Lee, S.K., Gundel, L.A. 2006. The effect of ozone on nicotine desorption from model surfaces: evidence for heterogeneous chemistry. *Environmental Science and Technologies*. 40(6):1799–1805.

13. EFSA. 2006. EFSA meeting summary report: EFSA/WHO International Conference with support of ILSI Europe on risk assessment of compounds that are both genotoxic and carcinogenic. 16 -18 November 2005, Brussels (pp. 290)

14. Ferrante, G., Simoni, M., Cibella, F., Ferrara, F., Liotta, Malizia, V., Corsello, G., Viegi, G., La Crutta, S. 2013. Third-hand smoke exposure and health hazards in children. *Monaldi Archives for Chest Disease*. 79(1): 38-43.

15. Hang, B., Sarker, A.H., Havel, C., Saha, S., Hazra, T.K., Schick, S., Jacob III., P., Rehan, V.K., Chenna, A., Sharan, D., Sleiman, M., Destaillats, H., Gundel, L.A. 2013. Thirdhand smoke causes DNA damage in human cells. *Mutagenesis*. 28: 381-391

16. Jacob, P., Benowitz, N.L., Destaillats, H., Gundel, L., Hang, B., Martins-Green, M., Matt, G.E., Quintana, P.J.E., Samet, J.M., Schick, S.F., Talbot, P., Aquilina, N.J., Hovell, M.F., Mao, J.H., Whitehead, T.P., 2017. Thirdhand smoke: new evidence, challenges, and future directions. *Chemical Research in Toxicology*. 30(1): 270–294.

17. Jung, J.W., Ju, Y.S., Kang, H.R. 2012.Association between paternal smoking behavior and children's respiratory morbidity: 5 year study inn an urban city of South Korea. *Pediatric Pulmonology*. 47:338-345.

18. Martins-Green, M., Adhami, N., Frankos, M., Valdez, M., Goodwin, B., Lyubovitsky, J., Dhall, S., Garcia, M., Egiebor, I., Martinez, B., Green, H. W.,Havel, C., Yu, L., , Liles, S., Matt, G., Destaillats, H., Sleiman, M., Gundel, L.A., Benowitz, N., Jacob III, P., Hovell, M., Winickoff, J.P., Curras-Collazo, M. 2014 Cigarette Smoke Toxins Deposited on Surfaces: Implications for Human Health. *PLoS ONE*. 9(1): e86391.

19. Matt, G.E., Quintana, P.J.E., Destaillats, H., Gundel, L.A., Sleiman, M., Singer, B.C., Jacob, P., Benowitz, N., Winickoff, J.P., Rehan, V., Talbot, P., Schick, S., Samet, J., Wang, Y., Hang, B., Martins-Green, M., Pankow, J.F., Hovell, M.F. 2011a. Thirdhand tobacco smoke: emerging evidence and arguments for a multidisciplinary research agenda. *Environmental Health Perspectives*. 119(9):1218–1226.

20. Matt, G.E., Quintana, P.J., Hovell, M.F., Bernert, J.T., Song, S., Novianti, N., Juarez, T., Floro, J, Gehrman, C., Garcia, M., Larson, S. 2004. Households contaminated by environmental tobacco smoke: sources of infant exposures. *Tobacco Control.*13:29–37.

21. Matt, G.E., Quintana, P.J., Hovell, M.F., Chatfield, D., Ma, D.S., Romero, R., Uribe, A. 2008. Residual tobacco smoke pollution in used cars for sale: air, dust, and surfaces. *Nicotine & Tobacco Research.* 10(9):1467–1475.

22. Matt, G.E., Quintana, P.J., Zakarian, J.M., Fortmann AL, Chatfield DA, Hoh E, Uribe, A.M., Hovell, M.F. 2011b. When smokers move out and nonsmokers move in: residential thirdhand smoke pollution and exposure. *Tobacco Control*. 20:e1.

23. Naufal, Z., Kathman, C., Wilson, C. 2009. Bayesian derivation of an oral cancer slope factor distribution for 4-(methylnitrosamino)-1-(3-pyridyl)-1-butanone (NNK). *Regulatory Toxicology and Pharmacology.* 55: 69–75.

24. Noble, R.E. 2000. Environmental tobacco smoke uptake by clothing fabrics. *The science of the total environment*. 262(1-2):1-3.

25. Northrup, T., Khan, A.M., Jacob III, P., Benowitz, N.L.,Hoh, E., Hovell, M.F., Matt, G.E., Stotts, A.L. 2016.Thirdhand smoke contamination in hospital settings: Assessing exposure risk for vulnerable pediatric patients. *Tobacco Control*. 25(6):619–623.

26. Paszkiewick, G.M., Pauly, J.L. 2008. Spectrofluorometric method for measuring tobacco smoke particulate matter on cigarette filters and Cambridge pads. *Tobacco Control*. 17(Suppl I):i53–i58.

27. Pauly, J.L., Allaart, H.A., Rodriguez, M.I., Streck, R.J. 1995. Fibers released from cigarette filters: an additional health risk to the smoker? *Cancer Research*. 55: 253-258.

28. Petrick, L., Destaillats, H., Zouev, I., Sabach, S., Dubowski. 2010. Sorption, desorption and surface oxidative fate of nicotine. *Physical Chemistry Chemical Physics*.12:10356–10364.

29. Pozuelos, G.L., Kagda, M.S., Schick, S., Girke, T., Volz, D.C., Talbot, P. 2019 Experimental acute exposure to thirdhand smoke and changes in the human nasal epithelial transcriptome: a randomized clinical trial. *JAMA Network Open*. 2(6):e196362.

30. Ramirez, N., Ozel, M.Z., Lewis, A.C., Marce, R.M., Borrull, F., Hamilton, J.F. 2014. Exposure to nitrosamines in thirdhand tobacco smoke increases cancer risk in non-smokers. *Environment International*. 71:139–147.

31. Saini, A., Rauert, C., Simpson, M.J., Harrad, S., Diamond, M.l. 2016. Characterizing the sorption of polybrominated diphenyl ethers (PBDEs) to cotton and polyester fabrics under controlled conditions. *Science of total environment*. 563–564:99–107.

32. Schick, S. F., and Glantz, S. 2007. Concentrations of the carcinogen 4-(methylnitrosamino)-1-(3-pyridyl)-1-butanone in side- stream cigarette smoke increase after release into indoor air: results from unpublished tobacco industry research. *Cancer Epidemiology, Biomarkers & Prevention.* 16:1547−53.

33. Schick, S.F., Farraro, K.F., Fang, J., Nasari, S., Kim, J., Lucas D., Wong, J., Giles, D.K., Jenkins, B. 2012. An Apparatus for generating aged cigarette smoke for controlled human exposure studies. *Aerosol Science and Technology*. 46:1246–1255.

34. Schick, S.F., Farraro K.F., Perrino, C., Sleiman, M., Van de Vossenberg, G., Trinh, M.P., Hammond, S.K., Jenkins, B.M., Balmes, J. 2014. Thirdhand cigarette smoke in an experimental chamber: evidence of surface deposition of nicotine, nitrosamines and polycyclic aromatic hydrocarbons and de novo formation of NNK. *Tobacco Control*. 23:152-159.

35. Sheu, R., Stonner, C., Ditto, J.C., Klupfel, T., Williams, J., Gentner, D.R. 2020. Human transport of thirdhand tobacco smoke: A prominent source of hazardous air pollutants into indoor nonsmoking environments. *Science Advances.* 6(10):eaay4109.

36. Sleiman, M., Destaillats, H., Smith, J.D., Liu, C., Ahmed, M., Wilson, K.R., Gundel, L.A. 2010a. Secondary organic aerosol formation from ozone-initiated reactions with nicotine and secondhand tobacco smoke. *Atmospheric Environment*. 44:4191-4198.

37. Sleiman, M., Gundel, L.A., Pankow, J.F., Jacob III, P., Singer, B.C., Destaillats, H. 2010b. Formation of carcinogens indoors by surface-mediated reactions of nicotine with nitrous acid, leading to potential thirdhand smoke hazards. *PNAS*. 107(15):6576–6581.

38. Whitehead, T.P., Havel, C., Metayer, C., Benowitz, N.L., Jacob III, P. 2015. Tobacco alkaloids and tobacco-specific nitrosamines in dust from homes of smokeless tobacco users, active smokers, and nontobacco users. *Chemical Research in Toxicology.* 28:1007-14

39. Xu, B., Chen, M., Yao, M., Ji, X., Mao, Z., Tang, W., Qiao, S., Schick, S.F., Mao, J.H., Hang, B., Xia, Y. 2015. Metabolomics reveals metabolic changes inn male reproductive cells exposed to thirdhand smoke. *Scientific Reports.* 5:15512.

Chapter 3

Nicotine Affects Multiple Biological Processes in EpiDerm Organotypic Tissues and Human Keratinocyte Monolayers

Abstract

Dermal exposure to nicotine is common due to the widespread use of tobacco products. Here we assessed the effects of nicotine at concentrations found in thirdhand smoke (THS) contaminated environments and electronic cigarette (EC) spills or leaks on a 3D human skin model (EpiDerm™) and on submerged keratinocyte cultures. Air liquid interface treatment of EpiDerm™ with 10 or 400 µg/mL of nicotine for 24 hours followed by proteomics analysis showed altered pathways related to inflammation, protein synthesis, cell-cell adhesion, apoptosis, and mitochondrial function. Submerged cultured keratinocytes were used to validate the proteomics data and further characterize the response of skin cells to nicotine. Mitochondrial phenotype changed from networked to punctate in keratinocytes treated with 10 or 400 µg/mL of nicotine for 48 hours and 24 hours, respectively. After 72 hours all concentrations of nicotine caused a significant decrease in the networked phenotype. In western blots, keratinocytes exposed to 400 µg/mL of nicotine had a significant decrease in mitofusin 2, while mitofusin 1 decreased after 72 hours. The shift from networked to punctate mitochondria correlated with a decrease in mitofusin 1/2, a protein needed to establish and maintain the networked phenotype. Mitochondrial changes were reversable after a 24-hour recovery period. Peroxisomes exposed to 400 µg/mL of nicotine for 24 hours became enlarged and were fewer in number. Nicotine concentrations in THS and EC spills altered the proteome profile in EpiDerm™ and damaged organelles including mitochondria and peroxisomes, which are

involved in ROS homeostasis. These changes may exacerbate skin infections, inhibit wound healing, and cause oxidative damage to cells in the skin, even after acute exposures.

1. Introduction

The consumption of tobacco products, such as combustible cigarettes and electronic cigarettes (ECs), contributes to environmental contamination by nicotine, a highly addictive chemical that can cause adverse responses in humans (Mishra *et al.*, 2015, Jacob *et al.*, 2017). Nicotine when internalized can be fatal in both adults and children at concentrations of 30-60 mg and 10 mg, respectively (Solario *et al.*, 2010, Tjocke *et al.*, 2020, Mayer et al. 2014). Uptake of nicotine can occur through inhalation, ingestion, or/and dermal contact. Dermal absorption of nicotine has been of interest due to occupational exposure during the harvesting of tobacco leaves (McKnight *et al.*, 2005) and the introduction of nicotine patches (Sorensen *et al.*, 2009). In both these examples, nicotine is readily absorbed through the skin, and in the case of the tobacco harvesters causes nausea, dizziness, and increases in heart rate and blood pressure. In spite of prior work on green tobacco disease and nicotine patches, very little is known about how the skin responds to nicotine at concentrations found in thirdhand smoke (THS) and EC fluids.

THS is the tobacco smoke residue that settles on indoor surfaces or clothing after smoking has stopped. THS may accumulate over long periods of time (Matt *et al.*, 2007, 2011a, 2011b; Jacob *et al.*, 2017) and may react with chemicals, such as HONO, to form carcinogens (Sleiman *et al.*, 2014). Nicotine, which is a dominant chemical in THS (Bahl *et al.*, 2014, 2016; Pozuelos *et al.*, 2021), has been detected on surfaces in smokers' homes and on homes of previous

smokers Matt et al. 2011b. Nicotine in THS can come into contact with the skin when contaminated clothing or surfaces are touched, leading to dermal exposure and uptake. Cotinine, a nicotine metabolite, was detected in the urine of children who live in THS contaminated households Matt et al. 2004. We have previously shown that in humid conditions nicotine is more readily extractible from fabrics, suggesting that exposure to nicotine could be greater in humid environments (Pozuelos et al. 2021).

ECs are nicotine delivery devices, which have gained popularity during the last 10 years. EC fluids (e-fluids) often contain high concentrations of nicotine, for example JUULTM fluids have ~ 60 mg/mL (Omaiye *et al.*, 2019a, Omaiye *et al.*, 2019b, Davis *et al.*, 2015), although many earlier generation products typically had 1-25 mg/mL (Davis *et al.*, 2015). EC users often come into contact with nicotine when handling products, when fluids spill, or when touching surfaces contaminated with ECs fluids or residue (Trtchourian *et al.*, 2010; Garcia *et al.*, 2016; Cantrell *et al.*, 2014; Khachatoorian *et al.*, 2019).. In vitro studies have demonstrated transmembrane absorbance of nicotine from e-liquids (Maina *et al.*, 2017), although its effects have not been characterized. Nicotine exposure from e-liquid spills have been reported in vape shops (Garcia *et al.*, 2016), and significant amounts of nicotine accumulated (4.571 g of nicotine) in a vape shop during a month of monitoring (Khachatoorian *et al.*, 2019). In addition, many EC products are leaky, and users come in contact with nicotine when handling ECs (Cantrell *et al.*, 2014; Khachatoorian *et al.*, 2019).

The purpose of this study was to examine the effect of nicotine on human skin using two in vitro models. First, we exposed EpiDerm™ tissue, a three-dimensional organotypic model of human epidermis, to nicotine at concentrations found in environmental settings (THS contaminated areas, vape shops, and EC fluids) and examined the effect of exposure on the EpiDerm™ proteome. Exposures were done at the air liquid interface (ALI) to replicate exposures humans would receive in field sites or when using ECs. We then used cultured monolayers of human keratinocytes to validate the proteomics data and to study the cellular responses to nicotine in more detail.

Materials and Methods

2.1. EpiDerm™ Treatment with Nicotine

EpiDerm™ (EPI-200) produced by Mat-Tek Corporation (Ashland, MA, USA) was used to analyze the effect of nicotine on a 3D human skin model. EpiDerm™ is a ready-to-use, highly differentiated 3D tissue model consisting of normal, human-derived epidermal keratinocytes grown on tissue culture inserts. EpiDerm™ allows topical application of chemicals at the air liquid interface and is widely used for highly predictive in vitro applications (Casas *et al.*, 2013 Kandárová *et al.*, 2018). EpiDerm™ was shipped on cell culture inserts in agarose. Upon receiving, inserts were removed from the agarose and incubated overnight in 0.9 mL EPI-100-NMM medium at 37 °C, 5% CO2. The following day, the culture medium was exchanged, and the apical surface of the tissues treated with PBS (phosphate buffered saline) only, 10 µg/mL (Nic100) or 400 µg/mL (Nic400) liquid (-)-nicotine (catalog N3876, Sigma-Aldrich, St. Louis, MO) diluted in PBS. A mesh was position on top of the tissue to assure equal distribution of the treatment. Inserts were treated for 24 hrs, after which EpiDerm™ tissues were lysed in 0.25% sodium deoxycholate, 1.0% Nonidet P-40 in Mol Bio H2O, 100 mM triethylamonium bicarbonate (TEAB) with 2mM phenylmethylsulfonyl fluoride (PMSF) and 25 µL of Halt Cocktail.

2.2. Sample Preparation for Proteomics

Samples were analyzed at the UCLA proteomics core. Briefly, EpiDerm™ protein samples were mixed with an equal volume of digestion buffer (8M urea,

0.1M Tris-HCl pH 8.5). Each sample was reduced and alkylated via sequential 20-minute incubation with 5 mM tris(2-carboxyethyl)phosphine (TCEP) and 10 mM iodoacetamide at room temperature in the dark while being mixed at 1200 rpm in an Eppendorf thermomixer. Carboxylate-modified magnetic beads (6 µL) (CMMB) also known as SP3 (Hughes *et al.*, 2014) and ethanol (50% final concentration) were added to each sample to induce protein binding to CMMB beads. CMMB beads were washed 3 times with 80% ethanol and then resuspended with 50 µl 50 mM TEAB. Protein samples were digested overnight in 0.1 µg LysC (Promega) and 0.8 µg trypsin (Pierce) at 37 °C. Following digestion, 1 mL of 100% acetonitrile was added to each sample to increase acetonitrile concentration (>95% final concentration) and induce peptide binding to CMMB beads. CMMBs were washed 3 times with 100% acetonitrile and the peptides eluted with 50 µL of 2% Dimethylsulfoxide (DMSO). Eluted peptide samples were dried by vacuum centrifugation and reconstituted in 5% formic acid before analysis by LC-MS/MS.

2.3 LC-MS Acquisition and Analysis

Samples were analyzed using a Thermo Orbitrap-Fusion Lumos Tribrid mass spectrometer. Peptides were separated in a 75µM ID, 25cm C18 column with 1.9 µM C18 particles (Dr. Maisch GmbH HPLC), with a 140-minute gradient of increasing acetonitrile concentration. MS/MS spectra were acquired using the Data Dependent Acquisition (DDA) mode.

MaxQuant, a quantitative proteomic software, was used for data analysis. The human reference proteome from EMBL (UP000005640_9606 HUMAN Homo sapiens, 20874 entries) was used for protein identification (Jürgen *et al.*, 2012). Statistical analysis of MaxQuant label-free quantitation data was performed with the art MS Bioconductor package (Jimenez-Morales *et al.*, 2019), which performs the relative quantification of protein abundance using the MSstats Bioconductor package (Choi *et al.*, 2014) (default parameters). The abundance of proteins missing from one condition but found in more than two biological replicates of the other condition for any given comparison were estimated by imputing intensity values from the lowest observed MS1-intensity across samples (Webb-Robertson *et al.*, 2015) and p-values were randomly assigned to those between 0.05 and 0.01 for illustration purposes. A p-value cut-off of 0.05 or less and an absolute log2 fold-change of 0.1 or greater were used to identify significant proteins.

2.4. Keratinocyte Culturing

A Keratinocyte transformed cell line (ATCC® CRL-2309TM) was cultured in poly-L-lysine coated flasks using keratinocytes-serum free medium (GIBCO 17005-042) with added keratinocyte supplements (Gibco 37000-015) and Bovine Pituitary Extract (BPE; Gibco 13028-014). Cells were cultured in a 37°C/5% CO2/95% relative humidity incubator for 24 to 48 hours before processing the cells for experiments. In experiments, keratinocytes were dispersed into single cells and seeded at a density of 100,000 cells/well in an Ibidi µ-Slide 8 Well

(#80826, IbidiGmbH, Gräfelfing, Germany). Cells were counted using a hemocytometer.

2.5 Cell Transfection

Keratinocytes were transiently transfected with sfGFP-Peroxisomes-2 (Plasmid #54601) and pMitoTimer (Plasmid #52659) purchased from Addgene (Cambridge, MA USA). Cells were transfected using a NEPA21 electron-kinetic transfection system (Bulldog bio). Briefly, 106 cells were electroporated with 10 µg/mL of sfGFP-Peroxisomes-2 and pMitoTimer. After transfection cells were distributed equally into Ibidi chamber slides in keratinocytes-serum free medium (GIBCO 17005-042) with added keratinocyte supplements (Gibco 37000-015) and Bovine Pituitary Extract (BPE; Gibco 13028-014). Cells re-covered for 48 hours prior to nicotine treatment.

2.6. Mitochondrial morphology analysis

Keratinocytes, transfected with pMitoTimer (Plasmid #52659) were treated with 10 µg/mL (Nic10) , 100 µg/mL (Nic100), 400 µg/mL (Nic400) of nicotine for 24, 48, and 72 hours prior to live cell imaging. Each cell was classified manually into three different clusters based on mitochondrial morphology. Cells with mitochondrial networks and at least 60 punctate mitochondria were categorized as “network”; cells with mitochondrial networks and more than 60 punctate mitochondria were classified as “network and punctate”; cells with only punctate and swollen mitochondria were classified as “punctate and swollen”.

2.7. Peroxisome morphology analysis

Keratinocytes after transfection with sfGFP-Peroxisomes-2 (Plasmid #54601) were treated with Nic10, Nic100, Nic400 of nicotine for 24 hours. Peroxisome image analysis was performed manually using ImageJ (Abramoff et al. 2004). Each peroxisome was traced using ImageJ to acquire peroxisome total area and the number of peroxisomes per cell (Abramoff et al. 2004).

2.8. Fluorescence Microscopy

Live cell imaging was performed using an Eclipse Ti microscope (Nikon Instruments, Melville, NY) using a 60X objective. Images were captured with a high-resolution Andor Zyla VSC-04941 camera (Andor, Belfast, UK). For live cell imaging, cells were maintained in a humidity-regulated incubation chamber (Pathology Devices Inc., San Diego, CA USA) at 37oC, 5% CO2, and 90% relative humidity.

2.9. Western Blot

Keratinocytes were plated at a concentration of 100,000 cells/well of a 6 well plate. Cells were attached for 24 hours prior to treatment with Nic10, Nic100, Nic400. After treatment, plates were placed on ice, washed with PBS to remove medium reside and 100 µL of RIPA (Radio-Immunoprecipitation Assay) buffer with protease inhibitor cocktails (ChemCruz, Dallas, TX, USA) was added to each well. The cells were scraped using a plastic cell scraper, collected and incubated at 30 min at 4°C on a plate shaker. The cells were spun at 16,000 x g for 15 min in a 4°C pre-cooled centrifuge, and the supernatant was transferred to

a fresh tube kept on ice. Protein concentration was performed using the Pierce BCA assay (Thermo Fisher Scientific, Waltham, MA). Laemmli buffer (Bio-Rad, Hercules, CA) was added to 10 µg of each sample and boiled at 95°C for 5 min. Samples were loaded on a Mini-PROTEAN TGX Precast SDS-PAGE gel (Bio-Rad, Hercules, CA USA) with molecular weight markers. The gel was run at 100 volts on the Bio-Rad Powerpac Basic power supply (Bio-Rad, Hercules, CA. Proteins were transferred to a PVDF membrane (Bio-Rad, Hercules, CA) overnight at 150 mAmps. The following day, the membrane was blocked in 5% milk in Tween in tris-buffered saline (TBST) for 30 min at room temperature. Membranes were washed 3x prior to adding the primary anti-bodies. Primary antibodies (Cell Signaling, Danvers, MA), of mitofusin 1 (D6E2S) mitofusin 2 (D2D10) and Glyceraldehyde-3-Phosphate Dehydrogenase (GAPDH) (14C10) (Cell Signaling, Danvers, MA) were diluted in 3% albumin in TBST separately. GAPDH was used as a loading control. Each individual antibody was added to their corresponding membranes and incubated at 4oC overnight. The membranes were washed and incubated with HRP-conjugated anti-rabbit secondary antibodies diluted in 5% milk in TBST (Tris-buffered saline, 0.1% Tween 20) for 2 hours at room temperature. The protein bands were imaged using Clarity Western ECL substrate (Bio- Rad, Hercules, CA).

3. Results

3.1. Proteomics Analysis of EpiDerm™ Treated with Nic10 or Nic400

Volcano plots show the differentially expressed proteins for the two comparisons (Nic10 vs PBS and Nic400 vs PBS) (Figure 1 A, B). In the Nic10 vs PBS set, a total of 352 proteins were significantly affected (206 upregulated and 146 downregulated) (Figure. 1A). In the Nic400 vs PBS set, a total of 313 proteins were significantly affected (150 up-regulated and 163 downregulated) (Figure 1B). There were 110 proteins that overlapped in the Nic10 vs PBS and Nic400 vs PBS sets (Figure 1C). Figure 1D shows the number of proteins that were up and downregulated in the Nic10 and Nic400 groups. When separated into up and down regulated proteins, there were 50 overlapping proteins for downregulated and 56 for upregulated (Figure 1D).

3.2. Canonical pathways affected in nicotine treated EpiDerm™

The Nic10 vs PBS set pathways with positive activated z-scores included “Protein Synthase Related Pathways” (EIF2 Signaling) and “Mitochondrial Related Pathway” (oxidative phosphorylation) (Table 1). Pathways with negative z-scores included “Apoptosis Related Pathways” (apoptosis signaling, induction of apoptosis by HIV1, TNFR1 signaling), “Cell-Cell Adhesion Related Pathway” (ILK signaling), and “Immune Related Pathways” (role of MAPK signaling in promoting the pathogenesis of influenza, IL-6 signaling, and IL-1 signaling, LPS-stimulated MAPK signaling, IL-15 production, IL-8 signaling) (Table 2).

In the Nic400 vs PBS set, pathways included “Protein Synthesis Related Pathway” (EIF2 signaling), which had a positive z score (Table 3). Pathways with negative z scores included “immune Related Pathways” (IL-1 signaling, ERK/MAPK signaling, MIF-mediated glucocorticoid regulation, MIF regulation of innate immunity), and “Apoptosis Related Pathway” (death receptor signaling) (Table 4).

Table 1: IPA Canonical Pathways for the 10 µg/mL of Nicotine vs PBS

Canonical Pathways	-log(p-value)	z-score	Proteins
Protein Synthesis Related Pathway			
EIF2 Signaling	19.2	2.53	EIF1, EIF3C, EIF3D, EIF3L, EIF4A2, MAP2K1, PTBP1, RPL15, RPL18A, RPL19, RPL24, RPL30, RPL38, RPL5, RPL6, RPL7A, RPS11, RPS13, RPS17, RPS2, RPS21, RPS24, RPS26, RPS3, RPS4X, RPS4Y2, RPS8, RPS9, RPSA
0xidative Stress Related Pathway			
Oxidative Phosphorylation	4.39	1	MT-ATP6, NDUFA4, NDUFB5, NDUFB8, NDUFS1, NDUFS6, UQCRC1, UQCRC2, UQCRQ

Table 2: Canonical Pathways for the 10 µg/mL of Nicotine vs PBS with Negative z-scores

Canonical Pathways	-log(p-value)	z-score	Proteins
Apoptosis related pathways			
Apoptosis Signaling	3.27	-0.378	BAX, CASP7, CASP8, LMNA, MAP2K1, NFKBIB, RELA
Induction of Apoptosis by HIV1	2.73	-1.342	BAX, CASP8, FADD, NFKBIB, RELA
TNFR1 Signaling	3.17	-2.236	CASP7, CASP8, FADD, NFKBIB, RELA
Cell-cell adhesion related pathways			
ILK Signaling	2.22	-1.342	DSP, GSK3A, ITGB4, KRT18, MTOR, RAC2, RELA, TMSB10/TMSB4X
Immune related Pathways			
Role of MAPK Signaling in Promoting the Pathogenesis of Influenza	1.68	-0.447	ATP6V1C1, BAX, MAP2K1, MAP2K3, NFKBIB
IL-6 Signaling	2.1	-0.816	IL36B, MAP2K1, MAP2K3, NFKBIB, RELA, TAB1
IL-1 Signaling	1.34	-1	MAP2K3, NFKBIB, RELA, TAB1
LPS-stimulated MAPK Signaling	1.55	-1	MAP2K1, MAP2K3, NFKBIB, RELA
IL-15 Production	1.59	-1.342	CSK, MAP2K1, MAP2K3, PTK2B, RELA
IL-8 Signaling	2.04	-1.89	BAX, EIF4EBP1, MAP2K1, MTOR, NFKBIB, PTK2B, RAC2, RELA

Table 3: Canonical Pathways for the 400 µg/mL of Nicotine vs PBS with Positive z- scores

	-log(p-value)	z-score	Proteins
Protein Synthesis Related Pathway			
EIF2 Signaling	6.91	2	EIF1, EIF2B2, EIF2S2, EIF3M, EIF4A2, PTBP1, RPL18A, RPL38, RPS12, RPS15, RPS24, RPS26, RPS3, RPS4X, RRAS2

Table 4: Canonical Pathways for the 400 µg/mL of Nicotine vs PBS with Negative z- scores

Ingenuity Canonical Pathways	-log(p-value)	z-score	Molecules
Immune related pathways			
IL-1 Signaling	2.15	-0.447	MAP2K3, NFKBIB, PRKAR1A, RELA, TAB1
ERK/MAPK Signaling	2.29	-0.707	PAK1, PLA2G4A, PLA2G4D, PPP2R5A, PRKAR1A, PRKCI, PTK2B, RRAS2
MIF-mediated Glucocorticoid Regulation	4.05	-1.342	MIF, NFKBIB, PLA2G4A, PLA2G4D, RELA
MIF Regulation of Innate Immunity	3.6	-1.342	MIF, NFKBIB, PLA2G4A, PLA2G4D, RELA
Apoptosis related Pathways			
Death Receptor Signaling	1.54	-1	ARHGDIB, CASP8, NFKBIB, RELA

3.3. IPA Toxicity analysis

Because treatment involved nicotine, a chemical with potentially harmful effects, a toxicological analysis was also performed using IPA (Table 5). The IPA toxicity list for the Nic10 vs PBS set included terms consistent with “Mitochondrial Dysfunction” and “Oxidative Stress”. The majority of the upregulated proteins associated with “Mitochondria Dysfunction” were part of the protein complexes in the electron transport chain (NDUFA8, NDUFA9, NDUFB8, NDUFS1, NDUFS6, UQCRC1, UQCRC2), suggesting increased ATP synthesis, which could lead to increased oxidative stress. Only two proteins (MFN1, PKM) were involved in the “Decreases Respiration of Mitochondria”. Proteins involved in “Increases Transmembrane Potential of Mitochondria” and Mitochondrial Membrane” were downregulated (BAX, CASP7, DNAJB1). Proteins involved in apoptosis were down regulated (BAX, CASP7, CASP8), suggesting an anti-apoptosis response to nicotine treatment.

The IPA toxicity list for the Nic400 vs PBS set was similar to the lower concentration (NIC10) in that it included terms related to “Mitochondrial Dysfunction” and “Oxidative Stress” (Table 5). Additional terms that appeared with the higher nicotine concentration were related to “PXP/RXR Activation”, “Hypoxia-inducible Factor Signaling”, “Aryl Hydrocarbon Receptor Signaling”, “Cholesterol Biosynthesis”, and “LXR/RxR Activation”.

Table 5: Toxicity Lists for the 10 µg/mL of Nicotine vs PBS comparison

IPA Toxicity Lists	-log(p-value)	Proteins
Mitochondrial Dysfunction	5.41	CASP8, CPT1A, MT-ATP6, NDUFA4, NDUFB5, NDUFB8, NDUFS1, NDUFS6, PARK7, UQCRC1, UQCRC2, UQCRQ
NRF2-mediated Oxidative Stress Response	2.27	AKR1A1, BACH1, DNAJB1, DNAJB11, DNAJB2, DNAJC11, DNAJC5, MAP2K1, MAP2K3
Decreases Respiration of Mitochondria	1.83	MFN1, PKM
Pro-Apoptosis	1.72	BAX, CASP7, CASP8
Increases Transmembrane Potential of Mitochondria and Mitochondrial Membrane	1.52	BAX, CASP7, DNAJB1
Mechanism of Gene Regulation by Peroxisome Proliferators via PPARα	1.4	MAP2K1, NFKBIB, RELA, TAB1

Table 5: Toxicity Lists for the 400 µg/mL of Nicotine vs PBS comparison

IPA Toxicity Lists	-log(p-value)	Proteins
Mitochondrial Dysfunction	4.34	CASP8, COX7A2, COX7C, NDUFA4, NDUFA8, NDUFA9, NDUFB5,NDUFS1, TXN2, UQCRQ
PXR/RXR Activation	2.95	GSTM2, PCK2, PRKAR1A, RELA, SCD
NRF2-mediated Oxidative Stress Response	2.59	AKR1A1, BACH1, CDC34, DNAJC13,DNAJC5, GSTM2, MAP2K3, PRKCI, RRAS2
Mechanism of Gene Regulation by Peroxisome Proliferators via PPARα	2.23	FAT1,NFKBIB,PRKAR1A,RELA,TAB1
Decreases Depolarization of Mitochondria and Mitochondrial Membrane	2.07	PAK1, PLA2G4A, PPIA
Hypoxia-Inducible Factor Signaling	1.99	EIF1, EIF2B2, EIF2S2, UBE2N
RAR Activation	1.91	PRKAR1A, PRKCI, PRMT1, RDH12, RELA,SDR16C5, SMARCC2
Aryl Hydrocarbon Receptor Signaling	1.87	ALDH3A1, CDKN2A, CTSD, GSTM2, NEDD8, RELA
Cholesterol Biosynthesis	1.81	IDI1, SQLE
LXR/RXR Activation	1.77	ACACA, IL36B, PLTP, RELA, SCD
Oxidative Stress	1.5	GSTM2, RELA, S100A7

3.4. IPA Regulator Effect Analysis for the NIC10 vs PBS Set

The top regulator effect network, shown in Figure S1, shows four predicted upstream regulators (IgG, SFN, CCN5, ESRRA) based on nine altered proteins in our data that lead to activation of “Survival of Organism” (Figure S1). Regulatory effects were not identified in the 400 µg/mL of nicotine treatment vs PBS comparison. The proteomics data collected using nicotine treated EpiDerm™ suggested that nicotine has stressed the EpiDerm™ and activated survival or stress responses without killing cells or inducing apoptosis.

3.5 Nicotine Alters Mitochondrial Morphology in Human Keratinocytes

Based on the IPA canonical pathways and toxicity lists, mitochondria were identified as targets of nicotine at both treatment concentrations. Mitochondrial morphology was further assessed in vitro using human keratinocytes transfected with the Mitotimer plasmid that specifically labels mitochondria and enables mitochondrial morphology to be evaluated (Figure 2 A-L). Mitochondria in control cells were generally elongated networks (Figures 2 A-C), while cells in treated groups appeared to have more punctate mitochondria, which were sometimes swollen (Figure 2D-L).

Mitochondrial phenotypes were quantified in each group (Figures 2 M-O). In keratinocytes treated with Nic400 for 24, 48, or 72 hours, there was a decrease in the percent of mitochondria with “network” morphology at all times and a corresponding increase in the percent with “network and punctate” (24 hours) and “punctate and swollen” (48 and 72 hours) (Figures 2 J-O). In the Nic10

treated group, “network” morphology decreased (48 and 72 hours) and “network and punctate” morphology in-creased (48 hours). In the Nic100 treated group, network morphology decreased following the 48 and 72 hour treatments. These data show that nicotine induces a progressive time and dose dependent transition from mainly networked mitochondria to the punctate and swollen form.

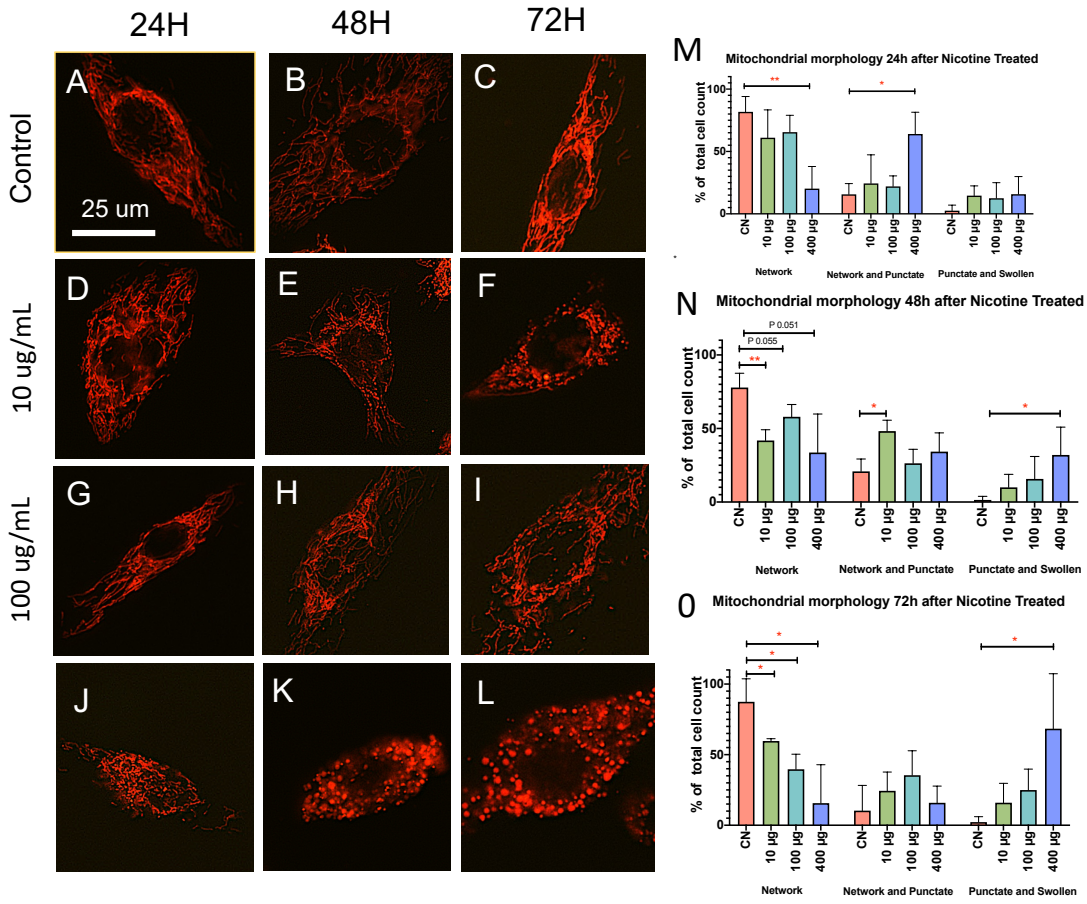

Figure 2. Mitochondria in Keratinocytes Treated with 10 (Nic10), 100 (Nic100), or 400 (Nic400) µg/mL of Nicotine for 24, 48, and 72 Hours. (A-L) Micrographs of mitochondria treated with various concentrations of nicotine and imaged at different times. (M) Mitochondrial morphology 24 after nicotine treatment. (N) Mitochondrial morphology 48h after nicotine treatment. (O) Mitochondrial morphology 72h after nicotine treatment. CN = Control Medium. All data are means ± the standard error of the mean for three independent experiments. * = $p < 0.05$, ** = $p < 0.01$

3.6. Mitofusin 1/2 Decreased in Keratinocytes Treated with Nic400

Mitochondria normally undergo cyclic fusion and fission, which are regulated by the mitofusins 1 and 2 (Chen et al. 2003). The previous experiment suggested that nicotine impaired mitochondrial fusion, which would favor an increase in the punctate form. We tested the hypothesis that nicotine suppressed the expression of mitofusins 1/2 using western blotting. Mitofusin 1 levels decreased after 72 hours in the Nic400 group (Figure 3 A-C). Mitofusin 2 levels significantly decreased in the Nic400 group at all exposure times (Figure 2 D-F).

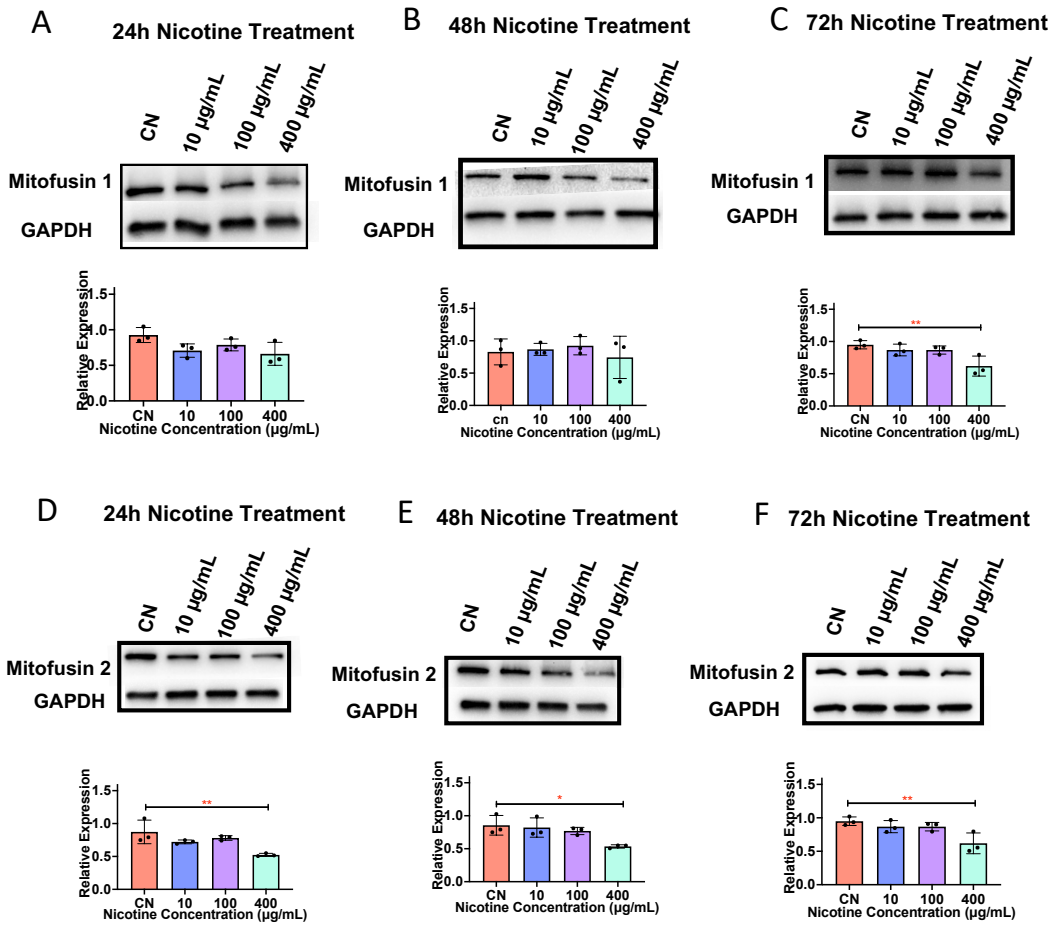

Figure 3. Mitofusin 1/2 Protein Expression in Keratinocytes after Nicotine Treatment. Mitofusin 1 protein expression in western blots after 24 hours (A), 48 hours (B), and 72 hours (C) of nicotine treatment. Mitofusin 2 protein expression in west-ern blots after 24 hours (D), 48 hours (E), and 72 hours (F) of nicotine treatment. CN = Control Medium. All data are means ± the standard error of the mean for three independent experiments. * = $p < 0.05$, ** = $p < 0$ .01

3.7. Recovery of Mitochondrial Morphology in Keratinocytes after Nicotine Treatment

To determine if the changes observed in mitochondrial morphology and mitofusin levels were reversible, a follow up experiment was done in which cells were treated with Nic400 and allowed to recover in nicotine-free medium for 24 or 48 hours. The percent of “network” and “network and punctate” mitochondria in the Nic400 treated group re-turned to control levels following a 24 or 48 hours recovery period in cell medium without nicotine (Figures 4I -J). To determine if longer treatment required longer recovery periods, cells were exposed to nicotine for 48 hours prior to recovery. In this case, it took 48 hours for mitochondrial morphology to return to control levels (Figures 4 K-L).

Western blots were performed to determine if mitofusin 1/2 recovered after nicotine treatment. In the Nic400 treated group, cells were exposed for 72 hours to produce a decrease in mitofusin1 as shown in Figure 3C. Mitofusin 1 recovered to control levels after 24 hours in culture medium without nicotine (Figure 5A). For mitofusin 2, exposure was reduced to 24 hours since this was adequate time to decrease the levels of this protein (Figure 3 D). In this case, recovery to control levels occurred in 48 hours (Figure 5 B). Figures in 5 need titles.

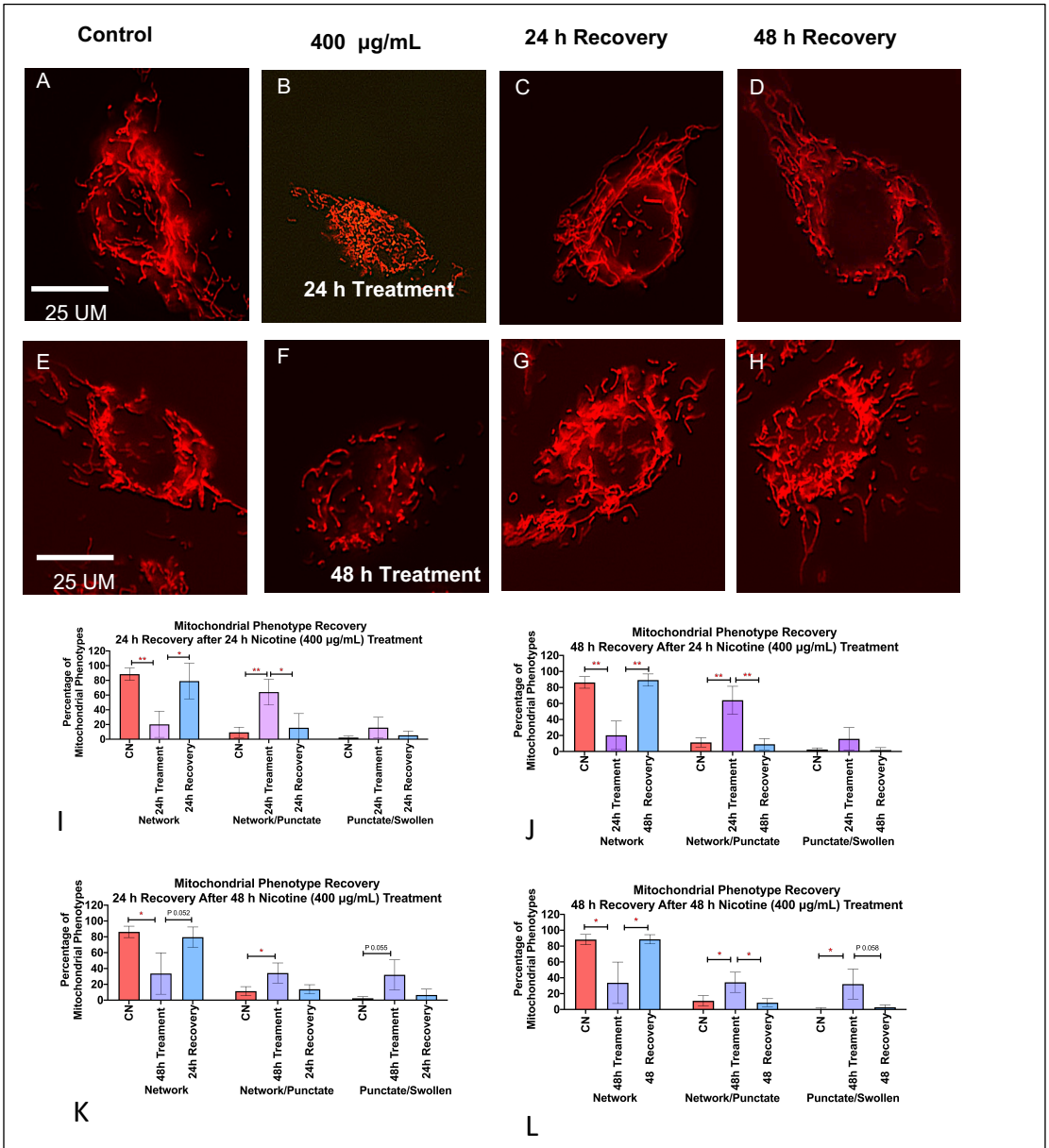

Figure 4. Mitochondrial Morphology in Nicotine Treated Keratinocytes Returns to Normal after 24 hours and 48 hours of Recovery in Cultured Medium. (A-H) Micrographs showing untreated controls, cells treated with nicotine and cells that re-covered 24 or 48 hours after treatment. (I) Mitochondrial morphology in keratinocytes treated for 24 hours and after 24 hours of recovery. (J) Mitochondrial morphology in keratinocytes treated for 24 hours and after a 48 hour recovery. (K) Mitochondrial morphology in keratinocytes treated for 48 hours and after 24 hours of recovery. (L) Mitochondrial morphology in keratinocytes treated for 48 hours and after 48 hours of recovery. CN = Control Medium. All data are means ± the standard error of the mean for three independent experiments. * = $p < 0.05$, ** = $p < 0$ .01

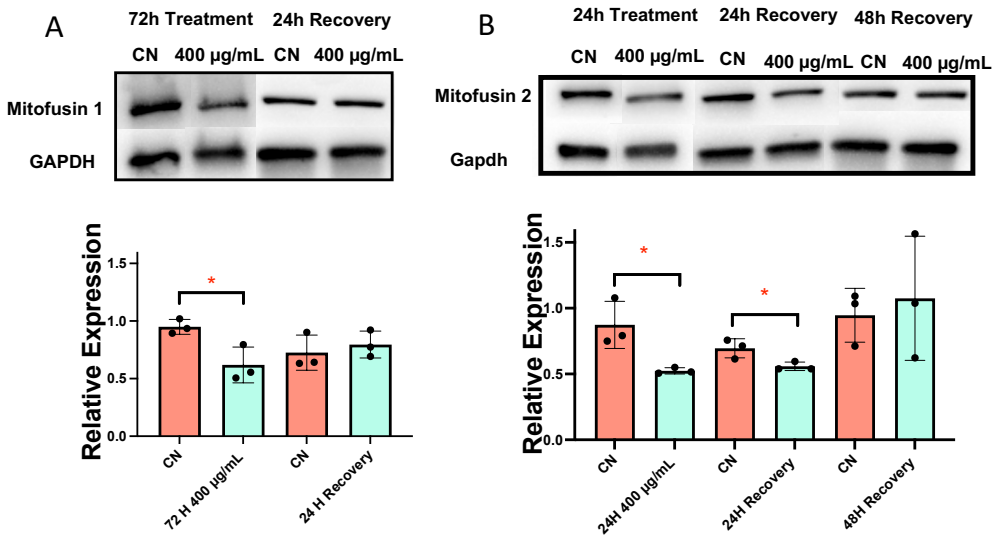

Figure 5. Mitofusin 1/2 Protein Expression in Nicotine Treated Keratinocytes after 24 and 48 Hours of Recovery. (A) Expression of mitofusin 1 in a western blot after 72 hours of exposure to 400 µg/mL (Nic400) of nicotine and after 24 hours of recovery. (B) Expression of mitofusin 2 after 24 hours of exposure to 400 µg/mL (Nic400) of nicotine, followed by 24 and 48 hours of recovery. CN = Control Medium. All data are means ± the standard error of the mean for three independent experiments. * = $p < 0.05$, ** = $p < 0$ .01

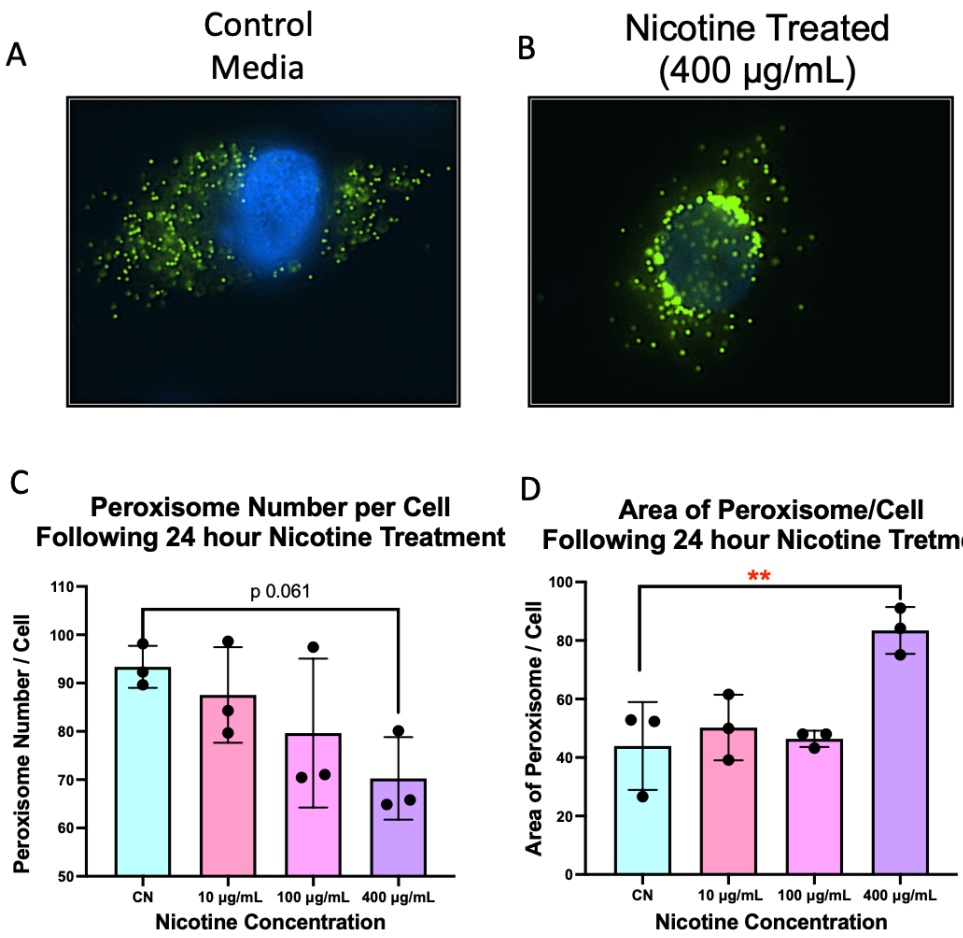

Figure 6. Peroxisome Morphology in Keratinocytes after Nicotine Treatment. (A) Micrograph of peroxisomes (green) in keratinocytes treated with medium only. (B) Micrograph of peroxisomes (green) in keratinocytes treated with 400 µg/mL (Nic400) of nicotine for 24 hours. (C) Number of peroxisomes per cell in keratinocytes following treatment with control medium, 10 µg/mL (Nic10), 100 µg/mL (Nic100), and 400 µg/mL (Nic400) of nicotine for 24 hours. (D) Area of peroxisomes per cell in keratinocytes following treatment with control medium, 10 µg/mL (Nic10), 100 µg/mL (Nic100), and 400 µg/mL (Nic400) of nicotine for 24 hours. CN = Control Medium. All data are means ± the standard error of the mean for three independent experiments. * = $p < 0.05$, ** = $p < 0$ .01

3.8 Nicotine Treatment Altered the Number and Size of Peroxisomes

Peroxisomes are involved in neutralizing ROS (Ganguli et al. 2019). Since we observed changes in the proteomics data related to oxidative stress, we examined the effect of nicotine on peroxisomes in keratinocytes transfected with the sfGFP-Peroxisomes-2 plasmid to visualize peroxisome size and number. Peroxisome morphology was altered in keratinocytes treated with Nic400 for 24 hours (Figures 6 A-B). The peroxisomes in the treated cells appeared to be fewer, larger, and more fluorescent (Figure 6 B). Peroxisome numbers and size were quantified manually. Nicotine treatment decreased the number of peroxisomes in all groups, with Nic400 being significantly lower than the untreated control (Figure 6C). The area of peroxisomes/cell increased in the Nic400 treated group (Figure 6D).

Discussion

The effects of nicotine in THS and EC products on human skin have not been well characterized. To our knowledge, this is the first proteomics study showing how EpiDerm™, a 3D model of human skin, responds to concentrations of nicotine found in THS and EC fluids during ALI exposure. Nicotine stimulated responses in the EpiDerm™ model that may negatively impact the skin and included: (1) an anti-inflammatory response that could promote bacterial infections and impair wound healing; (2) altered EIF2 protein synthesis that may initiate a stress response and suppress apoptosis; (3) an increase in proteins involved in oxidative phosphorylation; and (4) alterations in mitochondrial related pathways. Cultured human keratinocytes confirmed and extended the proteomics data. The nicotine-induced responses could lead to skin damage, infections, and progression to disease.

Nicotine concentrations used in this study were comparable to those in THS contaminated environments and EC liquid spills or leaks. The lowest concentration (Nic10) was based on nicotine concentrations in extracts from fabrics lightly exposed to cigarette smoke over 18 months in a laboratory setting (Pozuelos *et al.*, 2021). Higher concentrations (Nic100 and Nic 400) were used to simulate environmental settings without smoking bans, heavily exposed to cigarette smoke, and not frequently cleaned. The Nic400 concentration was also used to assess nicotine exposure through the handling of e-fluid, although this concentration is slightly outside the lower end of nicotine range in e-fluids (1

mg/mL - 60.9 mg/mL) (Omaiye et al. 2019a, Omaiye et al. 2019b, David et al. 2015).

At Nic10 and Nic400 concentrations, we observed inhibition of inflammatory related pathways in the EpiDermTM skin model, similar to in vivo animal and human studies (Tsoy *et al.*, 2011, Kalra et al. 2004 Staple et al. 2012 Scott et a. 2006, Misery et al. 2004). Although nicotine's anti-inflammatory properties may be beneficial for inflammatory skin diseases (Ingram *et al.*, 2008), such as psoriasis and atopic dermatitis, it can also facilitate bacterial infections in the skin and impair wound healing (Tsoy *et al.*, 2011, Staple *et al.*, 2012 Stegemann *et al.*, 2020). In in vivo animal studies, nicotine stimulated the cholinergic anti-inflammatory pathway and reduced antimicrobial peptide activity allowing susceptibility to staphylococcus aureus infection in the skin of mice (Tsoy *et al.*, 2011, Radek *et al.*, 2010, Kishibe *et al.*, 2015). Activation of α7 nAChR by nicotine inhibited the NF-kB pathway and toll-like receptor 2 (TLR2) signaling caused a decreased in receptor response to bacterial and other pathogens (Kishibe *et al.*, 2015). Inhibition of TLR2 activity is detrimental for proper modulation of pro-inflammatory signals needed to initiate wound healing. Recruitment of neutrophils to wounds helps eliminate pathogens, and macrophages secrete growth factors that stimulate cell proliferation to replace damage tissue (Cañedo-Dorantes *et al.*, 2019, Koh *et al.*, 2013, Seeger et al. 2015). TLR2 signaling is also involved in stimulating cell migration for proper wound healing. In keratinocytes, scratch assays migration is attenuated by

nicotine (10−9 M) through activation of α7 nAChR and suppression of TRL2 (Kishibe *et al.*, 2015). In EpiDerm^{TM}, nicotine (Nic10) decreased cell-cell adhesion proteins consistent with an in-crease in cell migration. Variations in results may depend on the cell type used and nicotine concentrations. Here we used a 3D skin model without wound incision and alteration of cell-cell adhesion proteins were only observed in Nic10 treatment. Increases in cell migration have been observed in human keratinocytes at different nicotine concentrations (10–7 M- 10-5M), which suggest migration is also concentration dependent (Chernyavsky *et al.*, 2009 Chernyavshy *et al.*, 2004). We show that EpiDermTM exposed to concentrations found in THS decreased inflammation related pathways that could contribute to pathogen infections and improper wound healing. In mice exposed to THS, wound healing in skin was impaired, and wounds were fragile (Martins *et al.*, 2004). Given our results, nicotine's an-ti-inflammatory properties may be the main contributor to the delay in wound healing observed in THS exposed mice (Martins *et al.*, 2004).

Proteomics analysis of EpiDerm treated with nicotine (Nic10 and Nic400) predicted an activated state of the EIF2 signaling pathway, which is involve in global protein synthesis. However, under stress conditions, eukaryotic translation initiation factor 2 alpha (eIF2α) may become phosphorylated and selectively translate only a subset of mRNAs necessary for cell survival and stress recovery, such as inhibitors of apoptosis (Lui *et al.*, 2014; Warnakulasuri-yarachchi *et al.*, 2004). Nicotine phosphorylation of EIF2 is depended on treatment concentration,

cell type, and experimental model (Huang *et al.*, 2016, Wong *et al.*, 2016, Placzek *et al.*, 2016). In our 3D EpiDermTM model, increased expression of proteins involved in the EIF2 pathway may be associated with stress-related protein synthesis, since: (1) mitochondrial stress related pathways were also observed (Nic10), (2) apoptosis pathways were decreased, and (3) expression of RPL19, a ribosomal protein involved in the activation of the unfolded protein response, was increased (Hong *et al.*, 2014).

Mitochondrial related pathways were the top hit on IPA's tox list analysis in the EpiDermTM treatments. Alterations in mitochondrial dynamics and oxidative stress have been observed in cells treated with nicotine (Meng *et al.*, 2021, Zahedi *et al.*, 2019). Nicotine binds to acetylcholine receptors in keratinocytes to stimulate a Ca+ influx (Grando *et al.*, 1996). Proteins altered in EpiDerm treated with nicotine included those in the electron transport chain. THS and nicotine altered mitochondrial morphology in mouse neural stem cells (mNSCs) (Zahedi *et al.*, 2019). In our study, nicotine at concentrations found in THS-exposed fabric de-creased mitochondrial networks, while increasing punctate and swollen mitochondria. Mitochondrial fragmentation was dependent on both nicotine concentration and time. The shift from networked to punctate mitochondria correlated with a decrease in mitofusin 1/2, proteins involved in mitochondrial fusion, which are needed to maintain the networked phenotype. A similar nicotine-induced mitochondrial fission accompanied by a decrease in mitofusin 1/2 was observed in neonatal rat ventricular cardiomyocytes and (Meng et al.

2021) in human multipotent embryonal carcinoma cells (Hirata *et al.*, 2016). Mitochondrial fragmentation was reversable in human keratinocytes, suggesting skin could recuperate after THS exposure. Alterations in mitochondria could lead to ROS imbalance, which may cause cellular oxidative stress in skin.

Mitochondrial alterations have been observed in stem cells exposed to THS, e-liquid, and nicotine. Unlike keratinocytes which have a networked morphology, stem cell mitochondria are punctate and undergo fission during cellular stress, leading to stress induced mitochondrial hyperfusion (SIMH). SIMH occurs in neural stem cells during exposure to THS, e-liquid or nicotine, and is regarded as a survival mechanism (Bahl *et al.*, 2016, Zahedi *et al.*, 2019). Our results suggest that stem cells and differentiated keratinocytes responded differently to nicotine. Stem cells mount a survival response via SIMH, while in differentiated keratinocytes, mitochondria fragment, which may occur in parallel with a survival response initiated by EIF2. In the mNSCs, punctate mitochondria have low activity when they are punctate and fuse to form networks when they need more energy.

Peroxisomes are essential for various cellular functions including maintenance of ROS homeostasis and degradation of hydrogen peroxides (Ganguli *et al.*, 2019, Ahuir *et al.*, 2017, Tripathi *et al.*, 2016). Abnormalities in peroxisomes can impair catalase activity and lead to inadequate detoxification of ROS, which in turn can cause oxidative stress and contribute to impaired mitochondrial function (Ganguli *et al.*, 2019). In our study, peroxisomes in

keratinocytes exposed to Nic400 were not normal and showed both a decrease in number and an increase in size relative to the controls. Changes in number may be caused by increased pexophagy, which occurs when peroxisomes are damaged (Till *et al.*, 2012) and can be triggered by excess ROS (Zhang *et al.*, 2015). The increase in size could be due to swelling of damaged peroxisomes, which has been reported in a PEX 11 knockout cell line (Beltran *et al.*, 2018). Swelling may also occur when peroxisomes are proliferating, which may have been occurring in our system to replace those lost by pexophagy. Dysfunction in peroxisomes can activate eIF2 transcription of stress pathways and increase ROS, leading to mitochondrial dysfunction (Huang *et al.*, 2019: 2021, Kim *et al.*, 2022). In a mouse model with dysfunctional peroxisomes, increased phosphorylation of eIF2-α led to activation of transcription factors that regulate expression of stress related genes (Huang *et al.*, 2016, Kovacs *et al.*, 2012 Kim *et al.*, 2022). EIF2 signaling was affected in our proteomics analysis and may be a response to peroxisome dysregulation. Impaired peroxisomes, which we observed in keratinocytes, also increase ROS and can trigger mitochondrial dysfunction, which was observed in both our proteomics data and phenotype analysis of mitochondria (Piao *et al.*, 2019, Oruqaj *et al.*, 2015, Ahlemeyer *et al.*, 2012, Lopez-Erauskin, Kim *et al.*, 2022). Liver cells from mice with dysfunctional peroxisomes developed swollen mitochondria, similar to our keratinocytes treated with NIC400 (Baumgart *et al.*, 2001). In our data, peroxisomes were abnormal by 24 hours of treatment, while mitochondrial swelling was observed

after 72 hours. Our data support the conclusion that treatment of human keratinocytes with nicotine may lead to peroxisome dysfunction, which in turn activates stress responses and produces mitochondrial dysfunction.

Conclusions

The EpiDermTM skin model and cultured keratinocytes treated with nicotine concentrations associated with environmental THS and EC are enough to penetrate and produce: (1) an anti-inflammatory response which could exacerbate skin infections and impaired wound healing, (2) alter the EIF2 signaling pathway that may activate a cellular stress response mechanism and inhibit apoptosis, (3) increased oxidative stress, and (4) alter both mitochondrial and peroxisome morphologies and disrupt ROS homeostasis. Even a short exposure to low concentrations of nicotine is sufficient to alter the EpiDerm^{TM} proteome and adversely affect organelles involved in oxidative stress. These data in conjunction with our earlier study showing alterations in the human nasal epithelium following inhalation of THS chemicals (Pozuelos *et al.*, 2019) provide strong evidence that humans are adversely affected by both dermal and inhalation exposure to THS. Together, these data demonstrate a need for a better understanding of the effects of THS on humans, the broadening of restrictions on indoor smoking, and development of policies for remediating contaminated environments.

References

1. Abramoff, M.D., Magalhaes, P.J., Ram, S.J. Image Processing with ImageJ. Biophotonics International, 2004.11(7) 36-42.

2. Ahlemeyer, B., Gottwald, M., Baumgart-Vogt, E. Deletion of a single allele of the Pex11β gene is sufficient to cause oxidative stress, delayed differentiation and neuronal death in mouse brain. *Dis. Model. Mech.* **2012**, *5*, 125–140.

3. Atena Zahedi, Rattapol Phandthong, Angela Chaili, Sara Leung, Esther Omaiye, Prue Talbot, Mitochondrial Stress Response in Neural Stem Cells Exposed to Electronic Cigarettes, iScience, Volume 16, 2019, Pages 250-269, ISSN 2589-0042, https://doi.org/10.1016/j.isci.2019.05.034. (https://www.sciencedirect.com/science/article/pii/S2589004219301713)

4. Bahl V, Jacob P 3rd, Havel C, Schick SF, Talbot P. Thirdhand cigarette smoke: factors affecting exposure and remediation. PLoS One. 2014 Oct 6;9(10):e108258. doi: 10.1371/journal.pone.0108258. PMID: 25286392; PMCID: PMC4186756.

5. Bahl V, Jacob P 3rd, Havel C, Schick SF, Talbot P. Thirdhand cigarette smoke: factors affecting exposure and remediation. PLoS One. 2014 Oct 6;9(10):e108258. doi: 10.1371/journal.pone.0108258. PMID: 25286392; PMCID: PMC4186756.

6. Bahl, V., Shim, H.J., Payton, J. III, Dias, K., Schick, S.F., Talbot, P. 2016. Thirdhand smoke: Chemical dynamics, cytotoxicity, and genotoxicity in outdoor and indoor environments. Toxicology in Vitro.32: 220–231

7. Baumgart E, Vanhorebeek I, Grabenbauer M, Borgers M, Declercq PE, Fahimi HD, Baes M. Mitochondrial alterations caused by defective peroxisomal biogenesis in a mouse model for Zellweger syndrome (PEX5 knockout mouse). Am J Pathol. 2001 Oct;159(4):1477-94. doi: 10.1016/S0002-9440(10)62534-5. PMID: 11583975; PMCID: PMC1850512.

8. Cantrell FL. Adverse effects of e-cigarette exposures. J Community Health. 2014 Jun;39(3):614-6. doi: 10.1007/s10900-013-9807-5. PMID: 24338077.

9. Cañedo-Dorantes, Luis, and Mara Cañedo-Ayala. 2019. Skin acute wound healing: a comprehensive review. *International journal of inflammation*.:3706315. doi: 10.1155/2019/3706315.
10. Casas, J.W., Lewerenz, G.M., Rankin, E.A., Willoughby, J.A., Blakeman, L.C., McKim, J.M., Coleman, K.P., 2013. In vitro human skin irritation test for

evaluation of medical device extracts. Toxicol In Vitro 27, 2175–2183. doi:10.1016/j.tiv.2013.08.006

11. Chen H, Detmer SA, Ewald AJ, Griffin EE, Fraser SE, Chan DC. Mitofusins Mfn1 and Mfn2 coordinately regulate mitochondrial fusion and are essential for embryonic development. J Cell Biol. 2003;160(2):189-200. doi:10.1083/jcb.200211046

12. Chernyavsky AI, Arredondo J, Qian J, Galitovskiy V, Grando SA. Coupling of ionic events to protein kinase signaling cascades upon activation of alpha7 nicotinic receptor: cooperative regulation of alpha2-integrin expression and Rho kinase activity. J Biol Chem. 2009 Aug 14;284(33):22140-22148. doi: 10.1074/jbc.M109.011395. Epub 2009 Jun 23. PMID: 19549780; PMCID: PMC2755938

13. Chernyavsky AI, Arredondo J, Marubio LM, Grando SA. Differential regulation of keratinocyte chemokinesis and chemotaxis through distinct nicotinic receptor subtypes. J Cell Sci. 2004 Nov 1;117(Pt 23):5665-79. doi: 10.1242/jcs.01492. Epub 2004 Oct 19. PMID: 15494367.

14. Choi M, Chang CY, Clough T, Broudy D, Killeen T, MacLean B, Vitek O. MSstats: An R package for statistical analysis of quantitative mass spectrometry-based proteomic experiments. Bioinformatics. 2014 Sep 1; 30(17): 2524-2526. PMID: 24794931.

15. Davis B, Dang M, Kim J, Talbot P. Nicotine concentrations in electronic cigarette refill and do-it-yourself fluids. Nicotine Tob Res. 2015 Feb;17(2):134-41. doi: 10.1093/ntr/ntu080. Epub 2014 May 26. PMID: 24862971; PMCID: PMC4892702

16. Ganguli Geetanjali, Mukherjee Utsav, Sonawane Avinash Peroxisomes and Oxidative Stress: Their Implications in the Modulation of Cellular Immunity During Mycobacterial Infection Frontiers in Microbiology 10 2019 https://www.frontiersin.org/article/10.3389/fmicb.2019.01121 10.3389/fmicb.2019.01121

17. Garcia R, Allem JP, Baezconde-Garbanati L, Unger JB, Sussman S. Employee and customer handling of nicotine-containing e-liquids in vape shops. Tob Prev Cessat. 2016;2(Suppl):10.18332/tpc/67295. doi:10.18332/tpc/67295

18. Grando SA, Horton RM, Mauro TM, Kist DA, Lee TX, Dahl MV. Activation of keratinocyte nicotinic cholinergic receptors stimulates calcium influx and enhances cell differentiation. J Invest Dermatol. 1996 Sep;107(3):412-8.

19. Hirata N, Yamada S, Asanagi M, Sekino Y, Kanda Y. Nicotine induces mitochondrial fission through mitofusin degradation in human multipotent embryonic carcinoma cells. Biochem Biophys Res Commun. 2016 Feb 5;470(2):300-305. doi: 10.1016/j.bbrc.2016.01.063. Epub 2016 Jan 13. PMID: 26774337.

20. Hong M, Kim H, Kim I. Ribosomal protein L19 overexpression activates the unfolded protein response and sensitizes MCF7 breast cancer cells to endoplasmic reticulum stress-induced cell death. Biochemical and biophysical research communications. 2014 Jul 18;450(1):673-8.

21. Hughes, C. S., Foehr, S., Garfield, D. A., Furlong, E. E., Steinmetz, L. M., & Krijgsveld, J. (2014). Ultrasensitive proteome analysis using paramagnetic bead technology. Molecular Systems Biology, 10(10), 757. https://doi.org/10.15252/msb.20145625

22. Huang W, Placzek AN, Viana Di Prisco G, Khatiwada S, Sidrauski C, Krnjević K, Walter P, Dani JA, Costa-Mattioli M. Translational control by eIF2α phosphorylation regulates vulnerability to the synaptic and behavioral effects of cocaine. Elife. 2016 Mar 1;5:e12052. doi: 10.7554/eLife.12052. PMID: 26928234; PMCID: PMC4786430

23. Jacob P 3rd, Benowitz NL, Destaillats H, et al. Thirdhand Smoke: New Evidence, Challenges, and Future Directions. Chem Res Toxicol. 2017;30(1):270-294. doi:10.1021/acs.chemrestox.6b00343

24. Jimenez-Morales D, Campos AR, Von Dollen. J. 2019. artMS: Analytical R tools for Mass Spectrometry. R package version 1.4.2. Available at https://bioconductor.org/packages/artMS/

25. Kalra R, Singh SP, Pena-Philippides JC, Langley RJ, Razani-Boroujerdi S, Sopori ML. Immunosuppressive and anti-inflammatory effects of nicotine administered by patch in an animal model. Clin Diagn Lab Immunol. 2004;11(3):563-568. doi:10.1128/CDLI.11.3.563-568.2004

26. Kandárová, H., Willoughby, J.A., De Jong, W.H., Letasiova, S., Milasova, T., Bachelor, M.A., Breyfogle, B., Handa, Y., la Fonteyne, De, L., Coleman, K.P., 2018. Pre-validation of an in vitro skin irritation test for medical devices using the reconstructed human tissue model EpiDermTM. Toxicology in Vitro 50, 407–417. doi:10.1016/j.tiv.2018.02.007

27. Kerui Huang, Jinoh Kim, Pham Vo, Ting Miao, Hua Bai, Peroxisome import stress impairs ribosome biogenesis and induces integrative stress response through eIF2α phosphorylation, bioRxiv 2020.11.19.390609; doi: https://doi.org/10.1101/2020.11.19.390609

28. Kim J, Bai H. Peroxisomal Stress Response and Inter-Organelle Communication in Cellular Homeostasis and Aging. Antioxidants (Basel). 2022 Jan 19;11(2):192. doi: 10.3390/antiox11020192. PMID: 35204075; PMCID: PMC8868334.

29. Khachatoorian C, Jacob P 3rd, Sen A, Zhu Y, Benowitz NL, Talbot P. Identification and quantification of electronic cigarette exhaled aerosol residue chemicals in field sites. *Environ Res*. 2019;170:351-358. doi:10.1016/j.envres.2018.12.027

30. Kishibe M, Griffin TM, Radek KA. Keratinocyte nicotinic acetylcholine receptor activation modulates early TLR2-mediated wound healing responses. *Int Immunopharmacol*. 2015;29(1):63-70. doi:10.1016/j.intimp.2015.05.047

31. Koh, Timothy J., and Luisa Ann DiPietro. "Inflammation and wound healing: the role of the macrophage." *Expert reviews in molecular medicine* 13 (2011).

32. Kovacs WJ, Charles KN, Walter KM, Shackelford JE, Wikander TM, Richards MJ, Fliesler SJ, Krisans SK, Faust PL. Peroxisome deficiency-induced ER stress and SREBP-2 pathway activation in the liver of newborn PEX2 knock-out mice. Biochim Biophys Acta. 2012 Jun;1821(6):895-907. doi: 10.1016/j.bbalip.2012.02.011. Epub 2012 Mar 13. PMID: 22441164; PMCID: PMC3366256

33. Liu B, Qian SB. Translational reprogramming in cellular stress response. Wiley Interdiscip Rev RNA. 2014 May-Jun;5(3):301-15. doi: 10.1002/wrna.1212. Epub 2013 Dec 23. PMID: 24375939; PMCID: PMC3991730.

34. López-Erauskin J, Galino J, Ruiz M, Cuezva JM, Fabregat I, Cacabelos D, Boada J, Martínez J, Ferrer I, Pamplona R, Villarroya F, Portero-Otín M, Fourcade S, Pujol A. Impaired mitochondrial oxidative phosphorylation in the peroxisomal disease X-linked adrenoleukodystrophy. Hum Mol Genet. 2013 Aug 15;22(16):3296-305. doi: 10.1093/hmg/ddt186. Epub 2013 Apr 20. PMID: 23604518

35. Maina, G., Castagnoli, C, Ghione, G, Passini, V., Adami, G., Filon, F. L., Crosera, M.2017. Skin contamination as pathway for nicotine intoxication in vapers. Toxicology in Vitro. 41:102-105. doi.org/10.1016/j.tiv.2017.02.022.

36. Martins-Green M, Adhami N, Frankos M, et al. Cigarette smoke toxins deposited on surfaces: implications for human health. 2014.*PLoS One*. 9(1):e86391. Published 2014 Jan 29. doi:10.1371/journal.pone.0086391

37. Matt, G.E., Quintana, P.J., Hovell, M.F., Chatfield D, Ma DS, Romero R, Uribe A. 2008.Residual tobacco smoke pollution in used cars for sale: air, dust, and surfaces. Nicotine Tob Res. 10(9):1467-75. doi: 10.1080/14622200802279898. PMID: 19023838

38. Matt GE, Quintana PJ, Destaillats H, Gundel LA, Sleiman M, Singer BC, Jacob P, Benowitz N, Winickoff JP, Rehan V, Talbot P, Schick S, Samet J, Wang Y, Hang B, Martins-Green M, Pankow JF, Hovell MF. Thirdhand tobacco smoke: emerging evidence and arguments for a multidisciplinary research agenda. Environ Health Perspect. 2011 Sep;119(9):1218-26. doi: 10.1289/ehp.1103500. Epub 2011A May 31. PMID: 21628107; PMCID: PMC3230406.

39. Matt GE, Quintana PJ, Hovell MF, Bernert JT, Song S, Novianti N, et al. 2004. Households contaminated by envi- ronmental tobacco smoke: sources of infant exposures. Tob Control 13:29–37.

40. Matt GE, Quintana PJ, Zakarian JM, Fortmann AL, Chatfield DA, Hoh E, Uribe AM, Hovell MF. When smokers move out and non-smokers move in: residential thirdhand smoke pollution and exposure. Tob Control. 2011B Jan;20(1):e1. doi: 10.1136/tc.2010.037382. Epub 2010 Oct 30. PMID: 21037269; PMCID: PMC3666918.

41. Mayer, B. How much nicotine kills a human? Tracing back the generally accepted lethal dose to dubious self-experiments in the nineteenth century. Arch Toxicol 88, 5–7 (2014). https://doi.org/10.1007/s00204-013-1127-0

42. Meng Ting-ting, Wang Wei, Meng Fan-liang, Wang Shu-ya, Wu Hui-hui, Chen Jia-min, Zheng Yan, Wang Guang-xin, Zhang Mao-xiu, Li Ying, Su Guo-hai Nicotine Causes Mitochondrial Dynamics Imbalance and Apoptosis Through ROS Mediated Mitophagy Impairment in Cardiomyocytes. Frontiers in Physiology12 2021 https://www.frontiersin.org/article/10.3389/fphys.2021.650055 DOI 10.3389/fphys.2021.650055

43. McKnight RH, Spiller HA. Green tobacco sickness in children and adolescents. Public Health Rep. 2005;120(6):602-605. doi:10.1177/003335490512000607 McKnight et al. 2005

44. Misery L. Nicotine effects on skin: are they positive or negative? Exp Dermatol. 2004 Nov;13(11):665-70. doi: 10.1111/j.0906-6705.2004.00274.x. PMID: 15500638.

45. Mishra A, Chaturvedi P, Datta S, Sinukumar S, Joshi P, Garg A. Harmful effects of nicotine. Indian J Med Paediatr Oncol. 2015;36(1):24-31. doi:10.4103/0971-5851.151771

46. Mohamad Sleiman, Jennifer M. Logue, Wentai Luo, James F. Pankow, Lara A. Gundel, and Hugo Destaillats Inhalable Constituents of Thirdhand Tobacco Smoke: Chemical Characterization and Health Impact Considerations Environmental Science & Technology 2014 48 (22), 13093-13101 DOI: 10.1021/es5036333

47. Omaiye et al. 2019A EE, McWhirter KJ, Luo W, Pankow JF, Talbot P. High-Nicotine Electronic Cigarette Products: Toxicity of JUUL Fluids and Aerosols Correlates Strongly with Nicotine and Some Flavor Chemical Concentrations. Chem Res Toxicol. 2019 Jun 17;32(6):1058-1069. doi: 10.1021/acs.chemrestox.8b00381. Epub 2019 Apr 17. PMID: 30896936; PMCID: PMC6579667.

48. Oruqaj, G.; Karnati, S.; Vijayan, V.; Kotarkonda, L.K.; Boateng, E.; Zhang, W.; Ruppert, C.; Günther, A.; Shi, W.; Baumgart-Vogt, E. Compromised peroxisomes in idiopathic pulmonary fibrosis, a vicious cycle inducing a higher fibrotic response via TGF-β signaling. *Proc. Natl. Acad. Sci. USA* **2015**, *112*, E2048–E2057

49. Omaiye et al. 2019B, E.E., McWhirter, K.J., Luo, W. et al. High concentrations of flavor chemicals are present in electronic cigarette refill fluids. Sci Rep 9, 2468 (2019). https://doi.org/10.1038/s41598-019-39550-2

50. Pascual-Ahuir A, Manzanares-Estreder S, Proft M. Pro- and Antioxidant Functions of the Peroxisome-Mitochondria Connection and Its Impact on Aging and Disease. Oxid Med Cell Longev. 2017;2017:9860841. doi: 10.1155/2017/9860841. Epub 2017 Jul 24. PMID: 28811869; PMCID: PMC5546064.

51. Piao, L.; Dorotea, D.; Jiang, S.; Koh, E.H.; Oh, G.T.; Ha, H. Impaired Peroxisomal Fitness in Obese Mice, a Vicious Cycle Exacerbating Adipocyte Dysfunction via Oxidative Stress. *Antioxid. Redox Signal.* **2019**, *31*, 1339–1351.

52. Placzek AN, Molfese DL, Khatiwada S, Di Prisco GV, Huang W, Sidrauski C, Krnjević K, Amos CL, Ray R, Dani JA, Walter P. Translational control of nicotine-evoked synaptic potentiation in mice and neuronal responses in human smokers by eIF2α. Elife. 2016 Mar 1;5:e12056.

53. Pozuelos GL, Kagda MS, Schick S, Girke T, Volz DC, Talbot P. Experimental Acute Exposure to Thirdhand Smoke and Changes in the Human Nasal

Epithelial Transcriptome: A Randomized Clinical Trial. *JAMA Netw Open.* 2019;2(6):e196362. doi:10.1001/jamanetworkopen.2019.6362

54. Pozuelos GL, Jacob P III, Schick SF, Omaiye EE, Talbot P. Adhesion and Removal of Thirdhand Smoke from Indoor Fabrics: A Method for Rapid Assessment and Identification of Chemical Repositories. International Journal of Environmental Research and Public Health. 2021; 18(7):3592. https://doi.org/10.3390/ijerph18073592

55. Scott DA, Martin M. Exploitation of the nicotinic anti-inflammatory pathway for the treatment of epithelial inflammatory diseases. *World J Gastroenterol*. 2006;12(46):7451-7459. doi:10.3748/wjg.v12.i46.7451

56. Seeger MA, Paller AS. The Roles of Growth Factors in Keratinocyte Migration. *Adv Wound Care (New Rochelle)*. 2015;4(4):213-224. doi:10.1089/wound.2014.0540

57. Solarino B, Rosenbaum F, Riesselmann B, Buschmann CT, Tsokos M. Death due to ingestion of nicotine-containing solution: case report and review of the literature. Forensic Sci Int. 2010 Feb 25;195(1-3):e19-22. doi: 10.1016/j.forsciint.2009.11.003. Epub 2009 Dec 1. PMID: 19954906.

58. Sørensen LT, Zillmer R, Agren M, Ladelund S, Karlsmark T, Gottrup F. Effect of smoking, abstention, and nicotine patch on epidermal healing and collagenase in skin transudate. Wound Repair Regen. 2009 May-Jun;17(3):347-53. doi: 10.1111/j.1524-475X.2009.00479.x. PMID: 19660042.

59. Staples, John, and Douglas Klein. 2012. “Can nicotine use alleviate symptoms of psoriasis?.” Canadian family physician Medecin de famille canadien vol. 58,4: 404-8.

60. Radek KA, Elias PM, Taupenot L, Mahata SK, O'Connor DT, Gallo RL. 2010. Neuroendocrine nicotinic receptor activation increases susceptibility to bacterial infections by suppressing antimicrobial peptide production. Cell Host Microbe.7(4):277-289. doi: 10.1016/j.chom.2010.03.009. Erratum in: Cell Host Microbe. 2010 Dec 16;8(6):552. PMID: 20413096; PMCID: PMC2916230.

61. Trtchounian, A., Talbot, P. 2010. Electronic nicotine delivery systems: is there a need for regulation? Tob. Control. 20, 47–52. Cantrell FL. Adverse effects of e-cigarette exposures. J Community Health. 2014 Jun;39(3):614-6. doi: 10.1007/s10900-013-9807-5. PMID: 24338077.

62. Tjoncke JA, Goncalves R, Castaing N, Molimard M, Tovagliaro F, Titier K. Death related to nicotine replacement therapy: A case report. Forensic Sci

Int. 2020 Apr;309:110223. doi: 10.1016/j.forsciint.2020.110223. Epub 2020 Feb 29. PMID: 3214630

63. Tsoyi K, Jang HJ, Kim JW, Chang HK, Lee YS, Pae HO, Kim HJ, Seo HG, Lee JH, Chung HT, Chang KC. 2011.Stimulation of alpha7 nicotinic acetylcholine receptor by nicotine attenuates inflammatory response in macrophages and improves survival in experimental model of sepsis through heme oxygenase-1 induction. Antioxid Redox Signal. 2011 Jun;14(11):2057-70. doi: 10.1089/ars.2010.3555. Epub. PMID: 21083424.

64. Tripathi. DN, Walker, CL. 2015 The peroxisome as a cell signaling organelle. Curr Opin Cell Biol. Apr;39:109-12. doi: 10.1016/j.ceb.2016.02.017. Epub 2016 Mar 9. PMID: 26967755; PMCID: PMC5657427.

65. Warnakulasuriyarachchi, D,Cerquozzi, S,Cheung HH, Holcik M. Translational induction of the inhibitor of apoptosis protein HIAP2 during endoplasmic reticulum stress attenuates cell death and is mediated via an inducible internal ribosome entry site element. J Biol Chem 2004, 279:17148–17157.

66. Webb-Robertson, B.J., Wiberg, H.K., Matzke, M.M., Brown, J.N., Wang J, McDermott JE, Smith RD, Rodland KD, Metz TO, Pounds JG, Waters KM. 2015. Review evaluation, and discussion of the challenges of missing value imputation for mass spectrometry-based label-free global proteomics. J Proteome Res. 14(5): 1993-2001. PMID: 25855118 PMCID: PMC4776766.

67. Wong, M. K., Holloway, A. C., & Hardy, D. B. 2016. Nicotine directly induces endoplasmic reticulum stress response in rat placental trophoblast giant cells. Toxicological Sciences, 151(1), 23-34.

68. Zhang J, Tripathi DN, Jing J, et al. 2015 ATM functions at the peroxisome to induce pexophagy in response to ROS. *Nat Cell Biol*. 17(10):1259-1269. doi:10.1038/ncb3230

Chapter 4

Acute Exposure to Thirdhand Smoke Leads to Rapid Changes in the Human Nasal Epithelial Transcriptome

Pozuelos GL, Kagda MS, Schick S, Girke T, Volz DC, Talbot P. Experimental Acute Exposure to Thirdhand Smoke and Changes in the Human Nasal Epithelial Transcriptome: A Randomized Clinical Trial. JAMA Netw Open. 2019 Jun 5;2(6):e196362. doi: 10.1001/jamanetworkopen.2019.6362. PMID: 31251375; PMCID: PMC6604097.

Abstract

Importance: This is the first study to show that acute inhalation of thirdhand smoke (THS) activates stress and survival pathways in human nasal epithelium.

Objective: To evaluate gene expression in the nasal epithelium of nonsmoking human females following acute inhalation of clean air and THS.

Design: Nasal epithelium was obtained from participants in a clinical trial (2011-2015) on the health effects of inhaled THS. In our crossover design, participants were exposed, head-only, to THS and to conditioned, filtered air. The order of exposures was randomized and exposures were separated by at least 21 days.

Setting: Experiments were performed in a controlled laboratory setting.

Participants: RNA in quantities sufficient for analysis was obtained from a subset of four healthy, nonsmoking women.

Exposures: By chance, the females in our subset had all been randomized to receive clean air exposure first and THS exposure second. Exposures lasted 3 hours.

Main Outcomes and Measures: Differentially expressed genes (DEGs) were identified using RNA sequencing with a false discovery rate < 0.1.

Results: Participants were four healthy nonsmoking human females 27-49 years old (mean = 42) with no chronic diseases. 389 DEGs were identified in THS exposed nasal epithelium, while only two genes, which were not studied further, were affected by clean air. Cluster-Profiler identified enriched Gene Ontology terms associated with stress-induced mitochondrial hyperfusion, such as respiratory electron transport

chain (q-value = $2.84E^{-03}$) and mitochondrial inner membrane (q-value = $7.21E^{-06}$). Reactome Pathway Analysis identified terms associated with up-regulation of DNA repair mechanisms, such as nucleotide excision repair (q-value = $1.05E^{-02}$). Enrichment analyses using Ingenuity Pathway Analysis identified canonical pathways related to stress-induced mitochondrial hyperfusion (e.g., increased oxidative phosphorylation) (p-value = $5.13E^{-04}$), oxidative stress (e.g., glutathione depletion phase II reactions) (p-value = $4.36E^{-02}$), and cell survival (z-score = 5.026). **Conclusions and Relevance:** Acute inhalation of THS caused cell stress leading to the activation of survival pathways. Some responses were consistent with stress-induced mitochondrial hyperfusion and similar to those demonstrated previously *in vitro*. These data will be valuable to physicians treating THS-exposed patients and will aid in formulating regulations for the remediation of THS contaminated environments.

Introduction

Thirdhand smoke (THS) is a subset of chemicals in secondhand cigarette smoke (sidestream smoke emitted by a burning cigarette and exhaled mainstream smoke) that sticks to indoor surfaces and persists after active smoking has occurred[1,2]. THS chemicals accumulate and can react with other compounds or can be re-emitted into the environment[1,2,3]. Nonsmokers can be exposed to chemicals in THS months or even years after smoking has stopped[3]. Many THS chemicals are toxic volatile and semi-volatile organic compounds[2,3,4]. Nicotine, a major chemical in THS, has a high affinity for surfaces[3] and can react with ambient nitrous acid to form tobacco-specific nitrosamines (TSNAs), some of which are carcinogens[5,6]. Nicotine-derived nitrosamines in THS include 4-(methylnitrosamino)-1-(3-pyridinyl)-1-butanone (NNK), and N-nitrosonornicotine (NNN)[5,6], which are also found in secondhand smoke and have been associated with the development of lung cancer[7]. Ozone can also react with nicotine to form formaldehyde, a known human carcinogen[8].

Due to the presence of these and other hazardous chemicals, such as acrolein, in THS, it is important to understand if there is a correlation between exposure to THS and human health, especially in nonsmokers. Previous studies have demonstrated that exposure of human cell lines to THS extracts for 24 hours increased DNA strand breaks and oxidative DNA damage[9,10]. Mouse neural stem cells undergo blebbing, fragmentation, cytoskeletal disruption, and vacuolization when treated with extracts of THS[11]. THS also causes stress-

induced mitochondrial-hyperfusion (SIMH), which is accompanied by increased mitochondrial membrane potential, ATP production, and reactive oxygen species (ROS)[12]. During SIMH, punctate mitochondria fuse and form tubular networks, which allow exchange of molecules including mitochondrial DNA as a survival mechanism[13]. Acrolein has been identified as a THS chemical that inhibits cell proliferation[11]. In a metabolomics study using male germ cells, THS exposure is correlated with down-regulation of several molecular pathways, including nucleic acid metabolism, ammonia metabolism and up-regulation of glutathione metabolism [14].

THS also causes adverse health effects in mice. Three-week old mice that were housed for 6 months in cages containing a THS-impregnated fabric and bedding showed an increase in inflammatory cytokines in lung tissue, impaired wound healing, and were hyperactive compared to controls[15]. Adult mice developed insulin resistance as a consequence of oxidative stress caused by THS and showed increased blood glucose, increased serum insulin, and accumulation of fat in viscera[16]. Oxidative stress in skeletal muscle and accumulation of H_2O_2 accompanied by low catalase activity was observed in chronically exposed mice[17]. After THS exposure, neonatal mice had significantly more eosinophils, increased platelet volume, lower hematocrit, and decreased mean cell volume than controls, while adult exposed mice had a significant increase in the percentage of B-cells and a decrease in myeloid cells[18].

Elimination of THS can be challenging, as it persists in houses previously owned by smokers even after 2 months of vacancy[19]. Cars previously owned by smokers also retain THS, and new owners may be at risk of exposure[20]. Common household fabrics retained THS chemicals 19 months after smoking had occurred[4]. Individuals absorb nicotine through their skin while wearing THS exposed clothes[21]. Moreover, infants whose mothers smoked outdoors had much higher levels of urine cotinine, a nicotine metabolite, than infants of nonsmoking parents[22]. Other examples of the persistence of THS have been reviewed recently[2].

Although these prior studies demonstrate humans are at risk of exposure to THS, the molecular effects of such exposure on humans have not been investigated. The purpose of this study was to evaluate the effects of inhalation of THS chemicals on gene expression in humans. Nasal epithelial cells were collected from nonsmokers before and after 3 hours of exposure to either clean air or to THS, subjected to mRNA sequencing (mRNA-seq), and analyzed for differential expression of genes (DEG). Significant changes in gene expression were found following THS exposure, but not exposure to clean air.

Materials and Methods

Ethics: The study was approved by University of California at San Francisco IRB Protocol number 12-09512. Details of participant recruitment, written informed consent screening, selection, compensation and involvement in the study appear in eMethods of the Supplement. The RNA-seq analysis was approved under IRB protocol HS-12-023 from UCR.

Study Population, Generation of THS, and THS exposure: The protocol for the primary study during which the nasal epithelial cell samples were collected appears in the CONSORT Flow Diagram (Figure 1) and eMethods in the Supplement. It was conducted at the University of California, San Francisco between 2011 and 2015. Briefly, 26 healthy nonsmokers who were not exposed to secondhand cigarette smoke (SHS) in daily life, were exposed, head-only to THS aerosol and to conditioned, filtered air for 3 hours, using an exposure chamber described previously[23]. Of these 26 individuals, 13 (8 women, 5 men) had nasal epithelial cell samples collected before and after each exposure. Nasal epithelial samples were collected from the anterior, inferior turbinate using small, sterile plastic curettes (RhinoPro, Arlington Scientific, Inc. Springville, UT, USA). These samples were immediately placed in RNAlater and shipped frozen to the University of California, Riverside, where RNA extraction and subsequent analyses were performed.

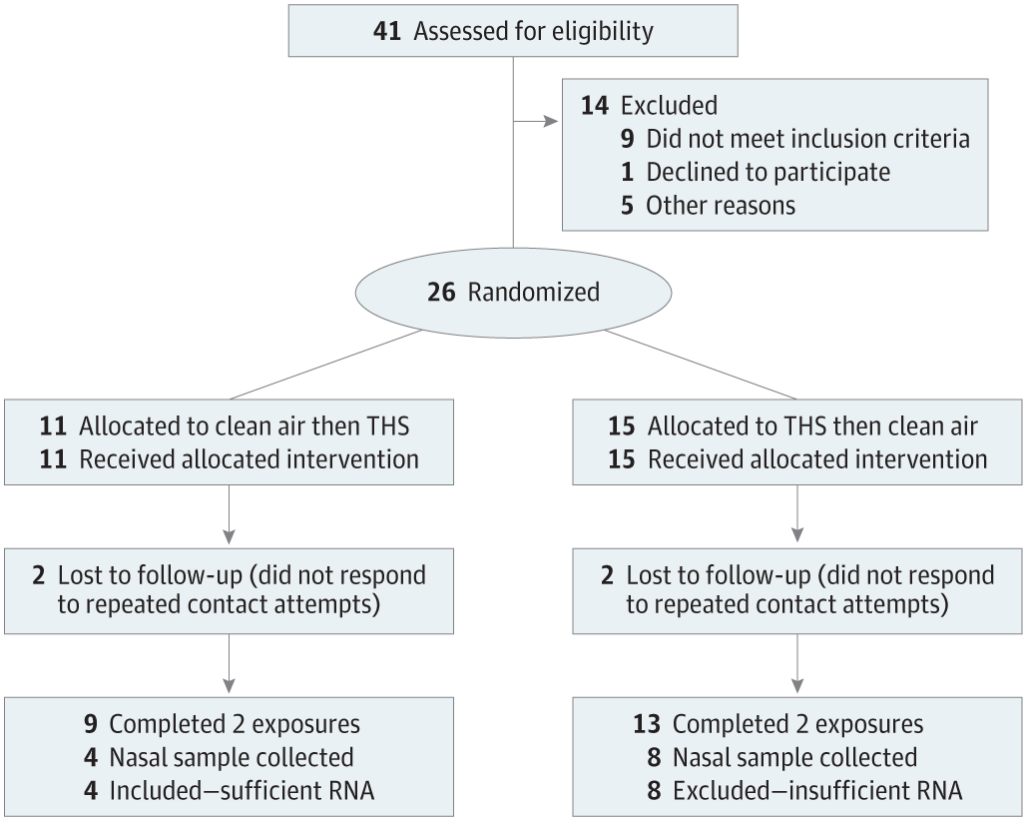

Figure 1. CONSORT Flow Diagram of Parent Study and Subset Sample.
Of 26 participants included in the parent study, nasal epithelial samples from 4 had sufficient RNA to be included in the subset sample.

***RNA Isolation**:* RNA was isolated from human nasal samples using RNeasy micro kits (Qiagen, Germantown, MD, USA) and stored at -80^{o}C. RNA was quantified using a NanoDrop ND-1000 spectrophotometer (Thermo Fisher Scientific, Waltham, MA, USA). Samples from four participants had RNA concentrations > 3 ng/µL, and these were used for subsequent analysis. Frozen

RNA samples were shipped to Cofactor Genomics (St. Louis, MO, USA) for library preparation and sequencing.

RNA Sequencing: Cofactor Genomics performed quality control on RNA samples, and RNA integrity was determined using a Bioanalyzer (Agilent 2100). Samples with RIN numbers between 8 -10 were used for library construction. Total RNA was reverse-transcribed using an Oligo(dT) primer, and limited cDNA amplification was performed using the SMARTer® Ultra® Low Input RNA Kit for Sequencing–v4 (Takara Bio USA, Inc., Mountain View, CA, USA). Full-length cDNA was fragmented and tagged, followed by limited PCR enrichment to generate the final cDNA sequencing library (Nextera® XT DNA Library Prep, Illumina, San Diego, CA, USA). Libraries were sequenced as single-end 75 base pair reads using an Illumina NextSeq500 following the manufacturer's instructions. Because the amount of nasal epithelium in each sample was very limited, we were not able to perform confirmatory qPCR.

Bioinformatics Analysis: Fastq files obtained from Cofactor were processed on a High Performance Computing Cluster (HPCC) at the University of California, Riverside. The RNA-Seq analysis workflow implemented by systemPipeR[24] was used to perform all the downstream data processing. Briefly, adapter sequences and low quality tails were removed from the raw reads using the Trimmomatic package[25]. The preprocessed reads were then aligned against the UCSC hg19 human reference genome with Tophat2 (Version 2.0.14)[26,27]. Read counting was performed with the *summarizeOverlaps* function of the GenomicsAlignment

package. Only unique reads overlapping the exonic gene regions were counted[28]. Using a cut-off value of at least 1 RPKM average across all samples, raw expression counts of the remaining 10,938 genes passing this filter were used for differential expression analysis with EdgeR[29]. Within each experimental group (Group 1, 2, 3, 4), the read counts from the four biological replicates were combined. For differential expression analysis, Groups 1 & 2 (before and after clean air) and Groups 3 & 4 (before and after THS) were treated as two separate experimental comparisons. Genes were considered to be DEGs if they had a false discovery rate (FDR) < 0.1 by EdgeR. Cluster-Profiler[30] and Reactome PA[31] (RPA) packages were used to identify over represented GO terms and enriched Reactome pathways, respectively, as described in the package manual. Additionally, enrichment analyses of pathways were performed using the Ingenuity Pathway Analysis (IPA) software (Qiagen, Germantown, MD, USA). Briefly, statistically significant transcripts were uploaded to IPA, and human homologs were automatically identified using NCBI's HomoloGene.

Statistical Analysis: The EdgeR package was used to obtain log-fold changes, p-values, and FDR scores (based on the Benjamini-Hochberg's method). A gene was considered significantly differentially expressed if the FDR was less than 0.1. ClusterProfiler and RPA packages used a Benjamini-Hochberg adjusted p-value of less than 0.05 to identify significantly enriched Gene Ontology terms and Reactome Pathways, respectively. IPA used the Fisher's Exact Test with a p-value threshold of 0.05 to identify statistically significant pathways; the algorithm

considered both direct and indirect relationships using the Ingenuity Knowledge Base (genes only) as the reference set.

Results

Exposure to THS Altered Gene Expression in Human Nasal Epithelium

The samples collected with this method were small and sufficient quantities of RNA for sequencing analysis could only be extracted from four women. By chance, these four participants had all been randomized to receive the clean air exposure first and THS exposure second, thus we were unable to determine the effect of order on RNA expression. After processing RNA-seq reads, data were analyzed to determine if there were differences in gene expression in the groups exposed to either clean air (Group 1 vs Group 2) or THS (Group 3 vs Group 4) (eFigure 1 in the Supplement). The dataset consisted of approximately 10,000 genes of which 2 and 389 were significantly differentially affected (FDR < 0.10) in clean air and THS-exposed subjects, respectively (eTable 1 in the Supplement). The data set is downloadable from SRA/GEO under submission number PRJNA514351/GSE129959. The two down-regulated genes (hemoglobin, alpha 1 and hemoglobin, alpha 2) identified when subjects were exposed to clean air had an absolute fold change of 8.2 and 8.7, respectively (eTable 2 in the Supplement). No genes were significantly up-regulated in the group exposed to clean air (eFigure 2 in the Supplement). Because these results showed that wearing the respirator for 3.5 hours and inhaling clean air did not significantly impact gene expression, clean air was not studied further.

Nasal samples collected after THS exposure had a significant number of DEGs compared to samples collected before exposure (eTable 1 and eFigure 2 in the Supplement). A total of 382 genes were significantly up-regulated (FDR < 0.1), while seven were down-regulated (eTable 1 in the Supplement). The log_2-fold changes for up-regulated genes ranged from 2 to 7, while down-regulated genes ranged from -2 to -9 (eTable 3 in the Supplement). These data demonstrate that inhalation of THS for a relatively short time significantly altered gene expression in human nasal epithelium.

GO Term Enrichment Analysis

We performed Gene Ontology (GO) enrichment analysis on the up-regulated DEGs to identify biological functions affected by THS (Figure 2A and B; eTables 4-6 in the Supplement). The GO database categorizes genes into different ontologies that represent biological knowledge[32]. Our analysis identified 11 functions enriched within the Biological Processes, 13 within Cellular Components, and 1 within Molecular Function. All the processes were significantly enriched (q-value of < 0.05) (eTables 4-6 in the Supplement). Most of the affected biological processes and cellular components in THS-exposed subjects involved mitochondrial function or RNA metabolism. The top GO Biological Process terms included Ribonucleoprotein Complex Biogenesis (GO:0022613), Cellular Respiration (GO:0045333), Respiration Electron Transport Chain (GO:0022904), and Mitochondrial ATP Synthesis Coupled Electron Transport (GO:0042775) (Figure 2A). Most of the remaining GO

Biological Processes included oxidative phosphorylation-related functions (eTable 4 in the Supplement). The top enriched GO Cellular Components terms included Mitochondria Protein Complex (GO:0098798), Mitochondrial Membrane Part (GO:0044455), Ribosomal Subunit (GO:0044391), Inner Mitochondrial Membrane Protein Complex (GO:0098800), Respiratory Chain (GO:0070469), Large Ribosomal Subunit (GO:0015934) and Respiratory Chain Complex (GO:0098803) (Figure 2B). All the remaining GO terms involved mitochondrial functions except for the two that were related to Ribosomal Subunit (eTable 5 in the Supplement). No enriched GO terms could be identified for the down-regulated genes in the THS experimental group, most likely due to the small number of genes in this set.

Reactome Enrichment Analysis

The Reactome enrichment analysis was used to further evaluate the up-regulated DEGs after THS exposure. This analysis yielded a total of 25 pathways that were significantly enriched (eTable 7 in the Supplement). The top six pathways (Figure 2C) included the Citric Acid Cycle (TCA) (R-HSA-1428517), Respiratory Electron Transport (R-HSA-611105), Translation (R-HSA-72766), Mitochondrial Protein Import (R-HSA-1268020), mRNA Splicing-Minor Pathway (R-HSA-72165), and Nucleotide Excision Repair (R-HAS-5696398). Figure 2C shows the genes associated with each pathway and their overlap, when they belong to multiple pathways. Also shown are the approximate fold-change values

of each gene.

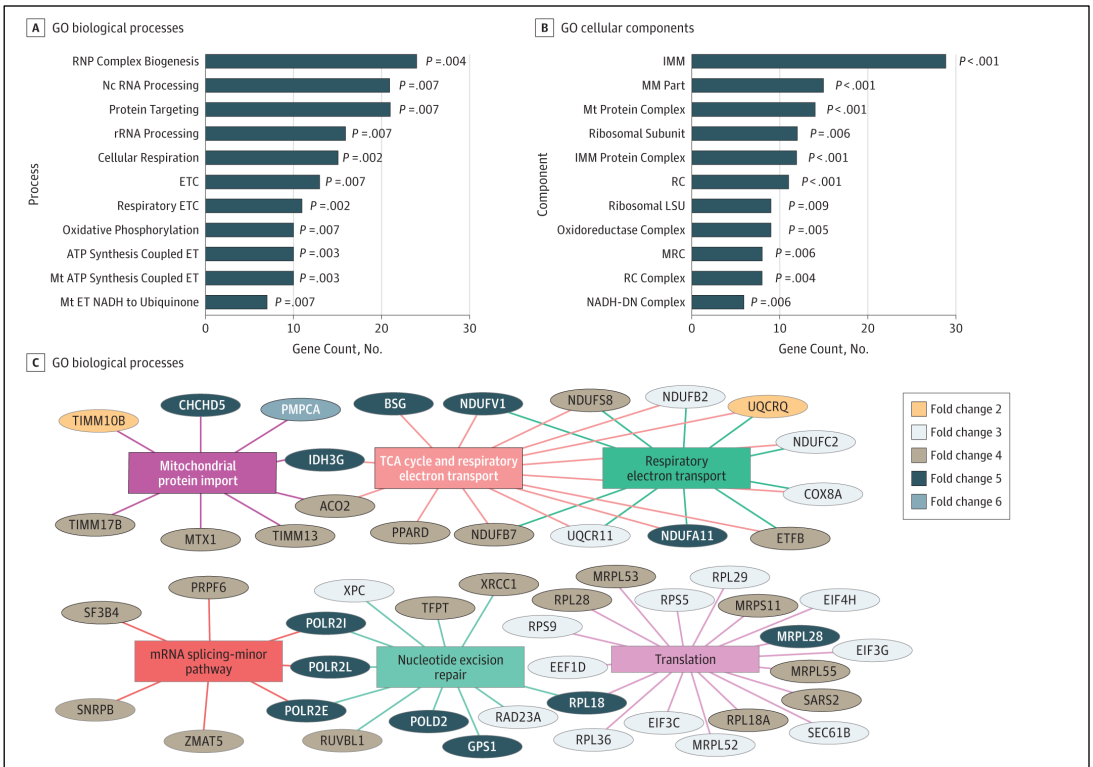

Figure 2. Gene Ontology (GO) and Reactome Pathway Enrichment Analysis of the Differentially Expressed Genes in Human Nasal Epithelium Exposed to Thirdhand Smoke. Bar charts show the most highly enriched biological process (A) and cellular component (B) GO terms. Each bar represents the number of genes identified in our study that are associated with each process or component. All biological processes and cellular components identified had an adjusted P value for multiple testing less than 0.05. (C) Network plot shows the top 6 enriched pathways and the associated genes using Reactome pathway analysis. Also shown are the approximate fold change values of each gene. The colored lines show the link between the genes and pathways identified. ATP indicates adenosine triphosphate; ET, electron transport; ETC, electron transport chain; IMM, mitochondrial inner membrane; LSU, large subunit; MM, mitochondrial membrane; MRC, mitochondrial respiratory chain; mRNA, messenger RNA; Mt, mitochondria; NADH-DN, nicotinamide adenine dinucleotide dehydrogenase complex; Nc, noncoding RNA; RC, respiratory chain; RNP, ribonucleoprotein; rRNA, ribosomal RNA; and TCA, trichloroacetic acid cycle.

Ingenuity Pathway Analysis

IPA was also performed using upregulated genes in the THS-exposed group. The top pathways identified included Sirtuin Signaling Pathways, EIF2 Signaling, Mitochondrial Dysfunction, and Oxidative Phosphorylation (Table 1). Some pathways identified in IPA overlapped with those identified using Reactome enrichment analysis, including Mitochondrial Related Pathways and DNA repair-related pathways. The top toxicological pathways identified included mainly processes related to mitochondrial activity, such as Mitochondrial Dysfunction, Increases Transmembrane Potential of Mitochondria & Mitochondrial Membrane, and Decreases Permeability Transition of Mitochondria & Mitochondrial Membrane. In addition, genes were linked to Glutathione Depletion Phase II Reactions (Table 1).

IPA identified Diseases and Functions that are associated with the DEGs after THS exposure (Table 2). These data were filtered and only functions with activated z-scores that predict transcriptional activation or inhibition based on literature reports are presented (Table 2). The identified functions included decreased cell death and increased cell viability, homologous recombination, and cell proliferation. eFigure 3 in the Supplement shows up-regulated genes associated with inhibition of cell death. The figure includes gene names and whether their expression could activate (orange lines) or inhibit (blue lines) cell death. For cell death, the majority of the up-regulated genes predict inhibition (blue lines). Based on each gene's biological role, IPA predicted that cell death

had an activation z-score of - 3.117 (overall process decreased) (Table 2). Complementary to cell death, cell viability (z-score = 5.026) (eFigure 4 in the Supplement) and homologous recombination (z score = 2.828) (eFigure 5 in the Supplement) both had increased activation states (Table 2)

Table 1. Ingenuity Pathway Analysis–Enriched Pathways After Exposure to Thirdhand Smoke

Pathway	*P* Value	*P* Value >.01	*P* Value <.01	Genes, No.
Canonical pathways				
Sirtuin signaling pathway	.01	X		11
EIF2 signaling	.006		X	10
Mitochondrial dysfunction	.002		X	9
Oxidative phosphorylation	.001		X	8
Hereditary breast cancer signaling	.03	X		6
Oncostatin M signaling	.003		X	4
Nucleotide excision repair pathway	.003		X	4
Colanic acid building blocks biosynthesis	.002		X	3
Methionine degradation I (to homocysteine)	.005		X	3
Cysteine biosynthesis III (mammalia)	.006		X	3
Glutathione-mediated detoxification	.008		X	3
Superpathway of methionine degradation	.02	X		3
Serine biosynthesis	.003		X	2
Superpathway of serine and glycine biosynthesis I	.006		X	2
γ-glutamyl cycle	.02	X		2
UDP-*N*-acetyl-D-galactosamine biosynthesis I	.02	X		1
Spliceosomal cycle	.03	X		1
L-DOPA degradation	.03	X		1
GDP-L-fucose biosynthesis I (from GDP-D-mannose)	.03	X		1
Top toxicological pathways				
Mitochondrial dysfunction	.003		X	9
Increased transmembrane potential of mitochondria and mitochondrial membrane	.06	X		3
Decreased permeability transition of mitochondria and mitochondrial membrane	.006		X	2
Glutathione depletion phase II reactions	.04	X		2

Table 2. Disease and Function Annotations From Ingenuity Pathway Analysis

Categories	Diseases or Functions Annotation	Predicted Activation State	Activation *z* Score	Molecules, No.	*P* Value	*P* Value	
						>.01	<.01
Cell death and survival	Cell death	Decreased	−3.117	77	.002		X
Cell death and survival	Apoptosis	Decreased	−3.686	63	.001		X
Cell death and survival	Necrosis	Decreased	−2.641	59	.04	X	
Cell death and survival	Cell death of tumor cell lines	Decreased	−3.029	50	.03	X	
Cell death and survival	Apoptosis of tumor cell lines	Decreased	−2.617	41	.02	X	
Cell death and survival	Cell viability	Increased	5.026	38	.01	X	
Cell death and survival	Cell viability of tumor cell lines	Increased	4.59	32	.02	X	
Cell death and survival	Cell viability of breast cancer cell lines	Increased	3.094	10	.02	X	
Cell death and survival	Cell viability of blood cells	Increased	2.195	6	.02	X	
Cell death and survival	Cell viability of leukocytes	Increased	2.2	5	.03	X	
Infectious diseases	Viral Infection	Increased	5.315	54	.002		X
Infectious diseases	Infection by RNA virus	Increased	4.494	31	.03	X	
Infectious diseases	Infection of cells	Increased	4.594	29	.009		X
Infectious diseases	Infection by HIV-1	Increased	4.301	23	.02	X	
Infectious diseases	Replication of RNA virus	Increased	3.087	19	.004		X
Infectious diseases	Infection of cervical cancer cell lines	Increased	3.772	18	.01	X	
Infectious diseases	Replication of influenza A virus	Increased	2.824	13	.005		X
Cell cycle, DNA replication, recombination, and repair	Homologous recombination of cells	Increased	2.828	8	<.001		X
Cellular development, cellular growth and proliferation	Cell proliferation of breast cancer cell lines	Increased	2.811	18	.03	X	

Discussion

The adverse health effects of THS have been studied in cultured cells and animal models[2], but similar investigations have not been previously performed on human subjects. Our study provides the first insight into the transcriptional responses of human respiratory epithelium to acute THS exposure. Remarkably, we found changes in gene expression in healthy nonsmokers following a 3-hour exposure to THS. The absence of an effect following clean air exposure provides evidence that the changes in gene expression following THS exposure are caused by THS *per se* and are not by the respirator worn during exposure. Because gene expression in the nasal epithelium is similar to the bronchial epithelium[33], our data are also relevant to the cells deeper in the respiratory system.

Our analyses demonstrate that brief exposure to THS affects mitochondrial activity. We previously reported that cultured mNSC undergo SIMH following exposure to THS extracts[12]. This process was originally described during treatment of mouse embryonic fibroblasts with UV light and cell cycle inhibitors, such as actinomycin D[13]. SIMH is characterized by fusion of mitochondria and subsequent increased production of ATP and superoxide[12]. We found an enrichment in pathways and biological processes related to increased mitochondrial activity and oxidative stress after THS exposure, such as mitochondrial ATP synthesis coupled electron transport chain (GO:0042773), respiratory electron transport (R-HSA-611105) and oxidative phosphorylation

(IPA). Increased expression of these pathways is also consistent with an increase in ATP synthesis, as occurs in SIMH[12]. Some genes related to the TCA cycle were also upregulated, which could also increase ATP production. Several studies have shown that cigarette smoking also induces activation of mitochondrial pathways similar to those found in our study[34,35,36].

While SIMH results in increased ATP production, it also increases ROS[12,13]. Our IPA analysis showed that Glutathione Depletion Phase II Reactions were upregulated after THS exposure. Specifically, there was an increase in glutathione synthetase (GSS) expression, which was also increased in a male germ cell line exposed to THS[14]. This gene is part of the glutathione (GSH) synthetase pathway, which scavenges ROS[37], suggesting the increase of the GSS gene is a cellular response to high levels of ROS.

In prior studies, increased ROS was associated with oxidative stress and damage of proteins, lipids and DNA[38], while THS treatment was correlated with DNA damage *in vitro*[10,9]. Our IPA-based enriched pathway analysis included up-regulation of the Nucleotide Excision Repair Pathway in THS exposed subjects. Two of the genes affected in this pathway included Xeroderma pigmentosum group C (XPC) and RNA polymerase II. The former is essential for recognition of DNA damage and plays a role in the early steps of the Nucleotide Excision Repair Pathway[39]. Up-regulation of RNA polymerase II has also been associated with a response to increased DNA damage[40]. IPA also identified an increased activation of homologous recombination. This pathway provides a repair

mechanism for double stranded DNA breaks[41]. Activation of the DNA repair pathways is also a cellular mechanism to facilitate survival[42]. In addition, an in vitro study showed that THS induces oxidation of mitochondrial proteins[12]. The increase in ROS as evidenced by upregulation of ROS scavenging genes in our data could also result in oxidation of mitochondrial proteins by high local concentrations of superoxide.

Our data further demonstrate that there is an overall increase in processes related to cell viability, which includes some genes involved in cell proliferation. Our results are consistent with previous *in vitro* studies showing increased proliferation of cultured mouse neural stem cells and human lung cancer cells exposed to THS extract[12, 43]. Nicotine, a major component of THS[4] and a chemical in our exposure chamber, can activate alpha nicotinic acetylcholine receptors (nAChRs) in normal human airway epithelial cells, leading to phosphorylation (activation) of serine/threonine kinase Akt, which is involved in many cellular survival pathways[44]. Akt can be activated within minutes of exposure to nicotine or NNK[44], further demonstrating that chemicals in THS could produce a rapid response. Nicotine is also associated with increased proliferation of human cancer cell lines by activating the 7α nAChR[45]. Considering that nicotine stimulates cell proliferation[45], it is possible that nicotine in THS contributes to the increase in cell viability pathways that we observed.

Nicotine is also involved in inhibiting apoptosis[46]. In our study, the increased expression of genes involved in inhibiting cell death (IPA) may have

been associated with nicotine, which was present in the THS at a concentration of 0.03 mg/m^3. Consistent with our study, cells exposed to THS *in vitro* showed decreased expression in pro-apoptotic genes[12]. The mechanism by which nicotine inhibits apoptosis has been studied in mouse liver cells[47]. Activation of 7α nAChRs in the mitochondrial outer membrane by nicotine inhibited hydrogen peroxide induced apoptosis by impairing Ca^{2+} accumulation in mitochondria and cytochrome C release[47]. However, this suppression of cell death may be transitory. Bahl et al.[12] showed that cells exposed to THS for 30 days had a decrease in cell proliferation and lost mitochondrial membrane potential, indicating that cells were entering apoptosis.

Limitations. This is an initial study based on four participants. Future work should be done to determine if similar data are obtained with a larger number of subjects that includes both genders.

In summary, this is the first exposure study to document an association between THS and gene expression in human subjects. Our results show that THS induced cell survival responses, which included up-regulation of genes involved in DNA repair, activation of cell viability, increased mitochondrial activity, and inhibition of cell death (Figure 3). These changes are very similar to those reported previously for in vitro cultured cells[9,11,12]. Importantly, the changes in gene expression in the current study were seen following a relatively short (3 hr) exposure, indicating that humans respond rapidly to THS. Future studies on long-term exposure in conjunction with our study would help complete our

understanding of the effects of THS on human health. Our study provides an important foundation for physicians treating patients exposed to THS and for future development of regulations dealing with remediation of indoor environments contaminated with THS.

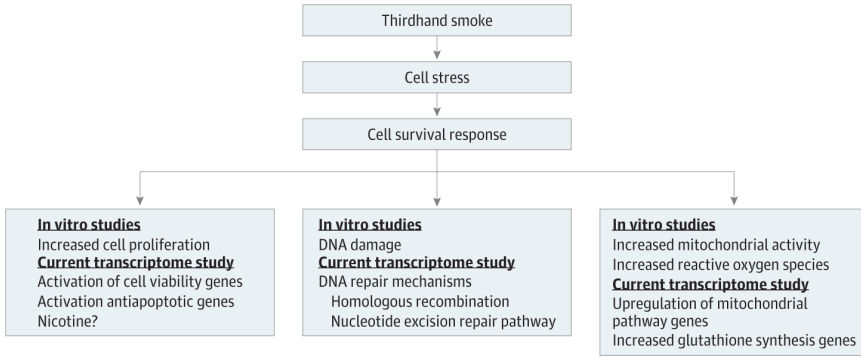

Figure 3. Schematic Diagram Summarizing the Responses of Human Nasal Epithelium to Thirdhand Smoke. Thirdhand smoke induced cellular stress leading to activation of cell survival responses, including activation of DNA repair pathways, increased cell proliferation, and increased mitochondrial activity in the human nasal epithelium. Previous in vitro studies have shown similar results in which thirdhand smoke causes DNA damage, increased cell proliferation, increased mitochondria activity and increased reactive oxygen species.

References

1. Matt GE, Quintana PJE, Destaillats, H, et al. Thirdhand tobacco smoke: Emerging evidence and arguments for a multidisciplinary research agenda. *Environmental Health Perspectives.* 2011:119(9):1218-1226.doi:10.1289/ehp.1103500.

2. Jacob III P, Benowitz NL, Destaillats H, et al. Thirdhand smoke: New evidence, challenges, and future directions. *Chemical Research in Toxicology.* 2017;30: 270−294. doi:10.1021/acs.chemrestox.6b00343.

3. Singer BC, Hodgson AT, Nazaroff WW. Gas-phase organics in environmental tobacco smoke: 2. Exposure-relevant emission factors and indirect exposures from habitual smoking. *Atmospheric Environment. 2003;*37: 5551–5561.doi:10.1016/j.atmosenv.2003.07.015.

4. Bahl V, Jacob III P, Havel C, et al. Thirdhand cigarette smoke: Factors affection exposure and remediation. *PLOS ONE*. 2014;9(10): e108258. doi:10.1371/journal.pone.0108258.

5. Sleiman M, Gundel LA, Pankow JF, et al. Formation of carcinogens indoors by surface-mediated reactions of nicotine with nitrous acid, leading to potential thirdhand smoke hazards. *PNAS.* 2010;107(15): 6576-6581.doi:10.1073/pnas.0912820107.

6. Schick SF, Farraro KF, Perrino C, et al. Thirdhand cigarette smoke in an experimental chamber: evidence of surface deposition of nicotine, nitrosamines and polycyclic aromatic hydrocarbons and de novo formation of NNK. *Tobacco Control.* 2014;23:152-159.doi: 10.1136/ tobaccocontrol-2012-050915.

7. Hoffmann D, Hecht SS. Nicotine-derived N-Nitrosamines and tobacco-related cancer: Current status and future directions. *Cancer Research*. 1985; 45; 935-944.

8. Petrick L, Destaillats H, Zouev I, et al. Sorption, desorption, and surface oxidative fate of nicotine. *Physical Chemistry Chemical Physics.* 2010*;*12:10356–10364.doi:10.1039/c002643c.

9. Hang B, Sarker AH, Havel C, et al. Thirdhand smoke causes DNA damage in human cells. *Mutagenesis.* 2013; 28(4): 381–391. doi:10.1093/mutage/get013.

10. Bahl V, Shim HJ, Jacob III P, et al. Thirdhand smoke: Chemicals dynamics, cytotoxicity, and genotoxicity in outdoor and indoor environments. *Toxicology in Vitro.* 2016; 32: 220-231. doi:10.1016/j.tiv.2015.12.007.

11. Bahl V, Weng NJH, Schick SF, et al. Cytotoxicity of thirdhand smoke and identification of acrolein as a volatile thirdhand smoke chemical that inhibits cell proliferation. *Toxicological Science*. 2016b;50(1): 234-246.doi:10.1093/toxsci/kfv327.

12. Bahl V, Johnson K, Phandthong R, et al. Thirdhand cigarette smoke causes stress-induced mitochondria hyperfusion and alters the transcriptional profile of stem cells. *Toxicological Science.* 2016c;53(1): 55–69. doi:10.1093/toxsci/kfw102.

13. Tondera D, Grandemange S, Jourdain A, et al. SLP-2 required for stress induced mitochondrial hyperfusion. *The EMBO Journal.* 2009;28:589–1600. doi:10.1038/emboj.2009.89.

14. Xu B, Chen M, Yao M, et al. Metabolomics reveals metabolic changes in male reproductive cells exposed to thirdhand smoke. *Scientific Reports.* 2015;5:15512.doi:10.1038/srep15512.

15. Martins-Green M, Adhami N, Frankos M, et al. Cigarette smoke toxins deposited on surfaces: Implications for human health. *PLoS ONE.* 2014;9(1): e86391. doi:10.1371/journal.pone.0086391.

16. Adhami, N, Starck, SR, Flores, C, and Martins-Green, M. A health threat to bystanders living in the homes of smokers: How some toxins deposited on surfaces can cause insulin resistance. *PLoS One*. 2016;11(3): e0149510. doi:10.1371/journal.pone.0149510.

17. Adhami N, Chen Y, Martins-Green M. Biomarkers of disease can be detected in mice
as early as 4 weeks after initiation of exposure to third-hand smoke levels equivalent to those found in homes of smokers. *Clinical Science*. 2017;131:2409-2426. doi:10.1042/CS20171053.

18. Hang B, Snijders, AM, Huang Y, et al. Early exposure to thirdhand cigarette smoke effects body mass and the development of immunity in mice. *Scientific Reports.* 2017*;* 7: 41915. doi:10.1038/srep41915.

19. Matt GE, Quintana PJE, Zakarina JM, et al. When smokers move out and non-smokers move in: residential thirdhand smoke pollution and exposure. *Tobacco Control*. 2011;20: e1
doi:10.1136/tc.2010.037382.

20. Matt GE, Quintana PJE, Hovell MF, et al. Residual tobacco smoke pollution in used cars for sale: Air, dust, and surfaces. *Nicotine & Tobacco Research.* 2008;10(9):1467-1475. doi: 10.1080/14622200802279898.

21. Beko G, Morrison G, Weschler CJ, Koch HM, et al. Dermal uptake of nicotine from air and clothing: Experimental verification. *Indoor Air. 2018;* 28: 247-257.doi: 10.1111/ina.12437.

22. Matt GE, Quintana PJE, Hovell MF, et al. Households contaminated by environmental tobacco smoke: sources of infant exposures. *Tobacco Control*. 2004;13: 29–37. doi: 10.1136/tc.2003.003889.

23. Schick SF, Farraro KF, Fang J, et al. An apparatus for generating aged cigarette smoke for controlled human exposure studies. *Aerosol Science and Technology.* 2012;46(11):1246–1255.doi:10.1080/02786826.2012.708947.

24. Backman TWH, Girke T. systemPiperR: NGS workflow and report generation environment. BMC Bioinformatics. *BMC Bioinformatics.* 2016;17:388.doi:10.1186/s12859-016-1241-0.

25. Bolger AM, Lohse M, Usadel B. Trimmomatic: a flexible trimmer for illumine sequence data. *Genome analysis.* 2014; 30(15): 2114-2120. doi:10.1093/bioinformatics/btu170.

26. Langmead B, Salzberg S. Fast gapped-read alignment wit Bowtie 2. *Nature Methods.* 2013;9(4):357–359. doi:10.1038/nmeth.1923.

27. Kim D, Pertea G, Trapnell C, et al. TopHat2: accurate alignment of transcriptomes in the presence of insertions, deletions and gene fusions. *Genome Biology.* 2013;14:R36. doi:10.1186/gb-2013-14-4-r36.

28. Lawrence M, Huber W, Pages H, et al. Software for computing and annotating genomics ranges. *PLoS Computational Biology.* 2013;9(8), e1003118. doi:10.1371/journal.pcbi.1003118.

29. Robinson MD, McCarthy DJ, Smyth GK. edgeR: a Bioconductor package for differential expression analysis of digital gene expression data. *Bioinformatics.* 2010;26(1):139-140. doi:10.1093/bioinformatics/btp616.

30. Yu G, Wang LG, Han Y, et al. clusterProfiler: an R Package for comparing biological themes among gene clusters. *Technical Communication.* 2012;16(5): 284-287. doi: 10.1089/omi.2011.0118.

31. Yu G, He QY. ReactomePA: an R/Bioconductor package for reactome

pathway analysis and visualization. *Molecular BioSystems* 2016;12: 477-479. doi: 10.1039/c5mb00663e

32. Blake JA, Christie KR, Dolan ME, et al. Gene Ontology Consortium: going forward. *Nucleic Acids Res*. 2015;43:D1046-56. doi: 10.1093/nar/gku1179.

33. Perez-Rogers JF, Gerrein J, Anderlind C, et al. Share gene expression alterations in nasal and bronchial epithelium for lung cancer detection. *JNCI Journal of the National Cancer Institute.* 2007;109(7):djw327. doi: 10.1093/jnci/djw327.

34. Suter M, Ma J, Harris AS, et al. Maternal tobacco use modestly alters correlated epigenome-wide placental DNA methylation and gene expression. *Epigenetics* 2011;6(11):1284-1294.doi:10.4161/epi.6.11.17819.

35. Wang J, Cui W, Wei J, et al. Genome-wide expression analysis reveals diverse effects of acute nicotine exposure on neuronal function-related genes and pathways. *Frontiers in Psychiatry*. 2011;2:5. doi: 10.3389/fpsyt.2011.00005.

36. Pierrou S, Broberg P, O'Donnell RA, et al. Expression of genes involved in oxidative stress responses in airway epithelial cells of smokers with chronic obstructive pulmonary disease. *American Journal of Respiratory and Critical Care Medicine*. 2007;175(6): 577–586. doi: 10.1164/rccm.200607-931OC.

37. Patlevic P, Vaskova J, Svorc PJ, et al. Reactive oxygen species and antioxidant defense in human gastrointestinal diseases. *Integrative Medicine Research.* 2016;5:250-258. doi: 10.1016/j.imr.2016.07.004.

38. Schieber M, Chandel NS. ROS function in redox signaling and oxidative stress. *Current Biology.* 2014;24(10): R453-R462. doi:10.1016/j.cub.2014.03.034.

39. Sears CR, Zhou H, Justice MJ, et al. Xeroderna pigmentosum group C deficiency alters cigarette smoke DNA damage cell fate and accelerates emphysema development. *American Journal of Respiratory Cell and Molecular Biology.* 2018;58(3):402-411. doi: 10.1165/rcmb.2017-0251OC.

40. Chiou YY, Hu J, Sancar A, et al. RNA polymerase II is released from the DNA template during transcription-coupled repair in mammalian cells. *J Biol Chem.* 2018;293(7):2476-2486. doi:10.1074/jbc.RA117.000971.

41. Jasin M, Rothstein R. Repair of strand breaks by homologous recombination. *Cold Spring Harbor Perspectives in Biology.* 2013;5: a012740. doi: 10.1101/cshperspect.a012740

42. Hoeijmakers JHJ. DNA Damage, aging, and cancer. *N Engl J Med*. 2009; 361:1475-85.doi: 10.1056/NEJMra0804615

43. Hang B, Wang Y, Huang Y, et al. Short-term early exposure to thirdhand cigarette smoke increases lung cancer incidence in mice. *Clinical Sciences*. 2018; 132:475-488. doi.org/10.1042/CS20171521

44. West KA, Brognard J, Clark AS, et al. Rapid Akt activation by nicotine and a tobacco carcinogen modulates the phenotype of normal human airway epithelial cells. *Journal of Clinical Invest*igation. 2003;111: 81–90. doi:10.1172/JCI200316147.

45. Dasgupta P, Rizwani W, Pillai S, et al. Nicotine induces cell proliferation, invasion and epithelial-mesenchymal transition in a variety of human cancer cell line. *International Journal of Cancer*. 2009;124:36–45. doi:10.1002/ijc.23894.

46. Mai H, May WS, Gao F, Jin Z, Deng X. A functional role for nicotine in Bcl2 phosphorylation and suppression of apoptosis. *The Journal Biological Chemistry.* 2003; 278:1886-1891. doi: 10.1074/jbc.M209044200

47. Gergalova G, Lykhmus O, Kalashnyk O, et al. Mitochondria express alpha-7 nicotinic acetylcholine receptors to regulate Ca^{2+} accumulation and cytochrome *c* release: study of isolated mitochondria. *PLoS ONE*. 2012; 7(2):e31361. doi:10.1371/journal.pone.0031361

Chapter 5

Transcriptomic Evidence that Switching from Tobacco to Electronic Cigarettes does not Reverse Damage to the Respiratory Epithelium

Abstract

The health benefits of switching from tobacco to electronic cigarettes (ECs) are not well characterized. To address this problem, we used RNA-seq analysis to compare the nasal epithelium transcriptome from the following groups (n=3 for each group): (1) former smokers who completely switched to second generation ECs for at least 6 months, (2) current tobacco cigarette smokers (CS), and (3) non-smokers (NS). Group three included one former cigarette smoker. The nasal epithelial biopsies from the EC users vs NS had a higher number of differentially expressed genes (DEGs) than biopsies from the CS vs NS and CS vs EC sets (1,817 DEGs total for the EC vs NS, 407 DEGs for the CS vs NS, and 116 DEGs for the CS vs EC comparison). In the EC vs NS comparison, enriched gene ontology terms for the downregulated DEGs were consistent with ciliogenesis and ciliary movement, while gene ontologies for upregulated DEGs included immune response, keratinization, and NADPH oxidase. Similarly, ontologies for cilium movement were enriched in the downregulated DEGs for the CS vs NS group. Reactome pathway analysis gave similar results and also identified keratinization and cornified envelope in the upregulated DEGs in the EC vs NS comparison. In the CS vs NS comparison, the enriched Reactome pathways for upregulated DEGs included biological oxidations and several metabolic processes. Regulator effects identified for the EC vs NS comparison were inflammatory response, cell movement of phagocytes and degranulation of phagocytes. Disease Ontology Sematic Enrichment analysis identified lung

disease, mouth disease, periodontal disease and pulmonary fibrosis in the EC vs NS comparison. Squamous metaplasia associated markers, keratin 10, keratin 13 and involucrin, were increased in the EC vs NS comparison. Our transcriptomic analysis showed that gene expression profiles associated with EC use are not equivalent to those from non-smokers. EC use may interfere with airway epithelium recovery by promoting increased oxidative stress, inhibition of ciliogenesis, and maintaining an inflammatory response. These transcriptomic alterations may contribute to the progression of diseases with chronic EC use.
Keywords: Electronic cigarettes, Cigarette smoke, Transcriptomic analysis, Immune response, Oxidative stress, Squamous metaplasia, Ciliogenesis

1. Introduction

Electronic cigarettes (ECs) are popular battery-operated devices, which aerosolize e-liquids (nicotine or non-nicotine containing flavored mixtures) using a heating coil (Trtchourian and Talbot 2010; NAS, 2018). Some studies have suggested that EC use may be a healthy long-term alternative to cigarette smoking that can help reverse and prevent progression of tobacco related respiratory diseases (Polosa *et al.,* 2014;2016; 2015;2018; Adriaens *et al.,* 2014, Goniewicz 2020). Some cigarette smokers who became EC users or dual users have self-reported reduction of respiratory symptoms after switching (Arnold *et al*. 2021, Polosa *et al.* 2014, 2016, 2018). In contrast, others have self-reported that respiratory symptoms worsen with EC use (Hua *et al.* 2013, 2020). In addition, a number of case studies have linked EC use to adverse effects in the respiratory, gastrointestinal, cardiovascular, neurological and immune systems (Hua *et al.,* 2016). In 2019, an outbreak of e-cigarette or vaping-related acute lung injury (EVALI) was reported in the United States. Patients with EVALI reported adverse respiratory symptoms such as coughing, dyspnea, pleuritic chest pain as well as abnormal pulmonary radiographic phenotypes (Jonas *et al.* 2020, EVALI ref). Lung injuries included acute eosinophilic pneumonia and diffuse alveolar damage (Kanne *et al.,* 2020).

To better understand the effect of vaping nicotine on pulmonary health, transcriptomic studies have examined gene expression in EC users. These studies differ in the techniques used in comparison groups, and the generation of

ECs used is sometimes variable or not given. A prior study used a Nanostring immune expression panel to analyze nasal epithelial biopsies from non-smokers, cigarette smokers and former cigarette users who had switched to ECs for at least 6 months (this group included dual users). This study identified decreased expression of immune-related genes in the EC users and cigarette users compared to the non-smokers (Martin *et al.,* 2016). In another study, immune responses were altered in the EC group, which including former smokers and dual users, following inoculation with live-attenuated influenza virus (Rebuli et al., 2021).

Bronchial airway epithelial brushings were analyzed from former smokers, tobacco cigarette smokers and former smokers who switched to ECs for at least 3 months using whole-transcriptomic arrays (Corbett *et al.,* 2019). This study did not contain non-smokers. Here interleukin receptor complex associated genes were upregulated, while genes involved in cilia were downregulated in EC users compared to former smokers (Corbett *et al*., 2019). Variations in the results of these EC studies may be due to differences in the compositions of the groups, puffs/day, cigarette/day, the generation of ECs used, flavor chemicals and overall differences in experimental designs

The purpose of this study was to compare gene expression in nasal epithelial biopsies from individuals who: (1) were non-smokers, (2) exclusive tobacco cigarette smokers (CS group) and (3) exclusive EC users who had switched completely from tobacco cigarettes to second generation nicotine-containing ECs

for at least 6 months (EC group). Our transcriptomic analysis showed that some gene expression profiles in EC group had not reverted to those found in the non-smoker group. Long-term use of ECs may contribute to the progression of several respiratory diseases.

2. Materials and Methods

2.1. Sample collection and RNA extraction

Nasal biopsies from 22 human participants were collected in RNA Later (Qiagen, Hilden, Germany 76104) and frozen at Roswell Park Cancer Institute, Buffalo, New York. These were shipped frozen to the University of California, Riverside and stored at -80^{o}C until analyzed. For RNA extraction, individual samples were thawed on ice prior to further processing. The samples were washed twice using Dulbecco's phosphate buffered saline (Lonza, Basel, Switzerland Cat. No. 17-513F). Qiagen RNeasy Plus Microkit (Cat No./ID: 74304) was used to extract total RNA, which was resuspended in 15 µL of RNase free distilled water. Sterile Eppendorf tubes containing RNA samples were snap frozen in liquid nitrogen before storing at -80^{o}C.

2.2. Sample information, selection, and demographics

Information regarding smoking history was obtained from all the patients, and the levels of urine cotinine were measured at Roswell Park (S Table 1). Nineteen of the nasal biopsies samples from females were selected for RNA-seq analysis. The selection was based matching gender (all females), age, and ethnicity, as well as urine cotinine concentrations and good RNA quality (RIN numbers). The cotinine concentrations were used to discard NS that tested positive and to include those in the CS and EC group with medium to high concentrations of cotinine. The group selected for further study consisted of white

females below the age of 50 that had urine cotinine levels of at least 400 ng/ml (CS and EC groups) and undetectable cotinine (<0.25 ng/ml; NS group).

2.3. Library preparation and sequencing

RNA from all samples was extracted in house and shipped to Cofactor Genomics (St. Louis, MO) on dry ice for library preparation and sequencing. RNA quality was checked using a Bioanalyzer. Samples having good RIN numbers (>7) were selected for RNA-seq library preparation (mRNAble Cat No. CFG001-30) and subsequent sequencing steps were performed by Cofactor Genomics. Total RNA reverse transcription was performed with an Oligo(Dt) primer followed by limited cDNA amplification using the SMARTer® Ultra® Low Input RNA Kit for Sequencing–v4 (Takara Bio USA, Inc., Mountain View, CA). Next, the full-length cDNA was subject to fragmentation followed by tagging. The final sequencing cDNA library was generated using limited PCR enrichment (Nextera® XT DNA Library Prep, Illumina, San Diego, CA). Single-end 75 base pair reads were generated using the Illumina NextSeq500 platform. Resulting FASTQ files containing all the reads were provided to us on a URL.

2.4. Hierarchical clustering and differential expression analysis

The FASTQ files were processed at the University of California on a High Performance Computing Cluster (HPCC). The files were preprocessed to remove adapter sequences and low-quality score reads using the Trimmomatic package (Bolger et al. 2014). The alignment, raw read count steps, and differential gene calling steps were performed using a pre-built RNA-seq workflow known as

systemPipeR (Backman T. W. H. and Girke T., 2016). The Human reference genome (UCSC hg19) was obtained from Illumina iGenomes (ftp.illumina.com). Preprocessed reads were then aligned to the reference genome using Tophat2 (2.0.14) (Langmead and Salzberg, 2012; Kim *et al.,* 2013). Raw read counts for exonic gene regions as well as normalized RPKM (reads per kilobase per million) values were calculated with the summarizedOverlaps function of the GenomicAlignment package from Bioconductor. Genes having low expression counts were removed using a cut-off of an average of one CPM across all samples leaving a total of 15,440 genes for analysis. Hierarchical clustering was performed with hclust function using Spearman's correlation values as a similarity matric to identify outliers within each of the groups. After outliers were removed, each group (EC, NS and CS) had three individuals. Analysis of differentially expressed genes (DEGs) was performed with EdgeR between EC vs NS, CS vs NS and CS vs EC. (Robinson et al., 2010). Raw FASTQ files were submitted to public databases and can be accesses in the National Center for Biotechnology Information SRA database (PRJNA666452).

2.5. Gene Ontology (GO) enrichment and Reactome Pathway Analyses

Enrichment analysis was performed for GO terms (clusterProfiler package from R/Bioconductor) (Yu *et al.,* 2012), pathways (ReactomePA package) (Croft et al., 2014 and Fabregat et al., 2016), and disease (DOSE- Disease Ontology Sematic and Enrichment) (Yu et al. 2015). In all cases, over-representation analysis with the Fisher's exact test was used as a statistical test. The required

gene sets were obtained from the DEG analysis results by applying the following filter setting: logFC ≥ 1 (upregulated; or ≤ -1 for downregulated) and an FDR ≤ 0.05. Over-represented GO terms, pathways, and disease terms had to have an adjusted p-value ≤ 0.05 using the Bonferroni Hochberg method for multiple testing correction. The heatmap was generated using z-scaled RPKM values in pheatmap and RcolorBrewer packages.

2.6. Ingenuity Pathway Analysis (IPA)

IPA software (QIAGEN Inc., https://digitalinsights.qiagen.com/IPA) was used to identify enriched Diseases and Biological Functions and Regulator Effects. A core analysis was performed using the “human” and “lung system” prefilters. Cutoff values were set as follows: log-fold change +/- 0.6, p-value 0.05, and q-value 0.05. Significance of Disease and Biological Functions was determined using a p-value calculated with a right-tailed Fisher’s exact test. Molecular networks were generated using the “Path Explorer” function, which identified molecular targets in our data associated with “e-cigarette aerosol”, “nicotine” or “cigarette smoke” exposure and their downstream effect on biological functions. The “Molecule Activity Predictor” tool predicted the activation state of biological functions. Regulator Effects were extracted to identify upstream regulators and biological processes affected in our data set.

3. Results

3.1. Differential Gene Expression (DEGs) in EC, CS, and NS: Initial Analysis

For the initial analysis, we used DEGs sets obtained with an FDR ≤ 0.05 and a log2 fold change (LFC) ≥ 1. DEGs are shown for each of the three comparisons (EC vs NS, CS vs NS, CS vs EC) in the volcano plots (Figures 1A-C). The highest number of DEGs (1,410 total, 570 upregulated and 1,243 downregulated) was in the EC vs NS comparison (Figure 1A). Within the CS vs NS comparison, a total of 366 DEGs were found (132 upregulated and 281 downregulated) (Figure 1B). Fewer genes were differentially expressed in the CS vs EC comparison (115 total, 52 up and 64 downregulated) (Figure 1C). Figure 1D shows the number of DEGs that were in common in the three comparisons. The greatest overlap in DEGs was in the EC vs NS and CS vs NS comparisons (Figure 1D). The number of DEGs that were up and downregulated in the EC vs NS and CS vs NS groups are shown in Figure 1E. The highest number of overlapping DEGs was in the downregulated sets (Figure 1E). The expression pattern of the RPKM values of individual DEGs was different in the three groups (Figure 1F).

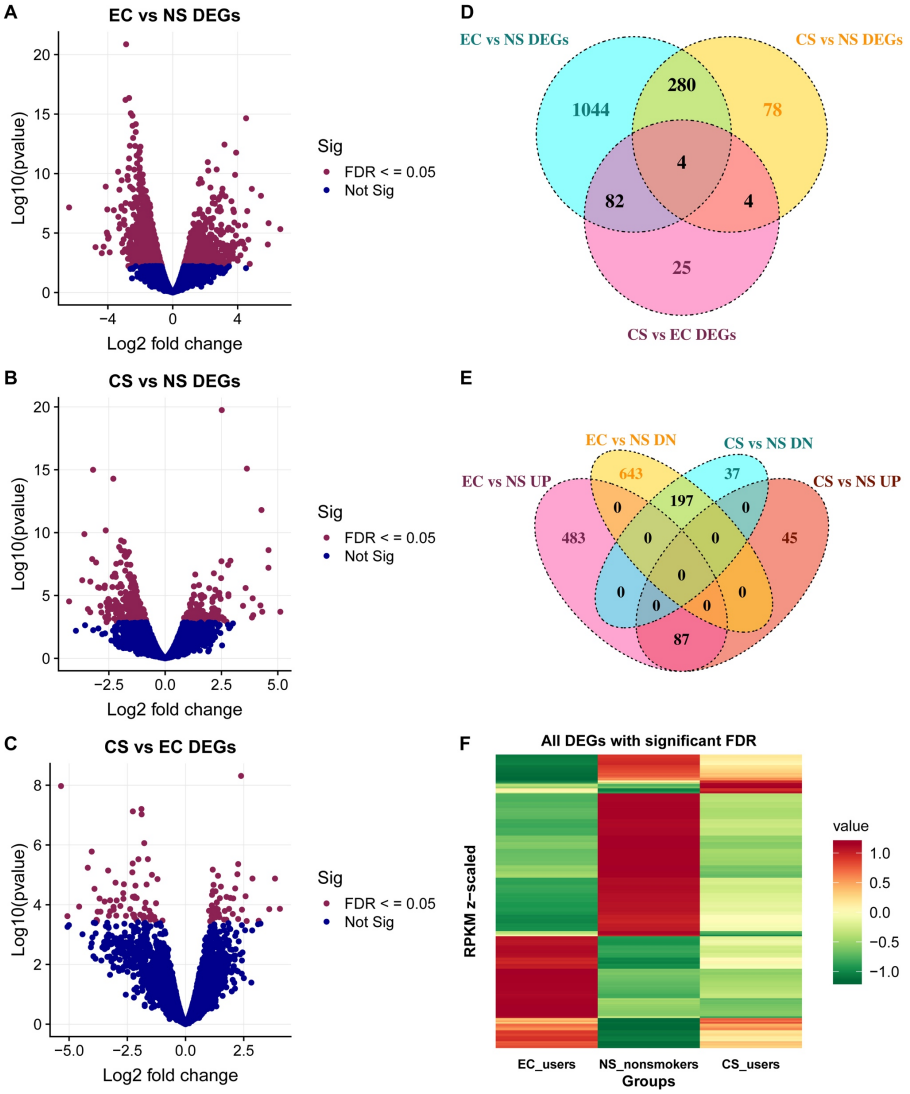

Figure 1: Differential gene expression in the EC, NS, and CS groups. Volcano plots showing DEGs in (A) EC vs NS, (B) CS vs NS, (C) CS vs EC. (D) Venn diagram showing all the DEGs in EC, NS and CS. (E) Venn diagram comparing the up and downregulated DEGs (FDR < 0.05) in the EC vs NS, CS vs NS, CS vs EC. (F) Heatmap showing the significant DEGs (FDR < 0.05) for each comparison.

3.2. GO term enrichment analysis for EC vs NS, CS vs NS, and CS vs EC

GO terms over-represented in the DEGs were identified using ClusterProfiler (Yu *et al.,* 2012) to obtain an overview of the processes affected in each group (Figure 2 and Tables S2- 4). Most of the enriched terms within the biological processes category for downregulated genes in the EC vs NS comparison included cilium organization (GO:0044782), cilium assembly (GO:0060271), cilium movement (GO:0003341), microtubule-based movement (GO:0007018), and plasma membrane bounded cell projection assembly (GO:0120031) (Figure 2A and Table S2A). Other biological processes included: nervous system process (GO:0050877), regulation of smoothened signaling pathway (GO:0008589), regulation of membrane potential (GO:0042391), and regulation of ion transport (GO:0043269) (Figure 2A and S Table 2A). For the downregulated DEGs, enriched cellular components included cilia-related terms and molecular functions included ion channel activity (GO:0005509, GO:0005216) and microtubule motor activity (GO:0003774, GO:0003777, GO:1990939, GO:0008569) (S Table 2B and Table S 2C).

Over-represented biological processes for upregulated genes in the EC vs NS comparison included inflammatory responses, such as neutrophil activation (GO:0042119), granulocyte activation (GO:0036230), and chronic inflammatory response (GO:0002544) (Figure 2B and Table S 2D). Other processes included response/regulation to wound healing (GO:0042060), response to bacterium (GO:0009611), blood coagulation and its regulation (GO:0030193), response to

xenobiotic stimulus (GO:0071466), and keratinization (GO:0031424) (Figure 2B and Table S 2D). The cellular component and molecular function terms for the upregulated DEGs included NADPH oxidase complex (GO:0043020) and superoxide-generating NADPH oxidase activator activity (GO:0008106) (S Table 2E and Table S 2F).

In the CS vs NS comparison, the biological processes and cellular components in the downregulated DEGs were similar to the EC vs NS group and included cilium assembly and organization (GO:0060271: GO:0044782: GO:0097014; GO:0005929) (Table S 3A-B). The molecular functions for the downregulated genes included ATP-dependent microtubule motor activity minus-end-directed (GO:0008569), dynein light chain binding (GO:0045503), dynein intermediate chain binding (GO:0045505), and ATP-dependent microtubule motor activity (GO:1990939) (S Table 3C). The upregulated biological processes included metabolic processes, such as monocarboxylic acid metabolic process (GO:0032787), anion transport (GO:0006820), and cellular response to xenobiotic stimulus (GO:0071466) (Fig 2D, S Table 3D). The enriched cellular components for the upregulated genes, were very-low-density lipoprotein particle (GO:0034361) and triglyceride-rich plasma lipoprotein particle (GO:0034385) (Supp. Table 3E). The molecular functions included glucuronosyltransferase activity (GO:0015020), monocarboxylic acid binding (GO:0033293), carboxylic acid binding (GO:0031406), organic acid binding (GO:0043177), and alcohol dehydrogenase (NADP+) activity (GO:0008106) (Supp. Table 3F).

The biological processes in the CS vs EC comparison for the downregulated genes included terms related to immune response, such as neutrophil activation (GO:0042119) and granulocyte activation (GO:0036230) (Figure 2E and Table S 4A). The cellular components for downregulated DEGs included secretory granule membrane (GO:0030667), keratin filament (GO:0045095) and intermediate filament (GO:0005882) (Supp. Table 4B). The biological processes and cellular components for upregulated genes were related to cilia assembly and movement (GO:0003341; GO:0060271; GO:0044782; GO:0097014, GO:0005929, GO:0044441) (Figure 2F, Table S 4D and Table S 4E). Dynein light chain binding (GO:0045503) was enriched by the upregulated DEGs (Table S 4F).

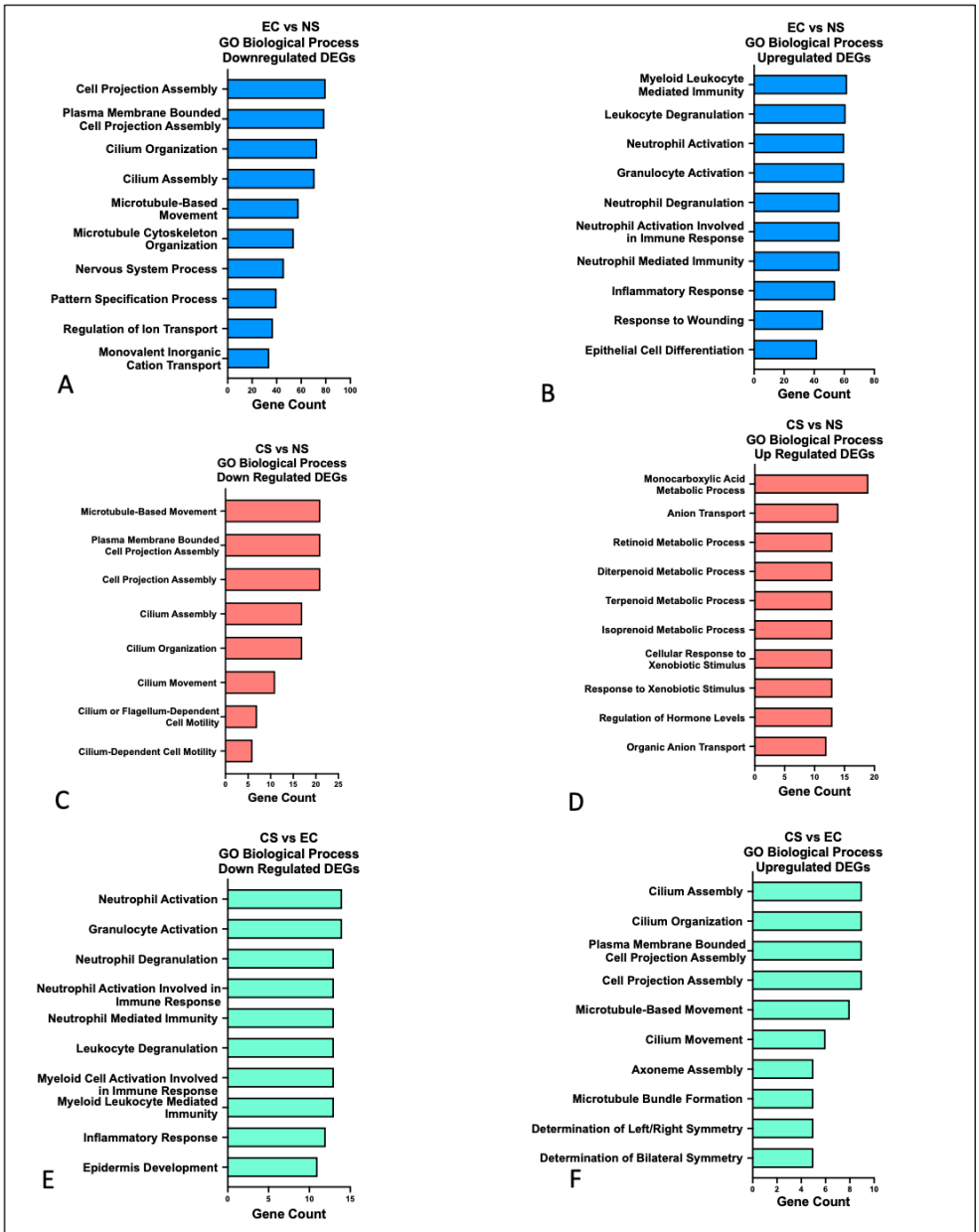

Figure 2: Top 10 enriched GO term annotations for each comparison. (A) Enriched downregulated biological processes in EC vs NS. (B) Enriched upregulated biological processes in EC vs NS. (C) Enriched downregulated biological processes in CS vs NS. (D) Enriched upregulated biological processes in CS vs NS. (E) Enriched downregulated biological processes in CS vs EC. (F) Enriched upregulated biological processes in CS vs EC. (FDR < 0.05).

3.3. IPA Biological Functions for EC vs NS

Biological functions analysis of lung-filtered data was done using IPA to make the analysis more specific to the lung and to obtain directionality. There was good agreement with results from the GO term analysis (Table S 5). The biological functions analysis in IPA for the EC vs NS comparison showed an increased predicted activation state (z-score > 2) for processes related to inflammatory response (e.g., response of myeloid cells, degranulation of phagocytes) and a decreased activation state (z-score < 2) for cilia formation. Other categories with increased activation states included cell-to-cell signaling, cell movement, and lipid metabolism (Table S 5). The other comparisons (CN vs NS and CN vs EC) did not have biological functions with a significant z-score (>2.0).

3.4. Reactome Pathway Enrichment Analysis for EC vs NS, CS vs NS and CS vs EC

Each comparison was also evaluated using Reactome enrichment analysis to identify the genes and pathways affected by smoking and EC use (Figure 3 and Figure S 1-3). In the EC vs NS comparison, the downregulated DEGs enriched pathways included organelle biogenesis and maintenance, cilium assembly, signaling by hedgehog, anchoring of the basal body to the plasma membrane, intraflagellar transport, and hedgehog “off state” (Figure 3A and Figure S 1A). The pathways identified with the upregulated DEGs of the EC vs NS comparison included neutrophil degranulation, keratinization, formation of

cornified envelope, cell surface interactions at the vascular wall, and interleukin-4 and 13 signaling (Figure 3B and Figure S 1B). For CS vs NS, the upregulated pathways included biological oxidations, metabolism of vitamins and cofactors, phase II – conjugation of compounds, and glucuronidation (Figure S 1C and Figure S 2). Pathways for the downregulated DEGs were not identified in the CS vs NS comparison. In the CS vs EC comparison, four pathways were enriched by the downregulated DEGs, which included neutrophil degranulation, signaling by interleukins, keratinization, and formation of cornified envelope (Figure S 1D and Figure S 3). No pathways were enriched by the upregulated DEGs.

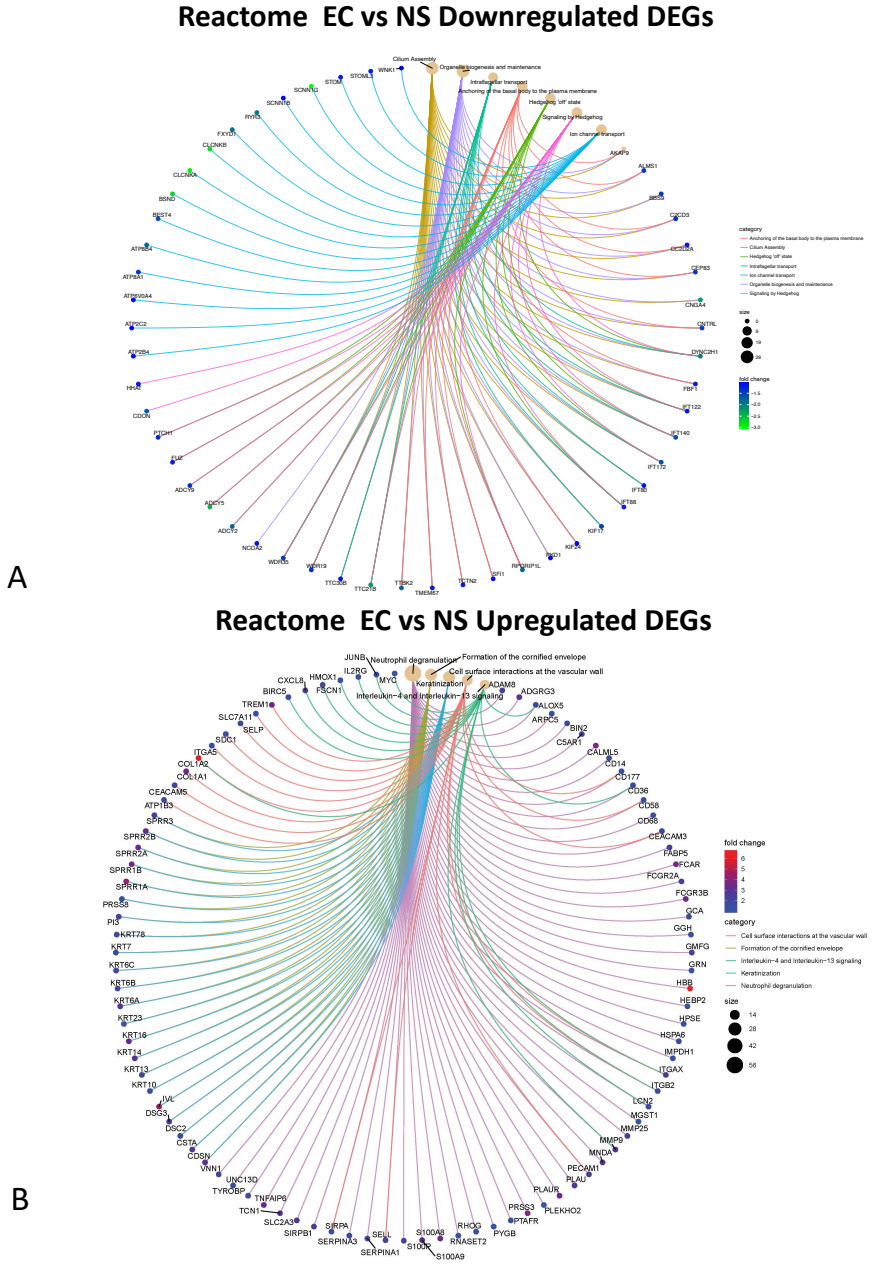

Figure 3. CNET diagrams showing the top altered Reactome pathways. (A) CNET diagram showing downregulated enriched pathways in EC vs NS. (B) CNET diagram showing upregulated enriched pathways in EC vs NS. Diagram shows the DEGs associated with each pathway and their fold changes (color key on right). Circle size key indicates the number of genes associated with each pathway.

3.4. Canonical Pathway using IPA

There was one significant canonical pathway identified using a lung filtered data set for the EC vs NS comparison, leukocyte extravasation signaling (z-score 2.668). For the CS vs NS data, there were no pathways with significant z-scores; however, methylglyoxal degradation III, a relevant pathway was significant. Only one canonical pathway with an activated z score was identified in the CS vs EC comparison (LXR/RXR activation, z score 2).

3.5. Networks Identified in the EC vs NS Comparison

DEGs in our data were compared to genes in the QIAGEN Knowledge Base to identify networks activated by “E-Cigarette Smoke”, “Nicotine”, or “Cigarette Smoke” using the “Path Explorer” tool in IPA (Figure 4). Pathway connections that were found included: (1) “E-cigarette Smoke” to “Activation of Mitochondria”, (2) “Nicotine” to “Dysfunction of Mitochondria”, and (3) “Cigarette Smoke” to activation of “Oxidative Phosphorylation” (Fig 4A-C). These networks are consistent with increases in mitochondria activity in the EC vs NS group. Additional networks were also found linking “Cigarette Smoke” to inhibition of “Formation of Cilia” and linking “E-Cigarette Smoke” to activation of “Would Healing Signaling Pathway” (Figures 5 A-B).

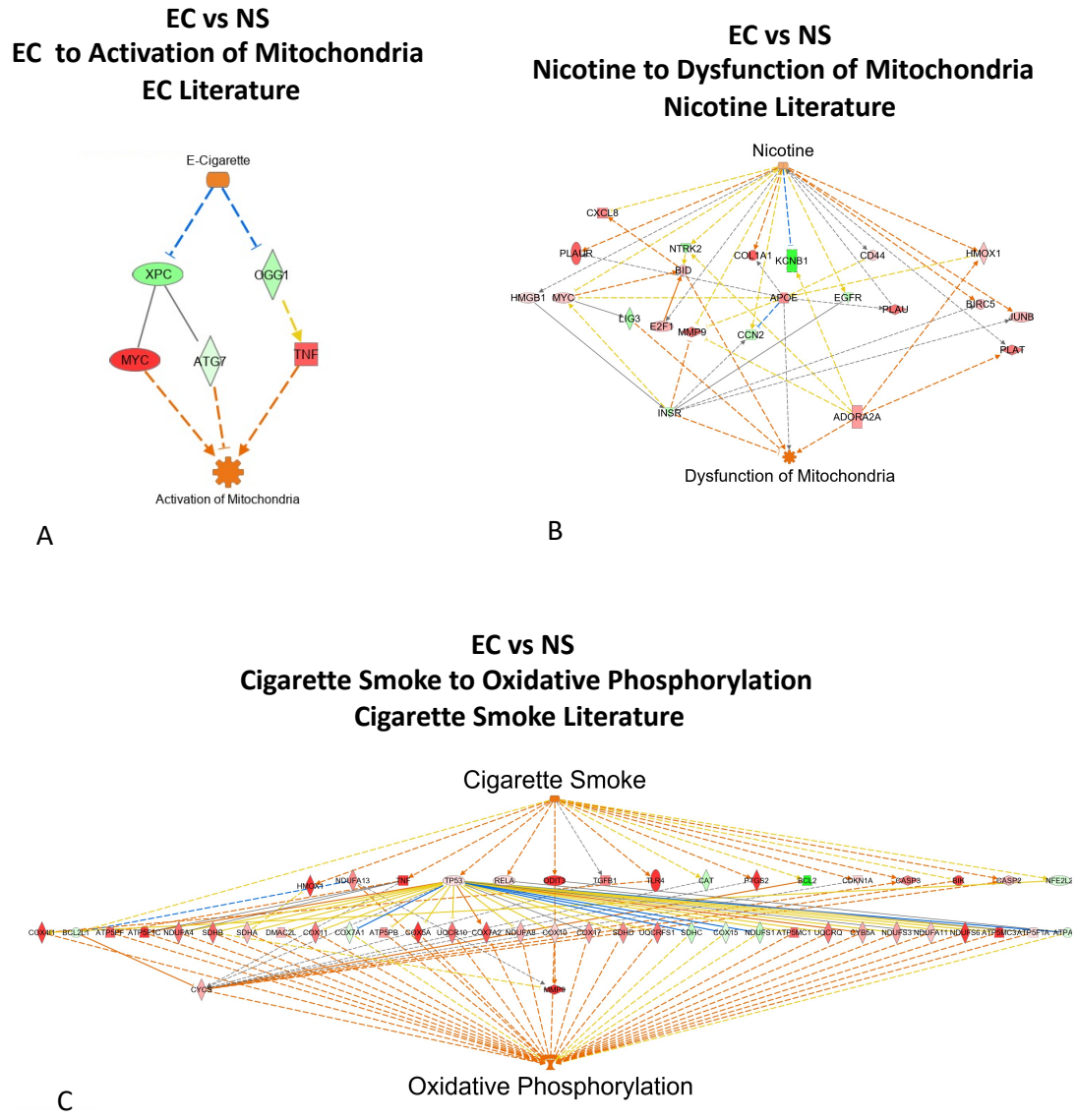

Figure 4: Mitochondrial pathways identified in EC vs NS data using IPA. (A) "Activation of Mitochondria" generated by overlaying our data on the EC literature. (B) "Dysfunction of Mitochondria" generated by overlaying our data on the nicotine literature. (C) "Oxidative Phosphorylation" generated by overlaying our data on the cigarette smoke literature.

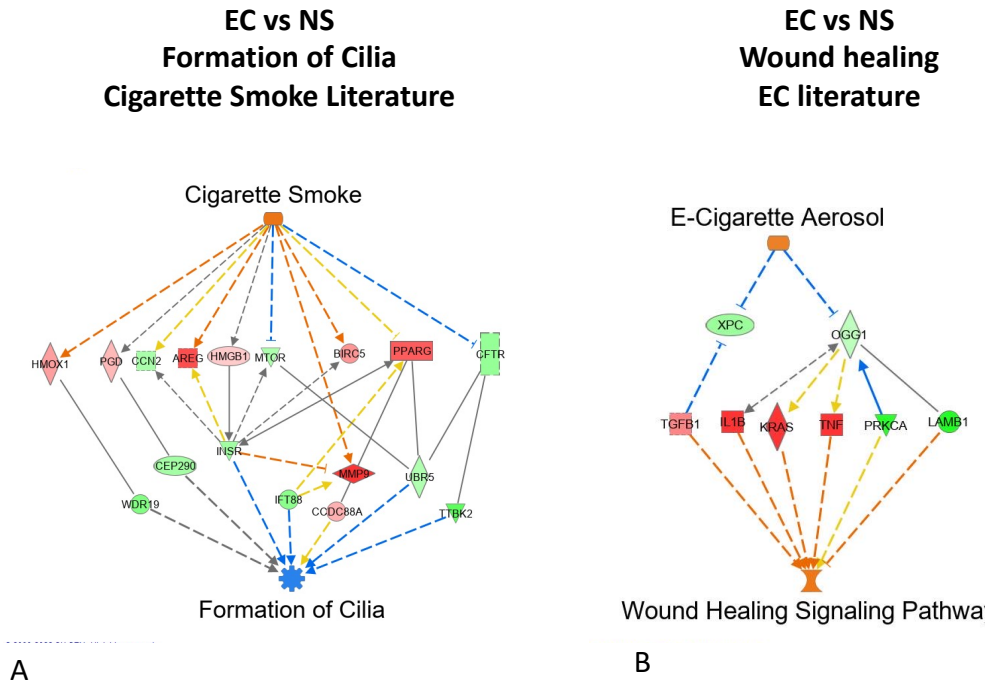

Figure 5: Pathways involved in formation of cilia and wound healing in our EC vs NS data identified using IPA. (A) "Formation of Cilia" generated by overlaying our data on the cigarette smoke literature. (B) "Wound Healing Signaling Pathway" generated by overlaying our data on the EC literature.

3.6. IPA Regulator Effect Analysis for the EC vs NS Comparison

The top regulator effect network, shown in Figure 6A, illustrates the five predicted upstream regulators, based on 12 DEGs in our data and three major downstream effector functions related to inflammation that are predicted to be activated (inflammatory response, homing of leukocytes, and degranulation of cells) (Figure 6A). With IPA's "Path Explorer" tool there was linkage between "Nicotine" and activation of "Accumulation of Leukocytes" and between "Nicotine" and activation of "Immune Response of Macrophages" (Figures 6 B-C).

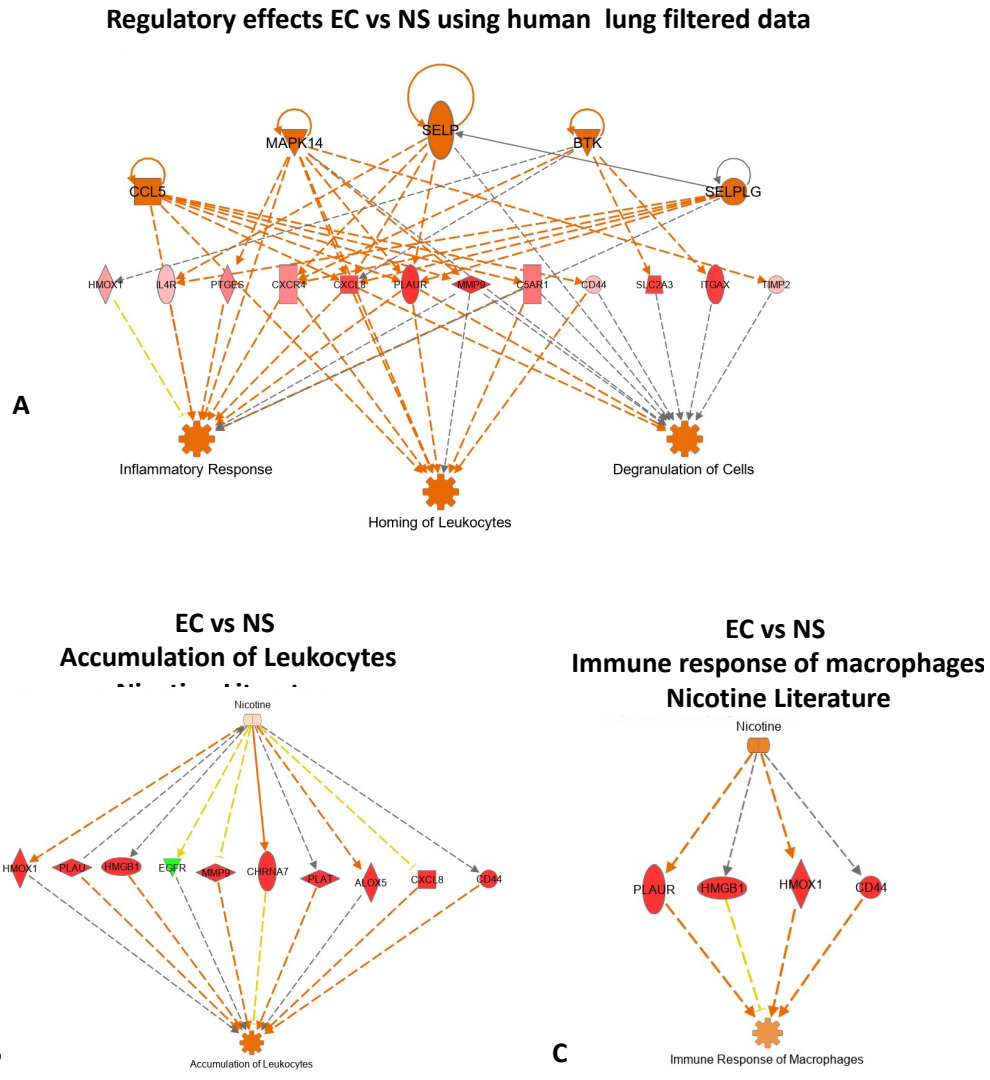

Figure 6: Evidence of an immune response in the EC vs NS comparison. (A) IPA regulator effects in EC vs NS. Downstream effects of five predicted upstream regulators based on DEG expression. Diagram shows predicted upstream regulators (upper row) and predicted downstream processes and functions (lower row) based on DEGs in our data (middle row). (B) "Accumulation of Leukocytes" generated by overlaying our data on the nicotine literature. (C) "Immune Response of Macrophages" generated by overlaying our data on the nicotine literature. Upregulated DEGs are pink-to-red depending on fold-change, while green DEGs indicate downregulation. Orange arrows represent predicted activation, yellow arrows indicate non-consistent activation and grey arrows represent effect not predicted.

3.7. Disease Ontology Semantic and Enrichment (DOSE)

DOSE analysis was performed for the DEGs that were down or upregulated in the EC vs NS comparison. For the upregulated genes the disease categories related to the respiratory system included lung disease, mouth disease, tooth disease, periodontal disease, and pulmonary fibrosis (Figure 7A). The DEGs associated with these respiratory diseases were often overlapping and were upregulated in more than one disease (Figure 7B). For example, FCGR2A, FCGR3B, PPARG, PLAU and MMP9 were associated with five diseases (Figure 7B). The two major disease categories for the downregulated DEGs were primary ciliary dyskinesia (p adjusted) and developmental disorder of mental health (FDR).

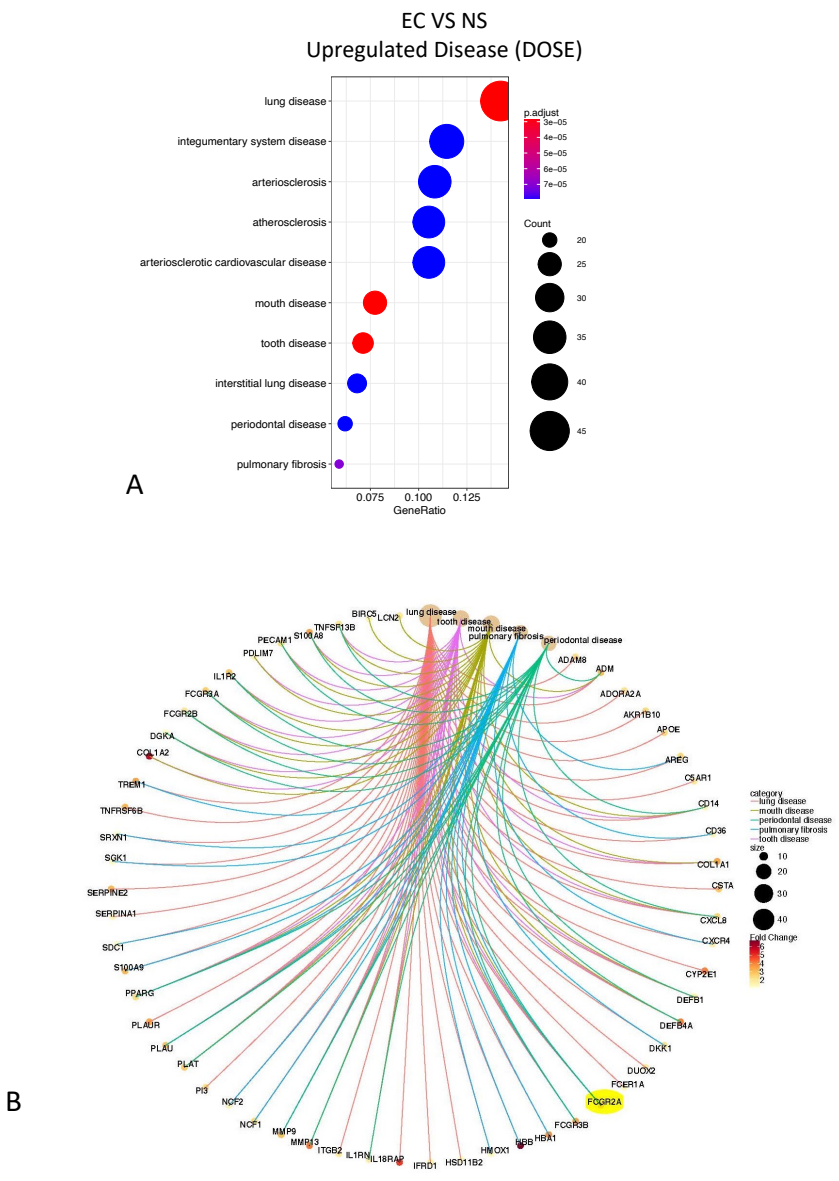

Figure 7: Disease Ontology Semantic and Enrichment (DOSE) analysis for upregulated genes in the EC vs NS comparison. (A) Diseases plotted vs gene ratio. Circles represent gene number associated with each disease and color represents the adjusted p-values. (B) CNET diagram showing the top DOSE diseases in EC vs NS. Diagram shows the DEGs associated with each disease and their fold changes (color key on right). The circle size key indicates the number of genes associated with each disease.

4. Discussion

Nasal epithelium from former smokers who switched to ECs was characterized by increased oxidative stress, an inflammatory response, keratinization, and impaired cilia formation when compared to non-smokers. Similar alterations have also been associated with tobacco cigarette use (Mosadomi et al. 1978 earlier, Tanriverdi et al. 2006, Lee et al. 2012, Brekman et al. 2014). In our study, the CS group had fewer transcriptomic alterations and was less robust than the EC group, nevertheless, cilia formation was decreased and oxidative stress was increased in CS group relative to the NS group.

Both the EC and CS groups showed evidence of oxidative stress ("NADPH oxidase" in EC and "Biological Oxidations" in CS). Oxidative stress via NADPH oxidase has been demonstrated in CS users and is associated with asthma, cystic fibrosis, chronic obstructive pulmonary diseases (Lee et al. 2012,). In our data, GO terms related to oxidative stress via NADPH oxidase were enriched in EC users, who showed increased expression of genes encoding cytoplasmic polypetide subunits (NCF1/p67phox, NCF2/47phox, NCF4/p40phox), which are necessary for the activation of the NADPH oxidase complex (Sumimoto *et al.,* 2005). These cytoplasmic polypeptide subunits bind to the transmembrane region on NADPH oxidase, which activates the enzymatic complex to produce Reactive oxygen species (ROS) (Sumimoto *et al.,* 2005). The elevation of NADPH oxidase by EC use is supported by several other studies. NADPH oxidase genes (NOX 1, NOX2, DUOX2) were upregulated in human bronchial

epithelial cells exposed to cinnamon flavored ECs at the air-liquid interface (Noel *et al.,* 2020). Increased ROS levels associated with NOX 2 elevation, a NADPH oxidase gene family member, was observed in the lungs of mice exposed acutely to EC aerosol (Kuntic *et al.,* 2020). The serum from non-smoking human subjects who vaped ECs increased ROS in human pulmonary microvascular endothelial cells by activating NADPH oxidase (Chatterjee *et al.,* 2019). Lung injury in cigarette smokers has been associated with increased ROS via NADPH oxidase (Yao *et al.,* 2008).

Inflammatory signals induced by cigarette smoking reverted to non-smoker levels 14 days after cessation (Darabseh *et al.,* 2021). In contrast, in our data, genes associated with inflammation were elevated 6 or more months after smokers had converted to EC use. Persistent inflammation in EC users could be due to the inhalation of EC aerosols. We detected upregulation of pro-inflammatory cytokines (CXCL8, CXCL13 and IL 36G) in EC users. In addition, MMP9, an inflammatory regulator released by neutrophils and macrophages, was upregulated in our study, in agreement with increased MMP9 and elevated neutrophilic granule enzymes in sputum from EC users (Reidel *et al.,* 2017). Degranulation of neutrophils is the major cause of tissue damage in smoking-related diseases, such as asthma and chronic obstructive pulmonary diseases (Barnes, 2000). In our study, GO terms and Reactome pathways associated with activation and degranulation of neutrophils were enriched in our EC users. Inflammation caused by ECs has been linked to nicotine, glycerol, propylene

glycol, and EC flavor chemicals (Lerner *et al.,* 2015, Escobar *et al.,* 2020, Escobar *et la.,* 2021, Nair *et al.,* 2021). Our data are consistent with the conclusion that ECs contain chemicals that maintain an inflammatory response, even after cigarette smoking has stopped.

Squamous metaplasia is a condition observed in the bronchial epithelia of smokers (Peters *et al.* 1993 Rigden *et al.* 2016). In smokers, squamous metaplasia may be partially reversible after smoking has stopped (Lapperre *et al.,* 2007). EC users in our study showed many characteristics of squamous metaplasia, including an increase in keratinization (keratin 10 and keratin 13), hyperproliferation of the epithelium, decrease expression of genes involved in ciliogenesis, and increase expression of involucrin (Schamberger *et al*., 2015, Rigden *et al.* 2016). Our data is consistent with the conclusion that squamous metaplasia existed in our EC group.

Accumulated evidence shows that both EC aerosol and cigarette smoke adversely affect cilia. In sheep, tracheal mucus velocity, an *in vivo* measure of mucociliary clearance, was reduced by EC vapor (Chung *et al.,* 2019). In a comparison of bronchial epithelium from former smokers vs EC users who were former smokers, genes that are indirectly involved in ciliogenesis were downregulated in the EC group (Corbett *et al.,* 2019). Our data extend these results by showing direct downregulation of genes involved in ciliogenesis and further compare the EC group directly to non-smokers. Our data support the conclusion that ciliogenesis had not returned to normal after switching from

cigarettes to ECs. Several *in vitro* studies have examined EC chemicals that may impair cilia biogenesis. Human bronchial epithelial cells exposed to cinnamon-flavored EC aerosols had shorter cilia than their controls (Noel *et al.,* 2020; Clapp *et al.,* 2019). Flavor chemicals (diacetyl and 2,3-pentanedione) caused downregulation of genes involved in ciliary biogenesis (TEKT1, CFAP70, PROM1, DNAH12, DNAI1, DNAH3, DNAAF1, CC2D2A, CFAP221, SPAG17, and DNAH6) in mature primary human airway epithelial cells exposed *in vitro* (Park et al. 2018). The same set of genes was downregulated in our study suggesting the effect observed in our human subjects was caused by these flavor chemicals, which are frequently observed in EC products (Omaiye *et al.,* 2019, 2020, Rachel Behar et al. 2016). Cilia-related transcription factors (FOXJ1, RFX2, and RFX3) that were downregulated in our EC group were also downregulated *in vitro* in human airway epithelium exposed to cigarette smoke (Brekman *et al.* 2014). Our data are consistent with EC aerosols and cigarette smoke inhibiting ciliogenesis via similar target genes and further indicate that defective ciliogenesis was not reversed by switching from cigarettes to ECs.

There is an urgent need to identify diseases associated with EC use. Research directly connecting diseases to ECs is limited, and many studies in both animals and humans are based on acute exposures. Understanding the long-term human health effects of EC use could require decades, as was the case for cigarette smoke related-diseases (Surgeon Report, 2014). The human subjects in our study were chronically exposed to cigarette smoke (CS) or EC

aerosol following smoking cessation (EC), and therefore give insight into both the phenotypes and diseases caused by these exposures. In the CS and EC group, the main phenotypes were dysregulation of cilia and increased oxidative stress. In the EC group, inflammation was also significantly increased. Ciliogenesis dysfunction can be indicative of ciliary dyskinesia syndrome, which inhibits clearance in the airways (Tilley *et al.,* 2015). In the EC group, increased oxidative stress via activation of NADPH oxidase was a dominant phenotype and could lead to epithelia remodeling (Siques *et al,.* 2018). In the CS group, oxidative stress likewise was increased, as has been reported in other studies of human smokers. Elevated ROS in the lung leads to disease such as respiratory distress syndrome, emphysema, and COPD, which are characterized by inflammation (Keller *et al.,* 2017). To further understand disease initiation and pathogenesis in our data, we took advantage of DOSE analysis. Many of the diseases enriched in the EC vs NS comparison included respiratory-related diseases (lung diseases, interstitial lung disease, and pulmonary fibrosis), which are commonly associated with cigarette smoking. Here we see that after switching from cigarette smoking to vaping for 6 months, evidence of lung disease was still apparent in the EC group. Other diseases detected in the DOSE analysis included the upper respiratory system (mouth disease, tooth disease, periodontal disease). These diseases have also been reported in cigarette smokers (Zhang *et al.,* 2019) and more recently in an epidemiological report on EC users (Jeong *et al.,* 2019). Taken together our data support the conclusion that switching from cigarette

smoking to EC use for 6 months does not restore the respiratory epithelium to that equivalent in the non-smoking group, suggesting that diseases that originate from oxidative stress, inflammation, and absence of cilia are present in the EC group.

Our study is affected by several factors. Our EC participants used second generation products which operate at high powers and may have generated aerosols that are more toxic than those produced by fourth generation products. A greater number of DEGs were identified in the EC vs NS set than in the CS vs NS and CS vs EC sets, similar to several previous studies (Rebuli *et al.,* 2021. Martin *et al.,* 2016). The lower number of DEGs in CS makes this group less robust and may explain why fewer enriched terms and pathways were identified. While exposures in the EC group were similar and represent what an average EC user would receive, the participants in the CS group were not exposed to equal numbers of cigarettes/day, which might have interfered with the identification of DEGs in the CS group. While we have found significant effects in both the EC and CS groups compared to the NS controls, future studies should be done using larger sample sizes and also include a group of ex-smokers who quit smokers without then using ECs.

5. Conclusions

Our data are consistent with the conclusion that switching from cigarette smoking to EC use for at least 6 months does not eliminate tissue damage in the respiratory epithelium. Nasal epithelium from EC users showed evidence of oxidative stress, increase inflammation, squamous metaplasia, and repressed ciliogenesis. These phenotypes were linked to lung diseases, interstitial lung disease, and pulmonary fibrosis. We cannot distinguish if the changes in the EC group were a consequence of cigarette smoking, fresh damage caused by EC use, or a combination of both. Our data clearly show evidence of tissue damage in EC users who have stopped cigarette smoking for at least 6 months.

References

1. Adriaens, K.; Van Gucht, D.; Declerck, P., Baeyens, F. 2014.Effectiveness of the Electronic Cigarette: An Eight-Week Flemish Study with Six-Month Follow-up on Smoking Reduction, Craving and Experienced Benefits and Complaints. Int. J. Environ. Res. Public Health.11, 11220-11248; doi:10.3390/ijerph111111220

2. Arnold, M.J., Nollen, N.L., Mayo, M. S., Ahluwalia, J.S., Leavens, E. L., Zhan, G., Rice ,M., Pulvers, K. 2021. Harm Reduction Associated with Dual Use of Cigarettes and e-Cigarettes in Black and Latino Smokers: Secondary Analyses from a Randomized Controlled e-Cigarette Switching Trial. Nicotine & Tobacco Research. 1–5 doi:10.1093/ntr/ntab069

3. Backman, T. W., & Girke, T. 2016. systemPipeR: NGS workflow and report generation environment. BMC bioinformatics,17(1), 388.

4. Barnes PJ. 2000. Mechanisms in COPD: differences from asthma. Chest. 117(2 Suppl):10S-4S. doi: 10.1378/chest.117.2_suppl.10s. PMID: 10673467.

5. Behar et al. 2016 RZ, Luo W, Lin SC, Wang Y, Valle J, Pankow JF, Talbot P. Distribution, quantification and toxicity of cinnamal dehyde in electronic cigarette refill fluids and aerosols. Tob Control. 2016 Nov;25(Suppl 2):ii94-ii102. doi: 10.1136/tobaccocontrol-2016-053224. Epub 2016 Sep 15. PMID: 27633763; PMCID: PMC5503843.

6. Bolger, A.M.; Lohse, M.; Usadel, B. 2014.Trimmomatic: a flexible trimmer for Illumina sequence data. Bioinformatics, 30(15), 2114-2120. https://doi.org/10.1093/bioinformatics/btu170

7. Brekman, A., Walters, M. S., Tilley, A. E., & Crystal, R. G. 2014. FOXJ1 prevents cilia growth inhibition by cigarette smoke in human airway epithelium in vitro. American journal of respiratory cell and molecular biology, 51(5), 688–700. https://doi.org/10.1165/rcmb.2013-0363OC

8. Chatterjee, S., Tao, J. Q., Johncola, A., Guo, W., Caporale, A., Langham, M. C., & Wehrli, F. W. 2019. Acute exposure to e-cigarettes causes inflammation and pulmonary endothelial oxidative stress in nonsmoking, healthy young sub-jects. American journal of physiology. Lung cellular and molecular physiology, 317(2), L155–L166. https://doi.org/10.1152/ajplung.00110.2019

9. Chung, S., Baumlin, N., Dennis, J. S., Moore, R., Salathe, S. F., Whitney, P. L., Sabater, J., Abraham, W. M., Kim, M. D., & Sal-athe, M. 2019. Electronic Cigarette Vapor with Nicotine Causes Airway Mucociliary Dysfunction Preferentially via TRPA1 Receptors. American journal of respiratory and critical care medicine, 200(9), 1134–1145. https://doi.org/10.1164/rccm.201811-2087OC

10. Clapp, P.W., Lavrich, K.S., van Heusden, C.A., Lazarowski, E.R., Carson, J.L., Jaspers, I. 2019. Cinnamaldehyde in flavored e-cigarette liquids temporarily suppresses bronchial epithelial cell ciliary motility by dysregulation of mitochondrial function. Am J Physiol Lung Cell Mol Physiol.; 16(3):L470-L486. doi: 10.1152/ajplung.00304.2018.

11. Corbett et al . 2019. Gene Expression Alterations in the Bronchial Epithelium of e-Cigarette Users. CHEST .DOI: https://doi.org/10.1016/j.chest.2019.05.022

12. Croft, D., Mundo, A.F., Haw, R., Milacic, M., Weiser, J., Wu, G., Caudy, M., Garapati, P., Gillespie, M., Kamdar, M.R., Jassal, B., Jupe, S., Matthews, L., May, B., Palatnik S, Rothfels K, Shamovsky V, Song H, Williams M, Birney E, Hermjakob H, Stein L, D'Eusta-chio P. 2014. The Reactome pathway knowledgebase. Nucleic Acids Res.:D472-7. doi: 10.1093/nar/gkt1102

13. Cross AR. 2000. p40(phox) Participates in the activation of NADPH oxidase by increasing the affinity of p47(phox) for flavocytochrome b(558). Biochem J. 113-7. doi: 10.1042/0264-6021:3490113. PMID: 10861218; PMCID: PMC1221127.

14. Darabseh, M.Z., Maden-Wilkinson, T.M., Welbourne, G. et al. 2021.Fourteen days of smoking cessation improves muscle fatigue resistance and reverses markers of systemic inflammation. Sci Rep 11, 12286. https://doi.org/10.1038/s41598-021-91510-x

15. Escobar, Y. H., Nipp, G., Cui, T., Petters, S. S., Surratt, J. D., & Jaspers, I. (2020). In Vitro Toxicity and Chemical Characteriza-tion of Aerosol Derived from Electronic Cigarette Humectants Using a Newly Developed Exposure System. Chemical re-search in toxicology, 33(7), 1677–1688. https://doi.org/10.1021/acs.chemrestox.9b004

16. Escobar YH, Morrison CB, Chen Y, Hickman E, Love CA, Rebuli ME, Surratt JD, Ehre C, Jaspers I. 2021. Differential responses to e-cig generated aerosols from humectants and different forms of nicotine in epithelial cells from nonsmokers and smokers. Am J Physiol Lung Cell Mol

Physiol.;320(6):L1064-L1073. doi: 10.1152/ajplung.00525.2020. Epub 2021 Apr 7. PMID: 33825493; PMCID: PMC8285624.

17. Fabregat A, Sidiropoulos K, Viteri G, Forner O, Marin-Garcia P, Arnau V, D'Eustachio P, Stein L, Hermjakob H. 2017.Reactome pathway analysis: a high-performance in-memory approach. BMC Bioinformatics. 18(1):142. doi: 10.1186/s12859-017-1559-2. PMID: 28249561; PMCID: PMC5333408.

18. Fryman, C, Lou, B, Weber, AG, Steinberg HN, Khanijo S, Iakovou A, Makaryus MR. 2020 Acute Respiratory Failure Associated With Vaping. Chest. 157(3):e63-e68. doi: 10.1016/j.chest.2019.10.057. PMID: 32145818.

19. Henry, T. S., Kanne, J. P., & Kligerman, S. J. 2019. Imaging of vaping-associated lung disease. New England Journal of Medi-cine, 381(15), 1486-1487.

20. Hua, M., Alfi, M., Talbot, P, 2013 Health-Related Effects Reported by Electronic Cigarette Users in Online Forums.J Med Internet Res. 2013;15(4):e59 doi: 10.2196/jmir.2324

21. Hua, M.; Sadah, S.; Hristidis, V.; Talbot, T. Health Effects Associated With Electronic Cigarette Use: Automated Mining of Online Forums. J Med Internet Res 2020;22(1):e15684) doi: 10.2196/15684

22. Hua, My, Talbot, P. 2016. Potential health effects of electronic cigarettes: A systematic review of case reports, Preventive Medicine Reports. 169-178.

23. Jeong, W., Choi, D. W., Kim, Y. K., Lee, H. J., Lee, S. A., Park, E. C., & Jang, S. I. (2020). Associations of electronic and conven-tional cigarette use with periodontal disease in South Korean adults. Journal of periodontology, 91(1), 55–64. https://doi.org/10.1002/JPER.19-0060

24. Jonas et al. Vaping-Related Acute Parenchymal Lung Injury. 2022 https://doi.org/10.1016/j.chest.2020.03.085

25. Kellner M, Noonepalle S, Lu Q, Srivastava A, Zemskov E, Black SM. ROS Signaling in the Pathogenesis of Acute Lung Injury (ALI) and Acute Respiratory Distress Syndrome (ARDS). Adv Exp Med Biol. 2017;967:105-137. doi: 10.1007/978-3-319-63245-2_8. PMID: 29047084; PMCID: PMC7120947.

26. Kim, D., Pertea, G., Trapnell, C., Pimentel, H., Kelley, R., & Salzberg, S. L. (2013). TopHat2: accurate alignment of transcrip-tomes in the presence of insertions, deletions and gene fusions. Genome biology, 14(4), R36.

27. Khanna A, Guo M, Mehra M, Royal W 3rd. 2013. Inflammation and oxidative stress induced by cigarette smoke in Lewis rat brains. J Neuroimmunol.254(1-2):69-75. doi:10.1016/j.jneuroim.2012.09.006

28. Kuntic M, Oelze M, Steven S, Kröller-Schön S, Stamm P, Kalinovic S, Frenis K, Vujacic-Mirski K, Bayo Jimenez MT, Kvandova M, Filippou K, Al Zuabi A, Brückl V, Hahad O, Daub S, Varveri F, Gori T, Huesmann R, Hoffmann T, Schmidt FP, Keaney JF, Daiber A, Münzel T. 2020. Short-term e-cigarette vapour exposure causes vascular oxidative stress and dysfunction: evidence for a close connection to brain damage and a key role of the phagocytic NADPH oxidase (NOX-2). Eur Heart J. 41(26):2472-2483. doi: 10.1093/eurheartj/ehz772.

29. Lee, T. , Chuen-Mao Yang. 2012. Role of NADPH oxidase/ROS in pro-inflammatory mediators-induced airway and pulmonary diseases. Biochemical Pharmacology.84; 581–590 http://dx.doi.org/10.1016/j.bcp.2012.05.005

30. Lee J, Taneja V, Vassallo R. 2012. Cigarette Smoking and Inflammation: Cellular and Molecular Mechanisms. Journal of Dental Research. 91(2):142-149. doi:10.1177/0022034511421200

31. Lerner CA, Sundar IK, Yao H, Gerloff J, Ossip DJ, McIntosh S, et al. (2015) Vapors Produced by Electronic Cigarettes and E-Juices with Flavorings Induce Toxicity, Oxidative Stress, and Inflammatory Response in Lung Epithelial Cells and in Mouse Lung. PLoS ONE 10(2): e0116732. doi:10.1371/ journal.pone.0116732

32. Loffredo, L., et al. 2018. Role of NADPH oxidase-2 and oxidative stress in children exposed to passive smoking. Thorax. 73:986–988. doi:10.1136/thoraxjnl-2017-211293

33. Lapperre, T. S., Sont, J. K., van Schadewijk, A., Gosman, M. M., Postma, D. S., Bajema, I. M., Timens, W., Mauad, T., Hiemstra, P. S., & GLUCOLD Study Group (2007). Smoking cessation and bronchial epithelial remodeling in COPD: a cross-sectional study. Respiratory research, 8(1), 85. https://doi.org/10.1186/1465-9921-8-85

34. Langmead, B., & Salzberg, S. L. (2012). Fast gapped-read alignment with Bowtie 2. Nature Methods, 9(4), 357-359.

35. Martin,E., Phillip W. Clapp, Meghan E. Rebuli, Erica A. Pawlak, Ellen Glista-Baker, Neal L. Benowitz, Rebecca C. Fry, and Ilona Jaspers. E-cigarette use results in suppression of immune and inflammatory-response genes in nasal epithelial cells similar to cigarette smoke. American Journal of Physiology Lung Cellular and Molecular Physiology 2016 311: 1, L135 L144 doi:10.1152/ajplung.00170.2016.

36. Mosadomi, A., Shklar, G., Loftus, E.R., Chauncey HH. 1978. Effects of tobacco smoking and age on the keratinization of palatal mucosa: a cytologic study. Oral Surg Oral Med Oral Pathol. 46(3):413-7. doi: 10.1016/0030-4220(78)90407-3.

37. Nair V, Tran M, Behar RZ, Zhai S, Cui X, Phandthong R, Wang Y, Pan S, Luo W, Pankow JF, Volz DC, Talbot P. Menthol in electronic cigarettes: A contributor to respiratory disease? Toxicol Appl Pharmacol. 2020 Nov 15;407:115238. doi: 10.1016/j.taap.2020.115238. Epub 2020 Sep 17. PMID: 32950532; PMCID: PMC8167901

38. National Academies of Sciences, Engineering, and Medicine, Health and Medicine Division, Board on Population Health and Public Health Practice, Committee on the Review of the Health Effects of Electronic Nicotine Delivery Systems, Eaton, D. L., Kwan, L. Y., & Stratton, K. (Eds.). (2018). Public Health Consequences of E-Cigarettes. National Academies Press (US).

39. Noël A, Hossain E, Perveen Z, Zaman H, Penn AL. 2020. Sub-ohm vaping increases the levels of carbonyls, is cytotoxic, and alters gene expression in human bronchial epithelial cells exposed at the air-liquid interface. Respir Res.21(1):305. doi: 10.1186/s12931-020-01571-1.

40. Omaiye, E.E., McWhirter, K.J., Luo, W. et al. High concentrations of flavor chemicals are present in electronic cigarette refill fluids. Sci Rep 9, 2468 (2019). https://doi.org/10.1038/s41598-019-39550-2

41. Park, HR., O'Sullivan, M., Vallarino, J. et al. Transcriptomic response of primary human airway epithelial cells to flavoring chemicals in electronic cigarettes. Sci Rep 9, 1400 (2019). https://doi.org/10.1038/s41598-018-37913-9

42. Peters, E. J., Morice, R., Benner, S. E., Lippman, S., Lukeman, J., Lee, J. S., Ro, J. Y., & Hong, W. K. (1993). Squamous metaplasia of the bronchial mucosa and its relationship to smoking. Chest, 103(5), 1429–1432. https://doi.org/10.1378/chest.103.5.1429

43. Polosa, R. Electronic cigarette use and harm reversal: emerging evidence in the lung. BMC Med 13, 54 (2015). Doi: 10.1186/s12916-015-0298-3

44. Polosa, R., Morjaria, J.B., Coponnetto, P., Prosperini, U., Russo, C., Pennisi., Bruno, C.M. (2016) Evidence for harm reduction in COPD smokers who switch to electronic cigarettesc. Respiratory Research.17:166 DOI 10.1186/s12931-016-0481-x

45. Polosa, R., Morjaria , J.B., Prosperini , U., Russo, Pennisi, A, Puleo, R., Caruso, M., Caponnetto, P. health effects in COPD smokers who switch to electronic cigarettes: a retrospective-prospective 3-year follow-up. International Journal of COPD. 2018

46. Polosa, R., Morjaria, J., Caponnetto, P., Caruso, M., Strano, S., Battaglia, E., Russo, C. (2014) Effect of Smoking Abstinence and Reduction in Asthmatic Smokers Switching to Electronic Cigarettes: Evidence for Harm Reversal. Int. J. Environ. Res. Public Health. 11; 4965-4977. doi:10.3390/ijerph110504965

47. Raju, S.V., Jackson, P.L. et al. 2013. Cigarette Smoke Induces Systemic Defects in Cystic Fibrosis Transmembrane Conductance Regulator Function Am J Respir Crit Care Med. 188; 11: 1321–1330

48. Rigden, H. M., Alias, A., Havelock, T., O'Donnell, R., Djukanovic, R., Davies, D. E., & Wilson, S. J. (2016). Squamous Metapla-sia Is Increased in the Bronchial Epithelium of Smokers with Chronic Obstructive Pulmonary Disease. PloS One, 11(5), e0156009. https://doi.org/10.1371/journal.pone.0156009

49. Rebuli, Glista-Baker, Hoffman, et al. 2021 E-Cigarettes Alter Response to LAIV. American Journal of Respiratory Cell and Mo-lecular Biology. 64

50. Reidel, B., Radicioni, G., Clapp, P. W., Ford, A. A., Abdelwahab, S., Rebuli, M. E., Haridass, P., Alexis, N. E., Jaspers, I., & Kesimer, M. (2018). E-Cigarette Use Causes a Unique Innate Immune Response in the Lung, Involving Increased Neutrophilic Activation and Altered Mucin Secretion. American Journal of Respiratory and Critical Care Medicine, 197(4), 492–501. https://doi.org/10.1164/rccm.201708-1590OC

51. Robinson, M. D., McCarthy, D. J., & Smyth, G. K. 2010. edgeR: a Bioconductor package for differential expression analysis of digital gene expression data. Bioinformatics, 26(1), 139-140.

52. Sakla, N.M., Gattu, R., Singh, G. et al. 2020. Vaping-associated acute respiratory distress syndrome. Emerg Radiol 27, 103–106. https://doi.org/10.1007/s10140-019-01736-6

53. Schamberger, A., Staab-Weijnitz, C., Mise-Racek, N. et al. Cigarette smoke alters primary human bronchial epithelial cell differentiation at the air-liquid interface. Sci Rep 5, 8163 (2015). https://doi.org/10.1038/srep08163

54. Sumimoto, H., Miyano, K., & Takeya, R. 2005. Molecular composition and regulation of the Nox family NAD(P)H oxidas-es. Biochemical and biophysical research communications, 338(1), 677–686. https://doi.org/10.1016/j.bbrc.2005.08.210

55. Siques Patricia, Brito Julio, Pena Eduardo. 2018. Reactive Oxygen Species and Pulmonary Vasculature During Hypobaric Hypox-ia. Frontiers in Physiology.https://www.frontiersin.org/article/10.3389/fphys.2018.00865 ,10.3389/fphys.2018.

56. Tarazona-Santos et al. 2013 E Machado M, Magalhães WC, et al. Evolutionary dynamics of the human NADPH oxidase genes CYBB, CYBA, NCF2, and NCF4: functional implications. Mol Biol Evol. 2013;30(9):2157-2167. doi:10.1093molbev/mst119

57. Tanriverdi, H., Evrengul, H., Kuru, O., Tanriverdi, S., Seleci, D., Enli, Y., Kaftan, H.A., Kilic, M. 2006 .Cigarette smoking induced oxidative stress may impair endothelial function and coronary blood flow in angiographically normal coronary arteries. Circ J. 70(5):593-9. doi: 10.1253/circj.70.593. PMID: 16636496.

58. Tilley AE, Walters MS, Shaykhiev R, Crystal RG. 2014.Cilia dysfunction in lung disease. Annu Rev Physiol. 2015;77:379-406. doi: 10.1146/annurev-physiol-021014-071931. Epub 2014 Oct 29. PMID: 25386990; PMCID: PMC4465242.

59. Trtchounian, A. and P. Talbot. (2010) Electronic nicotine delivery systems: is there a need for regulation? Tobacco Control. 20: 47e52. doi:10.1136/tc.2010.037259

60. US Department of Health and Human Services. The Health Consequences of Smoking–50 Years of Progress: A Report of the Surgeon General. Atlanta, GA: US Department of Health and Human Services, Centers for Disease Control and Prevention, National Center for

Chronic Disease Prevention and Health Promotion, Office on Smoking and Health; 2014.

61. Yee, K.K., Pribitkin, E.A., Cowart, B.J., et al. 2009.Smoking-associated Squamous Metaplasia in Olfactory Mucosa of Patients with Chronic Rhinosinusitis. Toxicologic Pathology. 37(5):594-598. doi:10.1177/0192623309338055

62. Yu, G, Wang, L, Han, Y, He, Q .2012. “clusterProfiler: an R package for comparing biological themes among gene clus-ters.” OMICS: A Journal of Integrative Biology, 16(5), 284-287. doi: 10.1089/omi.2011.0118.

63. Yu, G.; Wang, L.G; et al. 2015. DOSE: an R/Bioconductor package for disease ontology semantic and enrichment analysis, Bioinformatics. 31(4): 608–609, https://doi.org/10.1093/bioinformatics/btu684

64. Yao, Hongwei et al. 2008. Genetic ablation of NADPH oxidase enhances susceptibility to cigarette smoke-induced lung inflam-mation and emphysema in mice. The American journal of pathology vol. 172,5: 1222-37. doi:10.2353/ajpath.2008.070765

65. Zhang, Y., He, J., He, B., Huang, R., & Li, M. 2019. Effect of tobacco on periodontal disease and oral cancer. Tobacco Induced Diseases, 17, 40. https://doi.org/10.18332/tid/106187

Chapter 6: Conclusion

Environmental exposure to tobacco product residue and aerosol was assessed using both *in vitro* and *in vivo* models. We analyzed: (1) adhesion and release of THS chemicals from contaminated fabrics, (2) response of a 3D skin model and sub-cultured keratinocytes to nicotine, (3) transcriptomic alterations in human subjects who received inhalation exposure to THS, and (4) transcriptomic changes in in the nasal epithelium of former cigarette smokers who had switched to EC for at least 6 months, cigarette smokers, and non-smokers.

THS residue adhesion and release from cotton, terry cloth, polyester, and wool carpet was determined following different lengths of exposure to smoke. We introduced autofluorescence as a new method to compare and normalize THS concentrations across different batches, laboratories, and field sites. THS absorption increased with increased exposure. THS chemicals were more readily extracted from cotton and terry cloth than other fabrics. For polyester, chemicals became extractable when applying heat or maintained in a humid atmosphere. We showed THS chemical absorption and extraction were dependent on the chemical, fabric, temperature, time, and ambient humidity. These factors need to be considered when implementing remediation efforts in THS contaminated environments.

Nicotine concentrations in environments contaminated with THS and in EC fluids which often contact the skin were used to assess dermal protein alterations

upon nicotine exposure. Proteomics analysis of Epiderm™ exposed to nicotine showed alterations consistent with an anti-inflammation response, anti-apoptosis response, oxidative phosphorylation, mitochondrial dysfunction, and stress induced protein synthesis alterations. These changes were accompanied by mitochondrial fragmentation and enlarged peroxisomes in sub-cultured keratinocytes. Even a short exposure to low concentrations of nicotine is sufficient to alter the EpiDerm proteome and adversely affect organelles involved in oxidative stress. These proteomic changes may exacerbate skin infections, impair wound healing, and increase oxidative stress upon dermal contact to nicotine contaminated environments.

We were the first to report that inhalation of THS induced changes in the transcriptome of human nasal epithelium. Nasal biopsies from non-smokers were collected before and after acute exposure to THS. THS caused a cellular survival response, which included activation of anti-apoptotic genes, increased activation of DNA repair mechanisms, and upregulation of genes involved in mitochondrial pathways and glutathione synthesis. A relatively short exposure (3 hours) to THS was sufficient to alter the nasal transcriptome in humans.

Transcriptomic analysis of the nasal epithelium of former smokers who switched to EC use was also analyzed. Genes altered in current EC users had an increase in pathways associated with inflammation, oxidative stress, and keratinization, while ciliogenesis decrease when compared to non-smokers. These transcriptomic alterations support the conclusion that EC use interferes

with the recovery of airway epithelium in former smokers who switch exclusively to ECs. EC users showed evidence of markers associated with squamous metaplasia and alteration were linked to development of lung diseases.

Here we showed the molecular effects of nicotine, THS, and ECexposure on *in vitro* and *in vivo* models. We introduced autofluorescence as a method to quantify THS in contaminated fabrics and demonstrated that THS adhesion is dependent on factors such as fabric type and ambient humidity. We showed that human dermal contact with nicotine may promote skin damage through cellular oxidative stress and inhibition of an inflammatory response. Acute inhalation of THS is sufficient to alter the transcriptome in human nasal epithelium causing cellular stress that promotes activation of cell survival pathways. EC use inhibits airway epithelium recovery in former smokers by increasing inflammation and oxidative stress. These finding demonstrate the importance of remediation of THS and EC contaminated environments to minimize human exposure.

Appendix A: Supporting Information for Chapter 2

Supplementary Materials

Table S1. Cotton, terry, polyester and wool carpet daily smoke exposure for 1-month exposed fabrics

Date exposed	Hours of smoke	Total mg particles
9/3/15	3.35	17.58
9/4/15	3.98	49.41
9/10/15	3.82	30.95
9/11/15	3.15	66.10
9/17/15	1.87	13.48
9/18/15	4.33	70.60
9/28/15	4.50	49.61
9/29/15	5.42	84.87
10/1/15	3.13	36.93
10/2/15	5.80	68.44
10/6/15	5.95	207.69

Note: All fabrics were placed inside the smoking chamber on 8/31/15 and removed on 10/8/15

Table S2. Cotton, terry, polyester and wool carpet daily smoke exposure for 6-month exposed fabrics

Date exposed	Hours of smoke	Total mg particles
9/3/15	3.35	17.58
9/4/15	3.98	49.41
9/11/15	3.15	66.10
9/17/15	1.87	13.48
9/18/15	4.33	70.60
9/28/15	4.50	49.61
9/29/15	5.42	84.86
10/1/15	3.13	36.93
10/2/15	5.80	68.44
10/6/15	5.95	207.69
10/12/15	4.55	39.57
10/13/15	5.70	123.83
10/15/15	4.13	40.10
10/19/15	5.45	60.12
10/20/15	3.85	60.60
10/22/15	6.03	62.29
10/23/15	5.88	71.95
10/26/15	6.13	72.63
10/27/15	5.57	67.89
10/29/15	5.92	54.49
11/6/15	3.12	33.94
11/20/15	3.13	31.97
11/24/15	3.08	30.79
1/8/16	4.22	52.50
1/29/16	3.18	25.55
2/5/16	4.10	45.62

Note: All fabrics were placed inside the smoking chamber on 8/31/15 and removed on 3/8/16

Table S3. Cotton, terry, polyester and wool carpet daily smoke exposure for 12-month exposed fabrics

Date exposed	Hours of smoke	Total mg particles
9/3/15	3.35	17.58
9/4/15	3.98	49.41
9/10/15	3.82	30.95
9/11/15	3.15	66.10
9/17/15	1.87	13.48
9/18/15	4.33	70.60
9/28/15	4.50	49.61
9/29/15	5.42	84.87
10/1/15	3.13	36.93
10/2/15	5.80	68.44
10/6/15	5.95	207.69
10/12/15	4.55	39.57
10/13/15	5.70	123.83
10/15/15	4.13	40.06
10/19/15	5.45	60.12
10/20/15	3.85	60.60
10/22/15	6.03	62.29
10/23/15	5.88	71.95
10/26/15	6.13	72.63
10/27/15	5.57	67.89
10/29/15	5.92	54.49
11/6/15	3.12	33.94
11/20/15	3.13	31.97
11/24/15	3.08	30.79
1/8/2016I7	4.22	52.50
1/29/16	3.18	25.55
2/5/16	4.10	45.62
3/10/16	4.57	46.34
3/31/16	4.28	45.84
4/7/16	4.75	27.76
4/21/16	3.85	65.13
4/26/16	2.23	16.56
4/29/16	1.77	10.33
6/3/16	2.55	2.42
7/8/16	3.15	4.41
8/12/16	3.15	6.43

Note: All fabrics were placed inside the smoking chamber on 8/31/15 and removed on 9

Table S4. Cotton, terry, polyester and wool carpet daily smoke exposure for 18-month exposed fabrics

Date exposed	Hours of smoke	Total mg particles
9/3/15	3.35	17.58
9/4/15	3.98	49.41
9/10/15	3.82	30.95
9/11/15	3.15	66.10
9/17/15	1.87	13.48
9/18/15	4.33	70.60
9/28/15	4.50	49.61
9/29/15	5.42	84.86
10/1/15	3.13	36.93
10/2/15	5.80	68.44
10/6/15	5.95	207.69
10/12/15	4.55	39.57
10/13/15	5.70	123.83
10/15/15	4.13	40.10
10/19/15	5.45	60.12
10/20/15	3.85	60.60
10/22/15	6.03	62.30
10/23/15	5.88	71.95
10/26/15	6.13	72.63
10/27/15	5.57	67.89
10/29/15	5.92	54.49
11/6/15	3.12	33.94
11/20/15	3.13	31.98
11/24/15	3.08	30.79
1/8/2016I7	4.22	52.50
1/29/16	3.18	25.55
2/5/16	4.10	45.62
3/10/16	4.57	46.34
3/31/16	4.28	45.84
4/7/16	4.75	27.76
4/21/16	3.85	65.13
4/26/16	2.23	16.56
4/29/16	1.77	10.33

6/3/16	2.55	2.42
7/8/16	3.15	4.41
8/12/16	3.15	6.430
10/20/16	5.10	24.68
10/27/16	6.07	20.54
11/3/16	5.87	110.75
11/10/16	5.50	86.79
11/17/16	5.02	79.69
11/18/16	4.12	49.12
11/23/16	5.90	79.39
11/29/16	5.78	67.77
12/2/16	6.07	56.36
12/8/16	5.92	51.54
12/16/16	5.67	71.62
12/22/16	6.13	88.80
1/13/17	5.00	84.85
1/20/17	5.17	139.98
1/26/17	4.98	115.73
1/27/17	5.07	96.45
2/2/17	5.05	60.147
2/3/17	4.42	50.998
2/10/17	5.00	49.846
2/15/17	5.12	79.520
2/17/17	5.07	74.045
2/22/17	5.73	103.440
2/24/17	5.58	114.076
3/1/17	5.68	128.603
3/2/17	5.98	121.058
3/3/17	5.28	116.510

Note: All fabrics were placed inside the smoking chamber on 8/31/15 and removed on 3/7/17

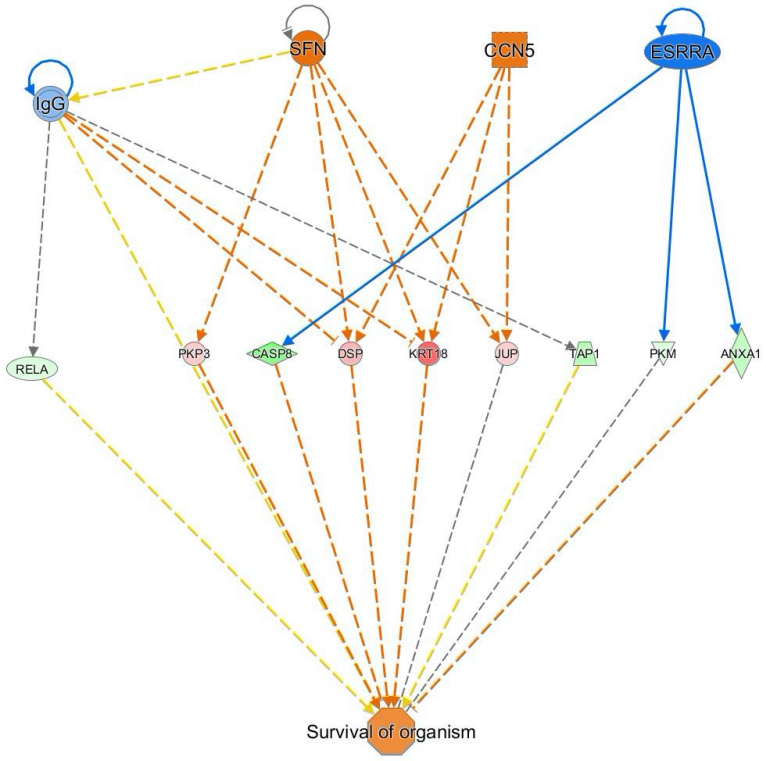

S Figure1. IPA regulator effects in EpiDerm™ Treated with10 µg/mL vs PBS .Downstream effects of four predicted upstream regulators based on DEG expression. Diagram shows predicted upstream regulators (upper row) and predicted downstream processes and functions (lower row) based on DEGs in our data (middle row).

Appendix C: Supporting Information for Chapter 4

eMethods

Background and Objectives

The goal of this study was to evaluate the effects of controlled exposure to thirdhand cigarette smoke on uptake of tobacco smoke chemicals and toxicants, inflammation, oxidative stress, cardiovascular health and the expression of genes in the mouth and nose of healthy nonsmokers. Secondhand smoke is a major preventable health risk around the world. Thirdhand smoke is a new term for the chemicals that stick to surfaces that are exposed to secondhand cigarette smoke. This was one of the first studies in the world to test whether breathing air from a room that has been smoked in had any detectable effects on people.

Methods

This was a controlled human exposure study with a crossover study design. Each participant received one three-hour exposure to THS and one three-hour exposure to conditioned, filtered air (clean air condition). Allocation of exposure order was randomized. Of the 26 participants, 11 received the clean air exposure first and 15 received the THS exposure first. The exposures were separated by a minimum of 21 days.

Participants

Participants were recruited using an online advertisement for healthy nonsmokers, ages 18-50, in the San Francisco area. At the screening visit, prospective participants signed a written consent form describing reasons for the study, the test procedures, time commitment and compensation, as well as the potential health risks of a single, brief

exposure to THS. A detailed medical and smoke exposure history was collected and a short physical was performed and blood, urine and saliva samples were collected. Urine samples were screened for metabolites of tetrahydrocannabinol, signs of urinary tract infection and (for women only) pregnancy. Saliva samples were screened for metabolites of nicotine. Blood samples were screened for signs of inflammation, diabetes, hyperlipidemia, and renal or hepatic impairment. Skin prick tests were conducted for 10 common aeroallergens.

Exclusion criteria for the primary study were:

1. Regular, current exposure to tobacco smoke, by history or saliva test (salivary cotinine > 10 ng/ml)
2. Physician diagnosis of asthma, heart disease, hypertension, thyroid disease, diabetes, glaucoma, or renal or hepatic impairment
3. Unstable psychiatric condition (such as current major depression, history of schizophrenia or bipolar disorder) or current use of more than two psychiatric medications
4. Pregnancy or breastfeeding
5. Alcohol or illicit drug dependence within the past 5 years
6. BMI > 35 and < 18
7. Current illicit drug use (by history or urine test)
8. More than 1 pack year smoking history
9. Ever a daily marijuana smoker
10. Smoked anything within the last 3 months
11. Unable to hold allergy or other OTC medications
12. Occupational exposure to smoke, dusts and fumes

13. Concurrent participation in another trial
14. Unable to communicate in English
15. BUN indicative of potential renal impairment
16. ALT or AST indicative of potential hepatic impairment
17. C-reactive protein concentration indicative of inflammation or infection
18. 2 or more of the following criteria:

    Systolic blood pressure > 140

    Diastolic blood pressure > 90

    Blood glucose > 110

    LDL >130

Study visits took place at the Zuckerberg San Francisco General Hospital campus, in the Human Exposure Laboratory, between 9:00 AM and 2:00PM.

Interventions

The respirable fraction of THS was generated by aging cigarette smoke in a six cubic meter stainless steel chamber overnight and then flushing the aerosol from the chamber with conditioned, filtered air. The cigarette smoke was generated by smoking a popular brand of cigarettes according to ISO protocol 3308: 2012 with a cigarette smoking machine (Model TE- 10z smoking machine, Teague Enterprises, Woodland, California, USA). The smoke was diluted to 1 mg/m^3 using conditioned, filtered air[23]. After a 1-hour smoking session, airflow through the system was turned off, and the aerosol was aged for 12 hours.

Study participants were exposed to clean air and THS head-only, using a modified pressurized air purifying respirator (3M Airmate # BE-10–3, 3M, Inc., St. Paul, MN, USA) with an aerosol flow rate of 200 lpm. The starting particle concentration in the

THS aerosol was 350-800 μg/m^3 and fell to below 20 μg/m^3 within 60 minutes. Clean air was supplied by the pressurized air purifying respirator with a HEPA filter (GVP-440, 3M, Inc., St. Paul, MN).

Nasal epithelial samples were collected from the anterior, inferior turbinate using small, sterile plastic curettes (RhinoPro, Arlington Scientific, Inc. Springville, UT, USA), before and after each exposure. Nasal epithelial samples were immediately placed in RNAlater, frozen, and stored at -80°C until RNA was isolated. Samples were shipped on dry ice to the University of California, Riverside for further processing.

Blood samples were collected before exposure, after 30 minutes of exposure, after exposure and at 22 hours after the exposure ended.

Urine samples were collected before exposure, after 30 minutes of exposure, after exposure, before bed, upon waking and at 22 hours after the exposure ended.

Blood pressure and heart rate were measured before exposure, after 30 minutes of exposure, after the exposure and at 22 hours after the exposure ended.

Participants who completed the study received $300 as compensation.

Outcomes

Parent study outcomes included urinary concentrations of 8-isoprostane, cotinine and NNAL, blood pressure and heart rate, circulating concentrations of IL-6 and VEGF.

Sample Size

Sample size was determined based on the number of people sufficient to detect increases in markers of inflammation in previous studies of secondhand cigarette smoke exposure.

Randomization, Allocation and Blinding

Participants were randomized after eligibility was determined and they had scheduled their first exposure visit. A single list of random numbers was used to assign exposure sequence by the staff who scheduled the participants. Participants did not know of their allocation until they entered the exposure chamber. Because of the distinctive odor of tobacco smoke, it was not possible to blind the participants or the staff. Sample containers provided to collaborators included a code indicating the timepoint and exposure.

Results

Participant Flow

See Consort Flow Chart.

Recruitment Dates

12/2011 to 7/2015. Study was ended when completion target of 22 individuals was met.

Baseline Data

20 participants completed the study (12 women and 10 men) ranging in age from 23 to 45 years (Mean = 35.4years, SD= 10.3 years). 13 participants identified as Caucasian, 5 as Asian, 1 as African American and 3 identified as 2 or more races and Hispanic.

Numbers Analyzed

See Consort Flow Chart.

Outcomes

Results of the parent study have been submitted for publication. Primary findings are increases in urinary metabolites of nicotine and the tobacco-specific nitrosamine, NNK. No changes were seen in cardiovascular measures or circulating markers of inflammation and oxidative stress.

eTable 1. Number of Differentially Expressed Genes (DEGs) for Clean Air and THS Exposure.

	Down Regulated DEGs	Up-Regulated DEGs
Clean Air Exposure	0	2
THS Exposure	7	382

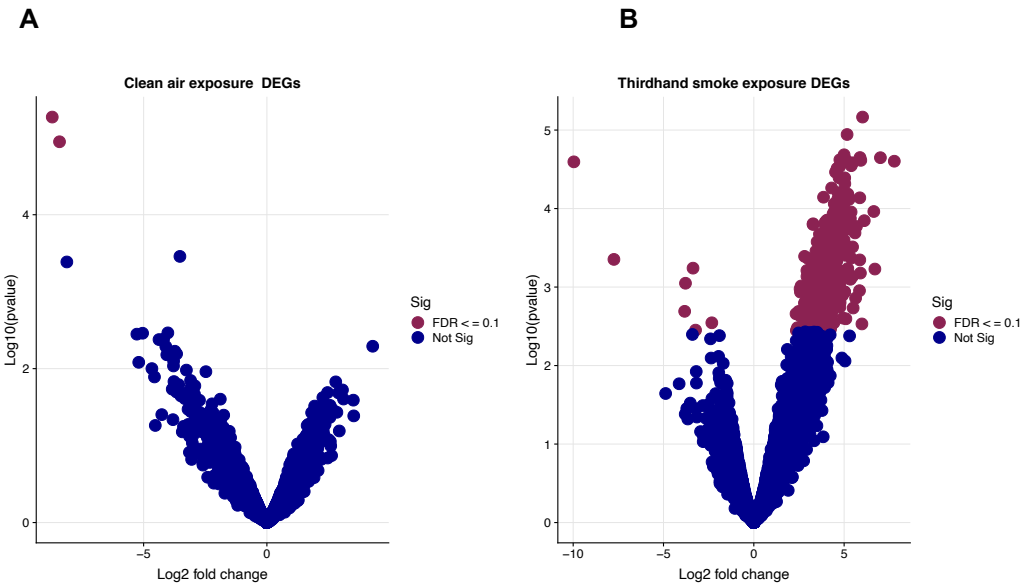

eFigure 1. Volcano Plots Showing the DEGs After Clean Air or THS Exposure.

(A) DEGs following clean air exposure and (B) following THS exposure. Blue dots represent genes that were not significant (FDR > 0.1), and magenta dots represent DEGs (FDR < 0.1).

eTable 2. Log_2-Fold Change, P-Values, and FDR Values, and of DEGs After Clean Air Exposure.

Genes	Log_2 -Fold Change	P-Value	FDR
HBA2	-8.71	5.38E-06	0.06
HBA1	-8.41	1.13E-05	0.06

eTable 3. Log_2 -Fold Change, P-Values, and FDR values and of DEGs After THS Exposure.

Genes	Log_2 -Fold Change	P-Value	FDR
ANAPC11	5.00	2.06E-05	0.02
CIB1	5.16	1.14E-05	0.02
COMT	4.61	3.07E-05	0.02
COPE	5.10	2.40E-05	0.02
ECH1	4.75	2.92E-05	0.02
HBG1	-9.96	2.54E-05	0.02
MAN1B1	6.02	6.83E-06	0.02
OSM	7.78	2.49E-05	0.02
PHPT1	5.47	2.61E-05	0.02
PPP5C	5.92	2.43E-05	0.02
TCEB2	4.76	2.39E-05	0.02
TFF3	7.01	2.25E-05	0.02
TMEM190	5.88	2.24E-05	0.02
ZMYND10	5.39	2.84E-05	0.02
ALDOA	4.52	3.43E-05	0.02
BRMS1	5.03	4.06E-05	0.03
PPP1CA	4.72	4.05E-05	0.03
AGTRAP	4.99	7.33E-05	0.03
ASL	5.14	7.25E-05	0.03
C19orf70	5.24	7.05E-05	0.03
NDUFV1	5.03	6.85E-05	0.03
PMPCA	5.87	7.29E-05	0.03
POLD2	5.21	6.53E-05	0.03
POLR2E	4.77	7.47E-05	0.03
POLR2I	4.65	7.55E-05	0.03
POLR2L	4.67	6.28E-05	0.03
R3HCC1	5.27	7.63E-05	0.03
ROMO1	4.31	5.46E-05	0.03
SNRPB	3.86	7.16E-05	0.03
TPPP3	5.04	4.82E-05	0.03
BSG	3.95	1.61E-04	0.03
BUD31	3.95	1.49E-04	0.03
C16orf71	4.96	1.43E-04	0.03
CCDC101	5.22	1.32E-04	0.03
CD151	4.03	1.43E-04	0.03
CENPM	6.64	1.09E-04	0.03
CFL1	3.28	1.59E-04	0.03
CHID1	4.76	1.25E-04	0.03
COMMD4	4.46	1.62E-04	0.03
DDX39A	4.95	1.67E-04	0.03
ETFB	4.45	8.69E-05	0.03
EXOSC5	6.12	1.43E-04	0.03
GPS1	4.99	1.63E-04	0.03

LGALS1	4.91	1.62E-04	0.03
MGMT	4.74	8.28E-05	0.03
MRPL28	4.99	8.66E-05	0.03
MVP	4.06	1.41E-04	0.03
NDUFA11	4.73	1.13E-04	0.03
NOC2L	5.35	1.34E-04	0.03
OTUB1	4.28	1.52E-04	0.03
PMEL	5.68	1.69E-04	0.03
PMF1-BGLAP	5.13	1.25E-04	0.03
PRPF6	4.39	1.17E-04	0.03
PTCD1	4.37	1.59E-04	0.03
RPL18	4.56	1.03E-04	0.03
SCRN2	5.29	1.70E-04	0.03
STRA13	4.53	1.50E-04	0.03
TARBP2	4.82	1.10E-04	0.03
TCF25	4.44	1.11E-04	0.03
TMEM265	3.29	1.56E-04	0.03
TOM1	4.31	1.55E-04	0.03
TRAPPC6A	5.00	1.33E-04	0.03
TSTA3	5.39	1.11E-04	0.03
VPS28	4.64	9.25E-05	0.03
WBP2	4.09	1.55E-04	0.03
ADGRE5	3.99	1.83E-04	0.03
ARL2	5.27	1.80E-04	0.03
C12orf57	4.71	1.83E-04	0.03
MAGED2	3.99	1.83E-04	0.03
SCAMP2	4.17	2.00E-04	0.03
SSSCA1	4.93	2.00E-04	0.03
CLK3	5.60	2.04E-04	0.03
WWP2	3.63	2.11E-04	0.03
AP2S1	4.43	2.30E-04	0.03
IDH3G	4.55	2.40E-04	0.03
KAT5	4.42	2.41E-04	0.03
LYPD2	3.84	2.39E-04	0.03
VMO1	3.76	2.41E-04	0.03
NHP2	4.06	2.50E-04	0.03
NRBP1	3.95	2.48E-04	0.03
TBRG4	5.00	2.53E-04	0.03
OAZ1	3.51	2.65E-04	0.03
PCIF1	4.34	2.68E-04	0.03
TEN1	4.98	2.73E-04	0.03
MTX1	4.05	2.77E-04	0.04
AAMP	3.81	2.99E-04	0.04
ARPC4	3.86	2.90E-04	0.04
CD82	3.71	2.99E-04	0.04
CDC42EP2	4.90	3.10E-04	0.04
MRPS11	4.26	3.11E-04	0.04
NDUFB7	4.34	2.96E-04	0.04
NDUFS8	4.14	2.94E-04	0.04
TEN1-CDK3	4.92	3.08E-04	0.04

YIPF2	4.71	3.07E-04	0.04
ZBTB48	5.47	3.08E-04	0.04
C19orf33	3.53	3.58E-04	0.04
CCDC103	4.13	3.50E-04	0.04
CRIP1	3.98	3.52E-04	0.04
KRT8	3.69	3.55E-04	0.04
LGALS3BP	3.77	3.48E-04	0.04
LINC00116	5.14	3.39E-04	0.04
MT2A	4.10	3.29E-04	0.04
PPAP2C	3.56	3.43E-04	0.04
WDR25	4.98	3.34E-04	0.04
YIF1B	3.44	3.48E-04	0.04
NAPA	4.00	3.66E-04	0.04
ALOX15P1	5.13	3.81E-04	0.04
GMPPA	4.67	3.75E-04	0.04
LMAN2	4.00	3.84E-04	0.04
SGSM3	4.26	3.77E-04	0.04
BCKDHA	4.45	3.96E-04	0.04
PRMT7	5.05	3.93E-04	0.04
PRSS8	4.26	3.99E-04	0.04
RPL28	3.88	4.02E-04	0.04
UBAC2	3.90	3.99E-04	0.04
FTSJ1	2.81	4.06E-04	0.04
ACO2	3.73	4.32E-04	0.04
C12orf10	4.38	4.22E-04	0.04
DPM3	5.39	4.27E-04	0.04
LYPLA2	4.13	4.31E-04	0.04
NDUFC2-KCTD14	3.00	4.32E-04	0.04
UBL7	4.25	4.15E-04	0.04
ZNHIT1	3.58	4.24E-04	0.04
ENTPD6	4.35	4.43E-04	0.04
HBG2	-7.74	4.44E-04	0.04
PMF1	4.07	4.38E-04	0.04
MIR4761	5.87	4.50E-04	0.04
ASCC2	3.93	4.85E-04	0.04
CHCHD5	4.59	4.72E-04	0.04
KIAA0195	4.09	4.83E-04	0.04
RUVBL1	3.75	4.75E-04	0.04
ZMAT5	4.47	4.78E-04	0.04
TIMM13	4.05	4.93E-04	0.04
PIGT	3.24	5.03E-04	0.04
ISG20	4.10	5.26E-04	0.04
TMEM205	3.85	5.14E-04	0.04
TNFSF12-TNFSF13	3.64	5.23E-04	0.04
TNFSF13	3.30	5.20E-04	0.04
RPP21	4.19	5.30E-04	0.04
ADGRG6	-3.36	5.74E-04	0.04
PEX16	5.20	5.81E-04	0.04
SCAMP3	4.24	5.81E-04	0.04
ST3GAL4-AS1	6.70	5.89E-04	0.04

GALE	3.82	6.18E-04	0.04
HIGD2A	3.18	6.12E-04	0.04
HN1	3.26	6.12E-04	0.04
NDUFB2	2.94	6.15E-04	0.04
SLC35C2	3.91	6.06E-04	0.04
WRAP53	4.40	6.18E-04	0.04
CATSPERD	4.84	6.27E-04	0.04
USP11	3.79	6.40E-04	0.05
ABHD11-AS1	5.90	6.63E-04	0.05
ARPC4-TTLL3	3.85	6.68E-04	0.05
CLN3	3.75	6.76E-04	0.05
CNN2	3.74	6.51E-04	0.05
DCPS	3.87	6.74E-04	0.05
SIL1	3.93	6.66E-04	0.05
TAX1BP3	3.25	6.64E-04	0.05
TSSC4	4.63	6.74E-04	0.05
DDX49	4.90	6.87E-04	0.05
HIST1H2BC	4.69	7.19E-04	0.05
H3F3C	2.94	7.30E-04	0.05
SDSL	5.46	7.32E-04	0.05
RPL18A	3.58	7.40E-04	0.05
CHCHD6	4.96	7.48E-04	0.05
GSS	3.18	7.60E-04	0.05
LRG1	3.31	7.60E-04	0.05
TEX264	3.85	7.86E-04	0.05
MEF2BNB-MEF2B	5.35	7.95E-04	0.05
TIMM17B	4.17	8.12E-04	0.05
VPS39	3.74	8.09E-04	0.05
PAFAH1B3	4.43	8.26E-04	0.05
PARP3	3.42	8.24E-04	0.05
PCNA-AS1	4.64	8.34E-04	0.05
SNAP47	3.64	8.33E-04	0.05
ANAPC5	3.21	8.39E-04	0.05
NANS	3.22	8.57E-04	0.05
TADA3	3.39	8.65E-04	0.05
USB1	3.52	8.62E-04	0.05
CYB561A3	3.37	8.79E-04	0.05
RPL36	3.14	8.79E-04	0.05
TEKT2	4.78	8.85E-04	0.05
LINC01224	-3.78	8.93E-04	0.05
RPP25L	4.31	9.00E-04	0.05
ANKZF1	3.96	9.13E-04	0.05
CHI3L1	3.65	9.19E-04	0.05
GPR162	3.77	9.21E-04	0.05
GSTP1	3.66	9.06E-04	0.05
AEN	4.22	9.46E-04	0.05
CXXC1	4.53	9.47E-04	0.05
DNAL4	3.91	9.40E-04	0.05
LSP1	4.10	9.47E-04	0.05
SIRT2	3.73	9.45E-04	0.05

ARF1	3.17	9.54E-04	0.05
EWSR1	2.62	9.69E-04	0.05
NARF	3.97	9.72E-04	0.05
SF3B4	3.50	9.68E-04	0.05
ST3GAL4	3.42	9.87E-04	0.05
RAD9A	3.93	1.00E-03	0.05
EIF4H	2.89	1.03E-03	0.06
ALG12	4.46	1.06E-03	0.06
NDUFC2	2.56	1.06E-03	0.06
RSPH9	3.86	1.06E-03	0.06
TUBG1	3.40	1.04E-03	0.06
CCDC57	4.73	1.08E-03	0.06
DUOXA1	3.49	1.09E-03	0.06
LOC105447645	4.26	1.09E-03	0.06
TECR	3.87	1.09E-03	0.06
TMED1	4.38	1.09E-03	0.06
ACOT8	4.33	1.12E-03	0.06
CDK10	5.85	1.11E-03	0.06
NDUFB2-AS1	4.20	1.12E-03	0.06
LRRC46	3.58	1.13E-03	0.06
AP4M1	4.02	1.15E-03	0.06
HIST2H4A	5.03	1.15E-03	0.06
HIST2H4B	5.03	1.15E-03	0.06
SEC61B	2.58	1.16E-03	0.06
SNCG	4.82	1.17E-03	0.06
U2AF1	2.86	1.14E-03	0.06
UQCR11	3.04	1.16E-03	0.06
STK36	3.58	1.18E-03	0.06
PPP1R32	4.89	1.19E-03	0.06
MUC20	3.15	1.19E-03	0.06
FAM195B	4.45	1.21E-03	0.06
ANPEP	3.26	1.26E-03	0.06
DMAP1	4.46	1.25E-03	0.06
IFI30	3.12	1.27E-03	0.06
NCF4	3.85	1.25E-03	0.06
NOL12	4.35	1.27E-03	0.06
C11orf49	3.23	1.28E-03	0.06
CCDC159	4.91	1.28E-03	0.06
C6orf1	4.03	1.29E-03	0.06
XRCC1	3.90	1.30E-03	0.06
DNPEP	2.99	1.31E-03	0.06
RAB5C	3.13	1.31E-03	0.06
ABHD16A	3.19	1.34E-03	0.06
C19orf48	4.46	1.34E-03	0.06
ELOF1	3.94	1.41E-03	0.06
GPX3	3.52	1.41E-03	0.06
HEXA	3.41	1.39E-03	0.06
LYPLA2P2	5.64	1.38E-03	0.06
PPARD	3.65	1.38E-03	0.06
RAD23A	3.23	1.41E-03	0.06

SLC16A5	3.27	1.39E-03	0.06
TAPBPL	3.51	1.40E-03	0.06
TBCD	3.95	1.38E-03	0.06
AK1	3.87	1.44E-03	0.06
CINP	4.26	1.44E-03	0.06
PPP2R1A	3.24	1.45E-03	0.06
RPS5	3.21	1.45E-03	0.06
XPC	3.25	1.43E-03	0.06
GCHFR	3.87	1.46E-03	0.06
MX1	2.93	1.46E-03	0.06
LAPTM5	3.08	1.47E-03	0.06
BIN3	3.65	1.50E-03	0.06
ARAF	3.36	1.53E-03	0.06
FLOT2	3.27	1.53E-03	0.06
BSCL2	3.39	1.54E-03	0.06
GAS8	3.85	1.55E-03	0.06
GPRC5C	3.26	1.57E-03	0.06
HS1BP3	4.78	1.58E-03	0.06
MLST8	4.01	1.56E-03	0.06
P2RX5-TAX1BP3	2.84	1.57E-03	0.06
ZNF576	4.35	1.56E-03	0.06
COX8A	2.80	1.60E-03	0.06
GRIPAP1	3.00	1.61E-03	0.06
NADSYN1	3.81	1.64E-03	0.07
NCAPH2	3.79	1.65E-03	0.07
SZRD1	3.16	1.65E-03	0.07
CYP2F1	3.07	1.69E-03	0.07
DDX41	3.77	1.69E-03	0.07
PHGDH	3.74	1.68E-03	0.07
SPTAN1	3.11	1.72E-03	0.07
STK11IP	4.38	1.77E-03	0.07
CARKD	3.27	1.78E-03	0.07
MUL1	3.57	1.79E-03	0.07
CCS	4.77	1.80E-03	0.07
KIF22	4.15	1.82E-03	0.07
MED24	3.37	1.82E-03	0.07
CDC37	3.63	1.83E-03	0.07
WFDC2	3.18	1.83E-03	0.07
BCL2L1	3.18	1.87E-03	0.07
C9orf114	3.54	1.87E-03	0.07
MFAP2	5.50	1.85E-03	0.07
RPL29	3.05	1.86E-03	0.07
ZDHHC12	4.11	1.86E-03	0.07
CPSF3L	3.84	1.88E-03	0.07
RPS9	3.14	1.88E-03	0.07
WDR55	3.11	1.90E-03	0.07
RABGGTA	3.54	1.92E-03	0.07
BLVRB	3.38	1.93E-03	0.07
DAGLB	4.13	1.94E-03	0.07
PHB	3.21	1.94E-03	0.07

HNRNPUL2-BSCL2	3.28	1.95E-03	0.07
ARHGAP1	2.97	1.97E-03	0.07
EXOC7	2.98	1.98E-03	0.07
TREX1	3.80	1.98E-03	0.07
MRPL53	4.09	2.00E-03	0.07
PRKCSH	3.60	2.00E-03	0.07
LOC101928223	-3.83	2.04E-03	0.07
GSTO1	2.48	2.04E-03	0.07
NUP188	4.19	2.08E-03	0.07
MRPL52	3.17	2.11E-03	0.07
TIMM10B	2.50	2.13E-03	0.08
MRPL55	3.56	2.15E-03	0.08
NTMT1	3.81	2.16E-03	0.08
PLEKHJ1	3.76	2.16E-03	0.08
SGTA	3.99	2.17E-03	0.08
CCDC37	3.64	2.18E-03	0.08
RBM23	2.34	2.19E-03	0.08
WDR45	3.31	2.21E-03	0.08
GPATCH3	4.21	2.24E-03	0.08
SRA1	2.76	2.24E-03	0.08
TFPT	4.32	2.24E-03	0.08
ITFG3	4.05	2.26E-03	0.08
LRPAP1	3.30	2.27E-03	0.08
NAP1L4	2.74	2.27E-03	0.08
COASY	3.33	2.32E-03	0.08
HLA-E	2.55	2.31E-03	0.08
URM1	3.36	2.32E-03	0.08
ARL16	3.13	2.36E-03	0.08
RNASEH2C	3.24	2.38E-03	0.08
DPP3	2.95	2.41E-03	0.08
ST20	3.93	2.41E-03	0.08
MSRB1	3.28	2.44E-03	0.08
ACY1	3.77	2.49E-03	0.08
LENG1	4.94	2.49E-03	0.08
RRP12	4.11	2.50E-03	0.08
ABHD14A-ACY1	3.69	2.54E-03	0.08
CLCNKB	5.10	2.53E-03	0.08
CXCL8	3.41	2.52E-03	0.08
EEF1D	3.07	2.54E-03	0.08
KRT17	3.25	2.52E-03	0.08
COG7	3.26	2.63E-03	0.08
DCP1B	3.56	2.63E-03	0.08
HMBS	3.45	2.61E-03	0.08
LOC102724814	3.90	2.61E-03	0.08
PDZK1IP1	3.71	2.62E-03	0.08
SARS2	4.06	2.62E-03	0.08
VSIG2	3.01	2.59E-03	0.08
WDR86-AS1	3.35	2.63E-03	0.08
POMT1	4.06	2.64E-03	0.08
LAMTOR4	3.35	2.66E-03	0.08

ZER1	3.17	2.68E-03	0.08
ABT1	3.06	2.70E-03	0.08
GLIPR2	2.82	2.71E-03	0.08
PSMG3	2.84	2.71E-03	0.08
PRMT1	3.43	2.75E-03	0.08
LIN37	4.43	2.85E-03	0.09
MMP3	-2.32	2.85E-03	0.09
SSNA1	3.45	2.85E-03	0.09
TXLNA	3.09	2.85E-03	0.09
DRG2	3.80	2.91E-03	0.09
EMP3	5.98	2.95E-03	0.09
NFYC	3.03	3.03E-03	0.09
SLC25A11	2.88	3.05E-03	0.09
POLR3H	2.87	3.08E-03	0.09
SLC44A4	3.11	3.10E-03	0.09
EIF3C	2.77	3.11E-03	0.09
EIF3CL	2.77	3.12E-03	0.09
THAP3	3.70	3.16E-03	0.09
BCL2A1	2.92	3.19E-03	0.09
CABP7	3.92	3.21E-03	0.09
DIABLO	2.62	3.21E-03	0.09
PISD	2.66	3.23E-03	0.09
SLC35A4	3.28	3.23E-03	0.09
CRELD1	4.08	3.26E-03	0.10
ABTB1	4.25	3.28E-03	0.10
ARFGAP2	3.35	3.31E-03	0.10
EIF3G	3.50	3.31E-03	0.10
SERPINF1	3.07	3.30E-03	0.10
UQCRQ	2.41	3.30E-03	0.10
COA3	2.56	3.39E-03	0.10
FBXO6	3.44	3.39E-03	0.10
NEU1	2.45	3.39E-03	0.10
PSMB10	2.86	3.36E-03	0.10
TPD52L2	3.33	3.39E-03	0.10
ZFYVE19	3.49	3.42E-03	0.10
TMEM219	2.70	3.46E-03	0.10
HCK	4.24	3.48E-03	0.10
C3orf30	-3.23	3.53E-03	0.10
IFI27L2	3.39	3.53E-03	0.10
TMEM9	3.02	3.54E-03	0.10
LGALS3	2.35	3.57E-03	0.10
NUDCD3	3.39	3.57E-03	0.10
PWP2	4.00	3.58E-03	0.10
SAE1	2.65	3.59E-03	0.10
HDAC11	4.19	3.62E-03	0.10
TMEM63A	3.52	3.61E-03	0.10

eTable 4. GO Terms: Biological Processes Enriched After THS Exposure

ID	Description	Gene Count	q-Value
GO:0045333	Cellular Respiration	15	2.39E-03
GO:0022904	Respiratory Electron Transport Chain	11	2.84E-03
GO:0042775	Mitochondrial ATP Synthesis Coupled Electron Transport	10	2.84E-03
GO:0042773	ATP Synthesis Coupled Electron Transport	10	2.84E-03
GO:0022613	Ribonucleoprotein Complex Biogenesis	24	4.19E-03
GO:0022900	Electron Transport Chain	13	6.97E-03
GO:0006605	Protein Targeting	21	6.97E-03
GO:0006120	Mitochondrial Electron Transport, NADH to Ubiquinone	7	6.97E-03
GO:0034470	ncRNA Processing	21	6.97E-03
GO:0006119	Oxidative Phosphorylation	10	7.24E-03
GO:0006364	rRNA Processing	16	7.24E-03

eTable 5. GO Terms: Cellular Components Enriched After THS Exposure

ID	Description	Gene Count	q-Value
GO:0005743	Mitochondrial Inner Membrane	29	7.21E-06
GO:0098798	Mitochondrial Protein Complex	14	8.30E-05
GO:0070469	Respiratory Chain	11	8.30E-05
GO:0098800	Inner Mitochondrial Membrane Protein Complex	12	2.36E-04
GO:0044455	Mitochondrial Membrane Part	15	2.77E-04
GO:0098803	Respiratory Chain Complex	8	4.38E-03
GO:1990204	Oxidoreductase Complex	9	4.76E-03
GO:0005746	Mitochondrial Respiratory Chain	8	5.60E-03
GO:0005747	Mitochondrial Respiratory Chain Complex I	6	5.60E-03
GO:0030964	NADH Dehydrogenase Complex	6	5.60E-03
GO:0045271	Respiratory Chain Complex I	6	5.60E-03
GO:0044391	Ribosomal Subunit	12	5.60E-03
GO:0015934	Large Ribosomal Subunit	9	8.75E-03

eTable 6. GO Terms: Molecular Function Enriched After THS exposure

ID	Description	Gene Count	q-Value
GO:0003954	NADH Dehydrogenase Activity	7	3.80E-03

eTable 7. Reactome Terms Enriched After THS exposure.

ID	Description	Gene Count	q-Value
R-HSA-1428517	The Citric Acid (TCA) Cycle and Respiratory Electron Transport	14	9.27E-03
R-HSA-611105	Respiratory Electron Transport	10	1.01E-02
R-HSA-72766	Translation	18	1.01E-02
R-HSA-1268020	Mitochondrial Protein Import	8	1.01E-02
R-HSA-72165	mRNA Splicing - Minor Pathway	7	1.05E-02
R-HSA-5696398	Nucleotide Excision Repair	10	1.05E-02
R-HSA-168273	Influenza Viral RNA Transcription and Replication	11	1.05E-02
R-HSA-73894	DNA Repair	18	1.05E-02
R-HSA-156827	L13a-mediated Translational Silencing of Ceruloplasmin Expression	10	1.05E-02
R-HSA-72706	GTP Hydrolysis and Joining of the 60S Ribosomal Subunit	10	1.05E-02
R-HSA-168255	Influenza Life Cycle	11	1.23E-02
R-HSA-72613	Eukaryotic Translation Initiation	10	1.23E-02
R-HSA-72737	Cap-dependent Translation Initiation	10	1.23E-02
R-HSA-446203	Asparagine N-linked Glycosylation	17	1.23E-02
R-HSA-8868773	rRNA Processing in the Nucleus and Cytosol	13	1.23E-02
R-HSA-163200	Respiratory Electron Transport, ATP Synthesis by Chemiosmotic Coupling, and Heat Production by Uncoupling Proteins.	10	1.23E-02
R-HSA-72689	Formation of a Pool of Free 40S Subunits	9	1.36E-02
R-HSA-72312	rRNA Processing	13	1.69E-02
R-HSA-168254	Influenza Infection	11	1.69E-02
R-HSA-6791226	Major Pathway of rRNA Processing in the Nucleolus and Cytosol	12	2.12E-02
R-HSA-156842	Eukaryotic Translation Elongation	8	2.80E-02
R-HSA-6799198	Complex I biogenesis	6	3.27E-02

R-HSA-5696394	DNA Damage Recognition in GG-NER	5	3.51E-02
R-HSA-203927	MicroRNA (miRNA) biogenesis	4	3.61E-02
R-HSA-446193	Biosynthesis of the N-glycan Precursor (dolichol lipid-linked oligosaccharide, LLO) and Transfer to a Nascent Protein	7	3.61E-02

eFigure 2. Diagram Showing the Cell Death Associated Genes that were Upregulated Following THS Exposure in the IPA Analysis.

Blue dotted lines indicate inhibition of cell death and yellow dotted lines indicate inconsistent findings to the predicted inhibition of Cell Death (z-score = -3.03). Grey lines indicate insufficient information to make a prediction. IPA predicted subcellular location (extracellular, plasma membrane, cytoplasm or nuclear) of each gene is shown.

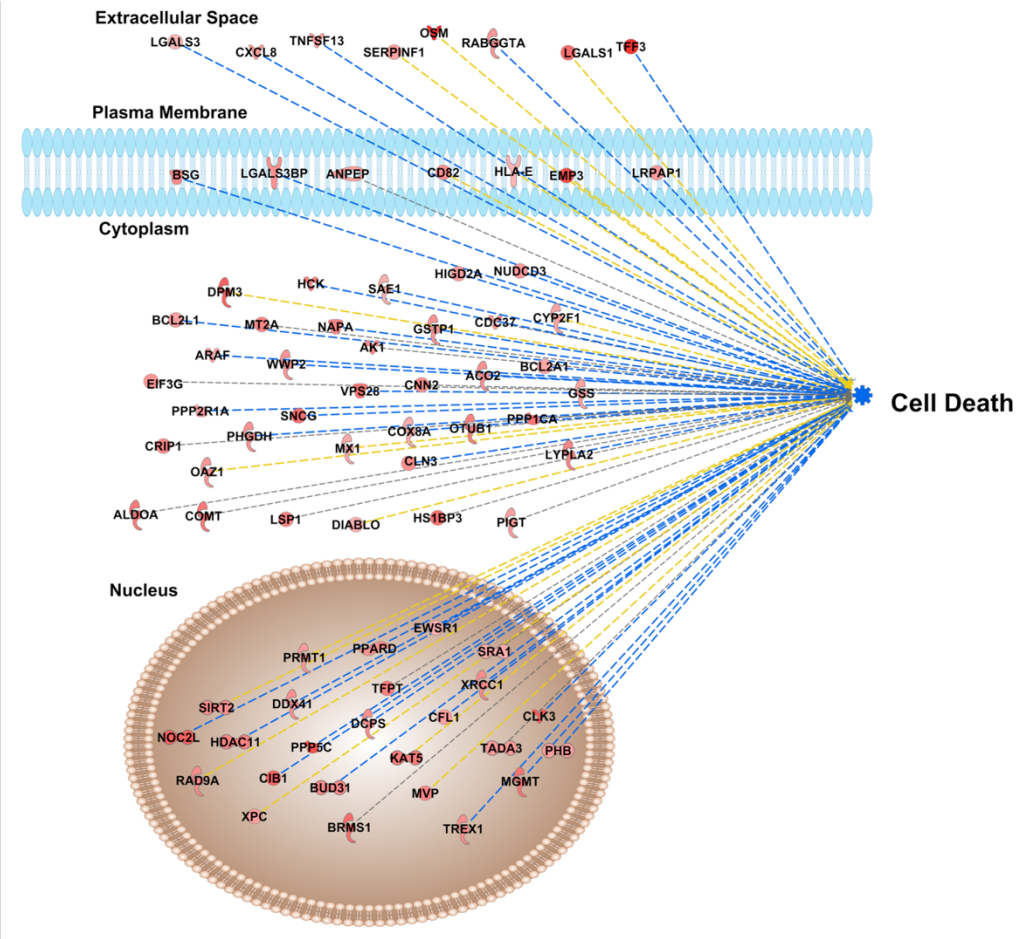

eFigure 3. Diagram Showing the Cell Viability Genes that were Upregulated Following THS Exposure in the IPA Analysis.

Orange dotted lines indicate activation of the process and yellow dotted lines indicate findings inconsistent with activation of cell viability (Z-score = 5.03). Predicted location of each gene (extracellular, plasma membrane, cytoplasm or nuclear) is shown.

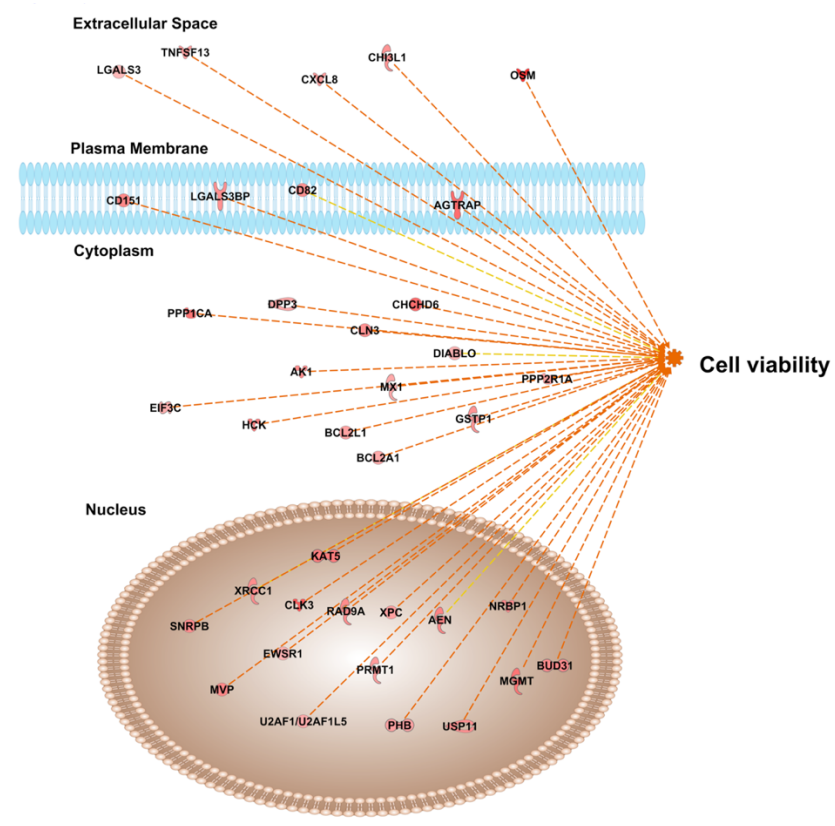

eFigure 4. Diagram Showing the Homologous Recombination Genes that were Upregulated Following THS Exposure in the IPA Analysis.

Orange dotted lines indicate activation of the process (z-score = 2.83). IPA based subcellular predicted location (extracellular, plasma membrane, cytoplasm or nuclear) of each gene is shown in the diagram.

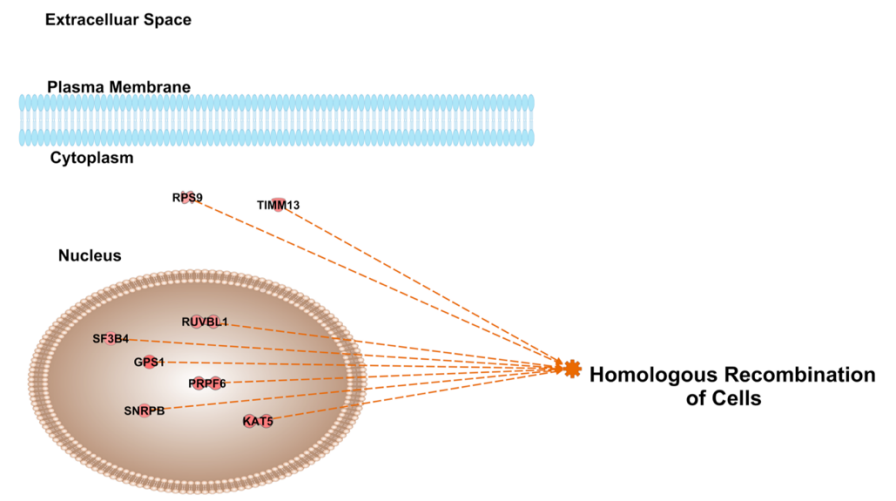

]

Supplement Table 1. Demographics and Biomarker Data

Sample Name	Age	Code	Group	Smoking History	Cigs per day	Puffs Per day	E-Cig Nicotine Concentration	Brand	Flavor currently using	Urine Cotinine Concentration (ng/ml)	NNAL (pg)
72	29	CN	E-Cigarette			90	6-9 mg (0.6-0.9%)	Smoov	Grape	1021.15457	3
132	32	EFY	E-Cigarette			96	16-24mg (1.6-2.4%)	Smoov	Pinnapple	711.214864	14.3
188	39	EFY	E-Cigarette			100	6-9 mg (0.6-0.9%)	ECTO	Jolly melon-watermelon	478.253462	0.4
75	48	NFY	Non-smoker	Never smoker						0	0.4
183	38	NFY	Non-smoker	Ex-smoker						0	0.6
254	26	NFY	Non-smoker	N/A						N/A	#VALUE!
40	33	SFY	Smoker		1					927.192474	684
85	33	SFY	Smoker		12					920.036049	108.3
98	41	SFY	Smoker		24					1103.99238	234.5

Table 2A: GO Biological Processes for the Downregulated DEGs in the EC vs NS Comparison

ID	Description	GeneRatio	BgRatio	pvalue	p.adjust	qvalue	geneID	Count
GO:0044782	cilium organization	73/629	332/12310	2.42E-27	9.03E-24	8.61E-24	AKAP9/ALMS1/ARMC4/BBS9/C2CD3/CC2D2A/CCDC103/CCDC113/CCDC114/CCDC13/CCDC151/CCDC39/CCDC40/CDC14A/CEP83/CFAP221/CFAP46/CFAP53/CFAP54/CFAP61/CFAP74/CNTRL/CROCC/DCDC2/DNAH1/DNAH3/DNAH5/DNAH6/DNAH7/DNAI1/DNAI2/DNAJB13/DYNC2H1/DZIP1L/FAM161A/FAM161B/FBF1/FOXJ1/FUZ/HYDIN/IFT122/IFT140/IFT172/IFT80/IFT88/KIF17/KIF24/KIF27/LRGUK/LRRC6/MAK/NEK1/PIH1D3/RFX2/RFX3/RP1/RPGRIP1L/RSPH1/RSPH4A/SFI1/SPAG17/STK36/SYNE2/TCTN2/TEKT1/TEKT2/TMEM67/TTBK2/TTC21B/TTC30B/UBXN10/WDR19/WDR35	73
GO:0060271	cilium assembly	71/629	322/12310	1.10E-26	2.05E-23	1.96E-23	AKAP9/ALMS1/ARMC4/BBS9/C2CD3/CC2D2A/CCDC103/CCDC113/CCDC114/CCDC13/CCDC151/CCDC39/CCDC40/CDC14A/CEP83/CFAP221/CFAP46/CFAP53/CFAP54/CFAP74/CNTRL/CROCC/DCDC2/DNAH1/DNAH3/DNAH5/DNAH6/DNAH7/DNAI1/DNAI2/DNAJB13/DYNC2H1/DZIP1L/FAM161A/FBF1/FOXJ1/FUZ/HYDIN/IFT122/IFT140/IFT172/IFT80/IFT88/KIF17/KIF24/KIF27/LRGUK/LRRC6/MAK/NEK	71

							1/PIH1D3/RFX2/RFX3/RP1/RPGRIP1L/RSPH1/RSPH4A/SFI1/SPAG17/STK36/SYNE2/TCTN2/TEKT1/TEKT2/TMEM67/TTBK2/TTC21B/TTC30B/UBXN10/WDR19/WDR35	
GO:0003341	cilium movement	31/629	59/12310	6.38E-25	7.95E-22	7.58E-22	ARMC4/CCDC103/CCDC114/CCDC151/CCDC39/CCDC40/CFAP221/CFAP46/CFAP53/CFAP54/CFAP61/DNAH1/DNAH11/DNAH3/DNAH5/DNAH7/DNAH9/DNAI1/DNAI2/HYDIN/LRRC6/MAATS1/PIH1D3/RFX3/RSPH4A/SPAG17/STK36/TEKT1/TEKT2/WDR66/WDR78	31
GO:0007018	microtubule-based movement	58/629	263/12310	6.26E-22	5.85E-19	5.57E-19	AP3M2/ARMC4/CCDC103/CCDC114/CCDC151/CCDC39/CCDC40/CFAP221/CFAP46/CFAP53/CFAP54/CFAP61/DNAH1/DNAH10/DNAH11/DNAH12/DNAH2/DNAH3/DNAH5/DNAH6/DNAH7/DNAH9/DNAI1/DNAI2/DYNC2H1/FMN2/FYCO1/HYDIN/IFT122/IFT140/IFT172/IFT80/IFT88/KIF17/KIF24/KIF26B/KIF27/KIF6/LRRC6/MAATS1/MAK/MAP1B/PIH1D3/RFX3/RSPH4A/SPAG17/SPG11/STK36/SYNE2/TEKT1/TEKT2/TTC21B/TTC30B/WDR19/WDR35/WDR63/WDR66/WDR78	58
GO:0120031	plasma membrane bounded cell projection assembly	79/629	483/12310	8.06E-21	5.98E-18	5.69E-18	AKAP9/ALMS1/ARHGEF26/ARMC4/BBS9/BCAS3/C2CD3/CC2D2A/CCDC103/CCDC113/CCDC114/CCDC13/CCDC151/CCDC39/CCDC40/CDC14A/CEP83/CFAP221/CFAP46/CFAP53/CFAP54/CFAP74/CNTRL/CROCC/DCDC2/DNAH1/DNAH3/DNAH5/DNAH6/DNAH7/DNAI1/DNAI2/DN	79

							AJB13/DYNC2H1/DZIP1L/FAM161A/FBF1/FOXJ1/FUZ/HYDIN/IFT122/IFT140/IFT172/IFT80/IFT88/KIF17/KIF24/KIF27/LPAR3/LRGUK/LRRC6/MAK/MTSS1/MYLK/NEK1/PIH1D3/PPP1R9A/RFX2/RFX3/RP1/RPGRIP1L/RSPH1/RSPH4A/SFI1/SLIT2/SPAG17/STK36/SYNE2/TCTN2/TEKT1/TEKT2/TENM2/TMEM67/TTBK2/TTC21B/TTC30B/UBXN10/WDR19/WDR35	
GO:0030031	cell projection assembly	80/629	495/12310	9.60E-21	5.98E-18	5.69E-18	AKAP9/ALMS1/ARHGEF26/ARMC4/BBS9/BCAS3/C2CD3/CC2D2A/CCDC103/CCDC113/CCDC114/CCDC13/CCDC151/CCDC39/CCDC40/CDC14A/CEP83/CFAP221/CFAP46/CFAP53/CFAP54/CFAP74/CNTRL/CROCC/DCDC2/DNAH1/DNAH3/DNAH5/DNAH6/DNAH7/DNAI1/DNAI2/DNAJB13/DYNC2H1/DZIP1L/FAM161A/FBF1/FOXJ1/FUZ/HYDIN/IFT122/IFT140/IFT172/IFT80/IFT88/KIF17/KIF24/KIF27/LPAR3/LRGUK/LRRC6/MAK/MTSS1/MYLK/NEK1/PIH1D3/PPP1R9A/RFX2/RFX3/RP1/RPGRIP1L/RSPH1/RSPH4A/SFI1/SLIT2/SPAG17/STK36/SYNE2/TCTN2/TEKT1/TEKT2/TENM2/TMEM67/TSGA10/TTBK2/TTC21B/TTC30B/UBXN10/WDR19/WDR35	80
GO:0035082	axoneme assembly	25/629	51/12310	2.28E-19	1.22E-16	1.16E-16	ARMC4/CC2D2A/CCDC103/CCDC114/CCDC151/CCDC39/CCDC40/CFAP46/CFAP74/DNAH1/DNAH3/DNAH5/DNAH7/DNAI1/DNAI2/DNAJB	25

							13/HYDIN/LRGUK/LRRC6/PIH1D3/RP1/RSPH1/RSPH4A/SPAG17/TEK T2	
GO:0001578	microtubule bundle formation	28/629	74/12310	8.15E-18	3.81E-15	3.63E-15	ARMC4/CC2D2A/CCDC103/CCDC114/CCDC151/CCDC39/CCDC40/CFAP46/CFAP74/DNAH1/DNAH3/DNAH5/DNAH7/DNAI1/DNAI2/DNAJB13/HYDIN/LRGUK/LRRC6/MAP1B/PIH1D3/RP1/RSPH1/RSPH4A/SPAG17/TEKT2/TPPP/TPPP3	28
GO:0070286	axonemal dynein complex assembly	15/629	28/12310	7.23E-13	3.00E-10	2.86E-10	ARMC4/CCDC103/CCDC114/CCDC151/CCDC39/CCDC40/DNAH1/DNAH3/DNAH5/DNAH7/DNAI1/DNAI2/LRRC6/PIH1D3/TEKT2	15
GO:0007368	determination of left/right symmetry	22/629	85/12310	1.62E-10	6.06E-08	5.77E-08	ARMC4/BICC1/C2CD3/CC2D2A/CCDC103/CCDC151/CCDC39/CCDC40/CFAP53/DLL1/DNAH11/DNAH5/DNAI1/DNAI2/FOXJ1/IFT140/IFT172/LRRC6/MEGF8/PCSK5/RFX3/RPGRIP1L	22
GO:0009855	determination of bilateral symmetry	22/629	90/12310	5.37E-10	1.82E-07	1.74E-07	ARMC4/BICC1/C2CD3/CC2D2A/CCDC103/CCDC151/CCDC39/CCDC40/CFAP53/DLL1/DNAH11/DNAH5/DNAI1/DNAI2/FOXJ1/IFT140/IFT172/LRRC6/MEGF8/PCSK5/RFX3/RPGRIP1L	22
GO:0007389	pattern specification process	40/629	266/12310	6.66E-10	1.94E-07	1.85E-07	AR/ARMC4/BICC1/C2CD3/CC2D2A/CCDC103/CCDC151/CCDC39/CCDC40/CDON/CELSR1/CFAP53/CXXC4/DLL1/DNAH11/DNAH5/DNAI1/DNAI2/DSCAML1/FOXJ1/FUZ/HIPK1/IFT122/IFT140/IFT172/IRX3/KMT2A/LEF1/LRP4/LRRC6/MEGF8/PCSK5/PTCH1/RFX3/RPGRIP1L/SEMA3C/SYNGAP1/TTC21B/WDR19/WLS	40

GO:0009799	specification of symmetry	22/629	91/12310	6.75E-10	1.94E-07	1.85E-07	ARMC4/BICC1/C2CD3/CC2D2A/CCDC103/CCDC151/CCDC39/CCDC40/CFAP53/DLL1/DNAH11/DNAH5/DNAI1/DNAI2/FOXJ1/IFT140/IFT172/LRRC6/MEGF8/PCSK5/RFX3/RPGRIP1L	22
GO:0000226	microtubule cytoskeleton organization	54/629	463/12310	9.70E-09	2.48E-06	2.36E-06	AKAP9/ARMC4/BCAS3/C2CD3/CC2D2A/CCDC103/CCDC114/CCDC13/CCDC151/CCDC39/CCDC40/CCDC78/CCDC8/CCDC88C/CDC14A/CFAP46/CFAP74/CROCC/DIXDC1/DNAH1/DNAH3/DNAH5/DNAH7/DNAI1/DNAI2/DNAJB13/EFHC1/EML1/FMN2/HYDIN/IFT172/KATNAL2/KIAA0753/KIF24/LRGUK/LRRC6/MAP1A/MAP1B/MAP6/PIH1D3/PKD1/RP1/RSPH1/RSPH4A/SAXO2/SPAG17/SYNE2/TEKT2/TMEM67/TPPP/TPPP3/TTBK2/TUBGCP6/ULK4	54
GO:0007156	homophilic cell adhesion via plasma membrane adhesion molecules	23/629	113/12310	9.96E-09	2.48E-06	2.36E-06	CDH22/CDHR3/CDHR4/CELSR1/DSCAML1/PCDH17/PCDHA10/PCDHA11/PCDHA12/PCDHA13/PCDHA4/PCDHA5/PCDHA6/PCDHA7/PCDHA8/PCDHA9/PCDHAC1/PCDHAC2/PCDHB1/PKD1/PTPRT/SDK1/SDK2	23
GO:0036159	inner dynein arm assembly	8/629	13/12310	4.56E-08	1.06E-05	1.01E-05	CCDC103/CCDC39/CCDC40/DNAH1/DNAH3/DNAH7/LRRC6/TEKT2	8
GO:0001539	cilium or flagellum-dependent cell motility	11/629	29/12310	8.46E-08	1.86E-05	1.77E-05	CCDC39/CFAP46/CFAP54/DNAH1/DNAH2/DNAH3/DNAH6/DNAH7/RFX3/TEKT1/TEKT2	11
GO:0036158	outer dynein arm assembly	8/629	14/12310	1.02E-07	2.11E-05	2.01E-05	ARMC4/CCDC103/CCDC114/CCDC151/DNAH5/DNAI1/DNAI2/LRRC6	8
GO:0097722	sperm motility	13/629	44/12310	1.71E-07	3.37E-05	3.21E-05	ATP2B4/CATSPERD/CCDC39/CCDC40/DNAH1/DNAH11/DNAH5/DNA	13

							I1/LRRC6/PIH1D3/TCTE1/TEKT1/TEKT2	
GO:0007224	smoothened signaling pathway	20/629	103/12310	2.07E-07	3.87E-05	3.69E-05	C2CD3/CC2D2A/CDON/DCDC2/FUZ/HHAT/HIPK1/IFT122/IFT140/IFT172/IFT80/MEGF8/PTCH1/RPGRIP1L/STK36/TCTN2/TTBK2/TTC21B/WDR19/WNT9A	20
GO:0098742	cell-cell adhesion via plasma-membrane adhesion molecules	26/629	167/12310	3.40E-07	6.04E-05	5.76E-05	CDH22/CDHR3/CDHR4/CELSR1/CLDN16/CLDN8/DSCAML1/PCDH17/PCDHA10/PCDHA11/PCDHA12/PCDHA13/PCDHA4/PCDHA5/PCDHA6/PCDHA7/PCDHA8/PCDHA9/PCDHAC1/PCDHAC2/PCDHB1/PKD1/PTPRT/SDK1/SDK2/TENM2	26
GO:0060285	cilium-dependent cell motility	10/629	28/12310	6.42E-07	0.000109	0.000103837	CCDC39/CFAP46/CFAP54/DNAH1/DNAH2/DNAH3/DNAH7/RFX3/TEKT1/TEKT2	10
GO:0030317	flagellated sperm motility	12/629	42/12310	7.68E-07	0.000124735	0.000118827	ATP2B4/CATSPERD/CCDC39/CCDC40/DNAH1/DNAH11/DNAH5/DNAI1/LRRC6/PIH1D3/TEKT1/TEKT2	12
GO:0003351	epithelial cilium movement	8/629	18/12310	1.23E-06	0.000191952	0.000182861	CCDC103/CCDC39/CCDC40/CFAP53/LRRC6/RFX3/SPAG17/STK36	8
GO:0035735	intraciliary transport involved in cilium assembly	11/629	40/12310	3.38E-06	0.000504808	0.000480898	DYNC2H1/IFT122/IFT140/IFT172/IFT80/IFT88/KIF17/TTC21B/TTC30B/WDR19/WDR35	11
GO:0042073	intraciliary transport	12/629	50/12310	5.79E-06	0.000831618	0.000792229	DYNC2H1/IFT122/IFT140/IFT172/IFT80/IFT88/KIF17/MAK/TTC21B/TTC30B/WDR19/WDR35	12
GO:0006814	sodium ion transport	21/629	140/12310	8.28E-06	0.001146617	0.001092308	ANK3/ATP2B4/CACNA1H/CAPS2/DMD/FXYD1/HCN4/PRKCE/SCN8A/SCNN1B/SCNN1G/SLC13A3/SLC13A4/SLC22A4/SLC23A1/SLC38A6/SLC41A1/SLC4A8/STOM/UTRN/WNK1	21
GO:0008589	regulation of smoothened signaling pathway	13/629	62/12310	1.17E-05	0.001562699	0.001488683	C2CD3/DCDC2/FUZ/IFT122/IFT140/IFT172/IFT80/ME	13

							GF8/PTCH1/RPGRIP1L/STK36/TTC21B/WNT9A	
GO:0035721	intraciliary retrograde transport	6/629	12/12310	1.23E-05	0.00158831	0.00151308	DYNC2H1/IFT122/IFT140/TTC21B/WDR19/WDR35	6
GO:0015672	monovalent inorganic cation transport	34/629	309/12310	2.00E-05	0.00248988	0.00237194	AKAP6/AKAP9/ANK3/ATP2B4/ATP6V0A4/CACNA1H/CAPS2/CNGA4/DMD/FXYD1/HCN4/KCNB1/KCNE1/KCNH3/KCNJ2/KCNMB2/KCNN3/KCNRG/PRKCE/SCN8A/SCNN1B/SCNN1G/SLC12A7/SLC13A3/SLC13A4/SLC22A4/SLC23A1/SLC2A12/SLC38A6/SLC41A1/SLC4A8/STOM/UTRN/WNK1	34
GO:0042391	regulation of membrane potential	28/629	236/12310	2.78E-05	0.00334912	0.00319049	AKAP6/AKAP9/ANK3/BCO2/CACNA1F/CACNA1H/CFTR/CNGA4/DMD/FGF14/FXYD1/GRIN3B/GRM5/HCN4/KCNB1/KCNE1/KCNH3/KCNJ2/KCNMB2/KMT2A/NRCAM/PIEZO2/PPP1R9A/PYCR1/SCN8A/SHANK2/SLC26A1/STOX1	28
GO:0043269	regulation of ion transport	37/629	358/12310	3.48E-05	0.00390811	0.00372300	AKAP6/AKAP9/ANK3/ATP2B4/ATP8A1/CACNA1F/CACNA1H/CFTR/CLCNKA/CLCNKB/CXCL10/CXCL11/CXCL9/DMD/FGF14/FXYD1/GRIN3B/GRM5/GRM7/HCN4/KCNB1/KCNE1/KCNH3/KCNJ2/KCNRG/LPAR3/MAOB/MYLK/PRKCE/RAB3B/SCN8A/SHANK2/STOM/STXBP1/THADA/UTRN/WNK1	37
GO:0035725	sodium ion transmembrane transport	15/629	88/12310	3.52E-05	0.00390811	0.00372300	ANK3/ATP2B4/CACNA1H/CAPS2/DMD/FXYD1/HCN4/PRKCE/SCN8A/SCNN1B/SCNN1G/SLC23A1/SLC41A1/STOM/UTRN	15
GO:0034765	regulation of ion transmembrane transport	29/629	252/12310	3.56E-05	0.00390811	0.00372300	AKAP6/AKAP9/ANK3/ATP2B4/CACNA1F/CACNA1H/CFTR/CLCNKA/CLCNKB/CXCL10/CXCL11/CXCL9/	29

							DMD/FGF14/FXYD1/GRM5/HCN4/KCNB1/KCNE1/KCNH3/KCNJ2/KCNRG/PRKCE/SCN8A/SHANK2/STOM/THADA/UTRN/WNK1	
GO:0050877	nervous system process	46/629	487/12310	3.98E-05	0.00424898	0.00404773	ABCC6/ADCY5/ANK3/ATP6V0A4/ATP8A1/BBS9/BTBD9/CACNA1F/CACNA1H/CHL1/CNGA4/CNTN5/DCDC2/EGFR/EYA4/FAM161A/FSCN2/GRM5/GRM7/HERC1/INSR/JAM3/KALRN/KCNE1/KCNMB2/KMT2A/LEF1/LRIG1/NAV2/NFASC/NRCAM/NRXN3/NTRK2/PDE6B/PIEZO2/RP1/SCN8A/SCNN1B/SCNN1G/SHANK2/SLC1A4/STRA6/SYNGAP1/TMPRSS3/TUB/WDR19	46
GO:0003002	regionalization	24/629	200/12310	8.56E-05	0.00873828	0.008324398	AR/CDON/CELSR1/CXXC4/DLL1/DSCAML1/FOXJ1/FUZ/HIPK1/IFT122/IFT140/IFT172/IRX3/KMT2A/LEF1/LRP4/MEGF8/PCSK5/PTCH1/RPGRIP1L/SEMA3C/TTC21B/WDR19/WLS	24
GO:1905515	non-motile cilium assembly	10/629	46/12310	8.65E-05	0.00873828	0.008324398	C2CD3/CC2D2A/CCDC13/FUZ/IFT122/IFT140/IFT172/IFT80/RP1/RPGRIP1L	10
GO:0001508	action potential	13/629	75/12310	9.68E-05	0.00951924 6	0.00906837 4	AKAP6/AKAP9/ANK3/CACNA1F/CACNA1H/DMD/HCN4/KCNB1/KCNE1/KCNJ2/KCNMB2/NRCAM/SCN8A	13

Supplement Table 2B: GO Cellular Components for the Downregulated DEGs in the EC vs NS Comparison

ID	Description	GeneRatio	BgRatio	pvalue	p.adjust	qvalue	geneID	Count
GO:0005929	cilium	103/665	426/12866	4.91E-42	2.22E-39	1.96E-39	ADCY5/AGBL2/AGBL4/AK8/ALMS1/ARMC4/ATP2B4/BBS9/C2CD3/CACNA1F/CATSPERD/CATSPERG/CC2D2A/CCDC103/CCDC114/CCDC151/CCDC39/CCDC40/CDC14A/CEP128/CEP170/CEP83/CERKL/CFAP221/CFAP45/CFAP46/CFAP53/CFAP54/CFAP58/CFAP61/CFAP70/CFAP74/CNGA4/CNTRL/CROCC/DCDC2/DNAH1/DNAH10/DNAH11/DNAH12/DNAH2/DNAH3/DNAH5/DNAH6/DNAH7/DNAH9/DNAI1/DNAI2/DNAJB13/DRC7/DYNC2H1/DZIP1L/EFHC1/ENKUR/FAM161A/FAM161B/FBF1/HYDIN/IFT122/IFT140/IFT172/IFT80/IFT88/KIF17/KIF27/LCA5/LRRC6/MAATS1/MAK/MAP1B/MOK/NEK4/PDE6B/PEX6/PIFO/PKD1/PKHD1L1/PROM1/PTCH1/RP1/RPGRIP1L/RSPH1/RSPH4A/SAXO2/SHANK2/SPAG17/STOML3/TCTE1/TCTN2/TEKT1/TEKT2/TMEM67/TSGA10/TTBK2/TTC21B/TTC30B/TTLL9/TUB/UBXN10/WDR19/WDR35/WDR66/WDR78	103

GO:0044441	ciliary part	80/665	334/12866	2.78E-32	6.29E-30	5.55E-30	AGBL2/AGBL4/AK8/ARMC4/ATP2B4/BBS9/C2CD3/CACNA1F/CATSPERD/CATSPERG/CC2D2A/CCDC103/CCDC114/CCDC151/CCDC39/CCDC40/CEP128/CEP170/CEP83/CERKL/CFAP221/CFAP46/CFAP54/CFAP61/CFAP74/CNGA4/CNTRL/CROCC/DCDC2/DNAH1/DNAH11/DNAH2/DNAH3/DNAH5/DNAH6/DNAH7/DNAH9/DNAI1/DNAI2/DNAJB13/DYNC2H1/DZIP1L/EFHC1/ENKUR/FAM161A/FBF1/HYDIN/IFT122/IFT140/IFT172/IFT80/IFT88/KIF17/MAATS1/MAK/MAP1B/MOK/NEK4/PDE6B/PEX6/PIFO/PKD1/PROM1/PTCH1/RP1/RPGRIP1L/RSPH1/RSPH4A/SAXO2/SHANK2/SPAG17/TCTN2/TMEM67/TTBK2/TTC21B/TTC30B/WDR19/WDR35/WDR66/WDR78	80
GO:0097014	ciliary plasm	40/665	97/12866	1.99E-26	3.00E-24	2.65E-24	AK8/ARMC4/CCDC103/CCDC114/CCDC151/CCDC39/CCDC40/CFAP221/CFAP46/CFAP54/CFAP61/CFAP74/DCDC2/DNAH1/DNAH11/DNAH2/DNAH3/DNAH5/DNAH6/DNAH7/DNAH9/DNAI1/DNAI2/DNAJB13/DYNC2H1/EFHC1/HYDIN/IFT140/IFT172/KIF17/MAATS1/NEK4/RP1/RPGRIP1L/RSPH4A/SAXO2/SPAG17/WDR35/WDR66/WDR78	40
GO:0005930	axoneme	39/665	96/12866	1.67E-25	1.90E-23	1.67E-23	AK8/ARMC4/CCDC103/CCDC114/CCDC151/CCDC39/CCDC40/CFAP221/CFAP46/CFAP54/CFAP61/CFAP74/DCDC2/DNAH1/DNAH11/DNAH2/DNAH3/DNAH5/DNAH6/DNAH7/DNAH9/DNAI1/DNAI2/DN	39

							AJB13/DYNC2H1/EFHC1/HYDIN/IFT140/IFT172/KIF17/MAATS1/RP1/RPGRIP1L/RSPH4A/SAXO2/SPAG17/WDR35/WDR66/WDR78	
GO:0032838	plasma membrane bounded cell projection cytoplasm	42/665	156/12866	2.11E-19	1.91E-17	1.69E-17	AK8/AP3M2/ARMC4/CCDC103/CCDC114/CCDC151/CCDC39/CCDC40/CFAP221/CFAP46/CFAP54/CFAP61/CFAP74/DCDC2/DNAH1/DNAH11/DNAH2/DNAH3/DNAH5/DNAH6/DNAH7/DNAH9/DNAI1/DNAI2/DNAJB13/DYNC2H1/EFHC1/HYDIN/IFT140/IFT172/KIF17/MAATS1/NEK4/RP1/RPGRIP1L/RSPH4A/SAXO2/SPAG17/WDR35/WDR66/WDR78/WLS	42
GO:0044447	axoneme part	18/665	28/12866	4.48E-17	3.38E-15	2.98E-15	CCDC114/CFAP61/DNAH1/DNAH2/DNAH3/DNAH5/DNAH6/DNAH7/DNAI1/DNAI2/HYDIN/MAATS1/RPGRIP1L/RSPH4A/SAXO2/SPAG17/WDR66/WDR78	18
GO:0031514	motile cilium	30/665	106/12866	7.37E-15	4.77E-13	4.21E-13	AK8/ALMS1/ATP2B4/CATSPERD/CATSPERG/CCDC103/CFAP61/DNAH1/DNAH11/DNAH2/DNAH9/DNAI2/DNAJB13/DRC7/DYNC2H1/ENKUR/IFT172/IFT88/MAATS1/PKD1/RSPH1/RSPH4A/SAXO2/SPAG17/TCTE1/TEKT1/TEKT2/TSGA10/WDR19/WDR66	30
GO:0099568	cytoplasmic region	53/665	393/12866	1.12E-10	6.34E-09	5.60E-09	AK8/AP3M2/ARMC4/ASTN2/CAP2/CCDC103/CCDC114/CCDC151/CCDC39/CCDC40/CFAP221/CFAP46/CFAP54/CFAP61/CFAP74/DCDC2/DCDC2B/DNAH1/DNAH11/DNAH2/DNAH3/DNAH5/DNAH6/DNAH7/DNAH9/DNAI1/DNAI2/DNAJB13/DYNC2H1/EFHC1/FMN2/GRM7/HYDIN/IF	53

							T140/IFT172/KIF17/MAATS1/MICAL3/MOBP/NEK4/PPP1R9A/RP1/RPGRIP1L/RSPH4A/SAXO2/SPAG17/STOX1/USP2/UTRN/WDR35/WDR66/WDR78/WLS	
GO:0005858	axonemal dynein complex	10/665	15/12866	3.02E-10	1.52E-08	1.34E-08	CCDC114/DNAH1/DNAH2/DNAH3/DNAH5/DNAH6/DNAH7/DNAI1/DNAI2/WDR78	10
GO:0030286	dynein complex	16/665	45/12866	3.45E-10	1.56E-08	1.38E-08	CCDC114/DNAH1/DNAH10/DNAH11/DNAH12/DNAH2/DNAH3/DNAH5/DNAH6/DNAH7/DNAH9/DNAI1/DNAI2/DYNC2H1/WDR63/WDR78	16
GO:0005875	microtubule associated complex	25/665	129/12866	8.37E-09	3.45E-07	3.04E-07	CCDC114/DNAH1/DNAH10/DNAH11/DNAH12/DNAH2/DNAH3/DNAH5/DNAH6/DNAH7/DNAH9/DNAI1/DNAI2/DYNC2H1/EML1/KIF17/KIF24/KIF26B/KIF27/KIF6/MAP1A/MAP1B/RP1/WDR63/WDR78	25
GO:0097730	non-motile cilium	17/665	75/12866	1.95E-07	7.34E-06	6.49E-06	CACNA1F/CDC14A/CERKL/DCDC2/FAM161A/IFT122/IFT140/KIF17/MAK/MAP1B/PDE6B/PEX6/PROM1/RP1/RPGRIP1L/SHANK2/WDR19	17
GO:0030990	intraciliary transport particle	11/665	31/12866	2.12E-07	7.40E-06	6.53E-06	IFT122/IFT140/IFT172/IFT80/IFT88/KIF17/TTC21B/TTC30B/UBXN10/WDR19/WDR35	11
GO:0005874	microtubule	42/665	353/12866	3.66E-07	1.18E-05	1.05E-05	BCAS3/CEP170/CSPP1/DCDC2/DCDC2B/DNAH1/DNAH10/DNAH11/DNAH12/DNAH2/DNAH3/DNAH5/DNAH6/DNAH7/DNAH9/DNAI1/DNAI2/DYNC2H1/EML1/EML6/FAM161A/FAM161B/KATNAL2/KIF17/KIF24/KIF26B/KIF27/KIF6/LRRC49/MAP1A/MAP1B/MAP6/RP1/RPGRIP1L/SAXO2/SPAG17/TEKT1/TEKT2/TPPP/TPPP3/TTLL9/TUBGCP6	42

GO:0036126	sperm flagellum	14/65	55/12866	5.13E-07	1.30E-05	1.15E-05	AK8/ATP2B4/CATSPERD/CATSPERG/DNAH1/DNAI2/DNAJB13/ENKUR/IFT172/RSPH1/SAXO2/TCTE1/TEKT1/TEKT2	14
GO:0097729	9+2 motile cilium	14/65	55/12866	5.13E-07	1.30E-05	1.15E-05	AK8/ATP2B4/CATSPERD/CATSPERG/DNAH1/DNAI2/DNAJB13/ENKUR/IFT172/RSPH1/SAXO2/TCTE1/TEKT1/TEKT2	14
GO:0097731	9+0 non-motile cilium	15/65	63/12866	5.16E-07	1.30E-05	1.15E-05	CACNA1F/CERKL/FAM161A/IFT122/IFT140/KIF17/MAK/MAP1B/PDE6B/PEX6/PROM1/RP1/RPGRIP1L/SHANK2/WDR19	15
GO:0097733	photoreceptor cell cilium	15/65	63/12866	5.16E-07	1.30E-05	1.15E-05	CACNA1F/CERKL/FAM161A/IFT122/IFT140/KIF17/MAK/MAP1B/PDE6B/PEX6/PROM1/RP1/RPGRIP1L/SHANK2/WDR19	15
GO:0044450	microtubule organizing center part	24/65	157/12866	1.66E-06	3.96E-05	3.50E-05	AGBL2/AGBL4/ALMS1/BBS9/C2CD3/CCDC113/CCDC13/CCDC146/CCDC151/CCDC78/CEP128/CEP170/CEP83/CROCC/DZIP1L/FBF1/IFT88/KIAA0753/KIF24/NEK1/SAXO2/SFI1/TTBK2/TUBGCP6	24
GO:0099513	polymeric cytoskeletal fiber	50/65	494/12866	3.81E-06	8.42E-05	7.43E-05	BCAS3/CEP170/CSPP1/DCDC2/DCDC2B/DNAH1/DNAH10/DNAH11/DNAH12/DNAH2/DNAH3/DNAH5/DNAH6/DNAH7/DNAH9/DNAI1/DNAI2/DYNC2H1/EML1/EML6/FAM161A/FAM161B/FBF1/FMN1/FSCN2/KATNAL2/KIF17/KIF24/KIF26B/KIF27/KIF6/LMNTD1/LRRC49/MAP1A/MAP1B/MAP6/PRPH/RP1/RPGRIP1L/RSPH1/SAXO2/SHANK2/SLC1A4/SPAG17/TEKT1/TEKT2/TPPP/TPPP3/TTLL9/TUBGCP6	50
GO:0035869	ciliary transition zone	13/65	56/12866	4.02E-06	8.42E-05	7.43E-05	BBS9/CC2D2A/FAM161A/IFT122/IFT140/KIF17/NEK4/RP1/RPGRIP1L/TCTN2/TMEM67/TTBK2/WDR19	13

GO:1902495	transmembrane transporter complex	23/65	154/12866	4.09E-06	8.42E-05	7.43E-05	ABCA2/AKAP6/AKAP9/BEST4/CACNA1F/CACNA1H/CATSPERD/CATSPERG/CFTR/CLCNKA/CLCNKB/FXYD1/GRIN3B/HCN4/KCNB1/KCNE1/KCNJ2/KCNMB2/RYR3/SCN8A/SCNN1B/SCNN1G/SHANK2	23
GO:0005814	centriole	19/65	117/12866	8.14E-06	0.000154172	0.000136134	AGBL2/AGBL4/ALMS1/C2CD3/CCDC146/CCDC151/CCDC78/CEP128/CEP170/CEP83/CROCC/DZIP1L/FBF1/IFT88/KIAA0753/KIF24/SAXO2/SFI1/TTBK2	19
GO:0097542	ciliary tip	11/65	43/12866	8.17E-06	0.000154172	0.000136134	DYNC2H1/IFT122/IFT140/IFT172/IFT80/IFT88/RP1/TTC21B/TTC30B/WDR19/WDR35	11
GO:1990351	transporter complex	23/65	162/12866	9.70E-06	0.000175771	0.000155206	ABCA2/AKAP6/AKAP9/BEST4/CACNA1F/CACNA1H/CATSPERD/CATSPERG/CFTR/CLCNKA/CLCNKB/FXYD1/GRIN3B/HCN4/KCNB1/KCNE1/KCNJ2/KCNMB2/RYR3/SCN8A/SCNN1B/SCNN1G/SHANK2	23
GO:0034702	ion channel complex	21/65	141/12866	1.11E-05	0.000193802	0.000171128	AKAP6/AKAP9/BEST4/CACNA1F/CACNA1H/CATSPERD/CATSPERG/CFTR/CLCNKA/CLCNKB/GRIN3B/HCN4/KCNB1/KCNE1/KCNJ2/KCNMB2/RYR3/SCN8A/SCNN1B/SCNN1G/SHANK2	21
GO:0036064	ciliary basal body	17/65	100/12866	1.30E-05	0.000212167	0.000187344	AGBL2/AGBL4/C2CD3/CCDC151/DZIP1L/FAM161A/IFT122/IFT140/IFT172/IFT88/KIF17/NEK4/PIFO/RPGRIP1L/SAXO2/TTBK2/WDR35	17
GO:0001750	photoreceptor outer segment	11/65	45/12866	1.31E-05	0.000212167	0.000187344	CACNA1F/CERKL/IFT140/MAK/MAP1B/PDE6B/PEX6/PROM1/RP1/SHANK2/WDR19	11
GO:0034703	cation channel complex	16/65	100/12866	5.03E-05	0.000785012	0.000693168	AKAP6/AKAP9/CACNA1F/CACNA1H/CATSPERD/CATSPERG/GRIN3B/HCN4/KCNB1/KCNE1/KCNJ2/KCNM	16

							B2/RYR3/SCN8A/SCNN1B/SCN N1G	
GO:0097223	sperm part	17/665	114/12866	7.40E-05	0.001116 83		.000986164 4/CATSPERD/CATSPE DNAI2/DNAJB13/ENKU GUK/PCSK4/RSPH1/S 8/TCTE1/TEKT1/TEKT 2	17
GO:0030992	intraciliary transport particle B	6/665	20/12866	0.000038 7177	0.005657 778	0.00499583	IFT172/IFT80/IFT88/KIF17/TTC30B/UBXN10	6
GO:0032391	photoreceptor connecting cilium	7/665	29/12866	0.000054 9097	0.007773 161	0.006863718	FAM161A/IFT122/IFT140/KIF17/RP1/RPGRIP1L/WDR19	7

Supplement Table 2C: GO Molecular Functions for the Downregulated DEGs in the EC vs NS Comparison

ID	Description	GeneRatio	BgRatio	pvalue	p.adjust	qvalue	geneID	Count
GO:0045503	dynein light chain binding	14/629	22/12391	1.44E-13	9.20E-11	8.46E-11	DNAH1/DNAH10/DNAH11/DNAH2/DNAH3/DNAH5/DNAH6/DNAH7/DNAH9/DNAI1/DNAI2/DYNC2H1/WDR63/WDR78	14
GO:1990939	ATP-dependent microtubule motor activity	16/629	41/12391	5.07E-11	1.62E-08	1.49E-08	DNAH1/DNAH10/DNAH11/DNAH2/DNAH3/DNAH5/DNAH6/DNAH7/DNAH9/DNAI1/DNAI2/DYNC2H1/KIF17/KIF27/WDR63/WDR78	16
GO:0008569	ATP-dependent microtubule motor activity, minus-end-directed	10/629	15/12391	2.53E-10	5.39E-08	4.95E-08	DNAH1/DNAH10/DNAH11/DNAH2/DNAH3/DNAH5/DNAH6/DNAH7/DNAH9/DYNC2H1	10
GO:0003777	microtubule motor activity	20/629	92/12391	2.56E-08	4.09E-06	3.76E-06	DNAH1/DNAH10/DNAH11/DNAH12/DNAH2/DNAH3/DNAH5/DNAH6/DNAH7/DNAH9/DNAI1/DNAI2/DYNC2H1/KIF17/KIF24/KIF26B/KIF27/KIF6/WDR63/WDR78	20
GO:0051959	dynein light intermediate chain binding	11/629	27/12391	3.27E-08	4.19E-06	3.85E-06	CCDC88C/DNAH1/DNAH10/DNAH11/DNAH2/DNAH3/DNAH5/DNAH6/DNAH7/DNAH9/DYNC2H1	11
GO:0005509	calcium ion binding	54/629	488/12391	4.76E-08	5.07E-06	4.67E-06	ADAMTS13/ASTN2/CAPS/CAPS2/CDH22/CDHR3/CDHR4/CELSR1/CLGN/DLL1/DNAH7/DNER/DUOX1/EFCAB2/EFCAB6/EFHB/EFHC1/EFHC2/EML1/HEG1/HSPG2/LRP4/LTBP2/MEGF8/N	54

							CALD/NELL2/PCDH17/ PCDHA10/PCDHA11/PCDHA12/PCDHA13/PCDHA4/PCDHA5/PCDHA6/ PCDHA7/PCDHA8/PCDHA9/PCDHAC1/PCDHAC2/PCDHB1/PLCB4/PLCH1/PROS1/RYR3/SLIT1/SLIT2/SNED1/SULF1/SVEP1/SYTL3/TENM2/ UMODL1/VCAN/VWA2	
GO:0045505	dynein intermediate chain binding	10/629	25/12391	1.73E-07	1.58E-05	1.45E-05	DNAH1/DNAH10/DNAH11/DNAH2/DNAH3/DNAH5/DNAH6/ DNAH7/DNAH9/DYNC2H1	10
GO:0003774	motor activity	20/629	104/12391	2.20E-07	1.76E-05	1.62E-05	DNAH1/DNAH10/DNAH11/DNAH12/DNAH2/ DNAH3/DNAH5/DNAH6/ DNAH7/DNAH9/DNAI1/DNAI2/DYNC2H1/KIF17/KIF24/KIF26B/KIF27/ KIF6/WDR63/WDR78	20
GO:0022838	substrate-specific channel activity	28/629	215/12391	4.20E-06	0.000298943	0.000274851	AQP7/BEST4/BSND/CACNA1F/CACNA1H/CFTR/CLCNKA/CLCNKB/CNGA4/FXYD1/ GRIN3B/HCN4/ KCNB1/KCNE1/ KCNH3/KCNJ2/ KCNMB2/KCNN3/NCALD/PIEZO2/PKD1/RASA3/RYR3/ SCN8A/SCNN1B/SCNN1G/SLC1A4/SLC26A1	28
GO:0005216	ion channel activity	27/629	206/12391	5.52E-06	0.000353092	0.000324635	BEST4/BSND/CACNA1F/CACNA1H/CFTR/CLCNKA/CLCNKB/ CNGA4 /FXYD1/GRIN3B/HCN4/KCNB1/KCNE1/KCNH3/KCNJ2/KCNMB2/KCNN3/NCALD/PIEZO2/PKD1/RASA3/RYR3/SCN8	27

							A/SCNN1B/SCN N1G/SL C1A4/SLC26A1	
GO:0 0168 87	ATPase activity	39/629	374/1 2391	1.51E- 05	0.00087 7917	0.0008 07163	ABCA13/ABCA 2/ABCA5/ABCC 6/ABCD2/ATP2 B4/ATP2C2/ATP 6V0A4/ ATP8A1/ATP8B 4/CFTR/CHD6/D HX35/DNAH1/D NAH10/DNAH1 1/DNA H12/DNAH2/DN AH3/DNAH5/D NAH6/DNAH7/ DNAH9/DNAI1/ DNAI2/ DYNC2H1/EIF4 A2/KATNAL2/K IF17/KIF24/KIF2 6B/KIF27/KIF6/ MDN1/ PEX6/RAD51B/ RNF213/WDR63 /WDR78	39
GO:0 0228 36	gated channel activity	22/629	160/1 2391	1.89E- 05	0.00090 1598	0.0008 28936	BSND/CACNA1 F/CACNA1H/CF TR/CLCNKA/C LCNKB/CNGA4 /GRIN3 B/HCN4/KCNB1 /KCNE1/KCNH3 /KCNJ2/KCNM B2/KCNN3/NC ALD/PIE ZO2/RASA3/RY R3/SCN8A/SCN N1B/SCNN1G	22
GO:0 0152 67	channel activity	28/629	233/1 2391	1.95E- 05	0.00090 1598	0.0008 28936	AQP7/BEST4/B SND/CACNA1F /CACNA1H/CFT R/CLCNKA/CL CNKB/C NGA4/FXYD1/ GRIN3B/HCN4/ KCNB1/KCNE1/ KCNH3/KCNJ2/ KCNMB 2/KCNN3/NCAL D/PIEZO2/PKD1 /RASA3/RYR3/ SCN8A/SCNN1 B/SCNN 1G/SLC1A4/SL C26A1	28
GO:0 0468 73	metal ion transmem brane transporter activity	29/629	246/1 2391	2.01E- 05	0.00090 1598	0.0008 28936	ATP2B4/ATP2C 2/CACNA1F/CA CNA1H/CAPS2/ CLDN16/CNGA 4/GRIN 3B/HCN4/KCN B1/KCNE1/KCN H3/KCNJ2/KCN MB2/KCNN3/P KD1/RAS	29

							A3/RYR3/SCN8A/SCNN1B/SCNN1G/SLC12A7/SLC13A3/SLC13A4/SLC23A1/SLC41A1/SLC4A8/SLC6A16/SLC6A20	
GO:0022803	passive transmembrane transporter activity	28/629	234/12391	2.11E-05	0.000901598	0.000828936	AQP7/BEST4/BSND/CACNA1F/CACNA1H/CFTR/CLCNKA/CLCNKB/CNGA4/FXYD1/GRIN3B/HCN4/KCNB1/KCNE1/KCNH3/KCNJ2/KCNMB2/KCNN3/NCALD/PIEZO2/PKD1/RASA3/RYR3/SCN8A/SCNN1B/SCNN1G/SLC1A4/SLC26A1	28
GO:0022839	ion gated channel activity	21/629	157/12391	4.43E-05	0.001770598	0.001627902	BSND/CACNA1F/CACNA1H/CFTR/CLCNKA/CLCNKB/CNGA4/GRIN3B/HCN4/KCNB1/KCNE1/KCNH3/KCNJ2/KCNMB2/KCNN3/NCALD/RASA3/RYR3/SCN8A/SCNN1B/SCNN1G	21
GO:0042623	ATPase activity, coupled	33/629	313/12391	5.48E-05	0.002063571	0.001897264	ABCA13/ABCA2/ABCA5/ABCC6/ABCD2/ATP2B4/ATP2C2/ATP6V0A4/ATP8A1/ATP8B4/CFTR/CHD6/DHX35/DNAH1/DNAH10/DNAH11/DNAH2/DNAH3/DNAH5/DNAH6/DNAH7/DNAH9/DNAI1/DNAI2/DYNC2H1/EIF4A2/KATNAL2/KIF17/KIF27/PEX6/RAD51B/WDR63/WDR78	33
	sodium ion ane ctivity	13/629	81/12391	0.000203189	0.0072245	0.006642263	CACNA1H/CAPS2/HCN4/SCN8A/SCNN1B/SCNN1G/SLC13A3/SLC13A4/SLC23A1/SLC41A1/SLC4A8/SLC6A16/SLC6A20	13

GO:0015077	monovalent inorganic cation transmembrane transporter activity	24/629	216/12391	0.000255346	0.008601127	0.007907944	ATP2C2/ATP6V0A4/CACNA1H/CAPS2/CNGA4/HCN4/KCNB1/KCNE1/KCNH3/KCNJ2/KCNMB2/KCNN3/SCN8A/SCNN1B/SCNN1G/SLC12A7/SLC13A3/SLC13A4/SLC23A1/SLC2A12/SLC41A1/SLC4A8/SLC6A16/SLC6A20	24
GO:0008324	cation transmembrane transporter activity	36/629	384/12391	0.000279182	0.00893384	0.008213843	ATP2B4/ATP2C2/ATP6V0A4/ATP8A1/CACNA1F/CACNA1H/CAPS2/CLDN16/CNGA4/GRIN3B/HCN4/KCNB1/KCNE1/KCNH3/KCNJ2/KCNMB2/KCNN3/PIEZO2/PKD1/RASA3/RYR3/SCN8A/SCNN1B/SCNN1G/SLC12A7/SLC13A3/SLC13A4/SLC1A4/SLC22A4/SLC23A1/SLC2A12/SLC41A1/SLC4A8/SLC6A16/SLC6A20/SLC7A2	36
GO:0005261	cation channel activity	18/629	142/12391	0.0003018	0.009197706	0.008456444	CACNA1F/CACNA1H/CNGA4/GRIN3B/HCN4/KCNB1/KCNE1/KCNH3/KCNJ2/KCNMB2/KCNN3/PIEZO2/PKD1/RASA3/RYR3/SCN8A/SCNN1B/SCNN1G	18
GO:0022890	inorganic cation transmembrane transporter activity	33/629	344/12391	0.000328382	0.009552929	0.008783038	ATP2B4/ATP2C2/ATP6V0A4/ATP8A1/CACNA1F/CACNA1H/CAPS2/CLDN16/CNGA4/GRIN3B/HCN4/KCNB1/KCNE1/KCNH3/KCNJ2/KCNMB2/KCNN3/PIEZO2/PKD1/RASA3/RYR3/SCN8A/SCNN1B/SCNN1G/SLC12A7/SLC13A3/SLC13A4/SLC23A1/SLC2A12/S	33

							LC41A1/SLC4A 8/SLC6 A16/SLC6A20	

Supplement Table 2D: GO Biological Processes for the Upregulated DEGs in the EC vs NS Comparison

ID	Description	GeneRatio	BgRatio	pvalue	p.adjust	qvalue	geneID	Count
GO:0031424	keratinization	27/484	71/12310	3.27E-20	1.27E-16	1.13E-16	ABCA12/CDSN/CNFN/CSTA/DSC2/DSG3/IVL/KRT10/KRT13/KRT14/KRT16/KRT23/KRT4/KRT6A/KRT6B/KRT6C/KRT7/KRT78/PI3/PRSS8/SFN/SPRR1A/SPRR1B/SPRR2A/SPRR2B/SPRR3/TMEM79	27
GO:0043588	skin development	43/484	222/12310	1.55E-18	2.99E-15	2.68E-15	ABCA12/AKR1C3/CD109/CDSN/CERS3/CNFN/COL1A1/COL1A2/CSTA/DKK1/DSC2/DSG3/EREG/FOXQ1/GJB3/GRHL3/HPSE/IVL/KRT10/KRT13/KRT14/KRT16/KRT23/KRT4/KRT6A/KRT6B/KRT6C/KRT7/KRT78/LTB/OVOL1/PI3/PRSS8/RYR1/SFN/SLC27A4/SPRR1A/SPRR1B/SPRR2A/SPRR2B/SPRR3/TMEM79/TRIM16	43
GO:0070268	cornification	24/484	63/12310	4.01E-18	5.16E-15	4.62E-15	CDSN/CSTA/DSC2/DSG3/IVL/KRT10/KRT13/KRT14/KRT16/KRT23/KRT4/KRT6A/KRT6B/KRT6C/KRT7/KRT78/PI3/PRSS8/SPRR1A/SPRR1B/SPRR2A/SPRR2B/SPRR3/TMEM79	24
GO:0042119	neutrophil activation	60/484	449/12310	3.71E-17	3.58E-14	3.21E-14	ADAM8/ADGRG3/ALOX5/ARPC5/BIN2/C5AR1/CALML5/CD14/CD177/CD36/CD58/CD68/CEACAM3/CXCL8/FABP5/FCAR/FCGR2A/FCGR2B/FCGR3B/GCA/GGH/GMFG/GRN/HBB/HEBP2/HPSE/HSPA6/IL18RAP/IMPDH1/ITGAX/ITGB2/LCN2/MGST1/MMP25/MMP9/MNDA/PECAM1/PLAU/PLAUR/PLEKHO2/PRSS3/PTAFR/PYGB/RHOG/RNASET2/S100A8/S100A9/S100P/SELL/SERPINA1/SERPINA3/SIRPA/SIRPB1/SLC2A3/SYK/TCN1/TNFAIP6/TYROBP/UNC13D/VNN1	60

GO:0036230	granulocyte activation	60/484	455/12310	7.03E-17	5.20E-14	4.65E-14	ADAM8/ADGRG3/ALOX5/ARPC5/BIN2/C5AR1/CALML5/CD14/CD177/CD36/CD58/CD68/CEACAM3/CXCL8/FABP5/FCAR/FCGR2A/FCGR2B/FCGR3B/GCA/GGH/GMFG/GRN/HBB/HEBP2/HPSE/HSPA6/IL18RAP/IMPDH1/ITGAX/ITGB2/LCN2/MGST1/MMP25/MMP9/MNDA/PECAM1/PLAU/PLAUR/PLEKHO2/PRSS3/PTAFR/PYGB/RHOG/RNASET2/S100A8/S100A9/S100P/SELL/SERPINA1/SERPINA3/SIRPA/SIRPB1/SLC2A3/SYK/TCN1/TNFAIP6/TYROBP/UNC13D/VNN1	60
GO:0002444	myeloid leukocyte mediated immunity	62/484	485/12310	9.38E-17	5.20E-14	4.65E-14	ADAM8/ADGRG3/ALOX5/ARPC5/BIN2/C5AR1/CALML5/CD14/CD177/CD36/CD58/CD68/CEACAM3/FABP5/FCAR/FCGR2A/FCGR2B/FCGR3B/GCA/GGH/GMFG/GRN/HBB/HEBP2/HMOX1/HPSE/HSPA6/IMPDH1/ITGAX/ITGB2/LCN2/MGST1/MILR1/MMP25/MMP9/MNDA/PECAM1/PLAU/PLAUR/PLEKHO2/PRSS3/PTAFR/PYGB/RAC2/RHOG/RNASET2/S100A8/S100A9/S100P/SELL/SERPINA1/SERPINA3/SIRPA/SIRPB1/SLC2A3/SPON2/SYK/TCN1/TNFAIP6/TYROBP/UNC13D/VNN1	62
GO:0030216	keratinocyte differentiation	32/484	135/12310	9.41E-17	5.20E-14	4.65E-14	ABCA12/AKR1C3/CD109/CDSN/CERS3/CNFN/CSTA/DSC2/DSG3/EREG/IVL/KRT10/KRT13/KRT14/KRT16/KRT23/KRT4/KRT6A/KRT6B/KRT6C/KRT7/KRT78/PI3/PRSS8/SFN/SPRR1A/SPRR1B/SPRR2A/SPRR2B/SPRR3/TMEM79/TRIM16	32

GO:0043299	leukocyte degranulation	61/484	475/12310	1.37E-16	6.61E-14	5.92E-14	ADAM8/ADGRG3/ALOX5/ARPC5/BIN2/C5AR1/CALML5/CD14/CD177/CD36/CD58/CD68/CEACAM3/FABP5/FCAR/FCGR2A/FCGR2B/FCGR3B/GCA/GGH/GMFG/GRN/HBB/HEBP2/HMOX1/HPSE/HSPA6/IMPDH1/ITGAX/ITGB2/LCN2/MGST1/MILR1/MMP25/MMP9/MNDA/PECAM1/PLAU/PLAUR/PLEKHO2/PRSS3/PTAFR/PYGB/RAC2/RHOG/RNASET2/S100A8/S100A9/S100P/SELL/SERPINA1/SERPINA3/SIRPA/SIRPB1/SLC2A3/SYK/TCN1/TNFAIP6/TYROBP/UNC13D/VNN1	61
GO:0002275	myeloid cell activation involved in immune response	60/484	481/12310	9.83E-16	3.55E-13	3.18E-13	ADAM8/ADGRG3/ALOX5/ARPC5/BIN2/C5AR1/CALML5/CD14/CD177/CD36/CD58/CD68/CEACAM3/FABP5/FCAR/FCGR2A/FCGR3B/GCA/GGH/GMFG/GRN/HBB/HEBP2/HMOX1/HPSE/HSPA6/IMPDH1/ITGAX/ITGB2/LCN2/MGST1/MILR1/MMP25/MMP9/MNDA/PECAM1/PLAU/PLAUR/PLEKHO2/PRSS3/PTAFR/PYGB/RAC2/RHOG/RNASET2/S100A8/S100A9/S100P/SELL/SERPINA1/SERPINA3/SIRPA/SIRPB1/SLC2A3/SYK/TCN1/TNFAIP6/TYROBP/UNC13D/VNN1	60
GO:0002283	neutrophil activation involved in immune response	57/484	440/12310	1.01E-15	3.55E-13	3.18E-13	ADAM8/ADGRG3/ALOX5/ARPC5/BIN2/C5AR1/CALML5/CD14/CD177/CD36/CD58/CD68/CEACAM3/FABP5/FCAR/FCGR2A/FCGR3B/GCA/GGH/GMFG/GRN/HBB/HEBP2/HPSE/HSPA6/IMPDH1/ITGAX/ITGB2/LCN2/MGST1/MMP25/MMP9/MNDA/PECAM1/PLAU/PLAUR/PLEKHO2/PRSS3/PTAFR/PYGB/RHOG/RNASET2/S100A8/S100A9/S100P/SELL/SERPINA1/SERPINA3/SIRPA/SIRPB1/SLC2A3/SYK/TCN1/TNFAIP6/TYROBP/UNC13D/VNN1	57

GO:0008544	epidermis development	42/84	257/12310	2.35E-15	7.48E-13	6.69E-13	ABCA12/AKR1C3/CALML5/CD109/CDSN/CERS3/CNFN/CSTA/DKK1/DSC2/DSG3/EMP1/EREG/FABP5/FOXQ1/GRHL3/HPSE/IVL/KLK7/KRT10/KRT13/KRT14/KRT16/KRT23/KRT4/KRT6A/KRT6B/KRT6C/KRT7/KRT78/OVOL1/PI3/PRSS8/SFN/SPRR1A/SPRR1B/SPRR2A/SPRR2B/SPRR3/TMEM79/TRIM16/WAS	42
GO:0002446	neutrophil mediated immunity	57/84	449/12310	2.51E-15	7.48E-13	6.69E-13	ADAM8/ADGRG3/ALOX5/ARPC5/BIN2/C5AR1/CALML5/CD14/CD177/CD36/CD58/CD68/CEACAM3/FABP5/FCAR/FCGR2A/FCGR3B/GCA/GGH/GMFG/GRN/HBB/HEBP2/HPSE/HSPA6/IMPDH1/ITGAX/ITGB2/LCN2/MGST1/MMP25/MMP9/MNDA/PECAM1/PLAU/PLAUR/PLEKHO2/PRSS3/PTAFR/PYGB/RHOG/RNASET2/S100A8/S100A9/S100P/SELL/SERPINA1/SERPINA3/SIRPA/SIRPB1/SLC2A3/SYK/TCN1/TNFAIP6/TYROBP/UNC13D/VNN1	57
GO:0009913	epidermal cell differentiation	32/84	172/12310	1.42E-13	3.92E-11	3.51E-11	ABCA12/AKR1C3/CD109/CDSN/CERS3/CNFN/CSTA/DSC2/DSG3/EREG/IVL/KRT10/KRT13/KRT14/KRT16/KRT23/KRT4/KRT6A/KRT6B/KRT6C/KRT7/KRT78/PI3/PRSS8/SFN/SPRR1A/SPRR1B/SPRR2A/SPRR2B/SPRR3/TMEM79/TRIM16	32

GO:0006954	inflammatory response	54/484	493/12310	6.07E-12	1.57E-09	1.40E-09	ACP5/ADAM8/ADORA2A/AIF1/ALOX5/APOE/C5AR1/CCRL2/CD14/CHST2/CLEC7A/CXCL13/CXCL8/CXCR4/FCGR2B/GGT1/HMOX1/IL18RAP/IL1R2/IL1RN/IL20RB/IL36G/ITGB2/KRT16/LY96/METRNL/MMP25/MYD88/NLRC4/PPARG/PTAFR/PTGES/RELB/RPS6KA4/S100A8/S100A9/SDC1/SELP/SEMA7A/SERPINA1/SERPINA3/SPHK1/SYK/THEMIS2/TMSB4X/TNFAIP6/TNFRSF10C/TNFRSF18/TNFRSF6B/TNIP3/TYRO3/UNC13D/VNN1/ZYX	54
GO:0050900	leukocyte migration	38/484	309/12310	3.70E-10	8.94E-08	8.00E-08	ADAM8/AIF1/ATP1B3/C5AR1/CD177/CD58/CEACAM3/CEACAM5/COL1A1/COL1A2/CXCL13/CXCL14/CXCL8/CXCR4/DAPK2/FUT7/HMOX1/ITGA5/ITGAX/ITGB2/MMP28/MMP9/MPP1/PDE4B/PECAM1/PTAFR/RAC2/S100A14/S100A8/S100A9/SDC1/SELL/SELP/SIRPA/SLC7A11/SYK/TNFRSF18/TREM1	38
GO:0050878	regulation of body fluid levels	39/484	347/12310	3.00E-09	6.83E-07	6.11E-07	ABCA12/ADM/ADORA2A/AK3/APOE/AQP2/ARRB2/CD177/CD36/COL1A1/COL1A2/DGKA/EHD1/GRHL3/GUCA1B/HBB/HPSE/HSD11B2/KCNN4/KRT16/PLAT/PLAU/PLAUR/PLEK/RAC2/RHOG/S100A9/SELP/SERPINA1/SERPINB2/SERPINE2/SFN/SH2B2/SLC7A11/STATH/SYK/TMEM79/TYRO3/WAS	39
GO:0042060	wound healing	41/484	387/12310	6.67E-09	1.43E-06	1.28E-06	ADORA2A/AK3/APOE/ARRB2/CD109/CD177/CD36/COL1A1/COL1A2/DGKA/DYSF/EHD1/EREG/GRHL3/HBB/HMOX1/HPSE/IFRD1/ITGA5/PHLDB2/PLAT/PLAU/PLAUR/PLEK/RAC2/RHOG/S100A8/S100A9/SDC1/SELP/SERPINA1/SERPINB2/SERPINE2/SH2B2/SLC7A11/SOX15/SPRR3/SYK/TNFRSF12A/TYRO3/WAS	41

GO:0009611	response to wounding	46/484	471/12310	1.02E-08	2.08E-06	1.86E-06	ADM/ADORA2A/AIF1/AK3/APOE/ARRB2/CD109/CD177/CD36/COL1A1/COL1A2/DGKA/DYSF/EHD1/EREG/FKBP1B/GRHL3/HBB/HMOX1/HPSE/IFRD1/ITGA5/PHLDB2/PLAT/PLAU/PLAUR/PLEK/RAC2/RHOG/S100A8/S100A9/SCARF1/SDC1/SELP/SERPINA1/SERPINB2/SERPINE2/SH2B2/SLC7A11/SOX15/SPRR3/SYK/TNFRSF12A/TSPO/TYRO3/WAS	46
GO:0006909	phagocytosis	26/484	200/12310	7.76E-08	1.50E-05	1.34E-05	ADORA2A/AIF1/ARPC5/BIN2/CD14/CD36/CLEC7A/FCGR2A/FCGR2B/FCGR3A/ICAM3/ITGB2/NCF2/NCF4/PECAM1/PPARG/RAC2/RAC3/RHOG/SIRPA/SIRPB1/SPON2/SYK/TYRO3/UNC13D/WAS	26
GO:1903034	regulation of response to wounding	18/484	105/12310	1.24E-07	2.28E-05	2.04E-05	APOE/CD109/CD36/FKBP1B/HPSE/PHLDB2/PLAT/PLAU/PLAUR/PLEK/S100A9/SCARF1/SELP/SERPINB2/SERPINE2/SOX15/SYK/TNFRSF12 A	18
GO:0009617	response to bacterium	37/484	369/12310	1.56E-07	2.74E-05	2.45E-05	ACP5/ADM/BPIFA2/C5AR1/CD14/CD36/CXCL13/CXCL8/DEFB1/DEFB4A/FCGR2B/GJB2/HIST1H2BJ/HPGD/JUNB/KLK7/LITAF/LY96/MGST1/MYD88/NLRC4/PDE4B/PTAFR/PTGES/RNASE7/S100A14/S100A8/S100A9/SELP/SPON2/STATH/SYK/TNFRSF10C/TNFRSF18/TNFRSF6B/TNIP3/TSPO	37
GO:0061041	regulation of wound healing	16/484	85/12310	1.64E-07	2.75E-05	2.46E-05	APOE/CD109/CD36/HPSE/PHLDB2/PLAT/PLAU/PLAUR/PLEK/S100A9/SELP/SERPINB2/SERPINE2/SOX15/SYK/TNFRSF12A	16

GO:0030855	epithelial cell differentiation	42/484	458/12310	2.68E-07	4.31E-05	3.86E-05	ABCA12/AKR1C1/AKR1C2/AKR1C3/CD109/CDSN/CERS3/CNFN/CSTA/DSC2/DSG3/EREG/ID1/IVL/KRT10/KRT13/KRT14/KRT16/KRT23/KRT4/KRT6A/KRT6B/KRT6C/KRT7/KRT78/MESP1/PI3/PPARG/PRSS8/PTK6/RHCG/SDC1/SFN/SLC7A11/SPRR1A/SPRR1B/SPRR2A/SPRR2B/SPRR3/TMEM79/TRIM16/UPK1B	42
GO:0007596	blood coagulation	28/484	242/12310	2.96E-07	4.58E-05	4.10E-05	ADORA2A/AK3/APOE/ARRB2/CD177/CD36/COL1A1/COL1A2/DGKA/EHD1/HBB/HPSE/PLAT/PLAU/PLAUR/PLEK/RAC2/RHOG/S100A9/SELP/SERPINA1/SERPINB2/SERPINE2/SH2B2/SLC7A11/SYK/TYRO3/W AS	28
GO:0050817	coagulation	28/484	243/12310	3.22E-07	4.79E-05	4.29E-05	ADORA2A/AK3/APOE/ARRB2/CD177/CD36/COL1A1/COL1A2/DGKA/EHD1/HBB/HPSE/PLAT/PLAU/PLAUR/PLEK/RAC2/RHOG/S100A9/SELP/SERPINA1/SERPINB2/SERPINE2/SH2B2/SLC7A11/SYK/TYRO3/W AS	28
GO:0030193	regulation of blood coagulation	12/484	50/12310	3.70E-07	5.11E-05	4.58E-05	APOE/CD36/HPSE/PLAT/PLAU/PLAUR/PLEK/S100A9/SELP/SERPINB2/SERPINE2/SYK	12
GO:1900046	regulation of hemostasis	12/484	50/12310	3.70E-07	5.11E-05	4.58E-05	APOE/CD36/HPSE/PLAT/PLAU/PLAUR/PLEK/S100A9/SELP/SERPINB2/SERPINE2/SYK	12
GO:0007599	hemostasis	28/484	246/12310	4.16E-07	5.54E-05	4.96E-05	ADORA2A/AK3/APOE/ARRB2/CD177/CD36/COL1A1/COL1A2/DGKA/EHD1/HBB/HPSE/PLAT/PLAU/PLAUR/PLEK/RAC2/RHOG/S100A9/SELP/SERPINA1/SERPINB2/SERPINE2/SH2B2/SLC7A11/SYK/TYRO3/W AS	28
GO:0018149	peptide cross-linking	9/484	27/12310	5.19E-07	6.69E-05	5.99E-05	CSTA/IVL/KRT10/PI3/SPRR1A/SPRR1B/SPRR2A/SPRR2B/SPRR3	9

GO:0042742	defense response to bacterium	19/484	129/12310	6.50E-07	8.10E-05	7.25E-05	ACP5/BPIFA2/C5AR1/CD36/CXCL13/DEFB1/DEFB4A/HIST1H2BJ/KLK7/MYD88/NLRC4/RNASE7/S100A14/S100A8/S100A9/SELP/SPON2/STATH/SYK	19
GO:0010466	negative regulation of peptidase activity	22/484	168/12310	6.90E-07	8.34E-05	7.46E-05	A2ML1/ADORA2A/ARRB2/BIRC5/CD109/CST7/CSTA/MMP9/NLRC4/PI3/PLAUR/PTTG1/PTTG3P/SERPINA1/SERPINA3/SERPINB2/SERPINB5/SERPINE2/SFN/SFRP2/TNFRSF10C/TNFRSF6B	22
GO:0050818	regulation of coagulation	12/484	53/12310	7.31E-07	8.56E-05	7.66E-05	APOE/CD36/HPSE/PLAT/PLAU/PLAUR/PLEK/S100A9/SELP/SERPINB2/SERPINE2/SYK	12
GO:0019730	antimicrobial humoral response	12/484	55/12310	1.12E-06	0.00012715 7	0.00011383 7	BPIFA2/DEFB1/DEFB4A/HIST1H2BJ/KLK7/LCN2/PI3/PRSS3/RNASE7/S100A8/S100A9/SPON2	12
GO:0007186	G-protein coupled receptor signaling pathway	41/484	471/12310	1.46E-06	0.00015703 2	0.00014058 3	ADGRF4/ADGRG3/ADM/ADORA2A/AKR1C2/AKR1C3/APOE/AREG/ARHGEF16/ARRB2/C5AR1/CA2/CAV2/CCK/CCRL2/CXCL13/CXCL8/CXCR4/DEFB1/DEFB4A/DGKA/EREG/GNG10/GPR153/GPR65/GPR87/GUCA1B/HCAR3/HOMER3/HPGD/KISS1/NMU/PDE4B/PLEK/PPARG/PTAFR/RAC2/RHOG/SFRP2/SPHK1/TYRO3	41
GO:0010951	negative regulation of endopeptidase activity	21/484	162/12310	1.46E-06	0.00015703 2	0.00014058 3	A2ML1/ADORA2A/ARRB2/BIRC5/CD109/CST7/CSTA/MMP9/NLRC4/PI3/PLAUR/PTTG1/SERPINA1/SERPINA3/SERPINB2/SERPINB5/SERPINE2/SFN/SFRP2/TNFRSF10C/TNFRSF6B	21
GO:1990266	neutrophil migration	13/484	70/12310	2.79E-06	0.00029113 9	0.00026064 3	ADAM8/C5AR1/CD177/CXCL8/DAPK2/ITGB2/MPP1/PDE4B/PECAM1/RAC2/S100A8/S100A9/SYK	13

GO:0032102	negative regulation of response to external stimulus	23/484	204/12310	5.31E-06	0.00054020	0.00048362	ACP5/ADORA2A/AIF1/APOE/CCK/CD109/CXCL13/FCGR2B/IL1R2/IL20RB/METRNL/MMP28/PHLDB2/PLAT/PLAU/PLAUR/PPARG/SEMA4G/SEMA7A/SERPINB2/SERPINE2/TNFAIP6/TYRO3	23
GO:0060326	cell chemotaxis	23/484	205/12310	5.77E-06	0.00057159	0.00051172	ADAM8/AIF1/ARHGEF16/ARRB2/BIN2/C5AR1/CXCL13/CXCL14/CXCL8/CXCR4/DAPK2/DEFB4A/ITGB2/MMP28/MPP1/PDE4B/RAC2/RHOG/S100A14/S100A8/S100A9/SYK/TMSB4X	23
GO:0006935	chemotaxis	37/484	430/12310	6.29E-06	0.00060825	0.00054539	ADAM8/AIF1/ARHGEF16/ARRB2/BIN2/C5AR1/CCRL2/CXCL13/CXCL14/CXCL8/CXCR4/DAPK2/DEFB1/DEFB4A/FOSL1/GPNMB/ITGB2/MMP28/MPP1/PDE4B/PDLIM7/PLAU/PLAUR/PTAFR/RAC2/RAC3/RHOG/S100A14/S100A8/S100A9/SEMA4G/SEMA7A/SPON2/SYK/TMSB4X/UNC5B/VASP	37
GO:0010469	regulation of signaling receptor activity	27/484	267/12310	6.56E-06	0.00061087	0.00054688	ADM/AREG/BMP1/CCK/CLCF1/CXCL13/CXCL14/CXCL8/DKK1/EREG/FCGR2B/GMFG/GPNMB/GRN/IL19/IL1RN/IL36G/LTB/METRNL/MIA/NAMPT/NCF1/PHLDA2/PLAU/SCGB3A1/SFRP2/TNFSF13B	27
GO:0042330	taxis	37/484	431/12310	6.64E-06	0.00061087	0.00054688	ADAM8/AIF1/ARHGEF16/ARRB2/BIN2/C5AR1/CCRL2/CXCL13/CXCL14/CXCL8/CXCR4/DAPK2/DEFB1/DEFB4A/FOSL1/GPNMB/ITGB2/MMP28/MPP1/PDE4B/PDLIM7/PLAU/PLAUR/PTAFR/RAC2/RAC3/RHOG/S100A14/S100A8/S100A9/SEMA4G/SEMA7A/SPON2/SYK/TMSB4X/UNC5B/VASP	37
GO:0006968	cellular defense response	9/484	36/12310	7.60E-06	0.00068323	0.00061167	ADORA2A/C5AR1/FOSL1/LSP1/LY96/MNDA/NCF1/NCF2/TYROBP	9

GO:0097530	granulocyte migration	14/484	89/12310	8.90E-06	0.00078176	0.00069987	ADAM8/C5AR1/CD177/CXCL8/DAPK2/ITGB2/MPP1/PDE4B/PECAM1/RAC2/S100A14/S100A8/S100A9/SYK	14
GO:0045861	negative regulation of proteolysis	25/484	243/12310	1.07E-05	0.00090276	0.00080826	A2ML1/ADORA2A/ARRB2/BIRC5/CAMK2N1/CD109/CST7/CSTA/IL1R2/MMP9/NLRC4/PI3/PLAT/PLAUR/PTTG1/PTTG3P/SERPINA1/SERPINA3/SERPINB2/SERPINB5/SERPINE2/SFN/SFRP2/TNFRSF10C/TNFRSF 6B	25
GO:0009410	response to xenobiotic stimulus	22/484	198/12310	1.07E-05	0.00090276	0.00080826	ACSL1/ADORA2A/AIF1/AKR1C1/ALDH3A1/APOBEC3A/CCNA2/CYP26A1/CYP2C18/CYP2E1/CYP2R1/CYP3A5/E2F1/FOSB/GGT1/GJB2/MGST1/NQO2/PPARG/PPP1R1B/PTAFR/RYR1	22
GO:0006690	icosanoid metabolic process	13/484	79/12310	1.12E-05	0.00092260	0.00082596	AKR1C1/AKR1C2/AKR1C3/AKR1C4/ALOX5/ALOX5AP/CYP2C18/CYP2E1/GGT1/HPGD/MGST1/PTGES/SYK	13
GO:0010035	response to inorganic substance	34/484	393/12310	1.34E-05	0.00108181	0.00096851	AKR1C3/ALOX5AP/AQP2/AREG/CA2/CCNA2/CD14/CD36/COL1A1/CYP2E1/CYP2R1/FKBP1B/FOSB/FOSL1/GGH/HBA1/HBA2/HBB/HMOX1/IL18RAP/JUNB/KCNMB4/KRT14/LDHA/MMP9/NCF1/NUDT1/PTGES/RASAL1/RYR1/S100A16/S100A8/SDC1/TSPO	34
GO:0033559	unsaturated fatty acid metabolic process	13/484	81/12310	1.48E-05	0.00117155	0.00104884	ACSL1/AKR1C1/AKR1C2/AKR1C3/AKR1C4/ALOX5/ALOX5AP/CYP2C18/CYP2E1/GLYATL2/HPGD/MGST1/PTGES	13
GO:0071466	cellular response to xenobiotic stimulus	17/484	133/12310	1.76E-05	0.00136104	0.00121848	ACSL1/AIF1/AKR1C1/ALDH3A1/APOBEC3A/CCNA2/CYP26A1/CYP2C18/CYP2E1/CYP2R1/CYP3A5/E2F1/GGT1/GJB2/MGST1/NQO2/RYR1	17

GO:0007159	leukocyte cell-cell adhesion	25/484	251/12310	1.87E-05	0.00141597	0.00126767	ADAM8/ADORA2A/AIF1/ASS1/CCDC88B/CD177/FAM49B/FCGR2B/GPNMB/IL20RB/ITGA5/ITGB2/PAG1/PECAM1/PTAFR/RAC2/S100A8/S100A9/SELL/SELP/SIRPA/SIRPB1/SYK/TNFSF13B/VNN1	25
GO:1902563	regulation of neutrophil activation	5/484	10/12310	1.97E-05	0.00146099	0.00130795	CD177/FCGR2B/ITGB2/PTAFR/SYK	5
GO:0052548	regulation of endopeptidase activity	28/484	300/12310	2.00E-05	0.00146099	0.00130795	A2ML1/ADORA2A/ARRB2/BID/BIRC5/BOK/CCK/CD109/CST7/CSTA/MMP9/MYC/NLRC4/PI3/PLAUR/PPARG/PTTG1/S100A8/S100A9/SERPINA1/SERPINA3/SERPINB2/SERPINB5/SERPINE2/SFN/SFRP2/TNFRSF10C/TNFRSF6B	28
GO:0032496	response to lipopolysaccharide	25/484	253/12310	2.14E-05	0.00151982	0.00136067	ACP5/ADM/C5AR1/CD14/CD36/CXCL13/CXCL8/GJB2/HPGD/JUNB/LITAF/LY96/MGST1/PDE4B/PTAFR/PTGES/S100A14/S100A8/SELP/SPON2/TNFRSF10C/TNFRSF18/TNFRSF6B/TNIP3/TSPO	25
GO:0002237	response to molecule of bacterial origin	26/484	269/12310	2.16E-05	0.00151982	0.00136067	ACP5/ADM/C5AR1/CD14/CD36/CXCL13/CXCL8/FCGR2B/GJB2/HPGD/JUNB/LITAF/LY96/MGST1/PDE4B/PTAFR/PTGES/S100A14/S100A8/SELP/SPON2/TNFRSF10C/TNFRSF18/TNFRSF6B/TNIP3/TSPO	26
GO:0052547	regulation of peptidase activity	29/484	320/12310	2.48E-05	0.00171256	0.00153318	A2ML1/ADORA2A/ARRB2/BID/BIRC5/BOK/CCK/CD109/CST7/CSTA/MMP9/MYC/NLRC4/PI3/PLAUR/PPARG/PTTG1/PTTG3P/S100A8/S100A9/SERPINA1/SERPINA3/SERPINB2/SERPINB5/SERPINE2/SFN/SFRP2/TNFRSF10C/TNFRSF6B	29

GO:0051346	negative regulation of hydrolase activity	29/484	322/12310	2.79E-05	0.00188397	0.00168663	A2ML1/ADORA2A/ANGPTL4/APOC1/ARRB2/BIRC5/CD109/CST7/CSTA/FKBP1B/GMIP/MMP9/NLRC4/PHACTR1/PI3/PLAUR/PPP1R14B/PPP1R1B/PTTG1/PTTG3P/SERPINA1/SERPINA3/SERPINB2/SERPINB5/SERPINE2/SFN/SFRP2/TNFRSF10C/TNFRSF6B	29
GO:0050865	regulation of cell activation	33/484	390/12310	2.83E-05	0.00188397	0.00168663	ADAM8/ADORA2A/AIF1/APOE/CCDC88B/CD177/CLCF1/FAM49B/FCGR2B/GPNMB/HMOX1/IL20RB/ITGB2/LMO4/LST1/MILR1/MNDA/PAG1/PLEK/PTAFR/RAC2/SAMSN1/SELP/SERPINE2/SIRPA/SIRPB1/SOX15/SYK/TNFRSF18/TNFSF13B/TYRO3/UNC13D/VNN1	33
GO:0015669	gas transport	5/484	11/12310	3.49E-05	0.00228887	0.00204906	CA2/HBA1/HBA2/HBB/MYC	5
GO:0006911	phagocytosis, engulfment	9/484	43/12310	3.56E-05	0.00229532	0.00205496	AIF1/BIN2/CD36/FCGR2B/ITGB2/PPARG/RAC2/RAC3/RHOG	9
GO:0046456	icosanoid biosynthetic process	8/484	34/12310	3.96E-05	0.00251289	0.00224682	AKR1C3/ALOX5/ALOX5AP/GGT1/HPGD/MGST1/PTGES/SYK	8
GO:0006959	humoral immune response	16/484	129/12310	4.50E-05	0.00280756	0.00251348	BPIFA2/C5AR1/CXCL13/DEFB1/DEFB4A/FCGR2B/HIST1H2BJ/KLK7/LCN2/PI3/PRSS3/RNASE7/S100A8/S100A9/SPON2/TREM1	16
GO:0097529	myeloid leukocyte migration	16/484	130/12310	4.95E-05	0.00303902	0.0027207	ADAM8/AIF1/C5AR1/CD177/CXCL8/DAPK2/ITGB2/MMP28/MPP1/PDE4B/PECAM1/RAC2/S100A14/S100A8/S100A9/SYK	16
GO:0006898	receptor-mediated endocytosis	21/484	205/12310	5.74E-05	0.00346682	0.00310367	ADM/APOBR/APOC1/APOE/ARRB2/CAV2/CD14/CD36/CLTB/CXCL8/DKK1/FCGR2B/HBA1/HBA2/HBB/ITGB2/LRP3/PDLIM7/SCARF1/SYK/TINAGL1	21

GO:1901568	fatty acid derivative metabolic process	15/484	120/12310	7.08E-05	0.00420895	0.00376808	ACSL1/AKR1C1/AKR1C2/AKR1C3/AKR1C4/ALOX5/ALOX5AP/CYP2C18/CYP2E1/DGAT2/GGT1/HPGD/MGST1/PTGES/SYK	15
GO:0055094	response to lipoprotein particle	6/484	20/12310	8.67E-05	0.00507738	0.00454558	APOE/CD36/ITGB2/MYD88/PPARG/SYK	6
GO:0042448	progesterone metabolic process	5/484	13/12310	9.11E-05	0.00525832	0.00470536	ADM/AKR1C1/AKR1C2/AKR1C3/AKR1C4	5
GO:0043300	regulation of leukocyte degranulation	8/484	38/12310	9.30E-05	0.00528698	0.00473199	CD177/FCGR2B/HMOX1/ITGB2/PTAFR/RAC2/SYK/UNC13D	8
GO:0002886	regulation of myeloid leukocyte mediated immunity	8/484	39/12310	0.00011303019	0.00633232	0.00566904	CD177/FCGR2B/HMOX1/ITGB2/PTAFR/RAC2/SYK/UNC13D	8
GO:0042554	superoxide anion generation	6/484	21/12310	0.00011735	0.00642972	0.00575623	ACP5/CD177/ITGB2/NCF1/NCF2/SYK	6
GO:0006820	anion transport	32/484	402/12310	0.00011961941	0.00642972	0.00575623	ABCA12/ABCC3/ACSL1/ADORA2A/AKR1C1/AKR1C4/APOC1/APOE/CA2/CCK/CD36/CLCA2/CLCA4/CLIC3/HBA1/HBA2/HBB/KCNN4/LRRC8A/OCA2/PLIN2/PPARG/PTAFR/SLC19A1/SLC22A16/SLC27A4/SLC2A3/SLC52A3/SLC7A11/SLCO1B3/SYK/TSPO	32
GO:0072593	reactive oxygen species metabolic process	20/484	200/12310	0.00011974747	0.00642972	0.00575623	ACP5/AIF1/AKR1C3/ASS1/CD177/CD36/DUOX2/EIF6/HBA1/HBA2/HBB/IL19/ITGB2/NCF1/NCF1B/NCF1C/NCF2/RAC2/SYK/TSPO	20
GO:0006692	prostanoid metabolic process	7/484	30/12310	0.00012879191	0.00672843	0.00602366	AKR1C1/AKR1C2/AKR1C3/AKR1C4/HPGD/MGST1/PTGES	7

GO:0006693	prostaglandin metabolic process	7/484	30/12310	0.00012879	0.0067284	0.0060236	AKR1C1/AKR1C2/AKR1C3/AKR1C4/HPGD/MGST1/PTGES	7
GO:0030595	leukocyte chemotaxis	17/484	156/12310	0.00013573	0.0069039	0.0061808	ADAM8/AIF1/C5AR1/CXCL13/CXCL14/CXCL8/CXCR4/DAPK2/ITGB2/MMP28/MPP1/PDE4B/RAC2/S100A14/S100A8/S100A9/SYK	17
GO:0002544	chronic inflammatory response	5/484	14/12310	0.00013719	0.0069039	0.0061808	CXCL13/PTGES/S100A8/UNC13D/VNN1	5
GO:0030593	neutrophil chemotaxis	10/484	62/12310	0.00013750	0.0069039	0.0061808	C5AR1/CXCL8/DAPK2/ITGB2/MPP1/PDE4B/RAC2/S100A8/S100A9/SY K	10
GO:0006801	superoxide metabolic process	9/484	51/12310	0.00014533	0.0072035	0.0064489	ACP5/CD177/CD36/ITGB2/NCF1/NCF1B/NCF1C/NCF2/SYK	9
GO:0071402	cellular response to lipoprotein particle stimulus	6/484	22/12310	0.00015603	0.0076360	0.0068361	APOE/CD36/ITGB2/MYD88/PPARG/SYK	6
GO:0099024	plasma membrane invagination	9/484	52/12310	0.00016973	0.0082024	0.0073432	AIF1/BIN2/CD36/FCGR2B/ITGB2/PPARG/RAC2/RAC3/RHOG	9
GO:0006979	response to oxidative stress	29/484	358/12310	0.00018425	0.0087942	0.0078731	AIF1/AKR1C3/APOE/AREG/CCNA2/CD36/COL1A1/CYP2E1/DUOX2/FKBP1B/FOSL1/GJB2/GPX2/HBA1/HBA2/HBB/HMOX1/IL18RAP/LDHA/MGST1/MMP9/NCF1/NCF2/NCF4/NUDT1/SDC1/SLC7A11/SRXN1/VN N1	29

GO:190303 6	positive regulation of response to wounding	8/484	42/12310	0.00019548	0.00916647 2	0.00820632 2	CD36/FKBP1B/HPSE/PLEK/S100A9/SCARF1/SELP/SOX15	8
GO:001613 7	glycoside metabolic process	5/484	15/12310	0.00019916 8	0.00916647 2	0.00820632 2	AKR1B10/AKR1C1/AKR1C2/AKR1C3/AKR1C4	5
GO:006143 6	establishment of skin barrier	5/484	15/12310	0.00019916 8	0.00916647 2	0.00820632 2	ABCA12/GRHL3/KRT16/SFN/TMEM79	5
GO:000270 3	regulation of leukocyte mediated immunity	15/484	132/12310	0.00020928 5	0.00951879 4	0.00852174	ARRB2/CD177/CLCF1/FAM49B/FCGR2B/HMOX1/IL18RAP/IL20RB/ITGB2/PTAFR/RAC2/SH2D1B/SYK/UNC13D/WAS	15

Supplement Table 2E: GO Cellular Components for the Upregulated DEGs in the EC vs NS Comparison

ID	Description	GeneRatio	BgRatio	pvalue	p.adjust	qvalue	geneID	Count
GO:0001533	cornified envelope	13/502	34/12866	1.82E-10	6.97E-08	6.20E-08	CDSN/CNFN/CSTA/DSC2/DSG3/IVL/KRT10/PI3/SPRR1A/SPRR1B/SPRR2A/SPRR2B/SPRR3	13
GO:0031225	anchored component of membrane	17/502	86/12866	2.83E-08	4.40E-06	3.92E-06	CD109/CD14/CD177/CD58/CEACAM5/CPM/FCGR3B/LY6D/LYPD3/MMP25/PLAUR/PRSS22/PRSS27/PRSS8/SEMA7A/TNFRSF10C/VNN1	17
GO:0030667	secretory granule membrane	31/502	262/12866	3.46E-08	4.40E-06	3.92E-06	ADAM8/ADGRG3/C5AR1/CAV2/CD109/CD14/CD177/CD36/CD58/CD68/CEACAM3/FABP5/FCAR/FCGR2A/FCGR3B/ITGAX/ITGB2/MGST1/MMP25/PECAM1/PLAU/PLAUR/PTAFR/RHOG/SELL/SELP/SIRPA/SIRPB1/SLC2A3/TYROBP/VNN1	31
GO:0060205	cytoplasmic vesicle lumen	30/502	270/12866	2.34E-07	1.67E-05	1.49E-05	ALOX5/APOE/ARPC5/BIN2/FABP5/FAM49B/GCA/GGH/GMFG/GRN/HBA1/HBA2/HBB/HEBP2/HPSE/HSPA6/IMPDH1/LCN2/MNDA/PYGB/RNASET2/S100A8/S100A9/S100P/SERPINA1/SERPINA3/SRGN/TCN1/TMSB4X/UNC13D	30
GO:0031983	vesicle lumen	30/502	271/12866	2.54E-07	1.67E-05	1.49E-05	ALOX5/APOE/ARPC5/BIN2/FABP5/FAM49B/GCA/GGH/GMFG/GRN/HBA1/HBA2/HBB/HEBP2/HPSE/HSPA6/IMPDH1/LCN2/MNDA/PYGB/RNASET2/S100A8/S100A9/S100P/SERPINA1/SERPINA3/SRGN/TCN1/TMSB4X/UNC13D	30
GO:0045095	keratin filament	8/502	19/12866	2.63E-07	1.67E-05	1.49E-05	KRT13/KRT14/KRT4/KRT6A/KRT6B/KRT6C/KRT7/KRT78	8
GO:0005882	intermediate filament	12/502	60/12866	2.77E-06	0.000150956	0.000134359	ADORA2A/KRT10/KRT13/KRT14/KRT16/KRT23/KRT4/KRT6A/KRT6B/KRT6C/KRT7/KRT78	12
GO:0034774	secretory granule lumen	26/502	258/12866	9.14E-06	0.000436356	0.000388379	ALOX5/ARPC5/BIN2/FABP5/FAM49B/GCA/GGH/GMFG/GRN/HEBP2/HPSE/HSPA6/IMPDH1/LCN2/MNDA/PYGB/RNASET2/S100A8/S100A9/S100P/SERPINA1/SERPINA3/SRGN/TCN1/TMSB4X/UNC13D	26
GO:0045111	intermediate filament	14/502	94/12866	1.57E-05	0.000659305	0.000586816	ADORA2A/KRT10/KRT13/KRT14/KRT16/KRT23/KRT4/KRT6A/KRT6B	14

1	t cytoskeleton						/KRT6C/KRT7/KRT78/PHLDB2/S100A8	
GO:0043020	NADPH oxidase complex	5/502	10/12866	1.90E-05	0.000659305	0.000586816	NCF1/NCF1B/NCF1C/NCF2/NCF4	5
GO:0101002	ficolin-1-rich granule	20/502	177/12866	1.90E-05	0.000659305	0.000586816	ADAM8/ALOX5/ARPC5/BIN2/CALML5/CD58/FCAR/GMFG/HBB/HSPA6/IMPDH1/ITGAX/ITGB2/MMP9/MNDA/PLEKHO2/SERPINA1/SIRPA/SLC2A3/TNFAIP6	20
GO:0031012	extracellular matrix	25/502	281/12866	0.000107591	0.003279826	0.002919217	AMTN/ANGPTL4/APOE/AZGP1/BMP1/COL1A1/COL1A2/COL6A2/COL6A6/FGFBP1/HPSE/LAD1/MMP13/MMP25/MMP28/MMP9/PI3/S100A9/SERPINA1/SERPINE2/SFRP2/SPON2/TINAGL1/TPSAB1/TPSB2	25
GO:0070820	tertiary granule	16/502	140/12866	0.000111617	0.003279826	0.002919217	ADAM8/CD177/CD58/FCAR/GGH/HBB/ITGAX/ITGB2/MMP9/PLAU/PRSS3/PTAFR/SIRPA/SLC2A3/TCN1/TNFAIP6	16
GO:0035578	azurophil granule lumen	11/502	75/12866	0.000145863	0.003979988	0.003542397	FABP5/GCA/GGH/GRN/HEBP2/IMPDH1/MNDA/PYGB/RNASET2/SERPINA3/UNC13D	11
GO:0009986	cell surface	35/502	471/12866	0.000195576	0.004980661	0.004433049	ADAM8/AREG/C5AR1/CD109/CD14/CD36/CD58/CEACAM5/CPM/CXCR4/FCER1A/FCGR2B/FCGR3A/FGFBP1/IL2RG/ITGA5/ITGAX/ITGB2/KRT4/LRRC8A/LY6D/LY9/PLAT/PLAU/PLAUR/PROM2/SDC1/SELL/SELP/SEMA7A/SERPINE2/SLC7A11/TNFRSF12A/TREML2/TYROBP	35
GO:0042581	specific granule	15/502	135/12866	0.000248188	0.005635682	0.005016052	ADAM8/ADGRG3/CD177/CD36/CEACAM3/FCAR/GGH/HPSE/ITGB2/LCN2/MMP25/PLAU/PLAUR/SLC2A3/TCN1	15
GO:0031091	platelet alpha granule	10/502	67/12866	0.000250803	0.005635682	0.005016052	CD109/CD36/FAM49B/PECAM1/SELP/SERPINA1/SERPINA3/SERPINE2/SRGN/TMSB4X	10
GO:0035579	specific granule membrane	11/502	81/12866	0.000292508	0.006207665	0.005525147	ADAM8/ADGRG3/CD177/CD36/CEACAM3/FCAR/ITGB2/MMP25/PLAU/PLAUR/SLC2A3	11

Supplement Table 2F: GO Molecular Functions for the Upregulated DEGs in the EC vs NS Comparison

ID	Description	GeneRatio	BgRatio	pvalue	p.adjust	qvalue	geneID	Count
GO:0033293	monocarboxylic acid binding	12/475	45/12391	7.96E-08	3.83E-05	3.26E-05	AKR1C1/AKR1C2/AKR1C3/AKR1C4/ALOX5AP/APOC1/CYP26A1/CYP27C1/FABP5/PPARG/S100A8/S100A9	12
GO:0048018	receptor ligand activity	26/475	210/12391	1.27E-07	3.83E-05	3.26E-05	ADM/AREG/BMP1/CCK/CLCF1/CXCL13/CXCL14/CXCL8/DEFB4A/DKK1/EREG/GMFG/GPNMB/GRN/IL19/IL1RN/IL36G/LTB/METRNL/MIA/NAMPT/SCGB3A1/SEMA4G/SEMA7A/SFRP2/TNFSF13B	26
GO:0004032	alditol:NADP+ 1-oxidoreductase activity	6/475	10/12391	5.67E-07	0.000106234	9.03E-05	AKR1B10/AKR1B15/AKR1C1/AKR1C2/AKR1C3/AKR1C4	6
GO:0030545	receptor regulator activity	26/475	229/12391	7.05E-07	0.000106234	9.03E-05	ADM/AREG/BMP1/CCK/CLCF1/CXCL13/CXCL14/CXCL8/DEFB4A/DKK1/EREG/GMFG/GPNMB/GRN/IL19/IL1RN/IL36G/LTB/METRNL/MIA/NAMPT/SCGB3A1/SEMA4G/SEMA7A/SFRP2/TNFSF13B	26
GO:0008106	alcohol dehydrogenase (NADP+) activity	7/475	17/12391	1.62E-06	0.000195464	0.000166171	AKR1B10/AKR1B15/AKR1C1/AKR1C2/AKR1C3/AKR1C4/ALDH3A1	7
GO:0001530	lipopolysaccharide binding	7/475	19/12391	3.93E-06	0.000394714	0.000335564	BPIFA2/CD14/HIST1H2BJ/PTAFR/RNASE7/SELP/SPON2	7
GO:0019825	oxygen binding	7/475	22/12391	1.20E-05	0.000906415	0.000770575	CYP26A1/CYP2C18/CYP2E1/CYP3A5/HBA1/HBA2/HBB	7
GO:0033764	steroid dehydrogenase activity, acting on the CH-OH group of donors, NAD or NADP as acceptor	7/475	22/12391	1.20E-05	0.000906415	0.000770575	AKR1B15/AKR1C1/AKR1C2/AKR1C3/AKR1C4/HSD11B2/HSD17B3	7
GO:0004033	aldo-keto reductase (NADP) activity	7/475	23/12391	1.67E-05	0.001049981	0.000892626	AKR1B10/AKR1B15/AKR1C1/AKR1C2/AKR1C3/AKR1C4/ALDH3A1	7
GO:0016176	superoxide-generating NADPH oxidas	5/475	10/12391	1.74E-05	0.001049981	0.000892626	NCF1/NCF1B/NCF1C/NCF2/NCF4	5

	e activator activity							
GO:0019865	immunoglobulin binding	6/475	17/12391	2.65E-05	0.00142251	0.001209326	FCAR/FCER1A/FCGR2A/FCGR2B/FCGR3A/FCGR3B	6
GO:0004252	serine-type endopeptidase activity	14/475	101/12391	2.94E-05	0.00142251	0.001209326	ADAM8/BMP1/KLK7/MMP13/MMP9/PLAT/PLAU/PRSS22/PRSS27/PRSS3/PRSS8/TMPRSS11D/TPSAB1/TPSB2	14
GO:0016229	steroid dehydrogenase activity	7/475	25/12391	3.07E-05	0.00142251	0.001209326	AKR1B15/AKR1C1/AKR1C2/AKR1C3/AKR1C4/HSD11B2/HSD17B3	7
GO:0005504	fatty acid binding	6/475	18/12391	3.85E-05	0.001651579	0.001404066	ALOX5AP/APOC1/FABP5/PPARG/S100A8/S100A9	6
GO:0030414	peptidase inhibitor activity	14/475	104/12391	4.11E-05	0.001651579	0.001404066	A2ML1/BIRC5/CD109/CST7/CSTA/NLRC4/PI3/PTTG1/PTTG3P/SERPINA1/SERPINA3/SERPINB2/SERPINB5/SERPINE2	14
GO:0061135	endopeptidase regulator activity	14/475	106/12391	5.09E-05	0.001687571	0.001434664	A2ML1/BIRC5/CD109/CST7/CSTA/NLRC4/PI3/PTTG1/SERPINA1/SERPINA3/SERPINB2/SERPINB5/SERPINE2/SFRP2	14
GO:0050664	oxidoreductase activity, acting on NAD(P)H, oxygen as acceptor	5/475	12/12391	5.13E-05	0.001687571	0.001434664	DUOX2/NCF1/NCF1B/NCF1C/NCF2	5
GO:0008236	serine-type peptidase activity	15/475	120/12391	5.32E-05	0.001687571	0.001434664	ADAM8/BMP1/CPM/KLK7/MMP13/MMP9/PLAT/PLAU/PRSS22/PRSS27/PRSS3/PRSS8/TMPRSS11D/TPSAB1/TPSB2	15
GO:0031406	carboxylic acid binding	16/475	134/12391	5.32E-05	0.001687571	0.001434664	AKR1C1/AKR1C2/AKR1C3/AKR1C4/ALOX5AP/APOC1/ASS1/CYP26A1/CYP27C1/FABP5/PPARG/S100A8/S100A9/SELP/SLC19A1/TNFAIP6	16
GO:0043177	organic acid binding	16/475	135/12391	5.82E-05	0.001755893	0.001492746	AKR1C1/AKR1C2/AKR1C3/AKR1C4/ALOX5AP/APOC1/ASS1/CYP26A1/CYP27C1/FABP5/PPARG/S100A8/S100A9/SELP/SLC19A1/TNFAIP6	16
GO:0005125	cytokine activity	14/475	109/12391	6.95E-05	0.001956383	0.001663193	AREG/BMP1/CLCF1/CXCL13/CXCL14/CXCL8/GRN/IL19/IL1RN/IL36G/LTB/NAMPT/SCGB3A1/TNFSF13B	14
GO:0016247	channel regulator activity	12/475	83/12391	7.14E-05	0.001956383	0.001663193	ANKRD36C/CHRNA7/FKBP1B/FXYD5/KCNMB4/KCNS1/KCNS3/LRRC26/PACSIN3/PRSS8/SGK1/SNTA1	12
GO:0017171	serine hydrolase activity	15/475	124/123	7.79E-05	0.002042893	0.001736735	ADAM8/BMP1/CPM/KLK7/MMP13/MMP9/PLAT/PLAU/PRSS22/PRSS2	15

			91				7/PRSS3/PRSS8/TMPRSS11D/TPSAB1/TPSB2	
GO:000486	endopeptidase inhibitor activity	13/475	10 0/123 91	0.0 001 107 84	0.002 69410 8	0.002 29035 6	A2ML1/BIRC5/CD109/CST7/CSTA/NLRC4/PI3/PTTG1/SERPINA1/SERPINA3/SERPINB2/SERPINB5/SERPINE2	13
GO:000449 7	monooxygenase activity	10/475	62/12 39 1	0.0 001 116 96	0.002 69410 8	0.002 29035 6	AKR1C1/AKR1C2/AKR1C3/AKR1C4/CYP26A1/CYP27C1/CYP2C18/CYP2E1/CYP2R1/CYP3A5	10
GO:000832 9	signaling pattern recognition receptor activity	5/475	14/12 39 1	0.0 001 217 4	0.002 71885 8	0.002 31139 7	CD14/CD36/CLEC7A/LY96/PTAFR	5
GO:003818 7	pattern recognition receptor activity	5/475	14/12 39 1	0.0 001 217 4	0.002 71885 8	0.002 31139 7	CD14/CD36/CLEC7A/LY96/PTAFR	5
GO:004690 6	tetrapyrrole binding	12/475	91/12 39 1	0.0 001 762 22	0.003 79506 3	0.003 22631 7	CYP26A1/CYP27C1/CYP2C18/CYP2E1/CYP2R1/CYP3A5/DUOX2/HBA1/HBA2/HBB/HMOX1/TCN1	12
GO:001620 9	antioxidant activity	10/475	66/12 39 1	0.0 001 911 26	0.003 97410 6	0.003 37852 8	ALOX5AP/APOE/DUOX2/GPX2/HBA1/HBA2/HBB/MGST1/S100A9/SR XN1	10
GO:000417 5	endopeptidase activity	23/475	26 5/123 91	0.0 002 223 61	0.004 46944 7	0.003 79963 4	ADAM8/BMP1/CAPN14/CAPNS2/CLCA2/CLCA4/GCA/KLK7/MMP13/MMP25/MMP28/MMP9/NRIP3/PLAT/PLAU/PRSS22/PRSS27/PRSS3/PRSS8/TINAGL1/TMPRSS11D/TPSAB1/TPSB2	23
GO:006113 4	peptidase regulator activity	15/475	13 7/123 91	0.0 002 405 02	0.004 67814 8	0.003 97705 9	A2ML1/BIRC5/CD109/CST7/CSTA/NLRC4/PI3/PTTG1/PTTG3P/SERPINA1/SERPINA3/SERPINB2/SERPINB5/SERPINE2/SFRP2	15
GO:002003 7	heme binding	11/475	83/12 39 1	0.0 003 116 38	0.005 87243 5	0.004 99236 4	CYP26A1/CYP27C1/CYP2C18/CYP2E1/CYP2R1/CYP3A5/DUOX2/HBA1/HBA2/HBB/HMOX1	11
GO:000488 8	transmembrane signaling receptor activity	32/475	43 7/123 91	0.0 003 435 59	0.006 27776 9	0.005 33695 3	ADGRF4/ADGRG3/ADORA2A/C5AR1/CCRL2/CD14/CHRFAM7A/CHRNA7/CXCR4/FCGR2B/GPR153/GPR65/GPR87/HCAR3/HPGD/IGSF6/IL1R2/IL20RB/IL2RG/ITGB2/PPARG/PTAFR/PTPRE/PTPRH/SCARF1/SFRP2/SPHK1/TNFRSF10C/TNFRSF18/TNFRSF6B/TYRO3/UNC5B	32
GO:001986 4	IgG binding	4/475	10/12 39 1	0.0 003 724 26	0.006 41636 6	0.005 45477 9	FCGR2A/FCGR2B/FCGR3A/FCGR3B	4
GO:003532 5	Toll-like receptor binding	4/475	10/12 39	0.0 003 724	0.006 41636 6	0.005 45477 9	CD36/S100A8/S100A9/SYK	4

			1	26				
GO:0004601	peroxidase activity	7/475	38/12391	0.00522885	0.00875832	0.00744576	ALOX5AP/DUOX2/GPX2/HBA1/HBA2/HBB/MGST1	7
GO:0004222	metalloendopeptidase activity	9/475	62/12391	0.00550986	0.00877555	0.00746049	ADAM8/BMP1/CLCA2/CLCA4/KLK7/MMP13/MMP25/MMP28/MMP9	9
GO:0016616	oxidoreductase activity, acting on the CH-OH group of donors, NAD or NADP as acceptor	12/475	103/12391	0.00564098	0.00877555	0.00746049	AKR1B10/AKR1B15/AKR1C1/AKR1C2/AKR1C3/AKR1C4/ALDH3A1/HPGD/HSD11B2/HSD17B3/IMPDH1/LDHA	12
GO:0050786	RAGE receptor binding	4/475	11/12391	0.00567573	0.00877555	0.00746049	S100A4/S100A8/S100A9/S100P	4

Supplement Table 3A: GO Biological Processes for Downregulated DEGs in the CS vs NS Comparison

ID	Description	Gene Ratio	Bg Ratio	pvalue	p.adjust	qvalue	geneID	Count
GO:0007018	microtubule-based movement	21/188	263/12310	5.49402E-10	1.24934E-06	1.22025E-06	ARMC4/CFAP54/DNAH1/DNAH10/DNAH11/DNAH2/DNAH3/DNAH5/DNAH6/DNAH7/DNAH9/DYNC2H1/FMN2/FYCO1/HYDIN/KIF26B/MAK/RFX3/TTC21B/WDR35/WDR66	21
GO:0003341	cilium movement	11/188	59/12310	1.1631E-09	1.32244E-06	1.29165E-06	ARMC4/CFAP54/DNAH1/DNAH11/DNAH3/DNAH5/DNAH7/DNAH9/HYDIN/RFX3/WDR66	11
GO:0001539	cilium or flagellum-dependent cell motility	7/188	29/12310	2.03559E-07	0.00015429 8	0.00015070 5	CFAP54/DNAH1/DNAH2/DNAH3/DNAH6/DNAH7/RFX3	7
GO:0060285	cilium-dependent cell motility	6/188	28/12310	3.33673E-06	0.00189693 3	0.00185276 5	CFAP54/DNAH1/DNAH2/DNAH3/DNAH7/RFX3	6
GO:0060271	cilium assembly	17/188	322/12310	8.78433E-06	0.00399511 1	0.00390209	ARMC4/CDC14A/CFAP54/DCDC2/DNAH1/DNAH3/DNAH5/DNAH6/DNAH7/DYNC2H1/HYDIN/MAK/RFX3/TTBK2/TTC21B/UBXN10/WDR3 5	17
GO:0044782	cilium organization	17/188	332/12310	1.31025E-05	0.00493510 9	0.00482020 1	ARMC4/CDC14A/CFAP54/DCDC2/DNAH1/DNAH3/DNAH5/DNAH6/DNAH7/DYNC2H1/HYDIN/MAK/RFX3/TTBK2/TTC21B/UBXN10/WDR3 5	17
GO:0120031	plasma membrane bounded cell projection assembly	21/188	483/12310	1.51916E-05	0.00493510 9	0.00482020 1	ARMC4/CDC14A/CFAP54/DCDC2/DNAH1/DNAH3/DNAH5/DNAH6/DNAH7/DYNC2H1/HYDIN/LPAR3/MAK/MTSS1/MYLK/RFX3/SLIT2/TTBK2/TTC21B/UBXN10/WDR35	21
GO:0030031	cell projection assembly	21/188	495/12310	2.19172E-05	0.00622995 4	0.00608489 7	ARMC4/CDC14A/CFAP54/DCDC2/DNAH1/DNAH3/DNAH5/DNAH6/DNAH7/DYNC2H1/HYDIN/LPAR3/MAK/MTSS1/MYLK/RFX3/SLIT2/TTBK2/TTC21B/UBXN10/WDR35	21

Supplement Table 3B: GO Cellular Components for Downregulated DEGs in the CS vs NS Comparison

ID	Description	Gene Ratio	Bg Ratio	pvalue	p.adjust	qvalue	geneID	Count
GO:0005930	axoneme	17/198	96/12866	8.20366E-14	1.49177E-11	1.34817E-11	ARMC4/CFAP54/DCDC2/DNAH1/DNAH11/DNAH2/DNAH3/DNAH5/DNAH6/DNAH7/DNAH9/DYNC2H1/HYDIN/PRKAR1A/SAXO2/WDR35/ WDR66	17
GO:0097014	ciliary plasm	17/198	97/12866	9.81429E-14	1.49177E-11	1.34817E-11	ARMC4/CFAP54/DCDC2/DNAH1/DNAH11/DNAH2/DNAH3/DNAH5/DNAH6/DNAH7/DNAH9/DYNC2H1/HYDIN/PRKAR1A/SAXO2/WDR35/ WDR66	17
GO:0005929	cilium	31/198	426/12866	4.47474E-13	4.5344E-11	4.09792E-11	ARMC4/CATSPERD/CDC14A/CFAP54/CFAP58/CNGA4/DCDC2/DNAH 1/DNAH10/DNAH11/DNAH2/DNAH3/DNAH5/DNAH6/DNAH7/DNAH9/ DYNC2H1/HYDIN/LCA5/MAK/NIN/PKHD1L1/PRKAR1A/SAXO2/SHANK2/TTBK2/TTC21B/TUB/UBXN10/WDR35/ WDR66	31
GO:0032838	plasma membrane bounded cell projection cytoplasm	18/198	156/12866	2.84199E-11	2.15991E-09	1.952E-09	ARMC4/CFAP54/DCDC2/DNAH1/DNAH11/DNAH2/DNAH3/DNAH5/DNAH6/DNAH7/DNAH9/DYNC2H1/HYDIN/PRKAR1A/SAXO2/WDR35/ WDR66/WLS	18
GO:0044447	axoneme part	9/198	28/12866	2.16543E-10	1.31658E-08	1.18985E-08	DNAH1/DNAH2/DNAH3/DNAH5/DNAH6/DNAH7/HYDIN/SAXO2/WD R66	9
GO:0044441	ciliary part	24/198	334/12866	3.19584E-10	1.61922E-08	1.46336E-08	ARMC4/CATSPERD/CFAP54/CNGA4/DCDC2/DNAH1/DNAH11/DNAH 2/DNAH3/DNAH5/DNAH6/DNAH7/DNAH9/DYNC2H1/HYDIN/MAK/NIN/PRKAR1A/SAXO2/SHANK2/TTBK2/TTC21B/WDR35/WDR66	24
GO:0030286	dynein complex	10/198	45/12866	1.18564E-09	5.14908E-08	4.65343E-08	DNAH1/DNAH10/DNAH11/DNAH2/DNAH3/DNAH5/DNAH6/DNAH7/D NAH9/DYNC2H1	10

GO:0005858	axonemal dynein complex	6/198	15/12866	5.49198E-08	2.08695E-06	1.88606E-06	DNAH1/DNAH2/DNAH3/DNAH5/DNAH6/DNAH7	6
GO:0099568	cytoplasmic region	21/198	393/12866	6.96736E-07	2.35342E-05	2.12688E-05	ARMC4/CAP2/CFAP54/DCDC2/DNAH1/DNAH11/DNAH2/DNAH3/DNAH5/DNAH6/DNAH7/DNAH9/DYNC2H1/FMN2/HYDIN/PRKAR1A/SAXO2/STOX1/WDR35/WDR66/WLS	21
GO:0005875	microtubule associated complex	11/198	129/12866	4.74998E-06	0.000144399	0.000130499	DNAH1/DNAH10/DNAH11/DNAH2/DNAH3/DNAH5/DNAH6/DNAH7/DNAH9/DYNC2H1/KIF26B	11
GO:0045211	postsynaptic membrane	10/198	138/12866	5.32071E-05	0.000147045	0.000132903	APBB1/DMD/GLRB/GRIN3B/GRM5/KCNB1/KCTD12/MPDZ/SHANK2/ SYNE1	10
GO:0031514	motile cilium	8/198	106/12866	0.000227095	0.000575308 4	0.000519929	CATSPERD/DNAH1/DNAH11/DNAH2/DNAH9/DYNC2H1/SAXO2/WD R66	8

Supplement Table 3C: GO Molecular Functions for Downregulated DEGs in the CS vs NS Comparison

ID	Description	Gene Ratio	Bg Ratio	pvalue	p.adjust	qvalue	geneID	Count
GO:0008569	ATP-dependent microtubule motor activity, minus-end-directed	10/186	15/12391	1.28247E-15	5.06578E-13	4.52241E-13	DNAH1/DNAH10/DNAH11/DNAH2/DNAH3/DNAH5/DNAH6/DNAH7/DNAH9/DYNC2H1	10
GO:0045503	dynein light chain binding	10/186	22/12391	2.52132E-13	4.97962E-11	4.44549E-11	DNAH1/DNAH10/DNAH11/DNAH2/DNAH3/DNAH5/DNAH6/DNAH7/DNAH9/DYNC2H1	10
GO:0045505	dynein intermediate chain binding	10/186	25/12391	1.22576E-12	1.61392E-10	1.44081E-10	DNAH1/DNAH10/DNAH11/DNAH2/DNAH3/DNAH5/DNAH6/DNAH7/DNAH9/DYNC2H1	10
GO:0051959	dynein light intermediate chain binding	10/186	27/12391	3.08236E-12	3.04383E-10	2.71734E-10	DNAH1/DNAH10/DNAH11/DNAH2/DNAH3/DNAH5/DNAH6/DNAH7/DNAH9/DYNC2H1	10
GO:1990939	ATP-dependent microtubule motor activity	10/186	41/12391	3.41477E-10	2.69767E-08	2.40831E-08	DNAH1/DNAH10/DNAH11/DNAH2/DNAH3/DNAH5/DNAH6/DNAH7/DNAH9/DYNC2H1	10
GO:0003777	microtubule motor activity	11/186	92/12391	1.21199E-07	7.97895E-06	7.12311E-06	DNAH1/DNAH10/DNAH11/DNAH2/DNAH3/DNAH5/DNAH6/DNAH7/DNAH9/DYNC2H1/KIF26B	11
GO:0005509	calcium ion binding	24/186	488/12391	2.93382E-07	1.65551E-05	1.47794E-05	CAPN13/CDHR3/DNAH7/DNER/EFHB/FBLN5/HEG1/NCALD/NELL2/NIN/PCDH19/PCDHA4/PCDHAC1/PCDHAC2/PCDHB1/PCDHB11/PLCH1/PROS1/SCUBE2/SLIT1/SLIT2/SNED1/SPOCK1/SULF1	24
GO:0003774	motor activity	11/186	104/12391	4.30206E-07	2.12414E-05	1.8963E-05	DNAH1/DNAH10/DNAH11/DNAH2/DNAH3/DNAH5/DNAH6/DNAH7/DNAH9/DYNC2H1/KIF26B	11

Supplement Table 3D: GO Biological Functions for upregulated DEGs in the CS vs NS Comparison

ID	Description	GeneRatio	BgRatio	pvalue	p.adjust	qvalue	geneID	Count
GO:0009812	flavonoid metabolic process	9/114	14/12310	7.0004E-16	7.20341E-13	6.42931E-13	UGT1A1/UGT1A10/UGT1A3/UGT1A4/UGT1A5/UGT1A6/UGT1A7/UGT 1A8/UGT1A9	9
GO:0052695	cellular glucuronidation	9/114	14/12310	7.0004E-16	7.20341E-13	6.42931E-13	UGT1A1/UGT1A10/UGT1A3/UGT1A4/UGT1A5/UGT1A6/UGT1A7/UGT 1A8/UGT1A9	9
GO:0001523	retinoid metabolic process	13/114	58/12310	4.07243E-15	2.79369E-12	2.49347E-12	AKR1B10/AKR1C1/AKR1C3/AKR1C4/APOC2/APOE/CYP26A1/SDC1/UGT1A1/UGT1A3/UGT1A7/UGT1A8/UGT1A9	13
GO:0016101	diterpenoid metabolic process	13/114	63/12310	1.30018E-14	6.68943E-12	5.97057E-12	AKR1B10/AKR1C1/AKR1C3/AKR1C4/APOC2/APOE/CYP26A1/SDC1/UGT1A1/UGT1A3/UGT1A7/UGT1A8/UGT1A9	13
GO:0006063	uronic acid metabolic process	9/114	19/12310	3.108E-14	1.06604E-11	9.51485E-12	UGT1A1/UGT1A10/UGT1A3/UGT1A4/UGT1A5/UGT1A6/UGT1A7/UGT 1A8/UGT1A9	9
GO:0019585	glucuronate metabolic process	9/114	19/12310	3.108E-14	1.06604E-11	9.51485E-12	UGT1A1/UGT1A10/UGT1A3/UGT1A4/UGT1A5/UGT1A6/UGT1A7/UGT 1A8/UGT1A9	9
GO:0006721	terpenoid metabolic process	13/114	70/12310	5.58708E-14	1.6426E-11	1.46608E-11	AKR1B10/AKR1C1/AKR1C3/AKR1C4/APOC2/APOE/CYP26A1/SDC1/UGT1A1/UGT1A3/UGT1A7/UGT1A8/UGT1A9	13
GO:0006720	isoprenoid metabolic process	13/114	88/12310	1.23091E-12	3.16653E-10	2.82624E-10	AKR1B10/AKR1C1/AKR1C3/AKR1C4/APOC2/APOE/CYP26A1/SDC1/UGT1A1/UGT1A3/UGT1A7/UGT1A8/UGT1A9	13
GO:0006805	xenobiotic metabolic process	12/114	92/12310	4.30656E-11	9.84766E-09	8.78941E-09	AKR1C1/ALDH3A1/CYP26A1/UGT1A1/UGT1A10/UGT1A3/UGT1A4/UGT1A5/UGT1A6/UGT1A7/UGT1A8/UGT1A9	12
GO:0071466	cellular response to xenobiotic stimulus	13/114	133/12310	2.59066E-10	5.33157E-08	4.75863E-08	AKR1C1/ALDH3A1/CYP26A1/E2F1/UGT1A1/UGT1A10/UGT1A3/UGT1A4/UGT1A5/UGT1A6/UGT1A7/UGT1A8/UGT1A9	13
GO:0003475	cellular hormone metabolic process	11/114	85/1231	3.16255E-10	5.838E-08	5.21063E-08	AKR1B15/AKR1C1/AKR1C2/AKR1C3/AKR1C4/CYP26A1/UG	11

4			0				T1A1/UGT1A3/UGT1A7/UGT1A8/UGT1A9	
GO:0042573	retinoic acid metabolic process	7/114	20/12310	3.40408E-10	5.838E-08	5.21063E-08	AKR1C3/CYP26A1/UGT1A1/UGT1A3/UGT1A7/UGT1A8/UGT1A9	7
GO:0009410	response to xenobiotic stimulus	13/114	198/12310	3.39661E-08	5.3771E-06	4.79926E-06	AKR1C1/ALDH3A1/CYP26A1/E2F1/UGT1A1/UGT1A10/UGT1A3/UGT1A4/UGT1A5/UGT1A6/UGT1A7/UGT1A8/UGT1A9	13
GO:0032787	monocarboxylic acid metabolic process	19/114	483/12310	8.54557E-08	1.2562E-05	1.1212E-05	AKR1C1/AKR1C2/AKR1C3/AKR1C4/APOC1/APOC2/CRAT/CYP26A1/GLYATL2/SDS/UGT1A1/UGT1A10/UGT1A3/UGT1A4/UGT1A5/UGT1A6/UGT1A7/UGT1A8/UGT1A9	19
GO:0042445	hormone metabolic process	11/114	150/12310	1.33584E-07	1.83278E-05	1.63582E-05	AKR1B15/AKR1C1/AKR1C2/AKR1C3/AKR1C4/CYP26A1/UGT1A1/UGT1A3/UGT1A7/UGT1A8/UGT1A9	11
GO:0016137	glycoside metabolic process	5/114	15/12310	1.73931E-07	2.23719E-05	1.99678E-05	AKR1B10/AKR1C1/AKR1C2/AKR1C3/AKR1C4	5
GO:0019748	secondary metabolic process	7/114	51/12310	4.01336E-07	4.85852E-05	4.33642E-05	AKR1B10/AKR1C1/AKR1C2/AKR1C3/AKR1C4/UGT1A7/UGT1A8	7
GO:1901661	quinone metabolic process	5/114	27/12310	4.2789E-06	0.000489221	0.000436648	AKR1B10/AKR1C1/AKR1C2/AKR1C3/AKR1C4	5
GO:0042448	progesterone metabolic process	4/114	13/12310	4.67719E-06	0.000497551	0.000444083	AKR1C1/AKR1C2/AKR1C3/AKR1C4	4
GO:0015893	drug transport	8/114	103/12310	4.83529E-06	0.000497551	0.000444083	ABCC3/CA2/FOLR2/HBA2/HBB/SLC7A11/SNCG/TCN1	8
GO:0010817	regulation of hormone levels	13/114	329/12310	1.07044E-05	0.001035693	0.000924395	AKR1B15/AKR1C1/AKR1C2/AKR1C3/AKR1C4/CCL5/CYP26A1/KISS1/UGT1A1/UGT1A3/UGT1A7/UGT1A8/UGT1A9	13
GO:0045833	negative regulation of lipid metabolic process	6/114	55/12310	1.10715E-05	0.001035693	0.000924395	AKR1C3/APOC1/APOC2/APOE/UGT1A1/UGT1A8	6
GO:0042440	pigment metabolic process	6/114	56/12310	1.23073E-05	0.001101233	0.000982892	UGT1A1/UGT1A10/UGT1A4/UGT1A7/UGT1A8/UGT1A9	6

GO:0016999	antibiotic metabolic process	8/114	119/12310	1.41084E-05	0.00120979	0.00107978	AKR1B10/AKR1C1/AKR1C2/AKR1C3/AKR1C4/HBA2/HBB/UGT1A1	8
GO:0006820	anion transport	14/114	402/12310	2.00059E-05	0.00164684	0.00146990	ABCC3/AKR1C1/AKR1C4/APOC1/APOC2/APOE/CA2/CLCA4/FOLR2/HBA2/HBB/SLC22A16/SLC7A11/STC1	14
GO:0044242	cellular lipid catabolic process	9/114	165/12310	2.1853E-05	0.00172974	0.00154386	AKR1B10/AKR1C3/APOC1/APOC2/APOE/CRAT/CYP26A1/FABP5/GL YATL2	9
GO:0017001	antibiotic catabolic process	5/114	38/12310	2.453E-05	0.00186972	0.00166803	AKR1B10/AKR1C3/HBA2/HBB/UGT1A1	5
GO:0015711	organic anion transport	12/114	311/12310	3.01774E-05	0.00221803	0.00197983	ABCC3/AKR1C1/AKR1C4/APOC1/APOC2/APOE/CA2/FOLR2/HBA2/HBB/SLC22A16/SLC7A11	12
GO:0005996	monosaccharide metabolic process	10/114	218/12310	3.37428E-05	0.00239457	0.00213724	SDS/UGT1A1/UGT1A10/UGT1A3/UGT1A4/UGT1A5/UGT1A6/UGT1A7/UGT1A8/UGT1A9	10
GO:0008202	steroid metabolic process	10/114	226/12310	4.58309E-05	0.00314403	0.00280641	AKR1B15/AKR1C1/AKR1C2/AKR1C3/AKR1C4/APOC1/APOE/CYP26A1/UGT1A1/UGT1A8	10
GO:0034368	protein-lipid complex remodeling	3/114	10/12310	8.85328E-05	0.00569367	0.00508101	APOC1/APOC2/APOE	3
GO:0034369	plasma lipoprotein particle remodeling	3/114	10/12310	8.85328E-05	0.00569367	0.00508101	APOC1/APOC2/APOE	3
GO:0008207	C21-steroid hormone metabolic process	4/114	28/12310	0.00012031	0.00710959	0.00634578	AKR1C1/AKR1C2/AKR1C3/AKR1C4	4
GO:0015669	gas transport	3/114	11/12310	0.00012091	0.00710959	0.00634578	CA2/HBA2/HBB	3
GO:0034367	protein-containing complex remodeling	3/114	11/12310	0.00012091	0.00710959	0.00634578	APOC1/APOC2/APOE	3
GO:0006692	prostanoid metabolic process	4/114	30/12310	0.00015875	0.00867203	0.00774066	AKR1C1/AKR1C2/AKR1C3/AKR1C4	4
GO:0006693	prostaglandin metabolic process	4/114	30/12310	0.00015875	0.00867203	0.00774066	AKR1C1/AKR1C2/AKR1C3/AKR1C4	4
GO:0051004	regulation of lipoprotein lipase activity	3/114	12/12310	0.00016012	0.00867203	0.00774066	ANGPTL4/APOC1/APOC2	3

GO:0015850	organic hydroxy compound transport	7/114	127/12310	0.00017381616	0.00917211717	0.00818645858	ABCC3/AKR1C1/AKR1C4/APOC1/APOC2/APOE/SNCG	7
GO:0042742	defense response to bacterium	7/114	129/12310	0.00019149495	0.00985243131	0.00879366464	ACP5/BPIFA2/HIST1H2BJ/KLRK1/S100A14/STAB1/STATH	7

Supplement Table 3E: GO Cellular Components for Upregulated DEGs in the CS vs NS Comparison

ID	Description	GeneRatio	BgRatio	pvalue	p.adjust	qvalue	geneID	Count
GO:0034361	very-low-density lipoprotein particle	3/15	10/12866	7.97513E-05	0.00785550404	0.00742946464	APOC1/APOC2/APOE	3
GO:0034385	triglyceride-rich plasma lipoprotein particle	3/15	10/12866	7.97513E-05	0.00785550404	0.00742946464	APOC1/APOC2/APOE	3

Supplement Table 3F: GO Molecular Functions for Upregulated DEGs in the CS vs NS Comparison

ID	Description	GeneRatio	BgRatio	pvalue	p.adjust	qvalue	geneID	Count
GO:0015020	glucuronosyltransferase activity	10/107	22/12391	8.90141E-16	2.77724E-13	2.16445E-13	B3GAT2/UGT1A1/UGT1A10/UGT1A3/UGT1A4/UGT1A5/UGT1A6/UGT1A7/UGT1A8/UGT1A9	10
GO:0033293	monocarboxylic acid binding	12/107	45/12391	2.07235E-15	3.23287E-13	2.51954E-13	AKR1C1/AKR1C2/AKR1C3/AKR1C4/APOC1/CYP26A1/FABP5/UGT1A1/UGT1A3/UGT1A7/UGT1A8/UGT1A9	12
GO:0031406	carboxylic acid binding	14/107	134/12391	7.78224E-12	6.72474E-10	5.24094E-10	AKR1C1/AKR1C2/AKR1C3/AKR1C4/APOC1/CYP26A1/FABP5/FOLR2/STAB1/UGT1A1/UGT1A3/UGT1A7/UGT1A8/UGT1A9	14
GO:0043177	organic acid binding	14/107	135/12391	8.62146E-12	6.72474E-10	5.24094E-10	AKR1C1/AKR1C2/AKR1C3/AKR1C4/APOC1/CYP26A1/FABP5/FOLR2/STAB1/UGT1A1/UGT1A3/UGT1A7/UGT1A8/UGT1A9	14
GO:0008106	alcohol dehydrogenase (NADP+) activity	7/107	17/12391	5.31801E-11	3.31844E-09	2.58623E-09	AKR1B10/AKR1B15/AKR1C1/AKR1C2/AKR1C3/AKR1C4/ALDH3A1	7
GO:0004032	alditol:NADP+ 1-oxidoreductase activity	6/107	10/12391	7.34975E-11	3.82187E-09	2.97858E-09	AKR1B10/AKR1B15/AKR1C1/AKR1C2/AKR1C3/AKR1C4	6
GO:0004033	aldo-keto reductase (NADP) activity	7/107	23/12391	6.42468E-10	2.86357E-08	2.23173E-08	AKR1B10/AKR1B15/AKR1C1/AKR1C2/AKR1C3/AKR1C4/ALDH3A1	7
GO:0001972	retinoic acid binding	6/107	14/12391	1.02195E-09	3.98559E-08	3.10618E-08	CYP26A1/UGT1A1/UGT1A3/UGT1A7/UGT1A8/UGT1A9	6
GO:0005501	retinoid binding	6/107	18/12391	6.14282E-09	2.12951E-07	1.65964E-07	CYP26A1/UGT1A1/UGT1A3/UGT1A7/UGT1A8/UGT1A9	6
GO:0019840	isoprenoid binding	6/107	19/12391	8.91527E-09	2.78156E-07	2.16782E-07	CYP26A1/UGT1A1/UGT1A3/UGT1A7/UGT1A8/UGT1A9	6
GO:0008194	UDP-glycosyltransferase activity	10/107	114/12391	4.85168E-08	1.37611E-06	1.07248E-06	B3GAT2/UGT1A1/UGT1A10/UGT1A3/UGT1A4/UGT1A5/UGT1A6/UGT1A7/UGT1A8/UGT1A9	10
GO:0005496	steroid binding	7/107	60/12391	7.78863	2.02504E-	1.57822E-	AKR1C1/AKR1C2/AKR1C3/AKR1C4/APOE/	7

				E-07	05	05	UGT1A1/UGT1A8	
GO:00 33764	steroid dehydroge nase activity, acting on the CH-OH group of donors, NAD or NADP as acceptor	5/1 07	22/12 391	1.02 399 E-06	2.457 58E-05	1.915 32E-05	AKR1B15/AKR1C1/A KR1C2/AKR1C3/AKR 1C4	5
	transferase sferring hexosyl	10/ 10 7	168/1 2391	1.81 938 E-06	4.054 62E-05	3.159 98E-05	B3GAT2/UGT1A1/U GT1A10/UGT1A3/UG T1A4/UGT1A5/UGT1 A6/UGT 1A7/UGT1A8/UGT1A 9	10
GO:00 16229	steroid dehydrogenas e activity	5/1 07	25/12 391	2.02 381 E-06	4.209 52E-05	3.280 7E-05	AKR1B15/AKR1C1/A KR1C2/AKR1C3/AKR 1C4	5
GO:00 16709	oxidoreductas e activity, acting on paired donors, with incorporation or reduction of molecular oxygen, NAD(P)H as one donor, and incorporation of one atom of oxygen	5/1 07	33/12 391	8.55 741 E-06	0.000 16686 9	0.000 13005	AKR1C1/AKR1C2/AK R1C3/AKR1C4/CYP26 A1	5
GO:00 16757	transfer ase activity , transfer ring glycosy l groups	10/ 10 7	223/1 2391	2.23 156 E-05	0.000 40955 8	0.000 31919	B3GAT2/UGT1A1/U GT1A10/UGT1A3/UG T1A4/UGT1A5/UGT1 A6/UGT 1A7/UGT1A8/UGT1A 9	10
GO:00 16616	oxidoreduct ase activity, acting on the CH-OH group of donors, NAD or NADP as acceptor	7/1 07	103/1 2391	2.94 889 E-05	0.000 51114 1	0.000 39835 9	AKR1B10/AKR1B15/A KR1C1/AKR1C2/AKR 1C3/AKR1C4/ALDH3 A1	7
GO:00 46982	protein heterodimeriz ation activity	12/ 10 7	348/1 2391	4.49 635 E-05	0.000 73834 8	0.000 57543 3	BOK/CABYR/HIST1 H2BJ/SYT5/UGT1A1/ UGT1A10/UGT1A3/ UGT1A4/ UGT1A6/UGT1A7/U GT1A8/UGT1A9	12
GO:00 16614	oxidored uctase activity, acting on CH-OH group of	7/1 07	117/1 2391	6.68 72E-05	0.001 04320 4	0.000 81302 3	AKR1B10/AKR1B15/A KR1C1/AKR1C2/AKR 1C3/AKR1C4/ALDH3 A1	7

	donors							
GO:00 16620	oxidoreductas e activity, acting on the aldehyde or oxo group of donors, NAD or NADP as acceptor	4/1 07	30/12 391	0.00 0121 162	0.001 79087 3	0.001 39572 1	AKR1B10/AKR1C3/A KR1C4/ALDH3A1	4
GO:00 04857	enzyme inhibitor activity	10/ 10 7	274/1 2391	0.00 0126 279	0.001 79087 3	0.001 39572 1	ANGPTL4/APOC1/A POC2/CSTA/PI3/PTT G3P/SFN/UGT1A1/U GT1A7/U GT1A8	10
GO:00 04497	monooxygena se activity	5/1 07	62/12 391	0.00 0191 301	0.002 59503 8	0.002 02244 8	AKR1C1/AKR1C2/AK R1C3/AKR1C4/CYP26 A1	5
	3 oxidoreductase acting on the or oxo group of onors	4/1 07	38/12 391	0.00 0309 487	0.004 02333	0.003 13559 1	AKR1B10/AKR1C3/A KR1C4/ALDH3A1	4
GO:00 05504	fatty acid binding	3/1 07	18/12 391	0.00 0464 849	0.005 80132 2	0.004 52127 3	APOC1/FABP5/UGT1 A8	3

Supplement Table 4A: GO Biological Processes for Downregulated DEGs in the CS vs EC Comparison

ID	Description	Gene Ratio	Bg Ratio	pvalue	p.adjust	qvalue	geneID	Count
GO:0042119	neutrophil activation	14/55	449/12310	6.67031E-09	5.37537E-06	4.60895E-06	C5AR1/CALML5/FCGR3B/GCA/IL18RAP/ITGB2/MME/MMP25/MMP9/QPCT/S100A7/SELL/SIGLEC14/TLR2	14
GO:0036230	granulocyte activation	14/55	455/12310	7.90128E-09	5.37537E-06	4.60895E-06	C5AR1/CALML5/FCGR3B/GCA/IL18RAP/ITGB2/MME/MMP25/MMP9/QPCT/S100A7/SELL/SIGLEC14/TLR2	14
GO:0070268	cornification	7/55	63/12310	1.09254E-08	5.37537E-06	4.60895E-06	DSC2/DSG3/IVL/KRT14/KRT16/KRT6A/KRT6B	7
GO:0008544	epidermis development	11/55	257/12310	1.40901E-08	5.37537E-06	4.60895E-06	CALML5/DSC2/DSG3/EMP1/IVL/KLK7/KRT14/KRT16/KRT6A/KRT6B/ S100A7	11
GO:0031424	keratinization	7/55	71/12310	2.55519E-08	7.79844E-06	6.68653E-06	DSC2/DSG3/IVL/KRT14/KRT16/KRT6A/KRT6B	7
GO:0043312	neutrophil degranulation	13/55	437/12310	4.43444E-08	1.04765E-05	8.98278E-06	C5AR1/CALML5/FCGR3B/GCA/ITGB2/MME/MMP25/MMP9/QPCT/S100A7/SELL/SIGLEC14/TLR2	13
GO:0002283	neutrophil activation involved in immune response	13/55	440/12310	4.80575E-08	1.04765E-05	8.98278E-06	C5AR1/CALML5/FCGR3B/GCA/ITGB2/MME/MMP25/MMP9/QPCT/S100A7/SELL/SIGLEC14/TLR2	13
GO:0002446	neutrophil mediated immunity	13/55	449/12310	6.09424E-08	1.16248E-05	9.96729E-06	C5AR1/CALML5/FCGR3B/GCA/ITGB2/MME/MMP25/MMP9/QPCT/S100A7/SELL/SIGLEC14/TLR2	13
GO:0043299	leukocyte degranulation	13/55	475/12310	1.17523E-07	1.88605E-05	1.61714E-05	C5AR1/CALML5/FCGR3B/GCA/ITGB2/MME/MMP25/MMP9/QPCT/S100A7/SELL/SIGLEC14/TLR2	13

GO:0030216	keratinocyte differentiation	8/55	135/12310	1.34067E-07	1.88605E-05	1.61714E-05	DSC2/DSG3/IVL/KRT14/KRT16/KRT6A/KRT6B/S100A7	8
GO:0002275	myeloid cell activation involved in immune response	13/55	481/12310	1.35954E-07	1.88605E-05	1.61714E-05	C5AR1/CALML5/FCGR3B/GCA/ITGB2/MME/MMP25/MMP9/QPCT/S100A7/SELL/SIGLEC14/TLR2	13
GO:0002444	myeloid leukocyte mediated immunity	13/55	485/12310	1.49647E-07	1.90301E-05	1.63168E-05	C5AR1/CALML5/FCGR3B/GCA/ITGB2/MME/MMP25/MMP9/QPCT/S100A7/SELL/SIGLEC14/TLR2	13
GO:0009913	epidermal cell differentiation	8/55	172/12310	8.59078E-07	0.00010084	8.64643E-05	DSC2/DSG3/IVL/KRT14/KRT16/KRT6A/KRT6B/S100A7	8
GO:0006954	inflammatory response	12/55	493/12310	1.3574E-06	0.000147956	0.000126861	C5AR1/C5AR2/CLEC7A/IL18RAP/IL1RN/IL36G/ITGB2/KRT16/MMP25/SOCS3/TLR2/TNFRSF10C	12
GO:0043588	skin development	8/55	222/12310	5.79058E-06	0.000589095	0.000505101	DSC2/DSG3/IVL/KRT14/KRT16/KRT6A/KRT6B/S100A7	8
GO:0051770	positive regulation of nitric-oxide synthase biosynthetic process	3/55	12/12310	1.80463E-05	0.001721166	0.001475746	LRRK2/NAMPT/TLR2	3
GO:0071621	granulocyte chemotaxis	5/55	79/12310	2.5923E-05	0.002326966	0.001995185	C5AR1/C5AR2/ITGB2/PDE4B/S100A7	5
GO:0051767	nitric-oxide synthase biosynthetic process	3/55	14/12310	2.96697E-05	0.002382949	0.002043185	LRRK2/NAMPT/TLR2	3
	9 regulation of nitric-nthase biosynthetic process	3/55	14/12310	2.96697E-05	0.002382949	0.002043185	LRRK2/NAMPT/TLR2	3
GO:0007568	aging	7/55	215/12310	4.47829E-05	0.003353876	0.002875676	ADM/ITGB2/KRT14/KRT16/LRRK2/MME/SOD2	7

GO:0097530	granulocyte migration	5/55	89/12310	4.61543E-05	0.00335376	0.00287567	C5AR1/C5AR2/ITGB2/PDE4B/S100A7	5
GO:0032496	response to lipopolysaccharide	7/55	253/12310	0.0001246676	0.00864798	0.00741494	ADM/C5AR1/CSF2RB/PDE4B/S100A7/TLR2/TNFRSF10C	7

Supplement Table 4B: GO Cellular Components for Downregulated DEGs in the CS vs EC Comparison

ID	Description	Gene Ratio	Bg Ratio	pvalue	p.adjust	qvalue	geneID	Count
GO:0030667	secretory granule membrane	20668	262/12866	1.62006E-05	0.00267310	0.00228514	C5AR1/FCGR3B/ITGB2/MME/MMP25/SELL/SIGLEC14/TLR2	8
GO:0045095	keratin filament	20515	19/12866	7.2037E-05	0.00594305	0.00508058	KRT14/KRT6A/KRT6B	3
GO:0005882	intermediate filament	20546	60/12866	0.000130952	0.00720238	0.00615706	KRT14/KRT16/KRT6A/KRT6B	4

Supplement Table 4C: GO Molecular Functions for Downregulated DEGs in the CS vs EC Comparison

ID	*Description*	*Gene Ratio*	*Bg Ratio*	*pvalue*	*p.adjust*	*qvalue*	*geneID*	*Count*

Supplement Table 4D: GO Biological Functions for upregulated DEGs in the CS vs EC Comparison

ID	Description	GeneRatio	BgRatio	pvalue	p.adjust	qvalue	geneID	Count
GO:0003341	cilium movement	14032	59/12310	2.28926E-08	1.93671E-05	1.77116E-05	CCDC40/DNAI1/DNAI2/LRRC6/MAATS1/SPAG17	6
GO:0060271	cilium assembly	14124	322/12310	4.28365E-07	0.000117159	0.000107145	CCDC40/CEP290/CROCC/DNAH6/DNAI1/DNAI2/LRRC6/SPAG17/TCT N2	9
GO:0035082	axoneme assembly	14001	51/12310	4.51949E-07	0.000117159	0.000107145	CCDC40/DNAI1/DNAI2/LRRC6/SPAG17	5
GO:0044782	cilium organization	14124	332/12310	5.53945E-07	0.000117159	0.000107145	CCDC40/CEP290/CROCC/DNAH6/DNAI1/DNAI2/LRRC6/SPAG17/TCT N2	9
GO:0007018	microtubule-based movement	14093	263/12310	1.09529E-06	0.000185323	0.000169482	CCDC40/CNIH2/DNAH6/DNAI1/DNAI2/LRRC6/MAATS1/SPAG17	8
GO:0070286	axonemal dynein complex assembly	13971	28/12310	1.49866E-06	0.000211311	0.000193248	CCDC40/DNAI1/DNAI2/LRRC6	4
GO:0001578	microtubule bundle formation	14001	74/12310	2.94377E-06	0.000355775	0.000325364	CCDC40/DNAI1/DNAI2/LRRC6/SPAG17	5
GO:0007368	determination of left/right symmetry	14001	85/12310	5.84848E-06	0.000618477	0.000565610	BICC1/CCDC40/DNAI1/DNAI2/LRRC6	5
GO:0009855	determination of bilateral symmetry	14001	90/12310	7.74892E-06	0.000692122	0.000632959	BICC1/CCDC40/DNAI1/DNAI2/LRRC6	5
GO:0009799	specification of symmetry	14001	91/12310	8.18111E-06	0.000692122	0.000632959	BICC1/CCDC40/DNAI1/DNAI2/LRRC6	5
GO:0036158	outer dynein arm assembly	13940	14/12310	9.64994E-06	0.000742168	0.000678728	DNAI1/DNAI2/LRRC6	3
GO:0120031	plasma membrane bounded cell projection assembly	14124	483/12310	1.20656E-05	0.000850628	0.000777917	CCDC40/CEP290/CROCC/DNAH6/DNAI1/DNAI2/LRRC6/SPAG17/TCT N2	9

GO:0030031	cell projection assembly	14124	495/12310	1.46868E-05	0.00095571	0.00087402	CCDC40/CEP290/CROCC/DNAH6/DNAI1/DNAI2/LRRC6/SPAG17/TCTN2	9
GO:0003351	epithelial cilium movement	13940	18/1231 0	2.1449E-05	0.00129613 4	0.00118534 1	CCDC40/LRRC6/SPAG17	3

Supplement Table 4E: GO Cellular Components for Upregulated DEGs in the CS vs EC Comparison

ID	Description	GeneRatio	BgRatio	pvalue	p.adjust	qvalue	geneID	Count
GO:0044447	axoneme part	14732	28/12866	2.09083E-08	3.55441E-06	3.10323E-06	DNAH6/DNAI1/DNAI2/MAATS1/SPAG17	5
GO:0005930	axoneme	14763	96/12866	4.6097E-07	2.10696E-05	1.83951E-05	CCDC40/DNAH6/DNAI1/DNAI2/MAATS1/SPAG17	6
GO:0097014	ciliary plasm	14763	97/12866	4.90248E-07	2.10696E-05	1.83951E-05	CCDC40/DNAH6/DNAI1/DNAI2/MAATS1/SPAG17	6
GO:0005929	cilium	14885	426/12866	4.95755E-07	2.10696E-05	1.83951E-05	CCDC40/CEP290/CROCC/DNAH6/DNAI1/DNAI2/LRRC6/MAATS1/SPAG17/TCTN2	10
GO:0044441	ciliary part	14855	334/12866	6.46514E-07	2.19815E-05	1.91913E-05	CCDC40/CEP290/CROCC/DNAH6/DNAI1/DNAI2/MAATS1/SPAG17/TCTN2	9
GO:0032838	plasma membrane bounded cell projection cytoplasm	14763	156/12866	7.87906E-06	0.00022324	0.00019490 3	CCDC40/DNAH6/DNAI1/DNAI2/MAATS1/SPAG17	6
GO:0005858	axonemal dynein complex	14671	15/12866	1.23435E-05	0.00029772	0.00026172	DNAH6/DNAI1/DNAI2	3
GO:0030286	dynein complex	14671	45/12866	0.00036085 7	0.00766821 4	0.00669484 9	DNAH6/DNAI1/DNAI2	3

Supplement Table 4F: GO Molecular Functions for upregulated DEGs in the CS vs EC Comparison

ID	Description	GeneRatio	Bg Ratio	pvalue	p.adjust	qvalue	geneID	Count
GO:0045503	dynein light chain binding	13575	22/1239 1	3.62984E-05	0.00490028 3	0.00447043 4	DNAH6/DNAI1/DNAI2	3

Supplement Table 5. IPA Top Biological Functions for EC vs. NS using human lung filtered data

Categories	Diseases or Functions Annotation	p-value	Predicted Activation State	Activation z-score	# Molecules
Cell-To-Cell Signaling and Interaction	Response of myeloid cells	0.00744	Increased	2.95	19
Cellular Compromise, Inflammatory Response	Degranulation of myeloid cells	8.35E-06	Increased	2.8	63
Cellular Compromise, Inflammatory Response	Degranulation of phagocytes	5.29E-06	Increased	2.8	63
Cellular Movement, Hematological System Development and Function, Immune Cell Trafficking	Homing of leukocytes	0.00737	Increased	2.735	34
Cellular Movement	Cell movement	0.0001	Increased	2.615	218
Cancer, Organismal Injury and Abnormalities, Respiratory Disease	Lung cancer	0.000446	Increased	2.608	350
Cell-To-Cell Signaling and Interaction	Response of granulocytes	0.000255	Increased	2.538	12
Cancer, Organismal Injury and Abnormalities	Extraadrenal retroperitoneal tumor	0.000127	Increased	2.449	329

Cellular Compromise, Inflammatory Response	Degranulation of leukocytes	1.33E-05	Increased	2.395	64
Lipid Metabolism, Small Molecule Biochemistry	Conversion of eicosanoid	0.00309	Increased	2.372	6
Cell Morphology, Cellular Assembly and Organization, Cellular Function and Maintenance	Formation of cilia	1.61E-07	Decreased	-2.158	30

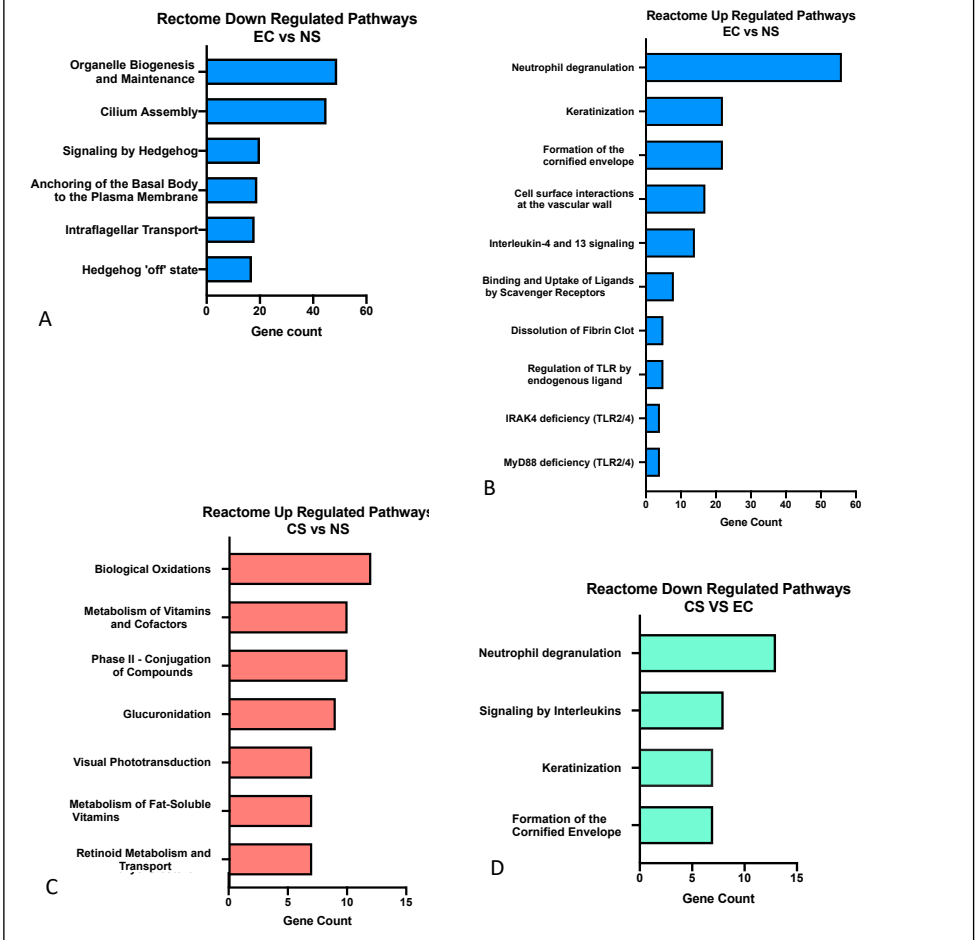

S Figure 1. Reactome enriched pathways. (A) Enriched pathways upregulated in EC vs NS. (B) Enriched pathways downregulated in EC vs NS. (C) Enriched pathways upregulated in CS vs NS. (D) Enriched pathways downregulated in CS vs EC. (FDR < 0.05)

Reactome CS vs NS Upregulated DEGs

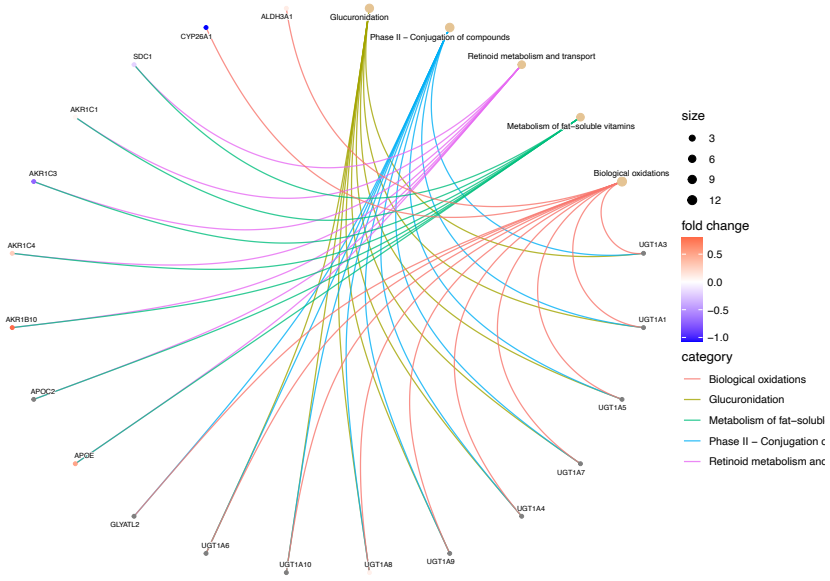

Supplement Figure 2. CNET diagram showing the top upregulated Reactome enriched pathways in CS vs E. Diagram shows the DEGs associated with each pathway and their fold changes (color key on right). Circle size key indicates the number of genes associated with each pathway.

Reactome CS vs NS Upregulated DEGs

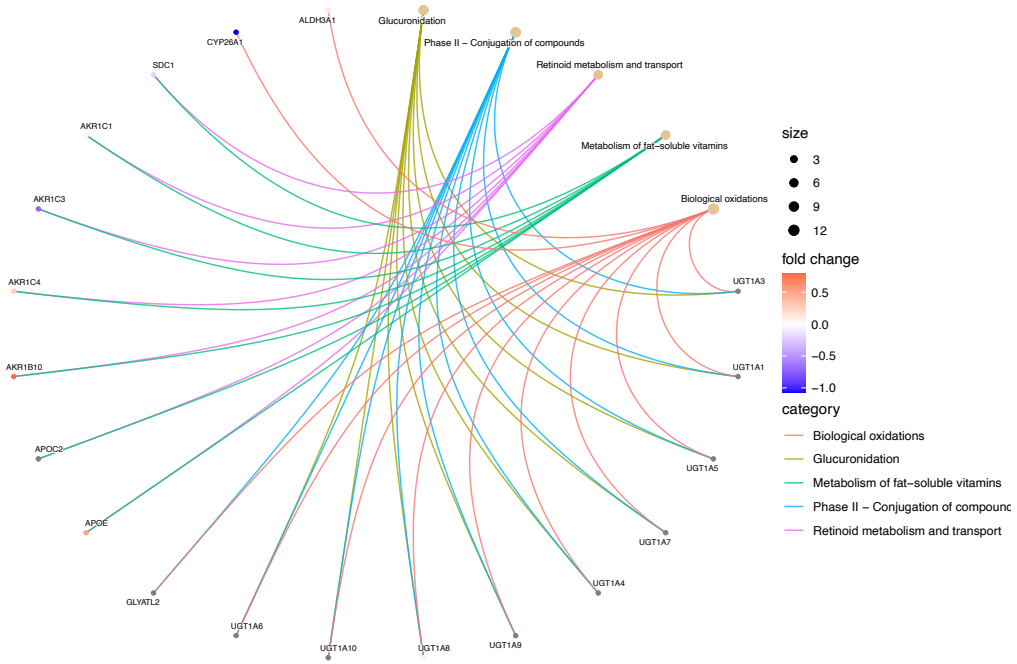

Supplement Figure 2. CNET diagram showing the top upregulated Reactome enriched pathways in CS vs E. Diagram shows the DEGs associated with each pathway and their fold changes (color key on right). Circle size key indicates the number of genes associated with each pathway